2001

Genetic and Molecular Analysis of Islet-and Liver-Enriched Transcription Factors in Metabolism and Development

David Quan Shih

Genetic and Molecular Analysis of Islet- and Liver- Enriched Transcription Factors in Metabolism and Development

A thesis presented to the faculty of
The Rockefeller University in
partial fulfillment of the requirements for
the degree of Doctor of Philosophy

David Quan Shih

The Rockefeller University
New York, New York
December 10, 2001

To my wife and best friend, Tien-An

Acknowledgments

Most of all, I would like to thank Markus Stoffel, who warmly welcomed me into his laboratory after my first Ph.D. advisor left Rockefeller University. He is a caring and patient mentor as well as a great scientist and teacher. He have firmly supported me in every possible way. I am extremely privileged to have had the opportunity to know him, to learn from him, and to work in his lab. There is no better environment in which to receive my scientific training—I owe him an immense debt of gratitude.

I thank all members of the Stoffel lab, past and present for making the lab an enjoyable place to work in every day. To Satoru Kuwajima, I am greatly indebted for all his tireless support especially with pancreatic islet isolation, he has been the most professional colleague I could ask for. I would like to thank Markus Heimesaat and Markus Bussen for their friendship, their collaborations, and for creating "The Pleasure Dome". I especially want to thank Markus Heimesaat and Satoru Kuwajima for sharing the responsibilities of animal work to help preserve my sanity. I would like to thank Christian Wolfrum for his friendship and for productive collaborations. Other lab members who I am grateful to include: Albert Barbera, Angeles Navas, Symi Richter, Pascal Boileau, and Vivian Lee for many insightful discussions and support, Rebecca Breslow, Jason Kim, Laura Garcia, and Stephanie Boger for their efficiency in all the things that keep the lab running smoothly.

I thank Ephraim Sehayek for his expertise in the characterization of cholesterol/bile acid defects in *hnf-1α*$^{-/-}$ mice, and for teaching me many techniques to better characterize plasma lipoproteins. I wish to thank Seamus Sreenan for playing an instrumental role in the characterization of the diabetic phenotype in *hnf-1α*$^{-/-}$ mice. I am very gratful for having the good fortune of working with Rohit Kulkarni. Rohit is terrifyingly efficient, knowledgeable, and is truly hardworking. I want to apologize to him for not mentioning many productive collaborations in this thesis.

I wish to thank the following people for their help, collaborations and valuable reagents in my research: Steven Duncan, Kevin Gerrish, Maureen Gannon, Christopher Wright, Roland Stein, Hayes Dansky, Martin Fleisher, Gerd Assmann, Stefan Fajans, Paul Cohen, Daniel Levine, Evelyn Ribary, Eleana Sphicas, Allan Wolkoff, Meenakshisundaram Ananthanarayanan, Benjamin Shneider, Frederick Suchy, Sarah

Shefer, Jaya Bollileni, Lou Philipson, Marco Pontoglio, Moshe Yaniv, Frank Gonzalez, Jenny Ono, Frank Isdell, Alison North, Bjorn Dittmer-Roche, Ruben Peraza, and Christopher Colon.

Nick Austriaco has played an important role in my early scientific training at MIT. He is amazingly smart, who as a graduate student independently thought up the Aging Project, believed that it will work, and started a new field of research in the Guarente Lab. He pushed me to be more confident, allowed me to carry out my own research ideas, and showed me that science is fun and addictive. I wish him the best in his spiritual calling to become a priest.

I would also like to thank my thesis committee members: Jan Breslow, James Darnell, Jeffrey Friedman, and Kenneth Polonsky who kindly traveled from St. Louis to participate in my thesis defense. They have provided me with invaluable scientific insights and encouragements. Their extensive accomplishments paved the way for much of the work presented here. In particular, I want to thank James Darnell for generously sharing reagents and mice that were generated by members of his lab.

Lastly, I cannot find the words to describe how grateful I am to my parents, Ping and Jean Shih, who I admire greatly. Without their support, guidance, encouragements, love and sacrifices, I could not be where I am today. I also want to thank my father and mother in law, Koahsiung and Chia-Ping Yang for their kindness and support.

Table of Contents

List of Figures

List of Tables

Abstract

Maturity-onset diabetes of the young (MODY) are monogenic forms of type 2 diabetes that are characterized by an early disease-onset, autosomal dominant inheritance, and defects in insulin secretion. Genetic studies have identified mutations in at least six genes associated with different forms of MODY. The majority of the MODY subtypes are caused by mutations in transcription factors that include hepatocyte nuclear factor (HNF)–4α, HNF-1α, PDX-1, HNF-1β, and NEURO-D1/BETA-2. In addition, genetic defects in the glucokinase gene, the glucose sensor of the pancreatic β-cells, and the insulin gene also lead to impaired glucose tolerance. Using molecular and genetic approaches, we demonstrated that the MODY genes are functionally related and form an integrated transcriptional network that plays an essential role in development and in different metabolic pathways.

Chapter 1: Introduction

The islets of Langerhans in the pancreas are specialized endocrine micro-organs composed of four distinct cell types: insulin-producing β-cells (65-90%), glucagon producing α-cells (5-20%), somatostatin-producing δ-cells (3-10%), and pancreatic polypeptide producing (PP) cells (≤1%). The precise interplay of these cell types results in the fine-tuned release of counterbalanced hormones that are important to maintain glucose homeostasis and plays a key role in the etiology of type 1 and type 2 diabetes mellitus. Type 1 diabetes is caused by an autoimmune destruction of pancreatic β-cells. Type 2 diabetes accounts for ≈90% of all diabetes and is characterized by hyperglycemia, insulin resistance, and impaired insulin secretion (1, 2).

Even though there is strong evidence that genetic factors are crucial for the development of NIDDM, few predisposing genes are presently known. This is due to the fact that the affliction is a multi-factorial polygenic disorder with unknown mode of inheritance. To better elucidate the molecular causes of NIDDM, a paradigm for genetic studies should be utilized. Maturity-onset diabetes of the young (MODY) is one such paradigm since the disease is monogenic (the disease is caused mutation in a single single gene) with high penetrance and a well-defined mode of inheritance (autosomal dominant) (3). Such characteristics allow for the collection of multigenerational pedigrees to confirm the linkage of susceptibility gene to disease. The information gathered from the study of MODY should also be applicable to NIDDM, allowing for a better understanding of its pathophysiology, risk assessment, and for the development of novel predictive and therapeutic approaches.

The findings that mutations in the transcription factors, hepatocyte nuclear factor (*HNF*)-1α, -1β, -4α, pancreatic and duodenal homeobox gene-1 (*PDX-1*), and neurogenic differentiation 1 (*NEUROD1*) are genes that cause MODY, suggest that MODY is a disorder of gene expression (4-9). These transcription factors belong to a network that plays important roles in β-cell development and function, and thus its impairment leads to islet cell dysfunction and causes MODY. In addition, this transcriptional network also plays a central role in regulating gene expression in the liver, kidney, and intestine, suggesting that patients with MODY may exhibit abnormal extra-pancreatic function. The identification of extra-pancreatic abnormalities in MODY patients might provide surrogate markers for the diagnosis of this disorder.

The introduction will review the pathophysiology of the two major types of diabetes and then focusing on the function and molecular defects of different MODY genes and the transcriptional network that they form. In the subsequent chapters, molecular and genetic studies will be presented that shows the involvement of this transcription factor network in the different metabolic pathways of pancreatic (Chapters 2-5) and extra-pancreatic (Chapters 6 and 7) tissues.

Diabetes Mellitus:

Diabetes mellitus refers to a variety of metabolic syndromes with a common feature of elevated plasma glucose levels (1, 2). There are 3 ways to diagnose diabetes and must be reconfirmed on a different day by any one of the 3 methods (10): 1) Symptoms of diabetes (polyuria, polydipsia, and unexplained weight loss) in addition to casual plasma glucose level ≥ 200mg/dl. Casual is defined as any time of the day. 2) Fasting plasma glucose (no caloric intake for at least 8 hours) ≥ 126 mg/dl. 3) 2 hour

postload glucose ≥ 200 mg/dl. There are 2 major categories of the disease, types 1 and 2. Type 1 diabetes, also known as insulin-dependent diabetes mellitus (IDDM), is a multifactorial autoimmune disease which results from the selective destruction of pancreatic β-cells by autoreactive T cells (11). Both CD4 (class II MHC restricted) and CD8 (class I MHC restricted) T cells are involved in its pathogenesis. Extensive studies have not yet identified the origins of the autoreactivity in IDDM, however a number of candidate autoantigens have been described including insulin, glutamic acid decarboxylase (GAD), tyrosine phosphatase (IA-2), and heat shock protein 60 (11, 12). Overt diabetes develops when over 90% of pancreatic β-cell are destroyed. Treatment of Type 1 diabetes is mostly based on daily self injection of insulin, but the long term diabetic complications including retinopathy, nephropathy, and neuropathy are not prevented. Transplantation of insulin producing islet cells may represent a cure, however lack of sufficient donor organs limits its potential. A novel way to generate a renewable souorce of functional islets-like structures to restore endocrine pancreatic function in type 1 diabetic patients is described in chapter 5.

Type 2 diabetes (NIDDM) is a clinically heterogeneous disorder for which susceptibility is determined by both environmental and genetic factors. The mechanisms leading to hyperglycemia and its complications remain largely unknown. Consequently, the usual treatments often fail to induce adequate glucose control and is a major public health problem affecting about 6-7% of the population and is the sixth leading cause of death in the US in 1997 (13). Diabetes occurs in all populations and age groups but is increasing in prevalence in the elderly, African Americans, Hispanics, Native Americans, and Asians (14). The diabetic complications including retinopathy, nephropathy,

neuropathy, and cardiovascular disease cause enormous human suffering. While the cost of human suffering is immeasurable, the health care cost due to NIDDM reaches 105 billion dollars annually, involves 10% of all US health care spending and 25% of Medicare dollars (15).

In a non-diabetic individual, plasma glucose levels are maintained in a very narrow range (80-120 mg/dL) despite variations in nutrient uptake. Normal glucose homeostasis depends on four factors (16): 1) insulin sensitivity: the ability of cells to take up glucose in the presence of insulin; 2) glucose sensitivity: the ability of cells to take up glucose in the absence of insulin; 3) first and second phase insulin secretion: the ability of the pancreatic β-cells to elicit both first and second phase insulin release. First phase insulin secretion lasts approximately 10 minutes with the maximum insulin release at 3-5 minutes after glucose load. Second phase insulin release is more prolonged and lasts as long as glucose levels remain elevated; 4) counter-regulatory hormones: counter-regulatory hormones such as glucagon must balance the anabolic effects of insulin to achieve glucose homeostasis.

Pathophysiologically, insulin resistance and insulin deficiency are the two major defects that cause diabetes. Insulin resistance, the decreased response of peripheral tissues to insulin, usually precedes overt diabetes. Reduced capacity of insulin stimulated glucose uptake in muscle and in fat appears to be the primary defect. Insulin resistance in fat results in increased lipolysis and elevated plasma fatty acid levels, which further accelerates the progression of insulin resistance by reducing glucose uptake in muscle and liver. To cope with insulin resistance, β-cell mass increases to provide sufficient insulin to maintain glucose homeostasis. At some point, the β-cells can no longer

compensate, failing to respond appropriately to elevated glucose levels. This presumably reflects a reduced capacity to adequately maintain or expand β-cell mass to meet the progressively worsening of insulin resistance. In this situation, first phase insulin secretion is lost, but the second phase insulin release is partially preserved. Eventually, β-cells severely decompensate, leading to the deterioration of glucose homeostasis, loss of both first and second phase insulin secretion, and complete metabolic decompensation with severe hyperglycemia and ketosis (17). The different metabolic stages of type 2 diabetes is diagrammed in figure 1-1.

Since insulin resistance and impaired insulin secretion are the key metabolic defects in type 2 diabetes, identification of the genetic components involved in insulin signaling, insulin secretion, and β-cell development are necessary towards a molecular understanding of the disease. However, because type 2 diabetes is clinically heterogeneous with a complex inheritance pattern, few predisposing genes to type 2 diabetes are presently known. Specific genetic defects have been identified for several uncommon monogenic subtypes of NIDDM including MODY.

Maturity-Onset Diabetes of the Young (MODY)

Although in most cases, type 2 diabetes appears to be a multi-factorial polygenic disorder, monogenic forms such as maturity-onset diabetes of the young (MODY) have been identified. MODY is a clinically heterogeneous disease that is characterized by an autosomal dominant inheritance and an early disease onset, usually before 25 years of age (3). In contrast to late-onset forms of type 2 diabetes in which β-cell defects develop as a result of insulin resistance, MODY is caused by a primary defect in pancreatic β-cell function and impaired glucose-stimulated insulin secretion (GSIS) (3). Using genetic

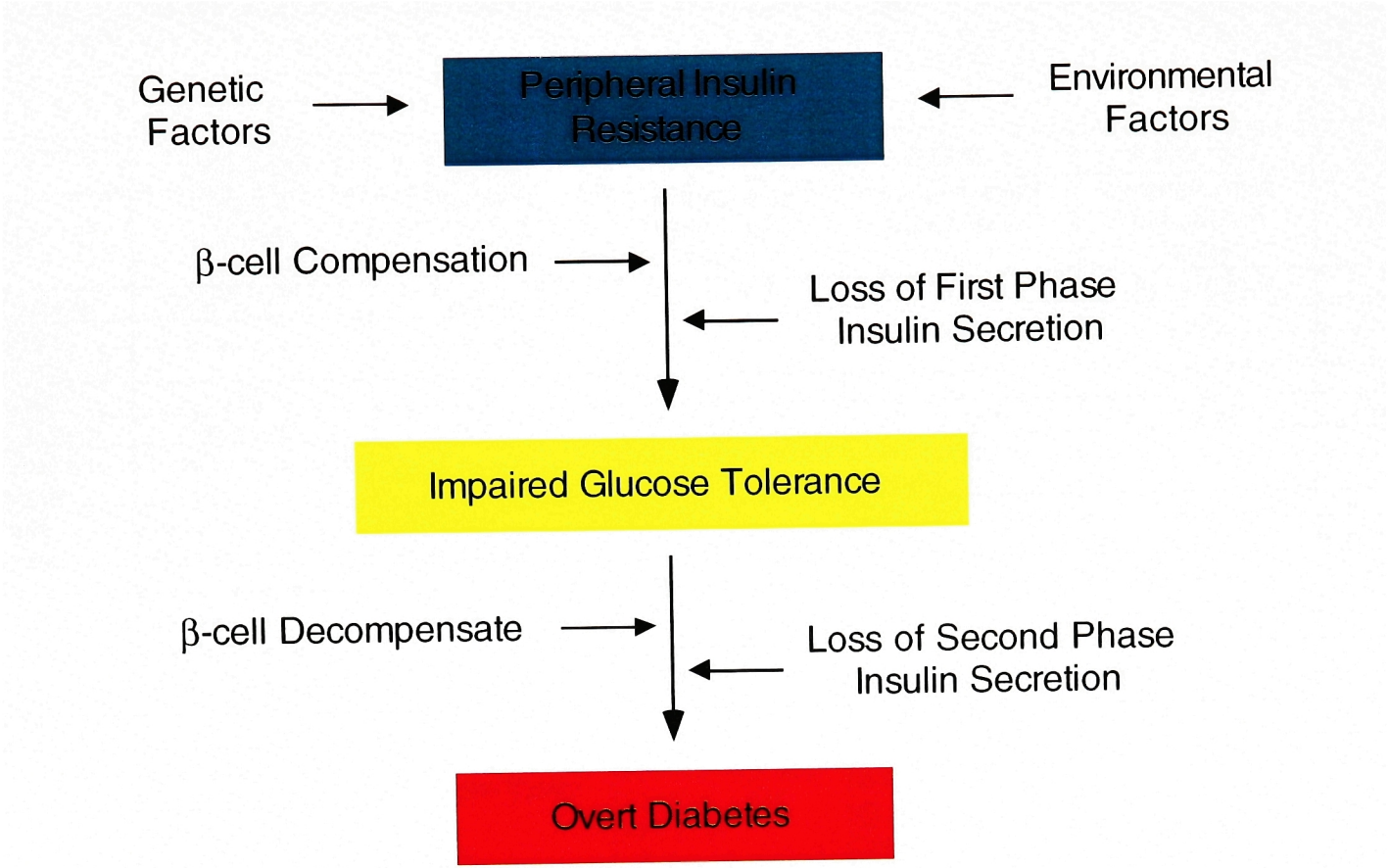

Figure 1.1: Metabolic Stages of Type 2 Diabetes. Peripheral insulin resistance is caused by both genetic and environmental factors. β-cell mass increases to cope with increased insulin demand. Insulin resistance in adipose tissue leads to increased fatty acid production which further aggrevate insuin resistance in the muscle and the liver. At some point, β-cells can no longer compensate and first phase insulin secretion is lost, leading to mild hyperglycemia. Eventually, β-cells decompensate leading to overt diabetes.

	HNF-4α	GCK	HNF-1α	PDX-1	HNF-1β	NeuroD1
Gene Family	Steroid Hormone Receptor	Glycolytic Enzyme	Homeodomain Transcription Factor	Homeodomain Transcription Factor	Homeodomain Transcription Factor	bHLH Transcription Factor
Genetic Locus	20q12-q13.1	7p15-p14	12q24.2	13q12.1	17cen-q21.3	2q32
Frequency * (%of MODY families)	3-7%	11-63%	21-73%	1-4%	1-5%	≤1%
Penetrance	High	100%	High	High	High	Medium?
Age at Diagnosis	Adolescent	Newborn	Adolescent	Postpubertal	Adolescent	Postpubertal
Most Common Treatment	Oral Hypoglycemic Insulin	Diet & Exercise	Oral Hypoglycemic Insulin	Oral Hypoglycemic Insulin	Insulin	Insulin
Clinical Features	Diabetes, Microvascular Complications, Reduced Apolipoproteins & Triglycerides	Diabetes, Impaired fasting glucose & GSIS	Diabetes, Microvascular Complications, Sensitivity to Sulfonylurea, glycosuria	Diabetes, Pancreatic Agenesis	Diabetes, Hypoplastic Glomerulocystic Kidney Disease, Mullerian Aplasia	Diabetes, Elevated Fasting Insulin
Molecular Defects	HNF-1α, PDX-1, SHP-1, AldoB, Apolipoproteins, L-PK, SR-B1, Bile Acid Transporters, Others	Glucose Sensing, Insulin Secretion, Glycogen Synthesis Others	HNF-4α, PDX-1, NEURO-D1, FXR, INS, IGF-2, PAH, GLUT-2, L-PK, Bile Acid Transporters, Others	β-cell Differentiation, INS, GLUT-2, GCK,IAPP,SST, Others	HNF1α, HNF3γ, BMP-6, TTR, AFP Apolipoproteins, Others	β-cell Differentiation, INS, Secretin, CCK, Others
Knockout Mouse Phenotype	Embryonic Lethal, Liver Steatosis	Diabetes, Perinatal Death	Diabetes, Dwarfism, Liver & kidney dysfunction	Diabetes, Pancreatic Agenesis	Embryonic Lethal	Perinatal Death, Diabetes, Epilepsy

Table 1-1. Characteristics of MODY Genes

*Different distributions in different populations

Abbreviations: HNF hepatocyte nuclear factor; GCK, glucokinase; PDX, pancreatic and duodenal homeobox gene; NeuroD1, neurogenic differentiation factor 1; bHLH, basic helix loop helix; GSIS, glucose stimulated insulin secretion; SHP-1, small heterodimer partner 1; AldoB, aldolase B; L-PK, liver pyruvate kinase; SR-B1, scavenger receptor B1; FXR, farnesoid X-activated recceptor; IGF-2, insulin growth factor 2; PAH, phenylalanine hydroxylase; Glut-2, glucose transporter 2; IAPP, islet amyloid polypeptide; SST, somatostatin; BMP-6, bone morphogenic protein 6; TTR, transthyretin; AFP, alpha fetal protein; CCK, cholecystokinin.

linkage and candidate gene approaches, mutations in genes on chromosome 2, 7, 12, 13, 19, and 20 have been linked to MODY and collectively may represent up to 5% of all patients with type 2 diabetes (18, 19). The gene on chromosome 7 (MODY2) encodes the glycolytic enzyme glucokinase (Gck) which plays a key role in generating the metabolic signal for insulin secretion and integrating hepatic glucose uptake (20). The genes on chromosome 20 (MODY1), 12 (MODY3), 19 (MODY5), 13 (MODY4), and 2 (MODY6) are caused by mutations in transcription factors *HNF–4α*, *HNF-1α*, *HNF-1β*, *PDX-1*, and *NeuroD1* respectively (4-6, 8, 9, 21). In addition to their expression in pancreatic β-cells, these genes are also expressed in the liver, kidney, and intestine. Therefore, abnormalities in extra-pancreatic might also be appreciated in some forms of MODY. The molecular basis as well as the clinical features of MODY genes are summarized in table 1-1 and described further below.

MODY1 (Hepatocyte Nuclear Factor-4α)

HNF-4α is a member of the superfamily of ligand-dependent transcription factors. It contains a zinc finger region (amino acids 48 to 128) and binds DNA as a homodimer. HNF-4α contains two transactivation domains, designated AF-1 and AF-2. AF-1 of transcription. The AF2 transactivation domain of HNF-4α, spanning amino acid residues 128-366, include the dimerization interface and a putative ligand binding domain. An *HNF-4α* promoter region named P2 is the major regulatory site for islet specific *HNF-4α* transcription. This enhancer element is located approximately 46 kb upstream of the previously identified P1 promoter of the *HNF-4α* gene and contains binding elements for HNF-1α and PDX-1 (22, 23).

HNF-4α plays a critical role in development, cell differentiation, metabolism and

is essential for the normal function of visceral endoderm, liver, intestine, kidney, and pancreatic islets (24, 25). The MODY1 locus was mapped to chromosome 20q (20q12-q13.1) and includes the gene encoding HNF-4α. Clinical studies demonstrated that loss-of-function mutation in HNF-4α cause MODY by compromising β-cell function. Prediabetic subjects with HNF-4α mutations have normal sensitivity to insulin and first-phase insulin responses to intravenous glucose (26). However, compared with normal subjects, MODY1 patients exhibit a decrease in absolute amplitude of insulin secretory oscillations and reduced insulin secretion rates in response to intravenous glucose infusions as blood glucose levels increase above 7mmol/l (26). Furthermore, HNF-4α haploinsufficiency leads to diminished glucagon secretory responses to arginine, suggesting a role of the MODY1 gene in α-cell function (27). Clinically, MODY1 patients frequently develop severe diabetes and complications, including micro- and macro-vascular angiopathy and peripheral neuropathy. About 30% of cases with MODY1 require insulin therapy and the remainder are treated with oral anti-diabetic drugs. Molecular studies indicate that HNF-4α deficiency lead to abnormal pancreatic islet gene expression which results in an impairment of insulin secretion. Several genes of the GSIS pathway in pancreatic β-cells are regulated by HNF-4α. They include the glucose transporter-2 (GLUT-2) and several enzymes of glycolysis (aldolase B, glyceraldehyde-3-phosphate dehydrogenase, L-pyruvate kinase) (Table 1-1). Furthermore, HNF-4α is an upstream transcriptional regulator of HNF-1α (the MODY3 gene) which itself is a transcriptional activator of the insulin gene (25). Together, these data suggest that diminished HNF-4α activity can impair GSIS by decreasing glucose entry and metabolism in pancreatic β-cells as well as insulin regulated gene transcription (25).

Since HNF-4α is not only expressed in pancreatic β-cells but also plays a key role in hepatocyte differentiation, mutations in this gene could be expected to result in pleiotropic phenotypes. Indeed, we show in chapter 7 that subjects with HNF-4α haploinsufficiency have diminished serum apolipoprotein (apo)AII, apoCIII, Lp(a) and triglyceride levels compared to normal controls or patients with other forms of early-onset diabetes (28).

MODY2 (Glucokinase)

The phosphorylation of glucose at the sixth carbon position is the first step in glycolysis and is catalyzed by a family of enzymes called hexokinases. Glucokinase (GCK), expressed mainly in the liver and endocrine pancreas, is a unique member of this family. In contrast to hexokinases 1, 2, and 3, GCK (hexokinase 4) is characterized by a high substrate specificity for glucose, a high Km of about 10mM (versus 0.1-0.001mM for the other hexokinases), and a lack of inhibition by metabolites such as glucose 6-phosphate or glucose 1,6 bisphosphate. These unique biochemical properties allow GCK to serve as the glucose sensor of the pancreatic β-cell by integrating glucose metabolism and insulin secretion (20). Impairment in the enzymatic activity of mutant GCK leads to decreased glycolytic flux in pancreatic β-cells (29). This translates *in vivo* as a rightward shift in the dose response curve relating blood glucose and insulin secretion rates (ISR) obtained during a graded intravenous glucose infusion. Average ISRs over a glucose range between 5 and 9 mM are 61% lower in MODY2 subjects than in control subjects (29). The release of insulin in response to arginine is preserved, indicating that the insulin secretion defect in MODY2 patients is due to glucose sensing. Complete loss of GCK activity in subjects with homozygous mutations in the *GCK* gene (T228M and M210K)

cause neonatal diabetes, a rare form of diabetes that requires insulin therapy within the first month of life (30). An activating GCK mutation (V455M) that causes a leftward shift of the dose-response curve relating blood glucose and insulin secretion rates has been reported to cause autosomal dominant familial hyperinsulinism (31). These genetic findings confirm the importance of GCK as a critical regulator for insulin secretion in pancreatic β-cells.

Gck-deficient mice are an excellent animal model to study the genetic defect in humans. Mice that lack Gck activity die perinatally with severe hyperglycemia and phenotypically resemble rare forms of neonatal diabetes. Heterozygous mice have elevated blood glucose levels and reduced insulin secretion. Expression of Gck in β-cells in the absence of expression in the liver can rescue Gck null mice, providing strong evidence for the critical need of β-cells Gck in glucose sensing and for maintaining normal glucose levels (32). 13C nuclear magnetic resonance spectroscopy studies have revealed that a hepatic glucose cycling defect also contributes to the molecular etiologies of the MODY2 phenotype. MODY 2 patients have decreased net accumulation of hepatic glycogen and augmented hepatic gluconeogenesis after meals (33). These results suggest that in addition to the altered β-cell function, abnormalities in liver glycogen metabolism play an important role in the pathogenesis of hyperglycemia in patients with GCK-deficient diabetes (Table 1-1) (33).

Fetal insulin secretion in response to maternal glycemia is an important determinant for intrauterine growth. Glucose sensing defects in pancreatic β-cells, caused by a heterozygous mutation in the *GCK* gene, reduce fetal growth and birth weight in addition to causing hyperglycemia after birth (34). The inheritance of a *GCK* mutation by

the fetus results in a reduction of birth weight of 521 g (p = 0.0002) compared to unaffected sibs (34). Maternal hyperglycemia due to a *GCK* mutations results in a mean increase in birth weight of 601 g (P = 0.001) (34). Since glucose, but not insulin crosses the placenta, it is likely that these changes in birth weight reflect changes in fetal insulin secretion that are influenced directly by the fetal genotype and indirectly, through maternal hyperglycemia, by the maternal *GCK*-genotype (34).

In contrast to MODY1 and MODY3 patients who frequently develop diabetes at the time of puberty, hyperglycemia in subjects with *GCK* mutation frequently manifest in the neonatal period and invariably develops before adolescence (Table 1-1) (34, 35). GCK deficiency is not associated with an increased incidence of diabetic complications, including retinopathy, neuropathy, or proteinuria, and other manifestations of the metabolic syndrome such as hypertension, obesity, or dyslipidemia (Table 1-1) (18, 35). This finding is also consistent with the low frequency of coronary heart disease seen in MODY2 patients.

MODY3 (Hepatocyte Nuclear Factor-1α)

HNF-1α is a homeodomain transcription factor composed of an N-terminal dimerization domain, a POU-homeobox DNA binding domain, and a C-terminal transactivation domain. HNF-1α is expressed in liver, kidney, intestine, and pancreatic islets where it directs tissue-specific gene expression. Mice with targeted inactivation of the *hnf-1α* gene have been shown to have NIDDM, dwarfism, renal Fanconi-like syndrome, glycogen storage disease 1b and defects in bile acid and plasma HDL-cholesterol metabolism (Chapter 6) (36-39). Pancreatic islets from Hnf-1α deficient mice have impaired β-cell glycolytic signaling proximal to mitochondrial oxidation (40, 41). In

chapter 3, we provide evidence that the glycolytic signaling impairment primarily results from abnormal gene expression caused by HNF-1α deficiency (42)

The gene encoding HNF-1α is located on the long arm of chromosome 12 (12q24.2) and was identified as the MODY3 gene through a combination of genetic linkage analysis and positional cloning (5). Mutations in the *HNF-1α* gene (MODY3) are the most common cause of MODY and depending on the population, may account between 21%-73% of all MODY (43, 44). The clinical features of MODY3 are similar to MODY1 since HNF-1α and HNF-4α regulate each other's expression. *HNF-1α* mutations lead to β-cell dysfunction and result in elevated fasting glycemia and glucose stimulated insulin secretion (GSIS) (45). Other clinical features of MODY3 include increased responsiveness to sulfonylureas and lower body mass index (BMI) (35, 45, 46). In addition to its effects on β-cell function, HNF-1α deficiency lead to decreased renal reabsorption of glucose (47, 48). *HNF-1α* mutations are highly penetrant, with 63% of MODY3 diagnosed by the age of 25 years, 78.6% by 35 years, and 95.5% by 55 years (49). Subjects with *HNF-1α* mutations have a more rapid deterioration in β-cell function than MODY2 subjects (Table 1-1) (35). MODY3 patients frequently require treatment with oral hypoglycemic agents or insulin (35).

MODY4 (Pancreatic and duodenal homeobox gene-1)

Pancreatic and duodenal homeobox gene-1 (PDX-1, IPF-1) is a homeodomain transcription factor that was originally isolated as a regulator of the insulin and somatostatin genes (50-52) . PDX-1 binds as a heterodimer with the ubiquitously expressed homeodomain protein PBX to target sites containing a consensus TGATTAAT motif (53). During development, PDX-1 is initially expressed at 8.5 dpc in the dorsal and

ventral gut epithelium that will later develop into a pancreas. At 9.5 dpc, PDX-1 expression marks the dorsal and ventral pancreatic buds of the gut and later is restricted to differentiating insulin producing β-cells and somatostatin producing δ-cell (50-52). Targeted disruption of the *pdx-1* gene results in a failure of the pancreas to develop (54, 55). Furthermore, β-cell-specific inactivation of the murine *pdx-1* gene indicates that Pdx-1 in the adult islet is required for maintenance of the β-cell phenotype, including expression of Nkx6.1, insulin, Glut-2, and Gck (56). Together, Pdx-1 appears to be a key regulator in early pancreas formation and later in maintaining islet pattern of hormone expression and normoglycemia.

Understanding the regulation of the *PDX-1* gene is of paramount importance since PDX-1 is an essential regulator of pancreas development and β-cell differentiation. Expression of PDX-1 in the adult islet is regulated by the feed forward loop formed by the transcription factor HNF-1α and HNF-4α as well as by the winged helix transcription factor HNF-3β (FOXA2) (Fig. 1-2) (42, 57-59). Recently, PDX-1 was found to be required for the expression of the fibroblast growth factor receptor-1 (FGFR1), an important signaling component in β-cells, indicating that PDX-1 acts upstream of FGFR1 signaling in β-cells to maintain proper glucose sensing, insulin processing, and glucose homeostasis (60).

The link between HNF-4α and PDX-1 is also found in humans by analyzing the promoter of *HNF-4α*. A mutation (-146T-C) in the *HNF-4αP2* promoter of a large MODY family was identified where a mutated *PDX-1* binding site in the P2 promoter cosegregates with diabetes (LOD score of 3.25) (22). This mutation lead to decreased

binding activity of PDX-1 to this site and reduced transcriptional activity. These data suggest that PDX-1 is an important activator of HNF-4α expression in pancreatic β-cells.

PDX-1 mutations are rare and most of the clinical findings of MODY4 are based on studies of a single family. Stoffers et al. (1997) identified a single nucleotide deletion within codon 63 (Pro63fsdelC) of the human *PDX-1* gene in a patient with pancreatic agenesis. This patient inherited the mutant allele from his parents who were heterozygous for the same mutation (6). Heterozygous family members have early-onset diabetes (range, 17 to 67 years) (7). The point deletion leads to an out-of-frame protein downstream of the PDX-1 transactivation domain, resulting in a non-functional protein lacking the homeodomain that is essential for DNA binding (6). Expression studies of the mutant PDX1(Pro63fsdelC) protein in eukaryotic cells revealed a second PDX-1 isoform that resulted from an internal translation initiating at an out-of-frame AUG (21). The reading frame crosses over to the wildtype *PDX-1* reading frame at the site of the point deletion just carboxy-proximal to the transactivation domain, resulting in a second PDX1 isoform that contains the COOH-terminal DNA-binding domain but lacks the amino-terminal transactivation domain (21). This terminal domain PDX-1 isoform may inhibit the transactivation functions of wildtype PDX-1, suggesting that a dominant negative mechanism may contribute to the development of diabetes in individuals with this mutation. Six affected members in this pedigree had severe impairment of insulin secretion during a hyperglycemic clamp study (61). However, none of the family members carrying the PDX-1(Pro63fsdelC) mutation showed ketosis or other indications of severe insulin deficiency (7).

MODY5 (Hepatocyte Nuclear Factor-1β)

HNF-1α and -1β are homologous proteins belonging to a large superfamily of homeodomain-containing transcription factors. As such, HNF-1β is structurally similar to HNF-1α with an N-terminal dimerization domain, a POU-homeobox DNA binding domain, and a C-terminal transactivation domain (62). HNF-1α and -1β bind to DNA as homo- and/or heterodimers. The *HNF-1* genes have an overlapping tissue distribution but HNF-1α/HNF1β ratios differ from one organ to another with HNF-1α being the predominant form in the liver and HNF-1β the major form in the kidney. Inactivation of the *hnf-1β* gene in mice results in early embryonic lethality by day 7.5 of development. Hnf-1β-deficient embryos exhibit an abnormal extraembryonic region, poorly organized ectoderm, and no discernible visceral endoderm (62, 63).

The gene encoding HNF-1β maps to chromosome 17q (17cen-q21.3) and genetic variation in this gene is responsible for several human disorders including MODY5, familial hypoplastic glomerulocystic kidney disease (renal cysts), and female genital abnormalities (vaginal aplasia with rudimentary uterus and bicornuate uterus) (8, 64-68). In contrast to other MODY types, patients with mutations in the *HNF-1β* gene have early and rapidly progressing familial hypoplastic glomerulocystic kidney disease different from the diabetic nephropathy in type 1 or type 2 diabetes. *HNF-1β* mutations are rare causes of MODY and only six MODY5 families have so far been reported. MODY5 develops early in life (range 10-25 years) and ultimately require insulin replacement therapy to control hyperglycemia (Table 1-1).

MODY6 (neurogenic differentiation-1)

NEUROD1/BETA2 belongs to the basic helix-loop-helix (bHLH) family of

transcription factors that is involved in determining cell type during development (69). NeuroD1 is composed of a bHLH DNA binding domain and a C-terminal transactivation domain that interacts with the cellular co-activator p300 and CBP. It was first isolated on the basis of its ability to activate the transcription of the insulin gene (69, 70). NEUROD1 is expressed in pancreatic islets, intestine, and the brain (69). Mice deficient for Neuro-D1 function have abnormal islet morphology, overt diabetes, and die shortly after birth (71).

Mutations in the *NEUROD1* gene have recently been reported as being associated with diabetes in two families with autosomal dominant inheritance (9). The first family carries a missense mutation (G to T transversion) causing a substitution of Arg to Leu (R111L) in the proximal bHLH domain and thereby, abolishes its DNA binding activity (9). The second mutation in the *NEUROD1* gene consists of an insertion of a cytosine residue in a polyC tract in codon 206 (206+C) (9). NeuroD(H206fsinsC) gives rise to a truncated polypeptide lacking the C-terminal transactivation domain, a region that associates with the co-activators CBP and p300 (72, 73). This mutant retains its ability to bind to DNA, however, it has lost its ability to activate transcription through the deletion of the protein domain that interacts with co-activator p300 (9). The clinical profile of patients with this truncated protein is more severe and shares clinical features of MODY such as non-obese diabetes, low endogenous insulin secretion (β-cell dysfunction) and early age of onset (range 17-56 years) (9). Therefore, mutations in NEUROD1 may result in another subtype of MODY.

MODY-X

Mutations in GCK and in islet enriched transcription factors indicate that MODY

is the result of abnormal gene expression involving effectors of glucose homeostasis. Additional MODY genes (MODY-X) may exist since there are families in which MODY does not co-segregate with markers tightly linked any of the known MODY loci. MODY-X may account for approximately 15% of Europeans and up to 80% of Japanese patients with the clinical diagnosis of MODY (15). Several mutations in genes involved in glucose metabolism including islet-brain-1 (IB-1, an inhibitor of JNK pathway for optimal insulin secretion), islet-1 (ISL-1, an islet enriched transcription factor required for β-cell development and function), and insulin were found to segregate with early-onset diabetes (74, 75) (76). However, these genes must be further characterized both genetically and clinically to determine their etiologies and assess if they might be the cause of MODY-X. Identification of genes responsible for MODY-X will enable a better understanding of the causes and pathophysiology of MODY and maybe type 2 diabetes.

The Transcriptional Network of the Pancreatic Islet

Numerous studies have shown that the HNFs as well as other islet enriched transcription factors fall into a regulatory network (Fig.1-2). Identification of these transcription factors as diabetes susceptibility genes and MODY highlights their importance in the normal function of the endocrine pancreas. This transcription network is also present in extra-pancreatic organs such as the liver, and is involved in their differentiation and as well as in various metabolic pathways.

In vitro studies have shown that the forkhead transcription factor HNF-3β is a transcriptional activator of PDX-1, HNF-4α, HNF-1α, and HNF-3α, suggesting that HNF-3β is a master regulator of this transcriptional hierarchy (57, 59, 77). The highly conserved DNA binding domain of the HNF-3 proteins is similar to that of linker

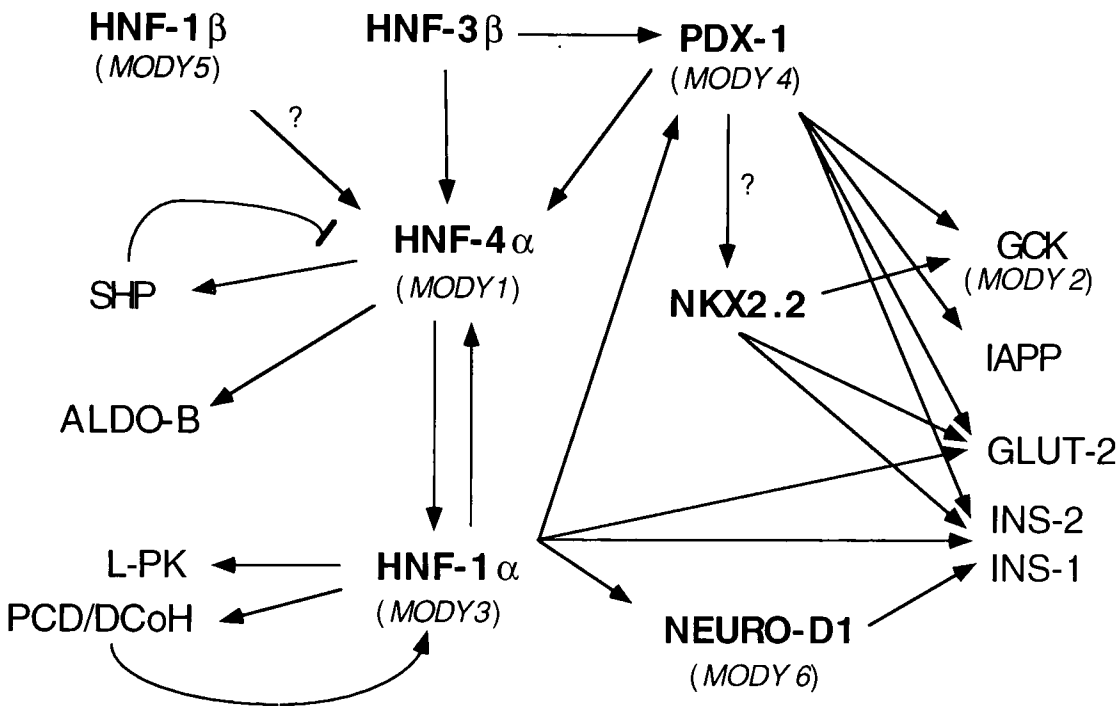

Figure 1-2. Proposed model for a hierarchical transcriptional network. This diagram shows the transcriptional regulation of transcriptional factors essential for endocrine pancreatic function. Arrows show positive transcriptional regulation. Bars show transcriptional repression. Black color indicates the transcriptional regulation in the liver and/or pancreatic islets. Red color indicates the transcriptional regulation that has only been found in the endocrine pancreas. Abbreviations: HNF: hepatocyte nuclear factor, GCK: glucokinase, IAPP: islet amyloid polypeptide, GLUT-2: glucose transporter-2, INS: Insulin, PDX-1: pancreatic and duodenal homeobox gene-1, SHP: small heterodimer protein, NEURO-D1: neurogenic differentiation-1, ALDO-B: aldolase B, L-PK: pyruvate kinase liver isoform, PCD: pterin-4-alpha-carbinolamine dehydratase.

histones H1 and H5. However, unlike the linker histones that compact DNA chromatin and repress gene expression, HNF-3β have been shown to decompact DNA from the nucleosome and is associated with transcriptionally active chromatin (78) (79). HNF-1β also occupies a preeminent position in the transcriptional network. It was shown that in *hnf-1β*$^{-/-}$ visceral endoderm, the expression of Hnf-4α and Hnf-1α are either markedly reduced or absent (62, 63). In the liver, HNF-4α regulates the expression of HNF-1α, whereas in pancreatic β-cells, HNF-4α and HNF-1α form an auto-regulatory loop in which HNF-1α also regulate the expression levels of HNF-4α (42, 80, 81). The regulatory feed-forward loop is further demonstrated with the recent identification and characterization of the major regulatory site (P2) for islet-specific HNF-4α expression which revealed a functional binding site for HNF-1α (22) (82). These data suggest that a defect in the autoregulatory loop between HNF-4α and HNF-1α may be responsible for the similar clinical features between MODY1 and MODY3. In addition, a functional PDX-1 binding site was also found in the P2 promoter, indicating that PDX-1 is a transcriptional activator of HNF-4α (22). Strong evidence showing that this functional hierarchy is also important in pancreatic β-cells came from the finding that MODY could be caused by a mutation in the PDX-1 binding site of the HNF-4αP2 promoter (22). Recent *in vitro* studies demonstrated that HNF-1α can bind to an evolutionarily conserved HNF-1α binding site in the PDX-1 promoter and activate its transcription (57). In addition, Pdx-1 expression levels are reduced in isolated Hnf-1α deficient islets, indicating that Hnf-1α is required for normal Pdx-1 expression in pancreatic β-cells (42). The importance of this transcriptional hierarchy in islet function and glucose homeostasis

is further investigated in chapter 4 by studying the epistatic relationship between different transcriptional components of the network.

A negative regulator that may be important to down-tune the activity of the network has been identified. Small dimerization partner (SHP-1) is an orphan nuclear factor of the steroid hormone superfamily that contains an AP2 domain but lacks the N-terminal DNA binding domain (83). SHP-1 can heterodimerize with various nuclear hormone receptors, including HNF-4α, and inhibit their transactivation activity (84). A recent study showed that the expression of Shp-1 is diminished in islets of *hnf-1α* null mice and this decrease is mediated secondarily by reduced expression of Hnf-4α in these islets (42). This report demonstrate that SHP-1 can regulate its own expression by inhibiting the function of its transcriptional activator HNF-4α, thus forming a negative feedback loop. SHP-1 may therefore serve as an important checkpoint to balance the activity of the islet transcriptional network (Fig. 1-2). However, additional studies are required to determine the physiological significance of this negative regulation.

This transcription factor network plays an important role in glucose homeostasis in pancreatic β-cells by coupling nutrient metabolism, insulin synthesis and secretion with electrical activity. After a meal, elevation of blood glucose leads to glucose transport into β-cells by glucose transporter-2 (GLUT-2), where it enters glycolysis and is broken down into pyruvate. The *GCK* and pyruvate kinase (*PK*) genes encode two glycolytic enzymes that catalyze the rate limiting and irreversible steps in glycolysis. Pyruvate then enters the mitochondria and undergoes oxidative phosphorylation, leading to an increase in ATP/ADP ratio and inhibition of ATP-sensitive, transmembrane potassium channels

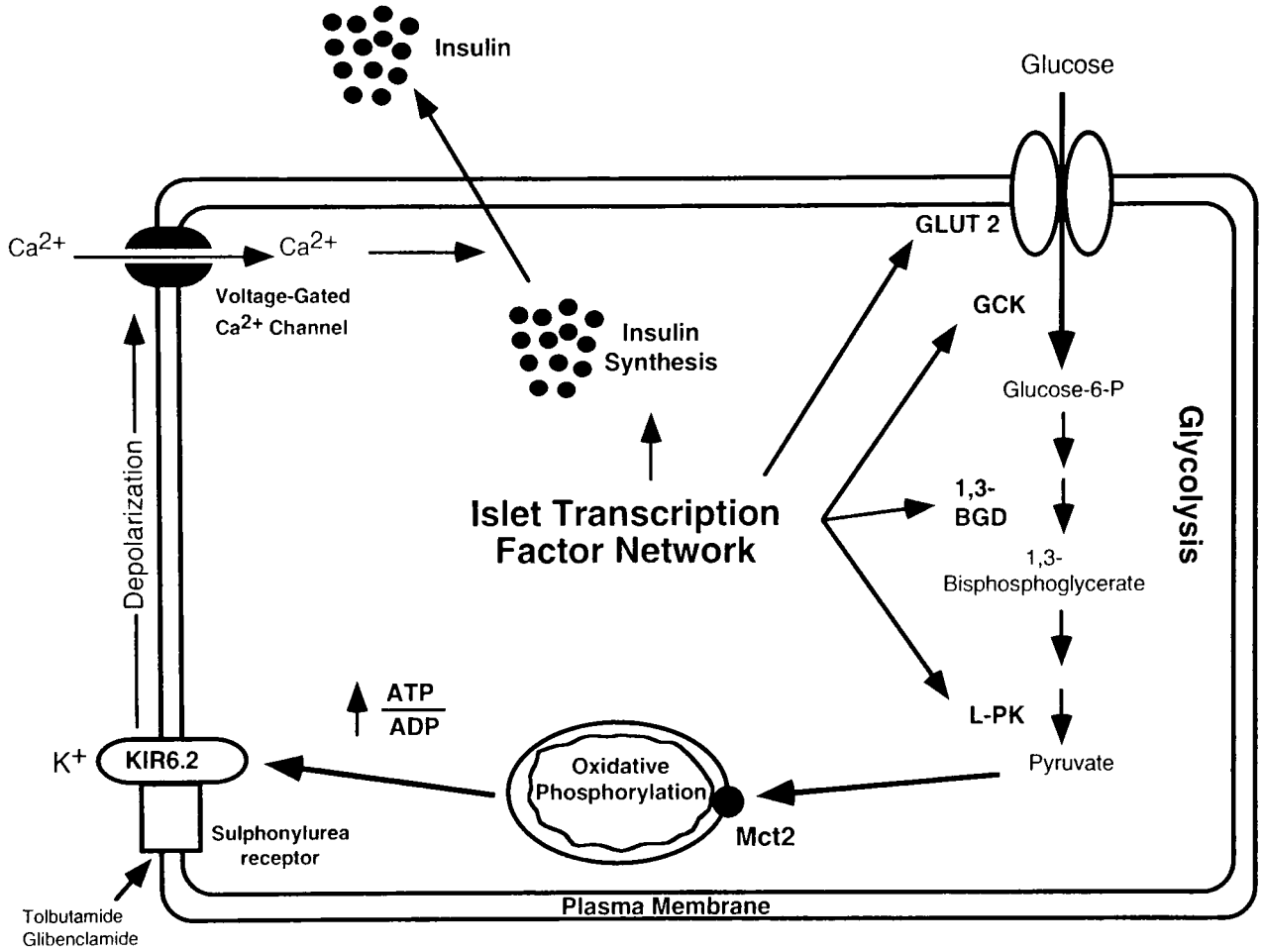

Figure 1-3. Metabolic signaling pathway in pancreatic β-cells. Glucose transporter-2 (GLUT-2) transports glucose into the β-cells where it enters glycolysis and is broken down into pyruvate. Pyruvate enters the mitochondria and undergoes oxidative phosphorylation, leading to an increase in ATP/ADP ratio that results in the depolarization of the β-cell plasma membrane by closing the ATP-sensitive potassium channels (KIR6.2). The resulting change in membrane potential activates voltage-gated calcium channel and leads to a rise in cytosolic calcium levels. Increased cytosolic calcium levels trigger secretion of pre-stored insulin vesicles. The islet transcription factor network regulates insulin secretion by regulating the expression of GLUT-2, glucokinase (GCK), glyceraldehyde-3-phosphate dehydrogenase (1,3 BGD), and insulin.

(KIR6.2). The change in membrane potential activates voltage-gated calcium channels and results in a rise in cytosolic calcium levels that trigger insulin release (Fig. 1-3).

The islet enriched transcription factors controls GSIS from β-cells at the following steps: 1) The transcription network regulate the entry of glucose into the β-cells by controlling the expression of GLUT-2, the major glucose transporter in the β-cells; 2) This network regulates the flux of glucose through glycolysis by regulating the expression of glucokinase, aldolase B, glyceraldehyde-3-phosphate dehydrogenase (1,3 BGD) and the liver pyruvate kinase isoform (L-PK); 3) Finally, this transcription network activates the transcription of the insulin gene itself. The combinatorial control of β-cell function by the islet enriched transcription factors generates both diversity and stringency for glucose homeostasis.

Summary

Type 2 diabetes among youth, is an emerging public health problem. Increasing evidence indicates that type 2 diabetes is a complex genetic disorder in which defects in insulin action (insulin resistance) and secretion contribute to the clinical features of the disease. Islet enriched transcription factors play a vital role in the normal development and function of the endocrine pancreas in animal models. The importance of this network is further underscored by its involvement in early-onset type 2 diabetes. Studying the pathophysiology of MODY and other early-onset diabetes of known etiology have provided important insights on glucose homeostasis and may provide novel insights into the etiology of β-cell dysfunction in more complex, late-onset type 2 diabetes.

Chapter 2: Impaired Glucose Homeostasis and Neonatal Mortality in Hepatocyte Nuclear Factor-3α Deficient Mice

Introduction

The hepatocyte nuclear factor 3 (HNF-3/FOXA) family of transcription factors in mammals are encoded by 3 unlinked genes designated HNF-3α, HNF-3β, and HNF-3γ. They all have in common a highly conserved 100 amino acid DNA-binding domain, which is centrally located in the HNF-3 proteins (85). The DNA-binding domain is made up of 3 α-helices and 2 characteristic loops (wings), resulting in the designation of this DNA-binding motif as the winged helix DNA binding domain that is responsible for monomeric recognition of specific DNA target sites (85). The structure of the highly conserved DNA binding domain of the HNF-3 proteins is similar to that of linker histones H1 and H5 (85). However, unlike linker histones that compact DNA in chromatin and repress gene expression, HNF-3 proteins have been shown to exhibit nucleosome-binding properties, decompact DNA from the nucleosome and are associated with transcriptionally active chromatin (78, 79). In addition to its DNA-binding domain, HNF-3 contain 4 trans-activation domains (86) (domains II-V).

HNF-3 transcription factors were discovered by their ability to bind to the promoters of the genes encoding α1-antitrypsin and transthyretin (87). Subsequently, HNF-3 binding sites have been discovered in numerous genes encoding hepatic and pancreatic enzymes, serum proteins and hormones (88). Based on their multiple targets in the liver and pancreas, an important role for HNF-3 proteins in metabolism has been suggested. In the adult, *hnf-3* genes have overlapping patterns of tissue expression

including gut, central nervous system, neuroendocrine cells, lung, and the liver (87, 89, 90). During development, HNF-3β is expressed first, followed by sequential expression of HNF-3α, and HNF-3γ in the definite endoderm, notochord, and floor plate of the neural tube (91-94). These observations suggest that in addition to their regulatory roles in metabolism in the adult, the HNF-3 proteins may play critical roles in the development of endodermal derived tissues (e.g. liver, pancreas).

The functional significance of the HNF-3 proteins *in vivo* was analyzed by gene targeting in mice. Targeted disruption of the *hnf-3β* in mice produces an embryonic lethal phenotype that lacks a notochord and exhibits defects in foregut and neural tube development (93, 95). Because of the early lethality of the homozygous mutant embryos, the role of Hnf-3β in the development of the gut, pancreas, and liver could not be characterized in detail. Tissue-specific deletion of *hnf-3β* in the liver during late fetal development (using Cre recombinase under the control of albumin promoter) have no effect on liver function and gene expression (96). This suggests that the main role of Hnf-3β is to set up a developmental program, and once such a transcriptional program is established, the function of HNF-3β in the liver seems dispensable. The function of Hnf-3β in pancreatic β-cell function was addressed by tissue specific deletion of *hnf-3β* using the Cre-loxP recombination system. Mice that lack Hnf-3β specifically in pancreatic β-cells resemble several pathophysiological aspects of familial hyperinsulinism such as dysregulated insulin secretion in response to both glucose and amino acids (97). The inappropriate hypersecretion of insulin is due to reduced expression of ATP-sensitive potassium channel (Kir6.2 and Sur1), the most common genes linked to familial hyperinsulinism (97). In addition, *hnf-3β*$^{-/-}$ mice may also exhibit an α-cell defect since

the plasma glucagon levels are inappropriately low (97). Together these data show that HNF-3β is required in pancreatic islets to maintain proper circulating levels of insulin and glucagon for glucose homeostasis.

In contrast to the *hnf-3β* null mice, *hnf-3γ* deficient embryos develop normally and show no obvious metabolic defects. The mild phenotype of *hnf-3γ*$^{-/-}$ mice can be explained in part by an upregulation of Hnf-3α and Hnf-3β (98). The role of Hnf-3α was analyzed in visceral endoderm derived from *hnf-3α* null embryonic stem (ES) cells (77). In this system, lack of Hnf-3α lead to an increase in the expression levels of several apolipoproteins and glycolytic enzymes including apolipoprotein (Apo)-A1, -AII, -AIV, B, -CII, glucose transporter (glut)-2, aldolase B, and liver pyruvate kinase (77). In addition, Hnf-3α regulate the expression of early-onset diabetes genes HNF-1α (MODY3) and HNF-4α (MODY1). Together, these data show that Hnf-3α is upstream of the liver and islet enriched transcription factor network that is required for both liver and pancreatic islet function. To test the function of Hnf-3α *in vivo*, we have generated mice lacking *hnf-3α* by gene targeting. We show that *hnf-3α* deficient mice develop a complex metabolic syndrome characterized by neonatal persistent hypoglycemia, hormonal insufficiencies, pancreatic α- and β-cell dysfunction, and increased expression of Hnf-3α target genes.

Results

Generation of *hnf-3α* Null Mice.

The *hnf-3α* gene was disrupted in ES cells by homologous recombination using a targeting vector in which most of exon 2 of the *hnf-3α* gene was deleted and fused in frame to the *Escherichia coli lacZ* gene and a pGK-neomycin cassette (Fig. 2-1A). One

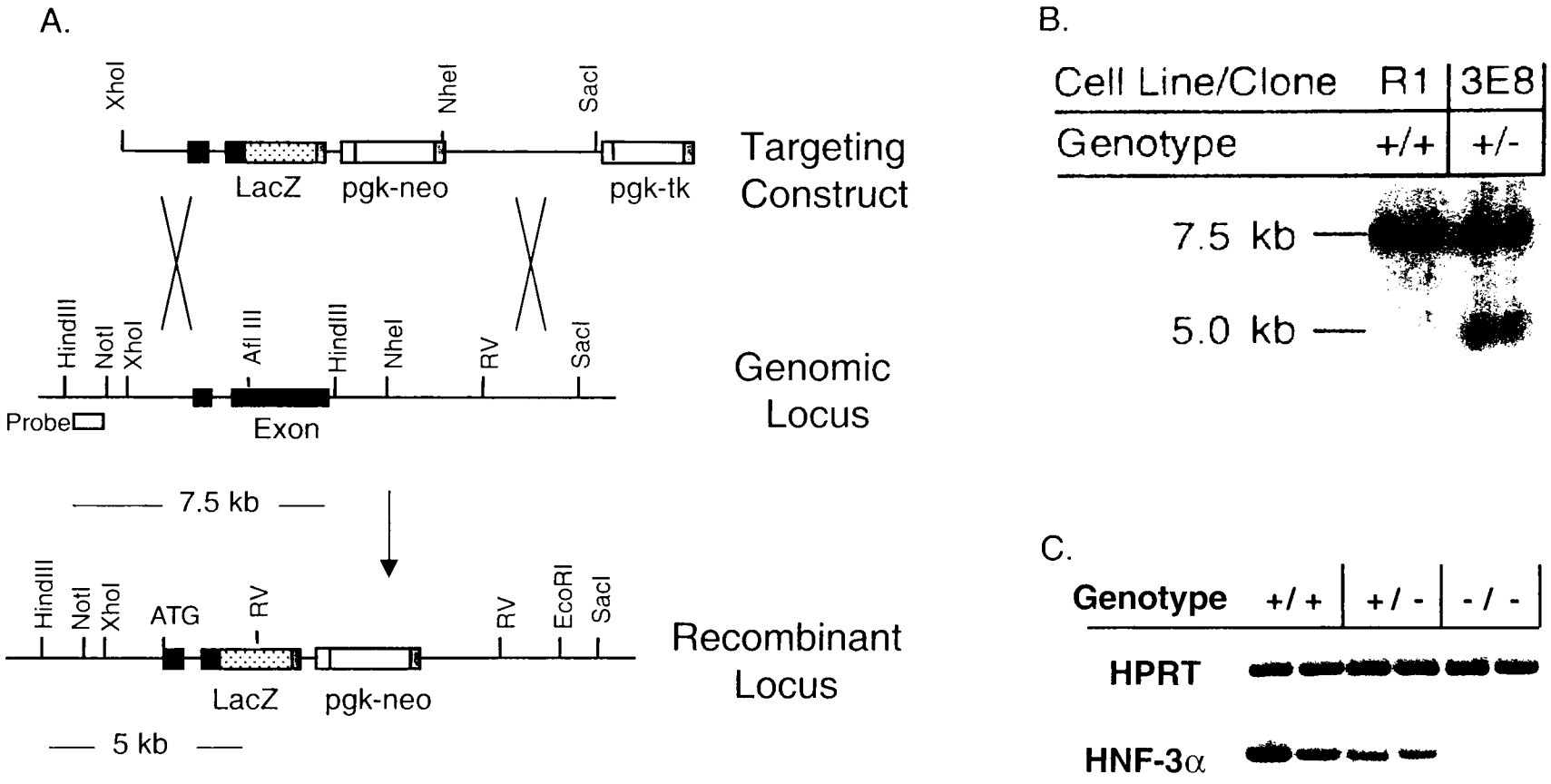

Figure 2-1. Disruption of the *hnf-3α* gene by homologous recombination. (A) Strategy for targeted disruption of the murine *hnf-3α* gene in ES cells. The genomic structure and restriction map of the mouse *hnf-3α* gene locus and targeting vector pPNT-2 used to disrupt the *hnf-3α* gene are shown. The targeting vector was constructed by deleting exon 2 including the DNA-binding domain downstream from the *Afl*II site and fusing it in-frame to the *E. coli lacZ* gene. The probe 3' of the left targeting arm was used for Southern blot analysis and is shown as a bar. (B) Southern blot analysis of transfected ES cells and *hnf-3α*$^{+/-}$ ES cells grown in the presence of G418. Genomic DNA was digested with *Hind*III and *Eco*RV. The wildtype allele shows a 7.5 kb band, and the targeted allele shows a 5.0 kb band. (C) No Hnf-3α message could be detected in *hnf-3α*$^{-/-}$ mice by RT-PCR.

ES cell clone that carried the targeted allele was used to generate chimeric male animals that passed the mutant allele to the offspring (Fig. 2-1B). *Hnf-3α* heterozygous mice were phenotypically indistinguishable from wildtype (wt) mice and were inbred to produce *hnf-3α*$^{-/-}$ mice. No *hnf-3α* mRNA could be detected in *hnf-3α*$^{-/-}$ mice by RT-PCR analysis (Fig. 2-1C).

Phenotypes of *hnf-3α*$^{-/-}$ Mice

Heterozygous *hnf-3α* mice, indistinguishable from wt animals, were intercrossed to generate offsprings with genotypes of Mendelian expectations. A total of over 1000 mice were generated and studied. The gross and histological morphologies of the gut, liver, and pancreas in *hnf-3α*$^{-/-}$ neonates are phenotypically indistinguishable from their littermates suggesting normal embryonic development. The mutant newborn mice are as active as their littermates, exhibit normal suckling behavior and have milk in their stomach. However, Hnf-3α is required for postnatal life since over 99% *of hnf-3α*$^{-/-}$ mice die between postnatal days 2-14 (only 1 out of over 200 *hnf-3α*$^{-/-}$ animals survived to 3 month of age). 1 to 2 days postnatally, *hnf-3α*$^{-/-}$ mice show signs of growth retardation (Fig. 2-2A, B). Although milk could be detected in the stomach throughout the life of *hnf-3α*$^{-/-}$ mice, milk volume in the stomach was drastically decreased after postnatal day 1 (Fig. 2-2C). Blood glucose and triglyceride levels were reduced 20-60%, whereas serum cholesterol was normal in 2- to 3-day old mutant mice compared with wt littermates (Fig. 2-2D, E).

Physiological Analysis of Hypoglycemia in *hnf-3α*$^{-/-}$ Mice

To investigate the physiological basis for postnatal persistent hypoglycemia and growth retardation in *hnf-3α*$^{-/-}$mice, we measured the level of hormones including insulin,

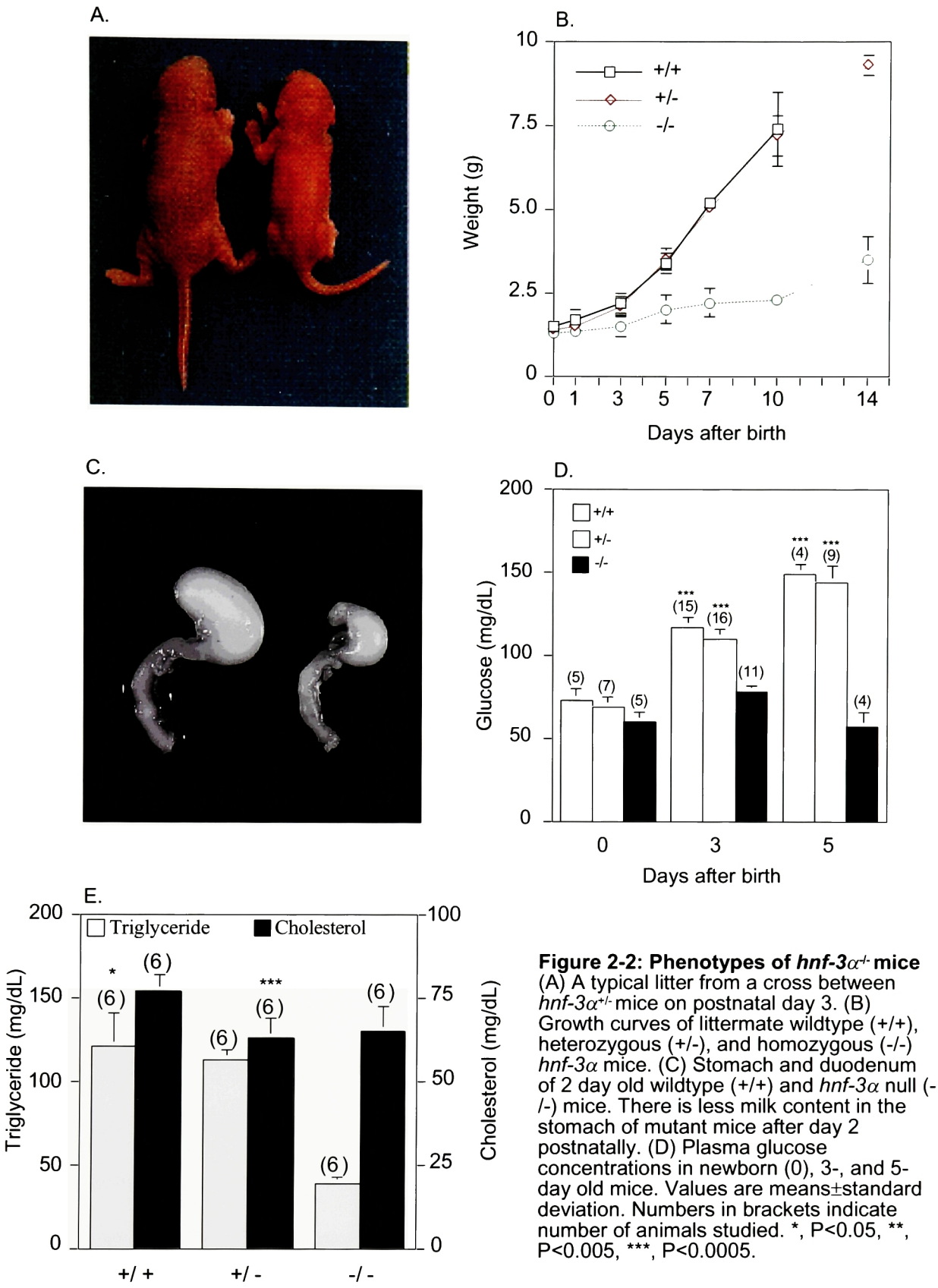

Figure 2-2: Phenotypes of *hnf-3α*$^{+/-}$ mice
(A) A typical litter from a cross between *hnf-3α*$^{+/-}$ mice on postnatal day 3. (B) Growth curves of littermate wildtype (+/+), heterozygous (+/-), and homozygous (-/-) *hnf-3α* mice. (C) Stomach and duodenum of 2 day old wildtype (+/+) and *hnf-3α* null (-/-) mice. There is less milk content in the stomach of mutant mice after day 2 postnatally. (D) Plasma glucose concentrations in newborn (0), 3-, and 5-day old mice. Values are means±standard deviation. Numbers in brackets indicate number of animals studied. *, P<0.05, **, P<0.005, ***, P<0.0005.

glucagon, cortisol, growth hormone, catecholemine (epinephrine and norepinephrine), and leptin that are known to regulate blood glucose concentrations. Serum insulin levels in mutant mice were reduced to approximately 50%, which is that found in wt mice after 24 hours of starvation (Fig. 2-3A). Plasma cortisol, growth hormone and catecholemine levels are significantly higher in *hnf-3α*$^{-/-}$ mice compared to their control littermates (Fig. 2-3B-D). These data suggest that the counter-regulatory responses to hypoglycemia of the pituitary gland, adrenal gland, and pancreatic β-cells that stimulate growth hormone, release of corticosteroid and catecholemine, and inhibition of insulin secretion, respectively, appeared normal. We found that the plasma leptin levels to be significantly lower in the *hnf-3α* null mice (Fig. 2-4E). Lowered plasma leptin level may be a secondary phenotype, due to the fact that *hnf-3α* deficient mice have very little adipose tissue. Lastly, we found that the plasma glucagon levels were decreased approximately 50% when compared with wt littermates (Fig. 2-3F). The paradoxical reduction in glucagon levels is further evident when compared to wt or heterozygous littermates that have been starved for 24 hours (Fig. 2-3F).

There are several mechanisms that could account for the reduced plasma glucagon levels in *hnf-3α*$^{-/-}$ mice including abnormalities in glucagon secretion and/or synthesis. To test if there is a defect in pancreatic α-cell secretory machinery, we performed *in vivo* glucagon secretion assay. Alanine, the principle endogenous aminogenic glucose precursor, is a potent stimulus of glucagon secretion and is used to evaluation α-cell function (99-103). Increased blood glucose levels due to glucagon can be used to assay for the integrity of glucagon secretory machinery. Alanine (0.25g/kg) was injected subcutaneously into 10 day old control mice and the peak alanine response as assayed by

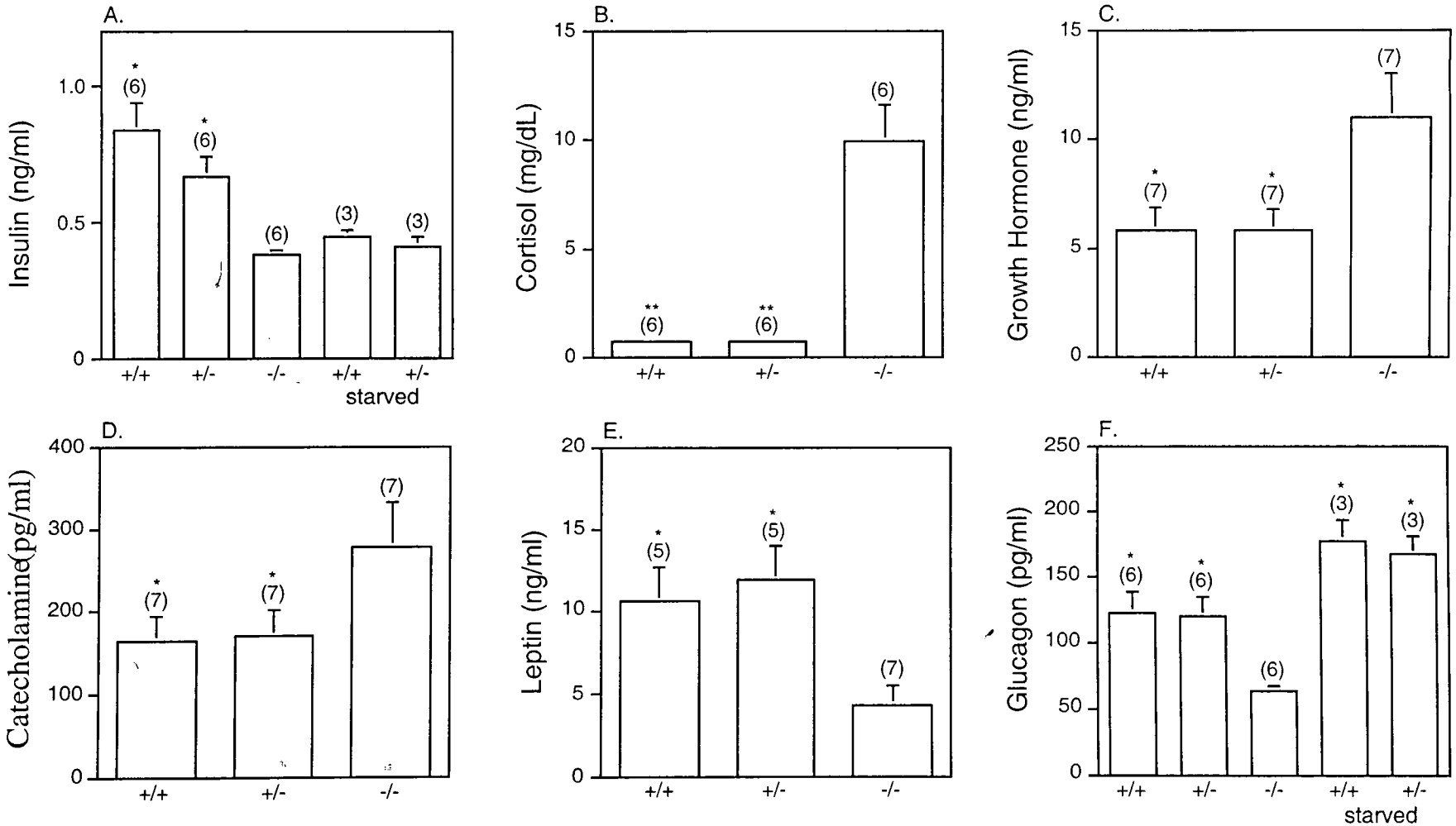

Figure 2-3: Hormone measurements in *hnf-3α* mutant mice. Plasma of 3 day old wildtype, *hnf-3α*$^{+/-}$, and *hnf-3α*$^{-/-}$ mice were obtained and the hormone levels were determined for insulin (A), cortisol (B), growth hormone (C), catecholamine (D), leptin (E), and glucagon (F). Starved animals in (A) and (F) indicate that these mice were separated from their mother for 12 hours. Values are mean ± standard deviation. Numbers in brackets indicate number of animals studied. *, P<0.05, **, P<0.005, ***, P<0.0005.

the rise in plasma glucose levels was determined to be 30 minutes post treatment (Fig. 2-4A). Once the time interval of alanine response is determined, we treated wt, *hnf-3α*$^{+/-}$, and *hnf-3α*$^{-/-}$ mice with alanine and measured glucose levels at 0, 15, and 30 minutes post treatment. We found that the rate of glucose increase is similar between mice of various genotypes (Fig. 2-4B). Since alanine is a gluconeogenic substrate, the rise in blood glucose levels may be secondary due to increased alanine concentration and not to increased glucagon secretion. To determine if alanine stimulated glucagon secretion directly, we measured plasma glucagon levels at 0 and 30 minutes post alanine treatment. We found that plasma glucagon levels increased at similar rate between wt and *hnf-3α*$^{-/-}$ mice (Fig. 2-4C). These data indicate that the reduced plasma glucagon levels in *hnf-3α*$^{-/-}$ mice are not due a defect in glucagon secretion. Furthermore, these data also suggest that the downstream effects of glucagon to increase blood glucose levels are not affected by *hnf-3α* deficiency.

Gene Expression Profiles in *hnf-3α* Null Mice

To study the molecular mechanisms that are responsible for the complex metabolic abnormalities in *hnf-3α*$^{-/-}$ mice, we analyzed steady state mRNA levels in the brain, liver, gut, and pancreas of newborn (<12 hours), 3, 5, and 7 day old mice. Gene expression of wt, heterozygous, and null mice were assayed by using reverse transcriptase (RT)-PCR. Each sample contained similar amounts of mRNA, as shown by the equal amplification of hypoxanthine phosphoribosyl transferase (HPRT) message. We analyzed the expression of 126 genes that were either reported to be regulated by Hnf-3 transcription factors or are known to affect glucose and energy homeostasis with similar expression pattern as Hnf-3α. Genes tested in the expression screen included

the rise in plasma glucose levels was determined to be 30 minutes post treatment (Fig. 2-4A). Once the time interval of alanine response is determined, we treated wt, *hnf-3α*$^{+/-}$, and *hnf-3α*$^{-/-}$ mice with alanine and measured glucose levels at 0, 15, and 30 minutes post treatment. We found that the rate of glucose increase is similar between mice of various genotypes (Fig. 2-4B). Since alanine is a gluconeogenic substrate, the rise in blood glucose levels may be secondary due to increased alanine concentration and not to increased glucagon secretion. To determine if alanine stimulated glucagon secretion directly, we measured plasma glucagon levels at 0 and 30 minutes post alanine treatment. We found that plasma glucagon levels increased at similar rate between wt and *hnf-3α*$^{-/-}$ mice (Fig. 2-4C). These data indicate that the reduced plasma glucagon levels in *hnf-3α*$^{-/-}$ mice are not due a defect in glucagon secretion. Furthermore, these data also suggest that the downstream effects of glucagon to increase blood glucose levels are not affected by *hnf-3α* deficiency.

Gene Expression Profiles in *hnf-3α* Null Mice

To study the molecular mechanisms that are responsible for the complex metabolic abnormalities in *hnf-3α*$^{-/-}$ mice, we analyzed steady state mRNA levels in the brain, liver, gut, and pancreas of newborn (<12 hours), 3, 5, and 7 day old mice. Gene expression of wt, heterozygous, and null mice were assayed by using reverse transcriptase (RT)-PCR. Each sample contained similar amounts of mRNA, as shown by the equal amplification of hypoxanthine phosphoribosyl transferase (HPRT) message. We analyzed the expression of 126 genes that were either reported to be regulated by Hnf-3 transcription factors or are known to affect glucose and energy homeostasis with similar expression pattern as Hnf-3α. Genes tested in the expression screen included

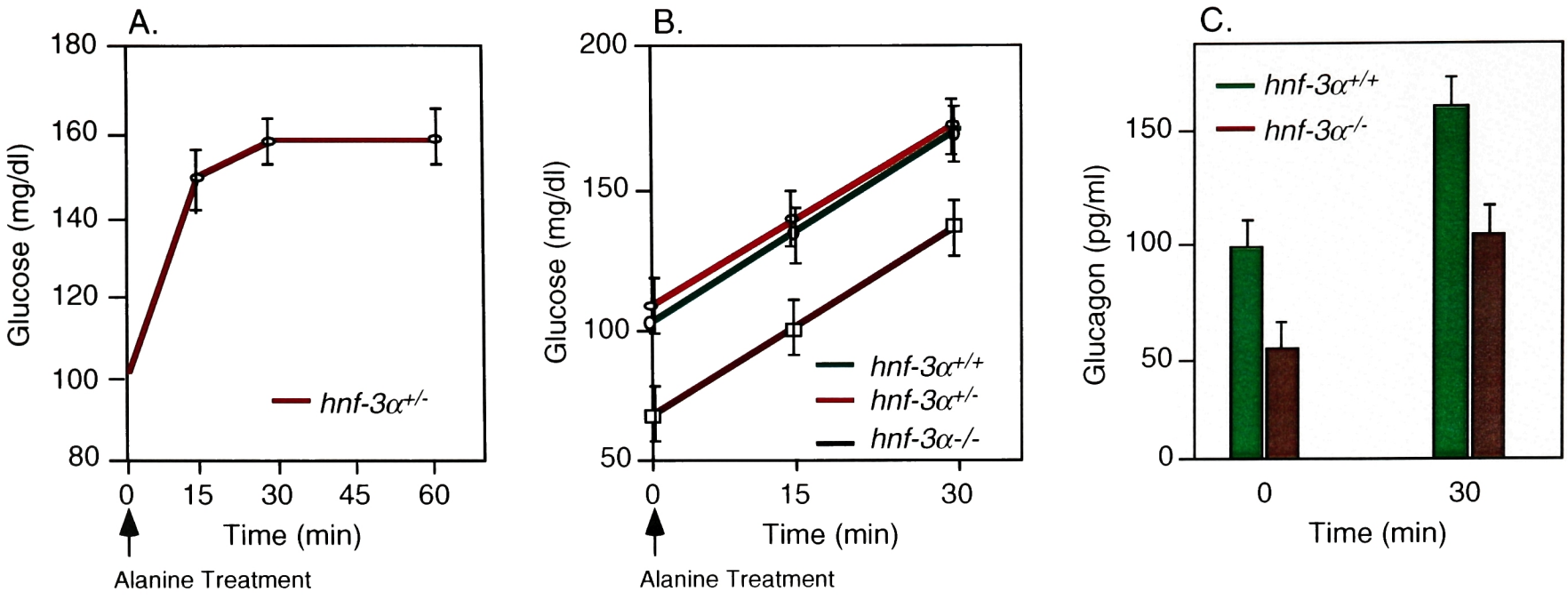

Figure 2-4. Glucagon secretion function in *hnf-3α*$^{-/-}$ mice. L-Alanine (0.25 g/kg) is injected (0 min) subcutaneously into 10 day old wildtype, *hnf-3α*$^{+/-}$, and *hnf-3α*$^{-/-}$ mice. Either glucose or glucagon is measured at the indicated time. (A) Alanine response curve showing that the glucose levels in *hnf-3α*$^{+/-}$ mice peaked at 30 min. (B) Blood glucose levels are measured at 0 min, 15 min, and 30 min post alanine injection. The rate of glucose increase is similar between wildtype, *hnf-3α*$^{+/-}$, and *hnf-3α*$^{-/-}$ mice. (C) Glucagon levels in the blood at 0 min and 30 min post alanine treatment. Plasma glucagon levels increased at similar rates in both wildtype and *hnf-3α*$^{-/-}$ mice.

hormones, peptide neurotransmitters and their receptors, glucose, amino acid and peptide transporters, transcription factors regulating metabolic pathways, enzymes of glycolysis, gluconeogenesis, glycogen synthesis and degradation, urea cycle, cholesterol and fatty acid synthesis and metabolism, intracellular storage proteins, and serum factors (the list of genes that were tested is in the appendix). No abnormalities in gene expression were detected in 3 day old mutant mice that would indicate primary defects in gluconeogenesis, glycogen metabolism, or fatty acid metabolism (data not shown). Thus, postnatal induction of mRNAs encoding gluconeogenic enzymes, glycogen breakdown, and fatty acid degradation enzymes are not impaired and cannot explain the hypoglycemia observed in these animals.

Consistent with the plasma hormone measurements, proglucagon mRNA was reduced ≈ 50% in the pancreas of *hnf-3α*$^{-/-}$ mice and remained low throughout life (Fig. 2-5A, data not shown). Hormones belonging to the same gene family such as secretin, gastric inhibitory peptide, vasoactive intestinal peptide, and cholecystokinin were unchanged. Surprising, proglucagon mRNA levels in the gut were indistinguishable in wt and *hnf-3α*$^{-/-}$ mice, suggesting that Hnf-3α is not required for expression of proglucagon transcription in intestinal L cells (Fig. 2-5B). Steady-state mRNA levels of neuropeptide Y (NPY) were also reduced by ≈ 50% shortly after birth, suggesting that Hnf-3α is required for transcriptional regulation of this gene. However, in contrast to pancreatic proglucagon mRNA levels, NPY transcription levels normalized after postnatal day 3 (Fig. 2-6), suggesting that other transcription factors can up-regulate NPY expression in *hnf-3α*$^{-/-}$ mice. In addition, steady-state mRNA levels of three genes not previously analyzed, were increased in *hnf-3α* deficient mice after postnatal day 3. Hexokinase I and

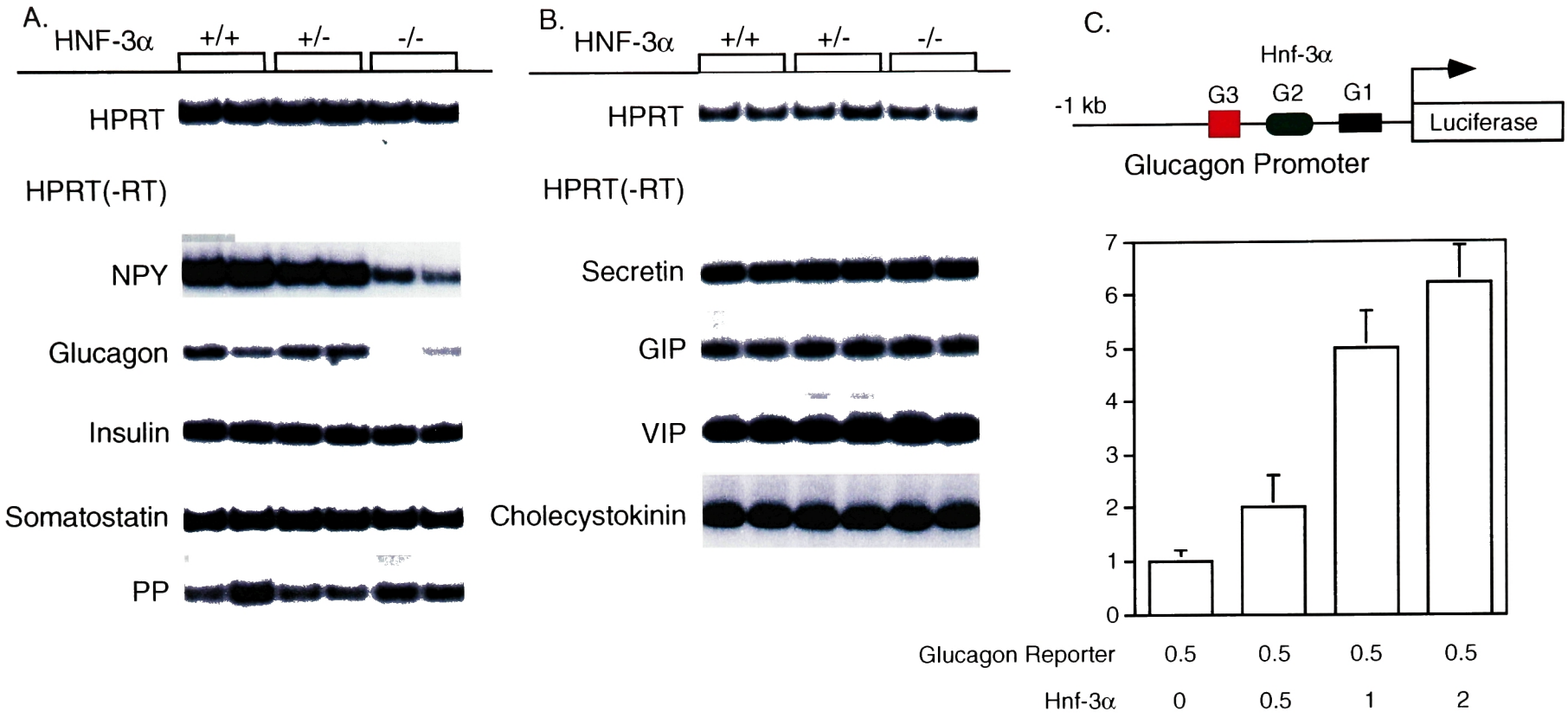

Figure 2-5. Gene expression analysis of islet and intestinal hormones. Steady-state mRNAs of pancreatic hormones (A) and intestinal hormones (B) were analyzed by reverse transcription-PCR. Glucagon and NPY transcripts were reduced in the pancreas of *hnf-3α*$^{-/-}$ mice. (C) The G2 element of the glucagon promoter contains a consensus Hnf-3 binding site. A schematic of the glucagon reporter contruct is shown. Co-transfection of Hnf-3α expression vector and glucagon reporter contruct in cos-7 cells. The average fold inductionss of two independent transfections performed in duplicates and normalized to β-galactosidase activity are shown. Error bars indicate standard error of the mean. NPY, neuropeptide Y; PP, pancreatic polypeptide; GIP, gastric inhibitory peptide; VIP, vasoactive intestinal peptide.

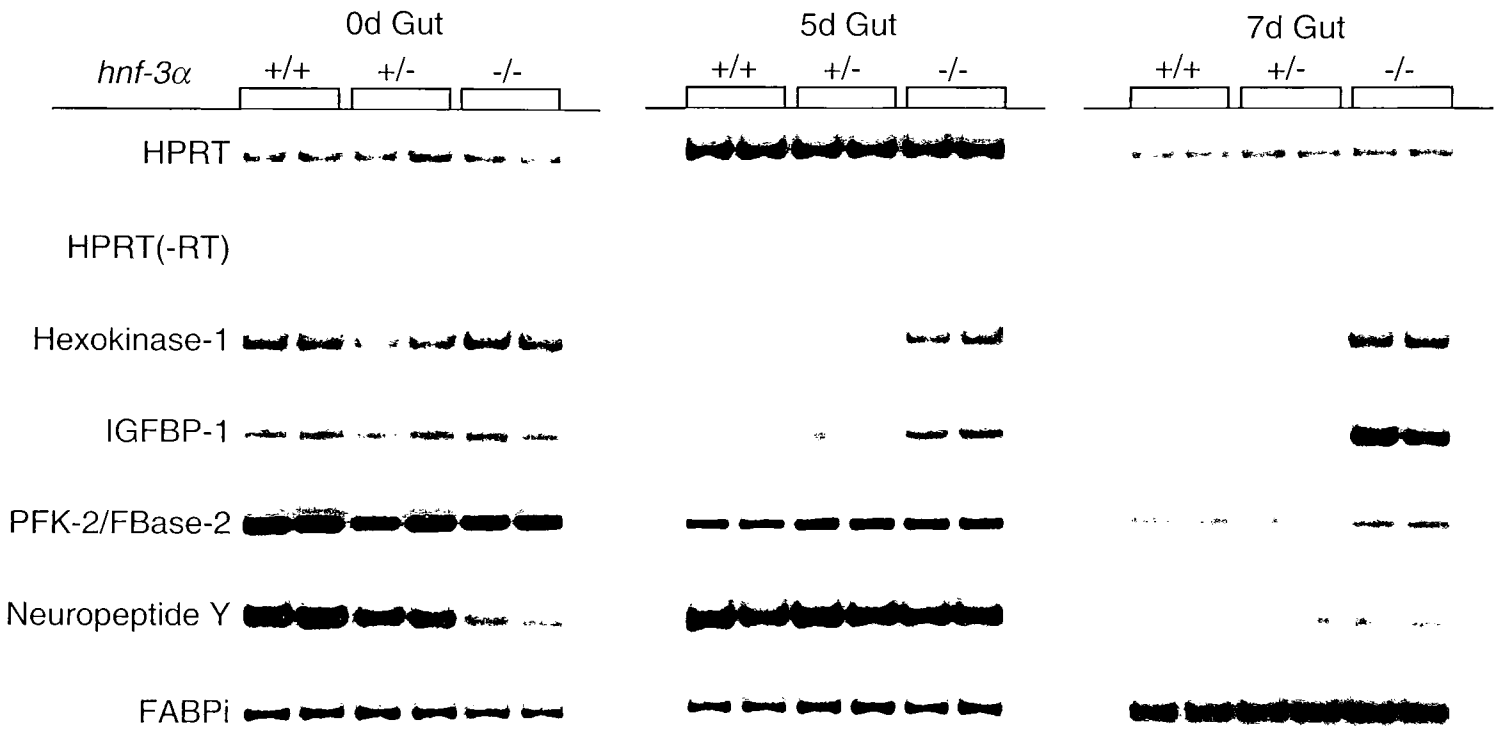

Figure 2-6. Steady-State mRNA Levels of Hnf-3α Target Genes. Steady state mRNA levels of hexokinase I, bifunctional enzyme phosphofructo-2/fructose-2,6-bisphosphatase-2 (PFK-2/FBase-2), and insulin growth factor binding protein-1 (IGFBP-1) are up-regulated in the intestine of *hnf-3α* null mice. HPRT hypoxanthine phosphoribosyltransferase; FABPi, intestinal fatty acid binding protein.

insulin growth factor binding protein-1 were significantly increased in 5 day old mutant animals, and phosphofructo-2-kinase/fructose-2,6-bisphophatase (PFK-2/FBase) was increased 2 fold in 7 day old *hnf-3α*$^{-/-}$ mice (Fig. 2-6).

The finding of reduced glucagon mRNA transcripts in *hnf-3α*$^{-/-}$ mice implies a previously unrecognized role for Hnf-3α in the regulation of glucagon gene expression. A conserved Hnf-3 binding site has been identified in the G2 element in the glucagon promoter (104). Hnf-3β was shown to bind to the G2 site, but it repressed the activity of the glucagon promoter construct in transient transfection experiments. In contrast to the postulated negative role of Hnf-3β on glucagon expression, deletion of the G2 binding site leads to a major loss of basal glucagon reporter activity in an islet cell line, implying that another member of the Hnf-3 family may activate glucagon expression through the G2 enhancer (104). To test if Hnf-3α can activate directly glucagon expression, we cloned a 1 kb rat glucagon promoter containing the G2 site and fused it upstream of a luciferase reporter gene (Fig. 2-5C). Transient co-transfections of Hnf-3α with the glucagon reporter construct lead to a dose-dependent 6-fold activation of luciferase activity (Fig. 2-5C). Together, these data indicate that Hnf-3α is a potent activator of glucagon transcription *in vitro* and *in vivo*.

To determine if the glucagon insufficiency in *hnf-3α* null mice is caused by reduced glucagon levels in pancreatic α-cells, we measured total intracellular glucagon contents from pancreas of wt and mutant animals. Total pancreatic glucagon content of *hnf-3α* null mice was also reduced 50% compared with wt littermates (3.2 vs. 6.4 μg/g pancreas, respectively). These results suggest that a decrease in pancreatic glucagon content in the pancreas is the primary defect of hypoglucagonemia in *hnf-3α*$^{-/-}$ mice.

The reduced total intracellular glucagon content in *hnf-3α*$^{-/-}$ mice may be caused by a block in pancreatic α-cell development. Pancreatic cell lineage allocation was assessed by looking for the presence of α- and β-endocrine cell types using immunohistochemistry. Islet structure and the number of glucagon and insulin-expressing cells are similar in wt and mutant pancreas (Fig. 2-7). These results indicate that the differentiation of the endocrine pancreas is normal in mice lacking Hnf-3α and that the reduced intracellular glucagon content is not due to decreased α-cell mass.

In several knockout mouse models, targeted mutation of one transcription factor lead to an up-regulation of other transcription factors belonging to the same gene family (98, 105). In addition, we previously showed that Hnf-3α negatively regulates the expression of the MODY genes Hnf-1α and Hnf-4α in embryoid bodies derived from ES cells lacking Hnf-3α (77). In this system, we also showed that the expression of genes required for normal metabolism, including apolipoproteins, aldolase B, and L-pyruvate kinase are increased. To test whether this is true in the liver, gut, and pancreas of *hnf-3α* null mice, we measured steady-state mRNA levels of these genes. Consistent with our previous findings, mRNA levels of Hnf-3β and Hnf-3γ were unchanged (data not shown). In contrast to the situation in embryoid bodies, there is no change in the transcript levels of Hnf-1α and Hnf-4α or other members of the HNF- transcription network (data not shown). Similarly, the mRNA levels for apolipoproteins (apo –AI, -AII, -AIV, -B, and –CII) were not affected by *hnf-3α* deficiency (data not shown).

Glucagon Signaling and Kidney Function in *hnf-3α*$^{-/-}$ Mice.

Since Hnf-3α is expressed in the liver, intestine, and kidney in addition to its expression in the pancreas, abnormalities in the function of these extra-pancreatic organs

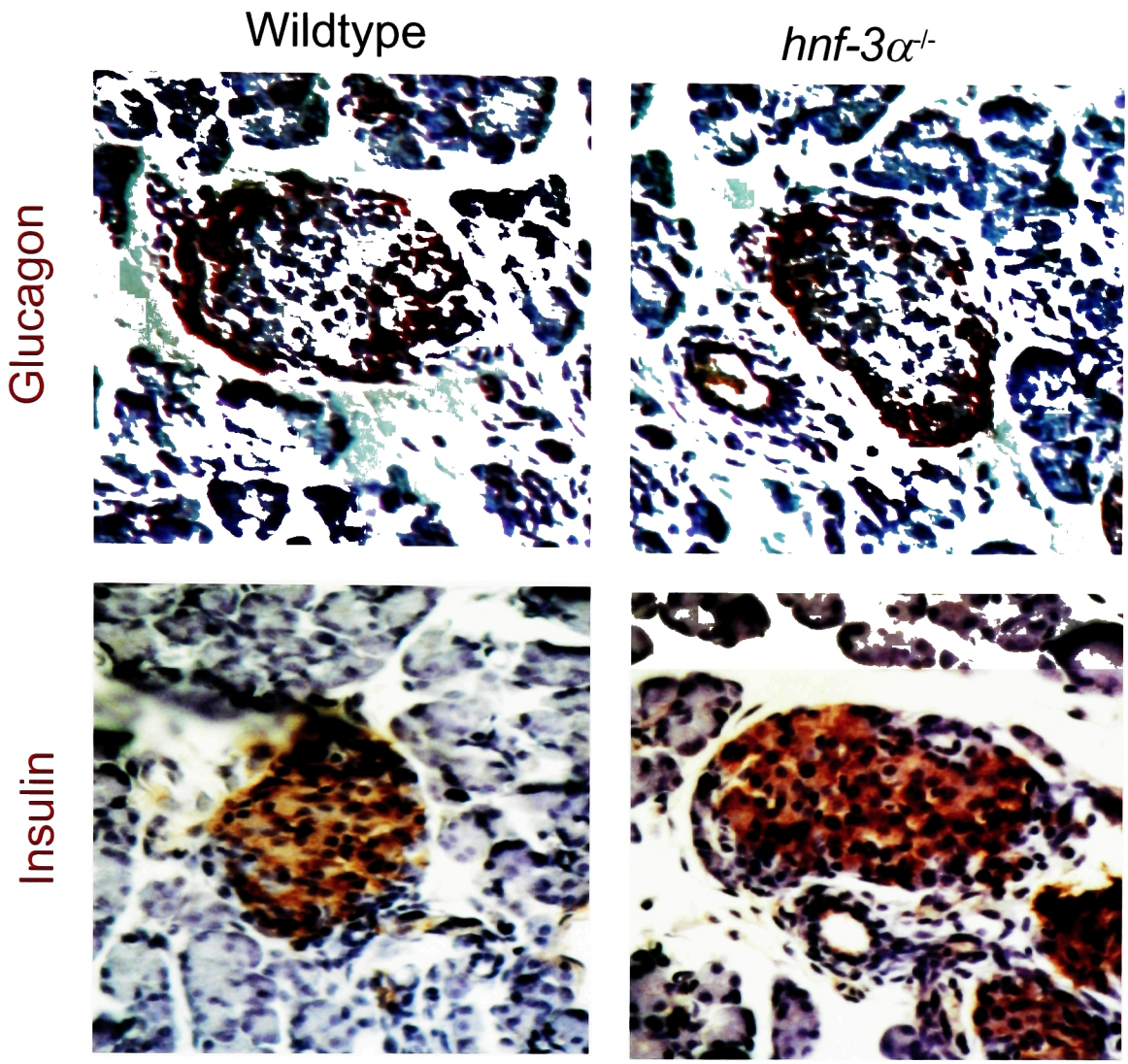

Figure 2-7. Normal pancreatic morphology in *hnf-3α*$^{-/-}$ Mice. Pancreatic tissue sections showing representative islets from 3-day old pancreata of wildtype and *hnf-3α* mutant mice. Sections were stained with antibodies against glucagon and insulin as described in Materials and Methods. Glucagon and insulin are detected in the characteristic cell-lineage patterns. Magnification 400X.

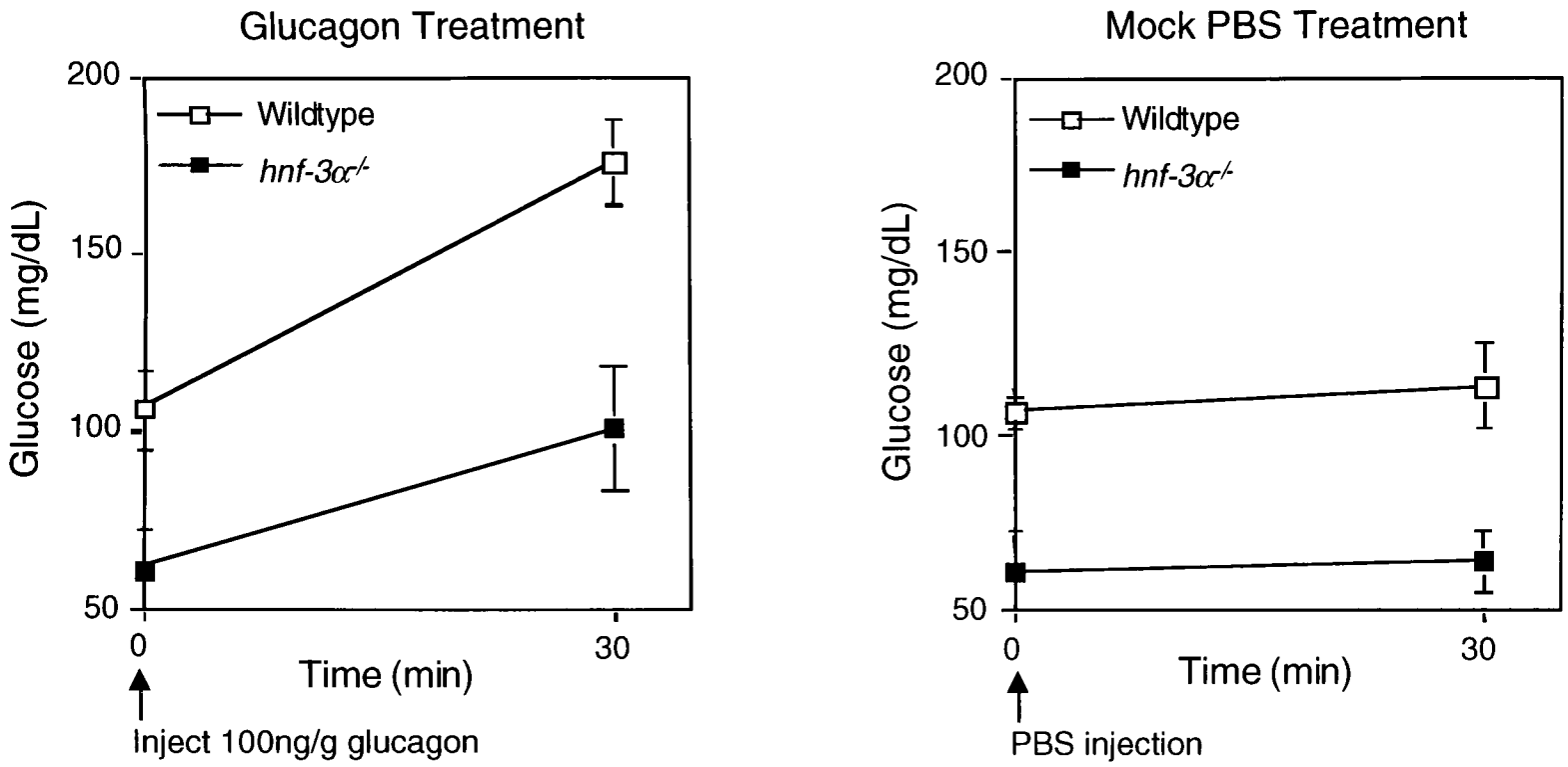

Figure 2-8. Intact glucagon signaling in *hnf-3α*$^{-/-}$ mice. Glucagon (100 ng/g) is injected (0 min) subcutaneously into 10 day old wildtype and *hnf-3α*$^{-/-}$ mice. Glucose is measured at the indicated time. (A) Glucagon increased the rate of plasma glucose levels similarly in both wildtype and *hnf-3α*$^{-/-}$ mice (A), in contrast, plasma glucose levels are not increased with mock PBS treatment. PBS, phosphate buffered saline.

may contribute to hypoglycemia in *hnf-3α*$^{-/-}$ mice. Glucagon is the primary hormone used in the neonatal period to maintain glucose homeostasis. To determine if the glucagon signaling pathway is intact in peripheral tissues such as the liver, we injected exogenous glucagon into 10 day old wt and *hnf-3α*$^{-/-}$ mice and measured plasma glucose levels at 0 and 30 minutes post treatment. We found that glucagon but not PBS increased plasma glucose concentration and that the rate of increase in glucose levels between wt and *hnf-3α*$^{-/-}$ mice are similar (Fig. 2-8). These data are consistant with the alanine response results and indicate that Hnf-3α deficiency does not impair glucagon signaling in extra-pancreatic tissues.

Liver glycogen is important for newborn pups as an energy source and later in life for glucose homeostasis (106). To investigate whether glycogen synthesis or degradation was impaired in the livers of *hnf-3α*$^{-/-}$ animals, total liver glycogen contents were measured in fasted states. We determined that glycogen content was similar overall in mutant and wt mice, suggesting that there was no intrinsic defect in glycogen metabolism (data not shown). Furthermore, mutant *hnf-3α* mice were able to increase their hepatic glycogen stores after intraperitoneal glucose administration, providing further support that glycogen synthesis in *hnf-3α*$^{-/-}$ mice is functional (data not shown). Finally, no differences were detected in the steady state mRNA of enzymes involved in gluconeogenesis (pyruvate carboxylase, phosphoenolpyruvate carboxylase, Fructose 1,6-bisphosphatase, and glucose 6 phosphatase), and glycogen metabolism (glycogen phosphorylase, phosphoglucomutase, UDP-glucose pyrophosphorylase, glycogen synthetase). These data further validate that *hnf-3α* deficiency does not diminish downstream effects of glucagon to increase blood glucose levels including

gluconeogenesis and glycogenolysis.

Ketone bodies are produced by the liver from free fatty acids at times of hypoglycemia, low insulin, and high serum glucagon concentrations. We therefore measured β-hydroxybutyrate plasma concentrations to study whether *hnf-3α*$^{-/-}$ mice maintain the ability to metabolically adapt to hypoglycemia by increasing fatty acid degradation. As expected, β-hydroxybutyrate concentrations were moderately elevated in the plasma of *hnf-3α* deficient mice and reached levels that were comparable to wt mice that had been starved for 24 hours (data not shown).

Hnf-1α null mice develop a Fanconi-like syndrome characterized by excessive loss of glucose and amino acids in their urine (36, 37). We therefore investigated whether a defect in renal reabsorption of glucose contributes to hypoglycemia in *hnf-3α*$^{-/-}$ mice by performing a quantitative urinalysis of glucose and amino acids. No glucose was detected in the urine of mutant *hnf-3α*$^{-/-}$ mice, and amino acid concentrations were similar to littermate control animals (Table 2-1). These results indicate that hypoglycemia and wasting of *hnf-3α*$^{-/-}$ mice cannot be explained by loss of glucose or amino acids in the urine.

Exocrine pancreas insufficiency due to decreased synthesis and/or secretion of amylase, proteinase, and lipases can lead to chronic malabsorption and hypoglycemia. We therefore test whether hypoglycemia in *hnf-3α*$^{-/-}$ mice might be caused by exocrine insufficiency. We assay the enzymatic activities of amylase, trypsin, chymotrypsin, and phospholipase from gut homogenate of wt and mutant mice. No significant differences were noted in these activities, suggesting that wasting is not caused by malabsorption due to decreased capacity to hydrolyze nutrients in the intestine.

Amino Acid	Wildtype (mole %)	*hnf-3α*$^{-/-}$ (mole %)
Thr	8.5	9.7
Ser	28.4	26.8
Pro	9.3	7.9
Gly	5.6	6.1
Ala	10.1	13.9
Val	2.3	2.9
Met	1.5	1.6
Ile	0.9	1.1
Leu	3.5	3.6
Tyr	5.7	5.4
Phe	1.9	1.7
His	1.5	1.3
Lys	19.1	16.6
Arg	1.4	1.1

Table 2-1. Quantitative Urinalysis on Wildtype and *hnf-3α*$^{-/-}$ Mice. Amino acid was quantitated from the urine of wildtype and *hnf-3α*$^{-/-}$ mice. We found that the amino acid contents were similar between urine obtained from wildtype and *hnf-3α* deficient mice. The 3 letter amino acid code are shown.

Pancreatic β-cell Function in *hnf-3α*$^{-/-}$ Mice

Hnf-3α is highly expressed in pancreatic β-cells and may be a part of a transcriptional network that is essential for normal pancreatic β-cell function (77). To assess pancreatic β-cell function in *hnf-3α*$^{-/-}$ mice, we challenged normal and mutant mice with glucose by parenteral administration. Three-day-old mice were given an intraperitoneal glucose infusion of 2 mg glucose/g total body weight and glucose and insulin levels were measured after 1 hour. Glucose levels were significantly elevated and insulin levels were markedly reduced in *hnf-3α*$^{-/-}$ mice as compared to wt and heterozygous littermates (Fig. 2-9A). Because hypoglycemia and starvation can have adverse effects on glucose-stimulated insulin secretion, we also performed intraperitoneal glucose tolerance in 4- to 6-week old wt and heterozygous *hnf-3α* mice that have indistinguishable body weight from wt mice and normal blood glucose levels. We observe that *hnf-3α*$^{+/-}$ mice had significantly higher blood glucose levels 30 minutes after glucose challenge and reduced plasma insulin concentrations at 60 and 120 minutes after glucose challenge (Fig. 2-9B, C). These data indicate that *hnf-3α* haploinsufficiency causes a mild insulin-secretory defect and that Hnf-3α is also critical for normal pancreatic β-cell function.

Discussion

We have used a genetic approach to study the function of Hnf-3α by generating mutant mice with a loss-of-function mutation in the *hnf-3α* gene. Mice that lack Hnf-3α expression develop neonatal persistent hypoglycemia. Persistent low blood-glucose levels can be caused by conditions of extreme malabsorption, underproduction of glucose (liver enzyme defects of glucose metabolism, hormone deficiencies, and acquired liver

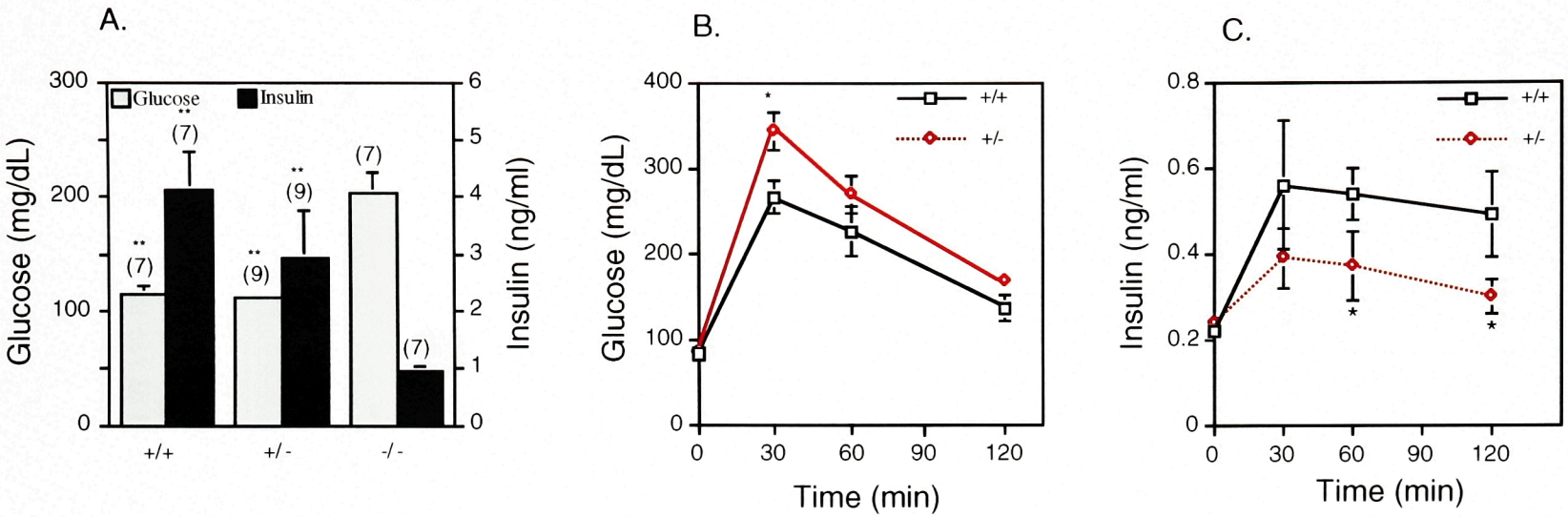

Figure 2-9. Analysis of Pancreatic β-cell Function in *hnf-3α* Mutant Mice. Plasma of 3 day old wildtype, *hnf-3α*$^{+/-}$, and *hnf-3α*$^{-/-}$ mice were obtained for glucose and insulin measurement. (A)measurement of plasma glucose and insulin levels in 3 day old mice 60 minutes after intraabdominal glucose administration. Blood glucose (B) and plasma insulin (C) levels during intraperitoneal glucose administration in adult wildtype and heterozygous littemates. Values are mean±standard deviation. Numbers in brackets indicate number of animals studied. *, P<0.05, **, P<0.005, ***, P<0.0005.

abnormalities), and overutilization of glucose because of hyperinsulinemia. The paradoxical reduction in circulating glucagon levels is most likely the cause of hypoglycemia. However, other mechanisms may contribute to the wasting syndrome because parenteral glucose and glucagon administration twice daily did not lead to weight gain or prolonged survival in *hnf-3α* null mice. One of the most dramatic phenotypes in *hnf-3α*$^{-/-}$ mice is an altered feeding behavior, as evidenced by reduced milk intake that is followed by malnutrition. The molecular and physiological mechanisms by which Hnf-3α regulates food intake and participates in glucose sensing are currently not understood. The hypothalamus plays a major role in normal control of appetite behavior, sensing hypoglycemia and mediating counter-regulatory responses (107). We have found Hnf-3α to be highly expressed in lateral and posterior part of the hypothalamus, and thus, cannot rule out that the abnormal feeding behavior is caused by a central nervous system defect. However, we have tested the expression of hypothalamic modulators of food intake such as galanin, orexin, peptide YY, cholecystokinin, and proopiomelanocortin and found the mRNA levels to be indistinguishable between mutant and WT neonates. Interestingly, expression of the orexigenic peptide NPY was normal in the hypothalamus but was significantly reduced in the pancreas and gut of newborn and 3 day old *hnf-3α* null mice. NPY transcripts increased after day 3 to normal levels, suggesting that elevated serum glucocorticoid levels and hypoinsulinemia, both known to increase NPY gene expression in the rat, can compensate for the transcriptional defect in NPY expression (108).

Hypoglycemia inhibits insulin secretion and stimulates rapid increases in the secretion of several hormones including glucagon, growth hormone, cortisol, and catechcolamines, that act in concert to increase plasma glucose concentrations (109).

Hnf-3α$^{-/-}$ mice fail to respond to low blood glucose by increasing glucagon secretion. The glucagon gene is expressed as a prohormone in α-cells of the endocrine pancreas, L cells of the intestine, and in the brain stem (110). Proglucagon is then processed differentially to generate glucagon and glucagon-like peptide-1, which are known to be the main biologically active hormones of the pancreas and intestine, respectively (111). Several mechanisms could account for this relative glucagon insufficiency in the *hnf-3α*$^{-/-}$ mice, including abnormalities in glucagon synthesis, glucagon secretion, and/or reduced number of α-cells. Hnf-3β, a related member of the Hnf-3 forkhead transcription factor family, was recently shown to regulate insulin secretion (97). Hnf-3α may have a similar action on pancreatic α-cells to regulate glucagon secretion. Impairment in glucagon secretion was ruled out since Hnf-3α deficient mice could secrete glucagon in response to a glucagon secretagogue (alanine). Recent gene targeting experiments of other islet enriched transcription factors such as Pdx-1 have revealed their importance in the development of the endocrine pancreas. Loss of Pdx-1 expression leads to pancreatic agenesis and β-cell specific abolition indicates that the Pdx-1 is required for late differentiation or maturation of the pancreatic β-cells (54-56). To rule out the possibility that *hnf-3α* deficiency impairs islet α-cell development, we assessed islet cell type composition by immunostaining with markers for α- and β- cells. Insulin producing β-cells, the predominant cell type in the islet, formed the core of the islets, whereas the less abundant glucagon expressing α-cells are distributed in the islet periphery. No differences in the ratio of α- to β-cells were observed between wt *and hnf-3α*$^{-/-}$ mice, thereby ruling out a developmental effect of Hnf-3α on the endocrine pancreas.

Low plasma glucagon levels in *hnf-3α*$^{-/-}$ mice most likely reflect a defect in transcriptional activation of the proglucagon gene in α-cells, because mRNA levels are reduced shortly after birth. The results of our transient transfection analysis on the glucagon promoter further validate our claim. Together, our results indicate that Hnf-3α is an essential regulator of glucagon transcription both *in vitro* and *in vivo*. Surprisingly, we did not find decreased pro-glucagon mRNA levels in the intestine of *hnf-3α*$^{-/-}$ mice, indicating that Hnf-3α is not required for transcriptional activation of proglucagon in intestinal L cells.

To determine if there may be a defect in glucagon signaling in peripheral tissues such as the liver that is masked by glucagon insufficiency, we performed glucagon challenge assays. We determined that blood glucose levels raised at similar rates in both wt and *hnf-3α*$^{-/-}$ mice, indicating that Hnf-3α deficiency does not impair glucagon signaling.

Hnf-3α is also expressed at high levels in insulin secreting pancreatic β-cells (92, 112, 113). To study pancreatic β-cell function in *hnf-3α* null mice, we performed glucose tolerance tests by intraperitoneal glucose administration. *Hnf-3α*$^{-/-}$ mice have markedly elevated glucose levels after 1 hour and significantly reduced insulin levels compared with littermate control mice. These results indicated that there might be an insulin secretory defect in pancreatic β-cells of *hnf-3α* deficient mice that is only revealed after a glucose challenge. Alternatively, impaired β-cell function could be caused by an indirect mechanism, since continuous exposure of pancreatic islets to low glucose can impair insulin secretion (114). To address this, we subjected adult wt and heterozygous littermates that have indistinguishable fasting blood-glucose levels to an intraperitoneal

glucose tolerance test. Blood glucose concentrations were significantly increased, whereas serum insulin levels were reduced in *hnf-3α*$^{+/-}$ animals compared with wt mice after a glucose challenge, providing further evidence that Hnf-3α is also important for normal pancreatic β-cell function.

We have identified three genes, hexokinase-1, phosphofructo-2-kinase/fructose-2,6-bisphosphatase, and insulin growth factor binding protein-1, that are up-regulated in *hnf-3α* mutant mice, suggesting an inhibitory role of Hnf-3α on transcription. Phosphofructo-2-kinase/fructose-2,6-bisphosphatase and insulin growth factor binding protien-1 were shown to contain functional Hnf-3 DNA-binding consensus sequences in their promoter/enhancer (115). However, changes in steady-state mRNA levels of these genes were only elevated after postnatal day 5, suggesting up-regulation of these 3 genes could be adaptive mechanisms for maximal absorption of glucose by maintaining an optimal glucose gradient across the intestinal epithelium.

We did not detect alterations in gene expression in the majority of Hnf-3 target genes that have previously been shown to be regulated by Hnf-3α and Hnf-3β in visceral endoderm of embryoid bodies (77). We believe that transcription of these genes is predominately regulated by Hnf-4α and Hnf-1α, which are targets of Hnf-3α in embryoid bodies. However, in *hnf-3α* null mice, no differences in Hnf-4α and Hnf-1α expression are observed (Fig. 2-10). Therefore, targets of Hnf-4α/Hnf-1α are not affected. In addition, it is also possible that Hnf-3β and Hnf-3γ, which are still present at wt levels in the *hnf-3α*$^{-/-}$ mice, can compensate for the loss of Hnf-3α without gross alterations in gene expression of most Hnf-3 target genes. We are currently testing this hypothesis by generating mice with combined allelic inactivation of Hnf-3α and Hnf-3β.

Mutations in hepatocyte nuclear factors-1α, -1β, and -4α have been associated with pancreatic β-cell defects resulting in maturity-onset diabetes of the young 3, 5, and 1 respectively. In this study, we have shown that another member of this transcriptional network, Hnf-3α, is essential for glucose homeostasis. In contrast to the other MODY genes, Hnf-3α regulates glucose homeostasis by controlling glucagon expression in pancreatic α-cells. No mutations have been described in *HNF-3α* gene in humans; however, Hnf-3α deficient mice share remarkable similarities to several reports of patients with neonatal persistent hypoglycemia and glucagon deficiency (101, 116). Sequencing the *HNF-3α* gene in a patient with severe neonatal hypoglycemia did not reveal any functional mutations (116, 117). This result does not preclude an involvement of HNF-3α as a cause of other cases of persistent neonatal hypoglycemia and HNF-3α may still be a candidate gene for human congenital glucagon deficiency syndromes.

Chapter 3: Hnf-1α Deficiency in Mice Leads to Abnormal Expression of Genes Involved in Pancreatic Islet Development and Metabolism

Introduction

HNF-1α is a homeodomain transcription factor composed of an N-terminal dimerization domain, a POU-homeobox DNA binding domain, and a C-terminal transactivation domain (118). HNF-1α is expressed in liver, kidney, intestine, and pancreatic islets (119). Clinical studies in humans have shown that heterozygous mutations in *HNF-1α* are associated with impaired pancreatic β-cell function that is characterized by impaired insulin secretion (45, 120). Surprisingly, although HNF-1α is expressed in extra-pancreatic tissues, the majority of phenotypic abnormalities identified to date in MODY3 patients involve pancreatic β-cell defects (45, 120). This suggests that HNF-1α plays an essential tissue-restricted role in pancreatic β-cells to maintain glucose homeostasis.

Mice with heterozygous mutations in *hnf-1α* gene are phenotypically normal. However, analogous to the MODY3 phenotype, *hnf-1α*$^{-/-}$ mice have severely blunted glucose-stimulated insulin secretion and develop overt diabetes (36, 37, 39). Previous physiological studies using pancreatic islets from *hnf-1α*-deficient mice showed that β-cell dysfuction in these animals is likely to result from its defective glycolytic signaling proximal to mitochondrial oxidation (40, 41). This conclusion is based on the following findings: (i) insulin secretion and intracellular calcium responses to glucose and

glyceraldehyde are reduced, (ii) glucose flux through glycolysis and the generation of ATP and NADH are reduced, (iii) ATP-sensitive K^+-currents (K_{ATP}) in β-cells from *hnf-1α*$^{-/-}$ mice are not suppressed by glucose but are sensitive to ATP, and (iv) mitochondrial substrates can suppress K_{ATP} and correct the insulin secretion defect of *hnf-1α*$^{-/-}$ islets. The results are also supported by recent studies showing reduced expression of liver pyruvate kinase (L-Pk) and glucose transporter 2 (Glut2) in islets of *hnf-1α*$^{-/-}$ mice and downregulation of Glut-2, L-Pk and insulin in cell lines that express a dominant-negative form of HNF-1α (81, 121). In contrast to the above reports, a recent *in vitro* study has suggested that a mitochondrial abnormalities may contribute to the β-cell defect in HNF-1α-deficient diabetes (122). In this report, a dominant negative HNF-1α, HNF1α-P291fsinsC, was expressed in insulinoma INS-1 cells and resulted in reduced expression levels of mitochondrial 2-oxoglutarate dehydrogenase (Ogdh) E1 subunit and increased expression of uncoupling protein 2 (Ucp2), thereby leading to impaired mitochondrial oxidation and consequently defective insulin secretory response (122). These inconsistent findings have yet to be resolved. In addition, the transcriptional control of β-cell genes by HNF-1α are still poorly understood.

In this study, the molecular basis by which Hnf-1α deficiency causes pancreatic β-cell dysfunction was explored. We compared pancreatic islet gene expression profiles from wt and *hnf-1α*$^{-/-}$ mice instead of relying exclusively on cell culture systems. We found that *hnf-1α* deficiency results in a pleiotrophic defect that includes dysregulation of glycolytic genes as well as other transcription factors of the islet transcription factor network. Our results localize the transcriptional defect in islets of *hnf-1α*$^{-/-}$ mice to nutrient entry and the glycolytic pathway, and provide evidence for a wider role of Hnf-

1α in the regulation of islet-enriched transcription factors that are critical for β-cell differentiation than has previously been anticipated. In addition, the liver steady-state mRNA levels of genes that we found to be regulated by Hnf-1α in the islet are determined. Interestingly, Hnf-1α target genes in the islet including Glut-2, L-PK, neutral and basic amino acid transporter (NBAT) and Hnf-4α are not regulated by Hnf-1α in the liver. Together, these results suggest that the selective pancreatic β-cell dysfunction in MODY3 may stem from the tissue specific requirement for HNF-1α function in pancreatic islets.

Results

Pancreatic Islet Gene Expression in *hnf-1α*$^{-/-}$ Mice

In keeping with previously reported data, insulin secretory responses to glucose are markedly reduced in *hnf-1α*$^{-/-}$ mice compared to littermate controls (40, 41). Methylpyruvate, an insulin secretagogue that freely permeates the mitochondrial membrane, can suppress ATP-dependent K^+-channel activity in *hnf-1α*$^{-/-}$ pancreatic islets suggesting that the defect in glucose metabolism is upstream of mitochondria (40). To test which genes involved in glucose metabolism was affected by the disruption of *hnf-1α*, we measured the mRNA levels of glucose transporters, amino-acid transporters, and all glycolytic enzymes. We also measured the proximal rate limiting enzymes of oxidative phosphorylation, including components of the pyruvate dehydrogenase complex (pyruvate decarboxylase, dihydrolipoyl dehydrogenase), aconitase, isocitrate dehydrogenase and α-ketoglutarate dehydrogenase complex (2-oxoglutarate dehydrogenase, dihydrolipoyl succinyl-transferase, dihydrolipoyl dehydrogenase) as well as uncoupling protein-2 (Ucp-2). Furthermore, we determined the mRNA levels of the

sulphonylurea receptor-1 (Sur-1), ATP-dependent K^+-channel (Kir6.2), prohormone convertase-2 and –3 (Pc2, Pc3), insulin, glucagon, somatostatin, and pancreatic peptide (PP).

Hypoxanthine phosporibosyltransferase (Hprt) expression levels were determined to show that each sample contained equivalent amounts of mRNA. No products were amplified in the absence of reverse transcriptase (Hprt-RT), indicating the absence of genomic DNA in the mRNA samples. The cDNA of each sample was derived from one animal, and 5-6 animals of each genotype (*hnf-1α*$^{+/+}$, *hnf-1α*$^{+/-}$, *hnf-1α*$^{-/-}$) were studied. We first assess the expression levels of the proximal steps of nutrient stimulated insulin secretion, mainly entry of nutrients into pancreatic β-cells and its breakdown by glycolysis. We found that the expression of genes encoding the liver isoform of pyruvate kinase (L-Pk), glucokinase (Gck), Glut-2, and neutral and basic amino acid transporter (Nbat) were significantly reduced (Fig. 3-1A). The absence of Glut-2 protein in mice that lack Hnf-1α was also confirmed by immunohistochemistry of pancreatic sections (Fig.3-2). The expression of other glucose (Glut-1) and amino acid (neutral amino acid transporter, Naat) transporters remain unchanged (Fig. 3-1A). The expression of the remaining glycolytic enzymes including phosphoglucose isomerase (Gpi), phosphofructokinase (Pfk), aldolase B (Aldo-B), triosephosphate isomerase (Tpi), glyceraldehyde 3-phosphate dehydrogenase (G3PD), phosphoglycerate kinase (Pgk), phosphoglycerate mutase (Pgam1 and 2), 2,3-bisphosphoglycerate mutase (Bpgm), α, β and γ-enolases were also similar in islets of *hnf-1α*$^{+/+}$ and *hnf-1α*$^{-/-}$ animals (Fig. 3-1B).

We next sought to determine if *hnf-1α* deficiency affect the expression of mitochondrial genes involved in nutrient stimulated insulin secretion. The expression of

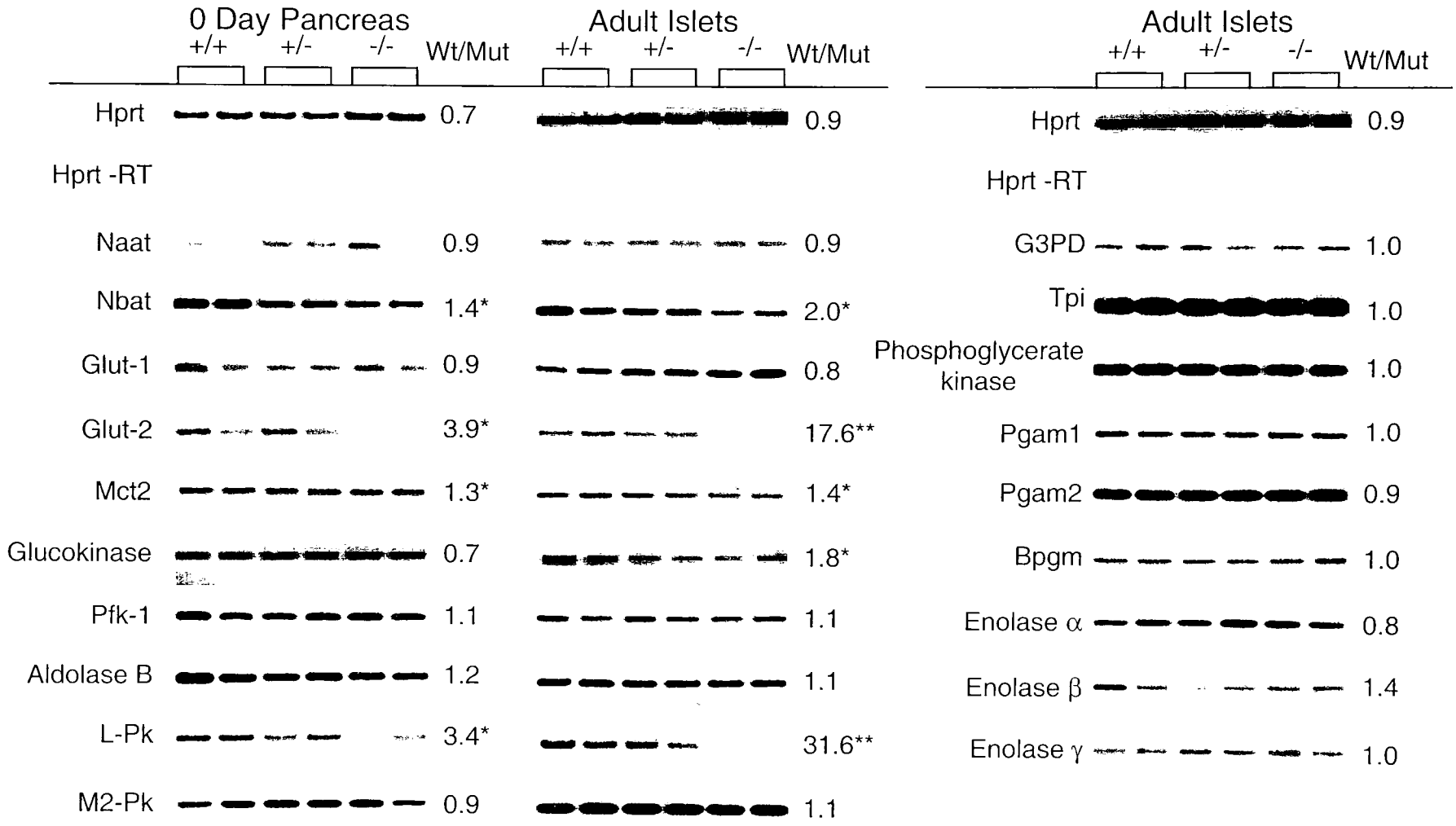

Fig. 3-1. Pancreatic islet gene expression in *hnf-1α*$^{-/-}$ mice. (A) RT-PCR analysis of nutrient transporters and enzymes catalyzing the energy dependent steps of glycolysis in pancreata of newborn mice and adult islets. (B) RT-PCR analysis of enzymes catalyzing the non-energy dependent steps in glycolysis. Quantitative measurements were obtained by densitometry. WT/Mut indicates the ratio of expression levels of the means of wildtype and *hnf-1α*$^{-/-}$ mice. Naat, neutral amino acid transporter; Nbat, neutral and basic amino acid transporter; Glut, glucose transporter; Pfk-1, phosphofructokinase 1; Pk, pyruvate kinase; G3PD, glyceraldehyde 3 phosphate dehydrogenase; Tpi, triose phosphate isomerase; Pgam, phosphoglycerate mutase; Bpgm, bisphosphoglycerate mutase. *:$p \leq 0.05$; **: $p \leq 0.01$.

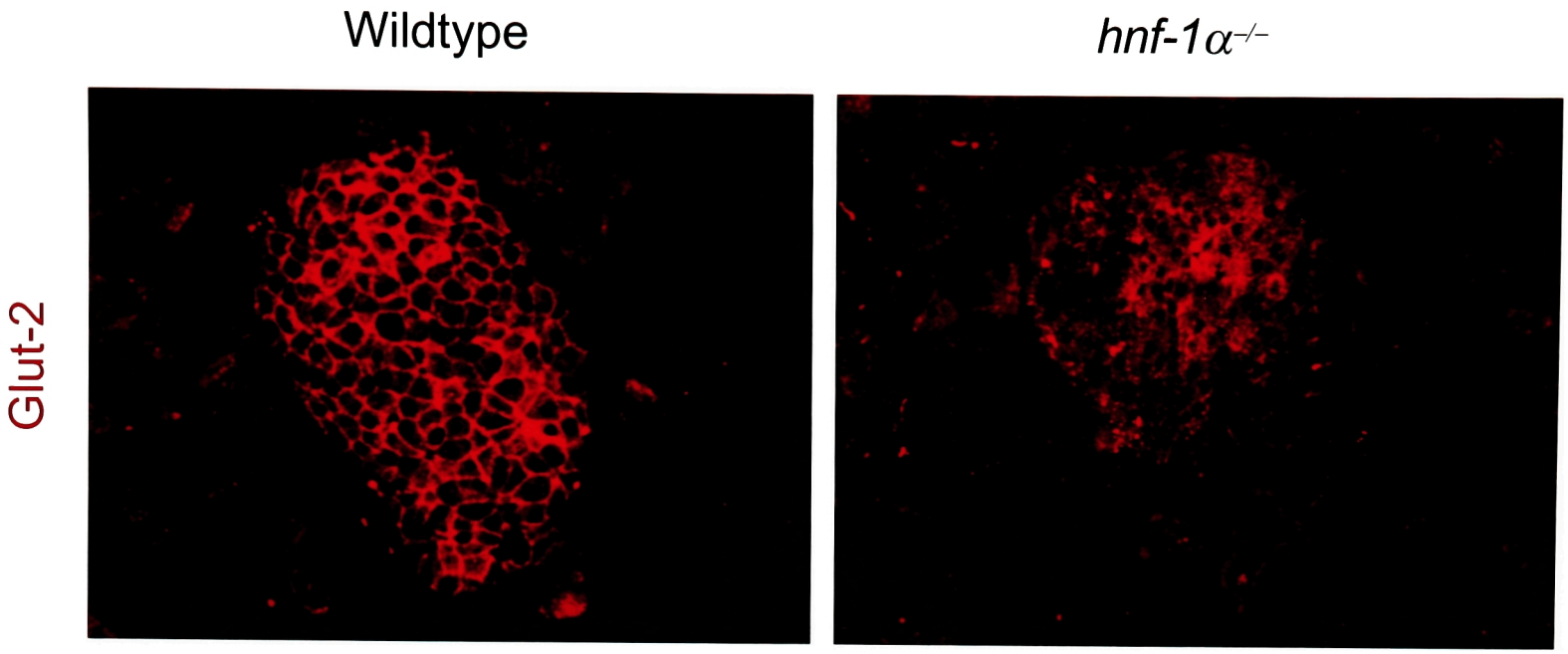

Figure 3-2. Immunofluorescent staining of Glut-2 protein in *hnf-1α*$^{-/-}$ islets. Pancreatic tissue sections showing representative islets from 4 weeks old *hnf-1α*$^{+/+}$ and *hnf-1α*$^{-/-}$ mice are shown. Sections were stained with antibodies against Glut-2. Pancreas sections from wildtype littermates demonstrated red fluorescent staining on the membranes of cells of pancreatic islets indicating the presence of Glut-2 in the membranes of pancreatic beta cells. In contrast, there was no staining evident in the islets of *hnf-1α*$^{-/-}$ mice. Staining in *hnf-1α* heterozygous mice was similar to that in the wildtype mice (data not shown).

all the genes involved in the tricarboxylic acid (TCA) cycle including Ogdh were similar between wt and *hnf-1α*$^{-/-}$ mice. Finally, we checked genes involved in insulin secretion that are distal to the TCA cycle such as the exocytotic machinery and the systems for processing peptide hormones. We did not detect any expression differences between insulin processing enzymes (PC2, PC3) or ATP-sensitive potassium channels (Kir 6.2, Sur-1) (Fig. 3-3A).

To confirm that impaired insulin secretion in *hnf-1α*$^{-/-}$ mice is not caused by a change in insulin steady-state mRNA levels or a change in the endocrine cell lineage allocation, we assessed islet composition quantitatively by determining the islet hormone expression levels. Consistent with the previous staining of islets with markers for α-, β-, δ-, and PP-cells (41), expression of different islet cell types markers such as Iapp, somatostatin, pancreatic polypeptide and total insulin (insulin 1 and 2) did not differ. Together these results suggest that the various islet cell types contributed equally in wt and *hnf-1α*$^{-/-}$ animals (Fig. 3-3B). However, we found decreased expression levels of insulin 1 and glucagon. Decreased expression level of insulin 1 is probably due to a consensus Hnf-1 binding site in –410 in the promoter of insulin 1 but not insulin 2. Decreased glucagon expression is probably due to hyperglycemia in *hnf-1α*$^{-/-}$ mice. To rule out a possible glucagon secretion defect that may be masked by hyperglycemia, we performed an *in vivo* glucagon secretion test using alanine as the glucagon secretagogue (99-103, 123). We found that there is no difference in glucagon secretion rate between wt and *hnf-1α*$^{-/-}$ mice (Fig. 3-4A, B).

Since hyperglycemia and hypoinsulinemia in *hnf-1α*$^{-/-}$ animals can lead to secondary changes in gene expression (124), the expression of the above mentioned

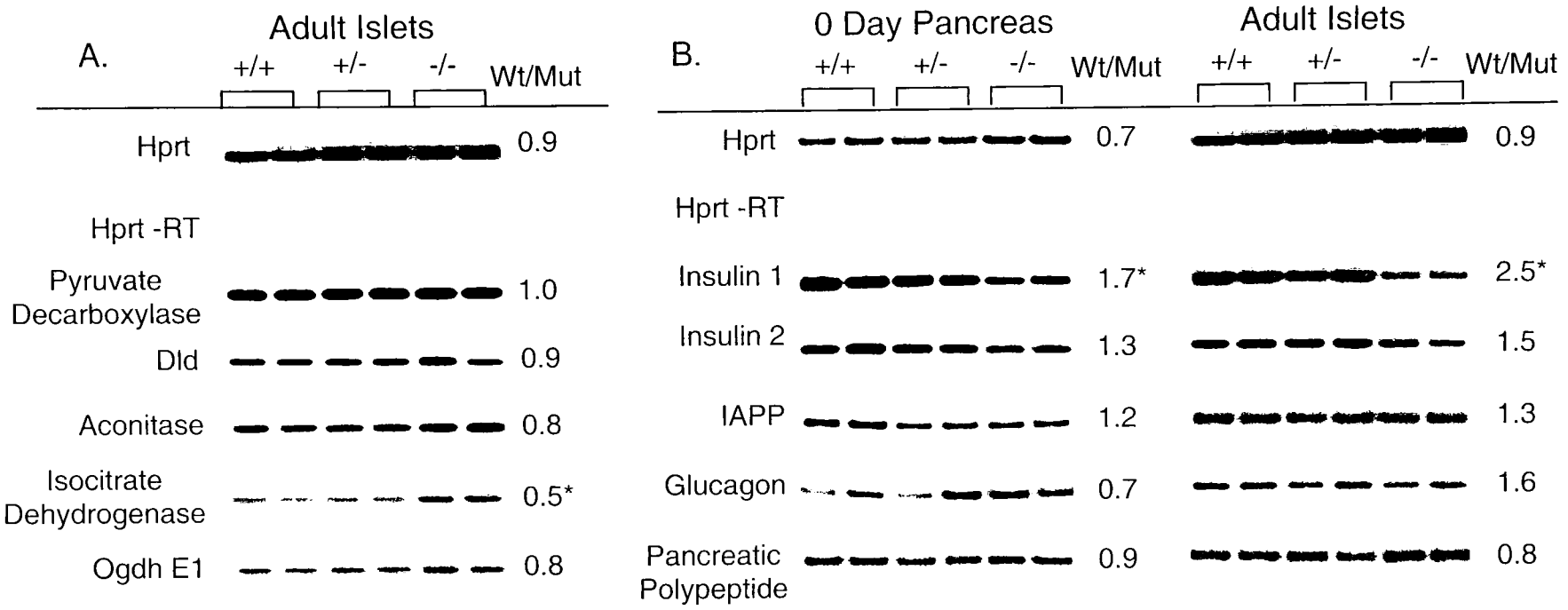

Fig. 3-3. Steady-state mRNA levels of genes involved in GSIS. (A) RT-PCR analysis of enzymes in the TCA cycle, hormone processing enzyme, and ion channels involved in GSIS in pancreata of newborn mice and adult islets. (B) RT-PCR analysis of hormones expressed in the endocrine pancreas. Quantitative measurements were obtained by densitometry. WT/Mut indicates the ratio of expression levels of the means of wildtype and *hnf-1α*$^{-/-}$ mice. Dld, dihydrolipoyl dehydrogenase; Ogdh, oxoglutarate dehydrogenase; E2k, dihydrolipoyl succinyltransferase; Ucp-2, uncoupling protein 2; PC, prohormone convertase; Kir6.2, ATP sensitive potassium channel; Sur-1, sulfonylurea receptor; IAPP, islet amyloid polypeptide. *:$p \leq 0.05$; **: $p \leq 0.01$.

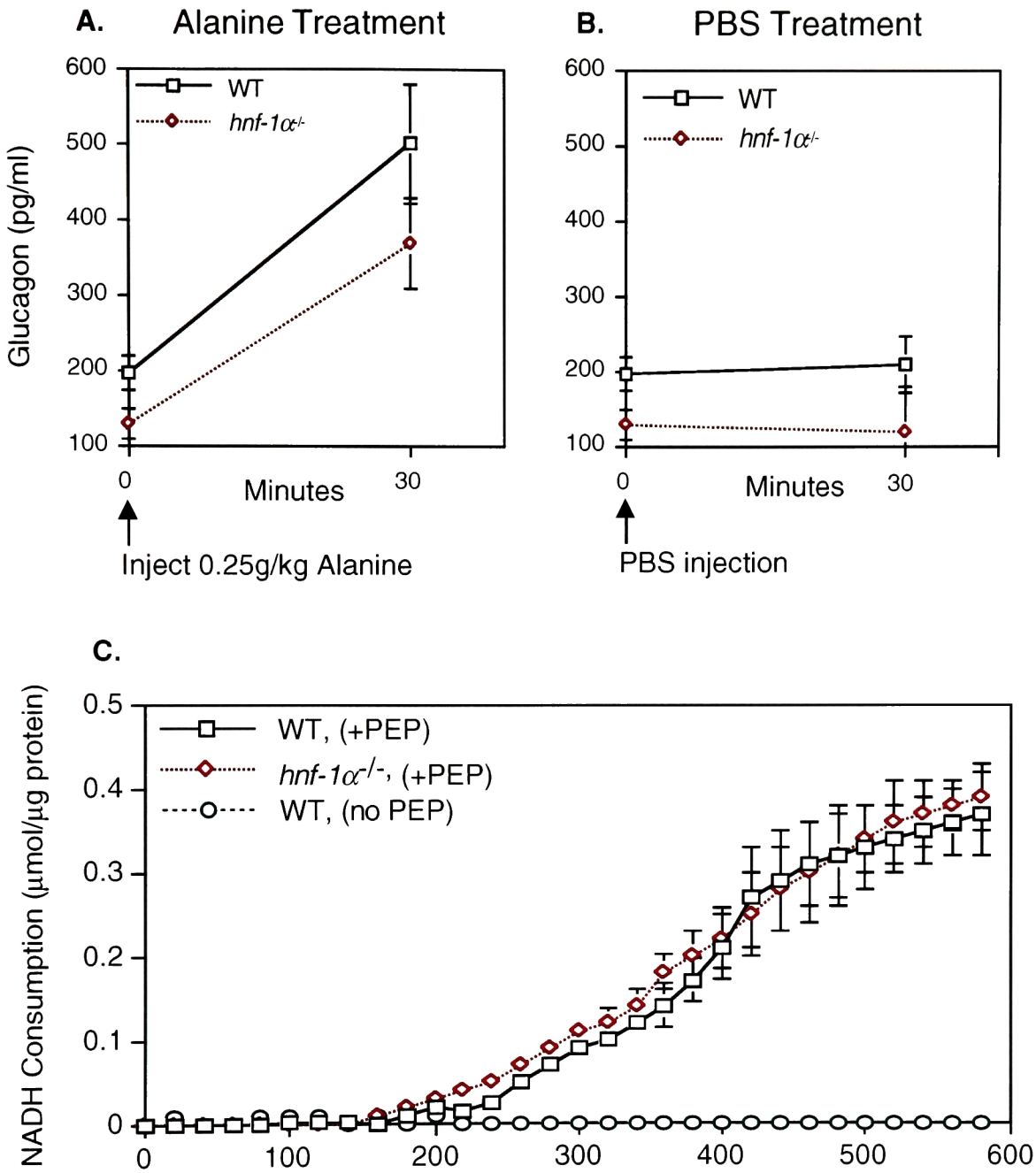

Figure 3-4: Analysis of pancreatic α-cell function and pyruvate kinase activity. Alanine (0.25 g/kg) (A) or PBS (B) is injected intraperitoneally into wildtype, and *hnf-1α*$^{-/-}$ mice. Glucagon is measured before and 30 minutes after alanine treatment. Plasma glucagon levels increased at similar rates in both wildtype and *hnf-1α*$^{-/-}$ mice. (C) Pyruvate kinase enzyme activity was measured in extracts of isolated islets. Pyruvate kinase activity is correlated to NADH consumption. The rates of consumption of NADH were similar in WT (n=4) and *hnf-1α*$^{-/-}$ (n=4) mice. PEP, phosphoenolpyruvate

genes were also studied in pancreata of newborn animals that had not been exposed to chronic hyperglycemia. We found that the expression of Glut-2, L-Pk, and Ins-1 was already decreased shortly after birth (Fig. 3-1A, 3-3B), suggesting that *hnf-1α* deficiency lead to the reduced expression of these genes. In contrast, glucagon and Gck mRNA levels were not altered in newborn pancreata (Fig. 3-1A, 3-3B), demonstrating that the decrease expression in *hnf-1α*$^{-/-}$ adult islets is likely due to hyperglycemia or hypoinsulinemia in these mice. Finally, we found that the expression of L-Pk was markedly reduced in islets of adult and newborn *hnf-1α*$^{-/-}$ animals. This transcriptional defect was specific for the liver isoform of pyruvate kinase (L-Pk) and expression levels of the muscle isoform (M_2Pk) were unchanged in *hnf-1α*$^{-/-}$ mice (Fig. 3-1A). To estimate the effect of the reduced L-Pk expression on overall pyruvate kinase activity, we measured total pyruvate kinase activity in islets of *hnf-1α*$^{+/+}$ and *hnf-1α*$^{-/-}$ mice (Fig 3-4C). Interestingly, no differences were detected in total pyruvate kinase activity, thus supporting previous findings that M2-Pk is the major pyruvate kinase isoform in pancreatic islets (125, 126).

Expression Analysis of Islet Enriched Transcription Factors in *hnf-1α*$^{-/-}$Mice

Hnf-1α belongs to a transcription network that controls the appropriate expression of β-cell genes to maintain glucose homeostasis (Fig. 1-3). Components of the islet enriched transcription network have been shown in the liver and extra-embryonic tissues to regulate the expression of other transcription factors in the same network (Fig. 1-2) (77, 80). To assess the effects of *hnf-1α* deficiency on the transcriptional regulatory network, we investigated the expression levels of islet-enriched transcriptional factors

that are important for either pancreas development or glucose metabolism in *hnf-1α*$^{-/-}$ mice.

We found that steady-state mRNA levels of Hnf-4α, an upstream regulator of Hnf-1α, was reduced in islets of *hnf-1α*$^{-/-}$ mice suggesting Hnf-1α is critical for the normal expression of Hnf-4α in pancreatic islets (Fig. 3-5). We also determined that the expression levels of several other islet-enriched transcription factors, including pancreatic and duodenal homeobox (Pdx)-1, neurogenic differentiation (NeuroD)-1, NK homeobox gene (Nkx) 2.2, Nkx6.1, dimerization cofactor of Hnf-1α (Dcoh) and small heterodimer partner (Shp)-1, were reduced approximately 1.4 to 11-fold in islets of *hnf-1α*$^{-/-}$ mice (Fig. 3-5). In contrast, the expression levels of Hnf-1β, -3α, -3β, -4γ, -6, Paired homeobox gene (Pax)-4, Pax-6, Islet-1, and caudal-type homeobox gene (Cdx) 2/3 did not differ between wt and *hnf-1α*$^{-/-}$ mice (Fig. 3-5 and data not shown). Steady state mRNA levels of Dcoh, Pdx-1, NeuroD1, Nkx2.2, and Nkx6.1 were also measured and found to be reduced in pancreata of newborn mice (Fig. 3-5). Our data indicate that Hnf-1α deficiency rather than nonspecific effects due to hyperglycemia compromised several components in the islet-enriched transcription network. These transcription factors may act together to impair nutrient stimulated insulin secretion by reducing glucose flux through glycolysis.

Liver Gene Expression Profiles in *hnf-1α*$^{+/+}$ and *hnf-1α*$^{-/-}$ Mice

Similar to the endocrine pancreas, the liver is an important organ for glucose metabolism. In addition, Hnf-1α as well as its target genes are expressed in the liver. To test if the changes in gene expression profiles of pancreatic islets are also present in the liver of *hnf-1α*$^{-/-}$ animals, we measured mRNA concentrations of all the above-mentioned

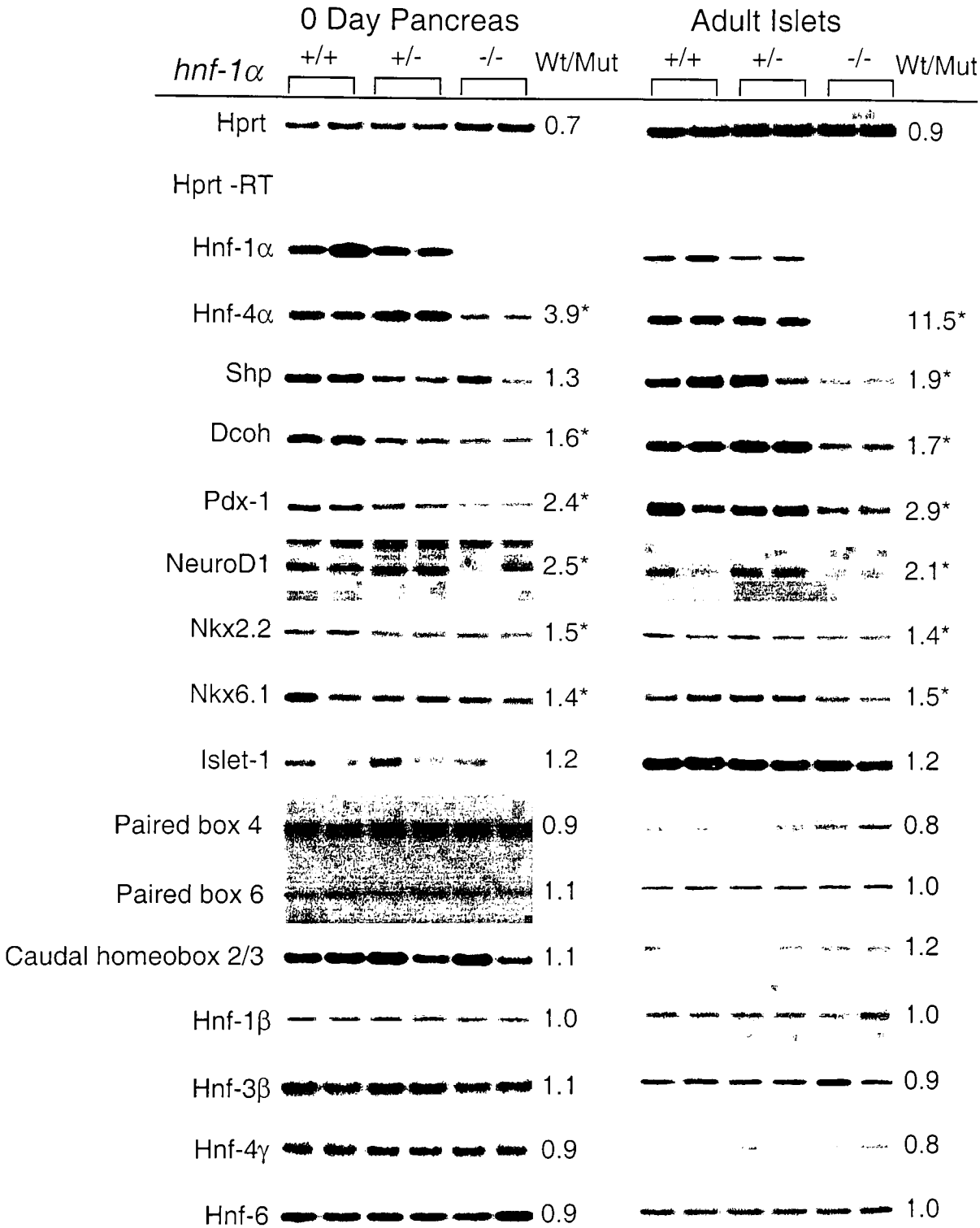

Figure 3-5. Analysis of islet enriched transcription factors in *hnf-1a*$^{-/-}$ mice. Steady-state mRNAs of islet enriched transcription factors were analyzed by RT-PCR by using [α-^{32}P]dCTP PCR products were separated by PAGE, and bands were visualized by autoradiography. We found that the expression of Hnf-4α, Shp, Dcoh, Pdx-1, NeuroD1, Nk box (Nkx) 2.2, Nkx6.1 are decreased in the absence of Hnf-1α.

genes in *hnf-1α* null, heterozygous and wt mice. Insulin growth factor 1 (Igf-1) was previously found to be reduced in *hnf-1α*$^{-/-}$ livers and is used as an expression control (37). We first tested all the glycolytic and TCA cycle enzymes involved in nutrient stimulated insulin secretion. Consistent with Hnf-1α regulation in the islets, the expression of Nbat was decreased in Hnf-1α deficient livers. In contrast to pancreatic endocrine pancreas, the liver is an important organ for glucose metabolism. In addition, Hnf-1α as well as its target genes are expressed in the liver. To test if the changes in gene expression profiles of pancreatic islets are also present in the liver of *hnf-1α*$^{-/-}$ animals, we measured mRNA concentrations of all the above-mentioned genes in *hnf-1α* null, heterozygous and wt mice. Insulin growth factor 1 (Igf-1) was previously found to be reduced in *hnf-1α*$^{-/-}$ livers and is used as an expression control (37). We first tested all the glycolytic and TCA cycle enzymes involved in nutrient stimulated insulin secretion. Consistent with Hnf-1α regulation in the islets, the expression of Nbat was decreased in Hnf-1α deficient livers. In contrast to pancreatic islets, the expression of Glut-1, Glut-2, Naat, and L-Pk was increased in *hnf-1α*$^{-/-}$ mice (Fig. 3-6). The expression of the remaining glycolytic and mitochondrial genes was similar in mice of different Hnf-1α genotypes (data not shown). These results show that Hnf-1α is required for expression of Glut-1, Glut-2, and L-Pk in insulin producing cells but not in other tissues which also co-express these genes.

We next assessed whether tissue-specific dependence on Hnf-1α can be extended to its interactions with other components of the transcription factor network. Consistent with the expression profile in the islets, transcript levels of DCoH were reduced in Hnf-1α null liver (Fig. 3-6). In contrast to pancreatic islets, the expression of Hnf-4α and Shp

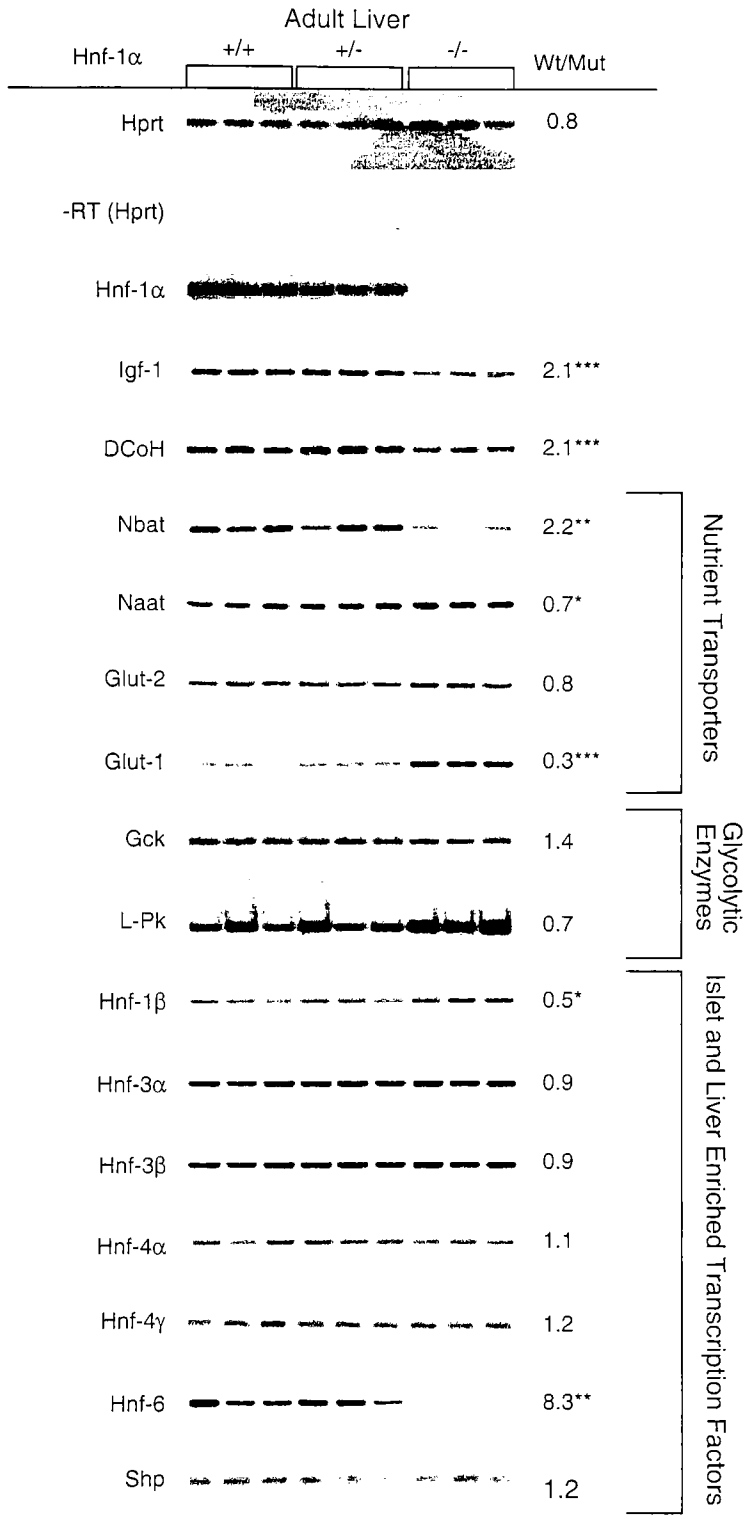

Figure 3-6. Steady state mRNA levels of Hnf-1α target genes in the liver. RT-PCR was performed from three separate RNA samples of each genotype as described in Methods. WT/Mut indicates the ratio of expression levels of the means of wildtype and *hnf-1α*$^{-/-}$ mice. *: $p \leq 0.05$; **: $p \leq 0.01$; ***: $p \leq 0.005$. Differences in L-Pk and Glut-2 expression in wildtype vs. mutant livers reached marginal significance ($p = 0.06$).

were unchanged in the liver of *hnf-1α*$^{-/-}$ mice. In analogy to the expression results obtained for Glut-1 and Naat, we found that Hnf-1β mRNA levels were significantly increased in the liver but not in pancreatic islets. Finally, Hnf-6 message was reduced in the liver but not in the pancreas (Fig. 3-6). The expression of other transcription factors including Hnf-3α, -3β and -4γ were unchanged in the liver (Fig. 3-6).

In summary, these data demonstrate that differences exist in the gene expression profiles of islets vs. liver in *hnf-1α*$^{-/-}$ mice. Therefore, in the liver other mechanisms may be operative that can activate Hnf-1α target genes, such as Glut-2 and L-Pk. These compensatory mechanisms may include elevated expression of Hnf-1β (which shares the same DNA binding sites as Hnf-1α) and/or unaltered expression levels of Hnf-4α.

Regulation of Small Heterodimer Partner in *hnf-1α*$^{-/-}$ Mice

The orphan nuclear receptor, small heterodimer partner (Shp), is one of only a few negative regulators of the islet and liver enriched transcription factor network. Shp can heterodimerize with various nuclear hormone receptors, including Hnf-4α, and inhibit their function (83, 84). These interesting properties in addition to our study which indicate that Hnf-1α may regulate Shp expression made it a fascinating candidate to analyze its promoter. Surprisingly, the promoter regions of both the human and murine *Shp* promoter did not contain any Hnf-1 binding sites (127). In contrast, a putative Hnf-4α consensus binding sequence was identified at position –551 to –570 bp in the human *SHP* promoter. This binding site was also evolutionary conserved at a similar location in the murine *shp* promoter (Fig. 3-7A) (Genbank accession numbers for murine and human sequences are AF044315 and AF044316, respectively). We therefore hypothesized that the downregulation of Shp may be due to the reduced Hnf-4α message in *hnf-1α*$^{-/-}$ mice.

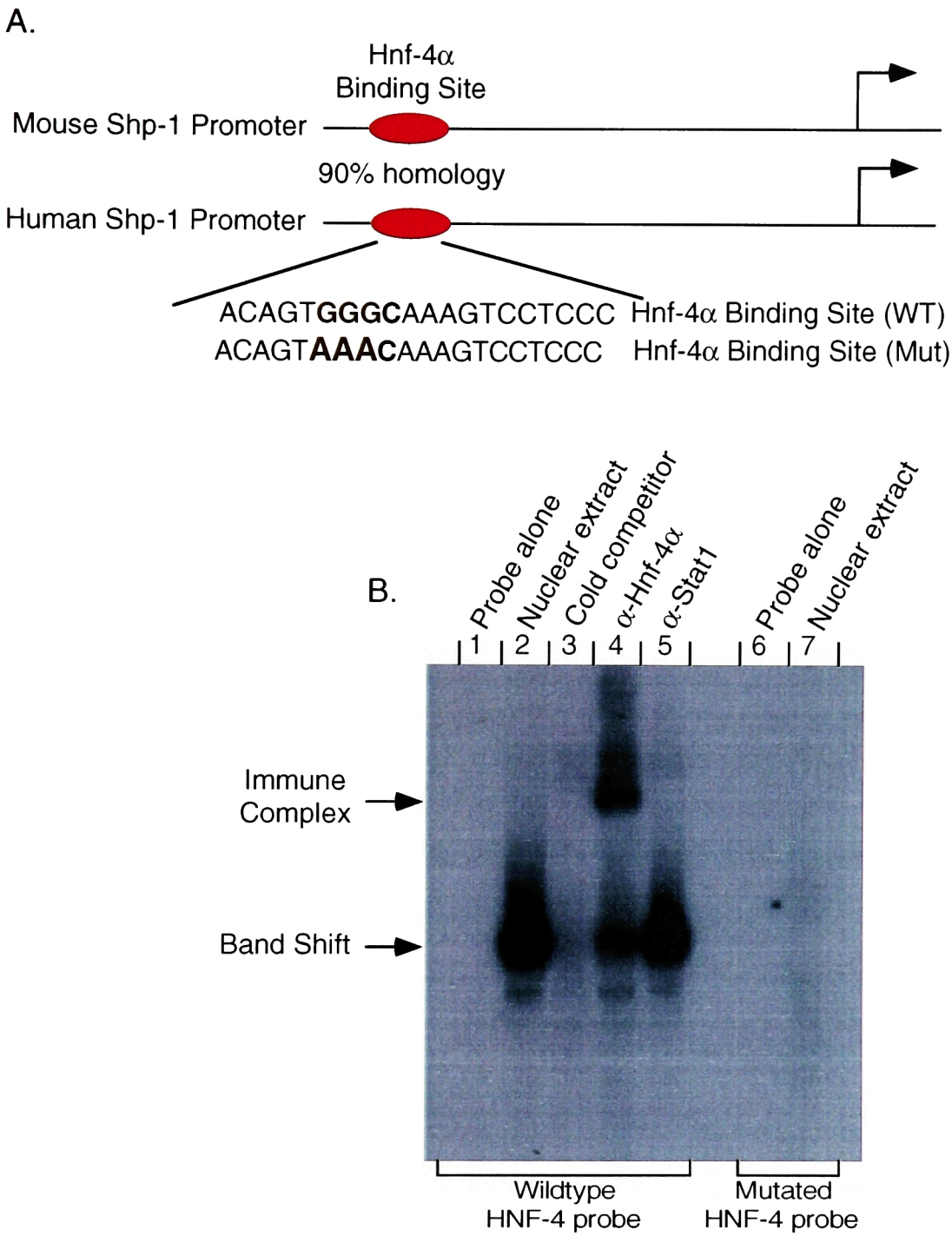

Figure 3-7. Analysis of the *SHP-1* promoter. (A) Comparison between the human and murine *SHP-1* promoter that shows 90% homology in the HNF-4 binding site. The wildtype and mutant sequences of the HNF-4 binding site is shown. (B) EMSA analysis of the HNF-4 binding site in the *SHP-1* promoter. The DNA binding activity was measured using a ^{32}P-labeled double stranded oligonucleotide containing the HNF-4 binding site as a probe and nuclear extracts of HIT-T15 cells that were transfected with pCMV-pHNF4α. Competition was carried out with a 20-fold excess of cold probe (lane 3), and supershifts were performed with a polyclonal α-HNF-4α antiserum or an α-Stat-1 control antiserum (lanes 4 and 5, respectively). No binding activity was detected with a probe containing a mutated HNF-4 binding site (Lane 7). Free probe on the bottom of the gel is not shown.

Electrophoretic mobility shift assays (EMSA) were performed to investigate if Hnf-4α can bind to the putative HNF-4 binding site in the *SHP* promoter. A major DNA/protein complex was detected with a ^{32}P-labeled oligonucleotide that contained the HNF-4 binding site (Fig. 3-7B, lane 2). This binding activity could be competed by an unlabeled excess of cold Hnf-4 binding oligonucleotide (Fig. 3-7B, lane 3). Furthermore, a supershift of the complex was observed after pre-incubation of extract with a monospecific anti-Hnf-4α antiserum (α-445), but not with anti-STAT-1 antibodies (Fig. 3-7B, lanes 4 and 5) demonstrating that Hnf-4α can bind to the HNF4 site in the *SHP* promoter. As expected, Hnf-4α was not able to bind to the mutated Hnf-4 site (Fig. 3-7B, lane 7).

Next, we addressed the question of whether Hnf-4α can act as a direct transcriptional activator in co-transfection assays by cloning a 582 bp of the 5'- human *SHP* promoter containing the putative HNF-4 binding site and linked it to a luciferase reporter gene (pGL2-pSHP). Co-transfection of pGL2-pSHP with a Hnf-4α expression vector (pcDNA3-pHNF-4α) showed an approximately 2- to 5- fold dose-dependent activation of the *SHP* promoter in three different cell lines, Cos7 (kidney), HepG2 (liver) and HIT-T15 (islet) cells (Fig. 3-8A to C). In contrast, Hnf-1α expression did not result in the transcriptional activation of this reporter construct (Fig. 3-8A to C). To confirm that Hnf-4α can directly activate the *SHP* promoter, we mutated one hexamer half of the HNF-4 binding site in the reporter plasmid pGL2-pSHP (Fig. 3-7A). Transcriptional activation of HNF-4α on the resulting SHP reporter plasmid (pGL2-pSHPmut) was

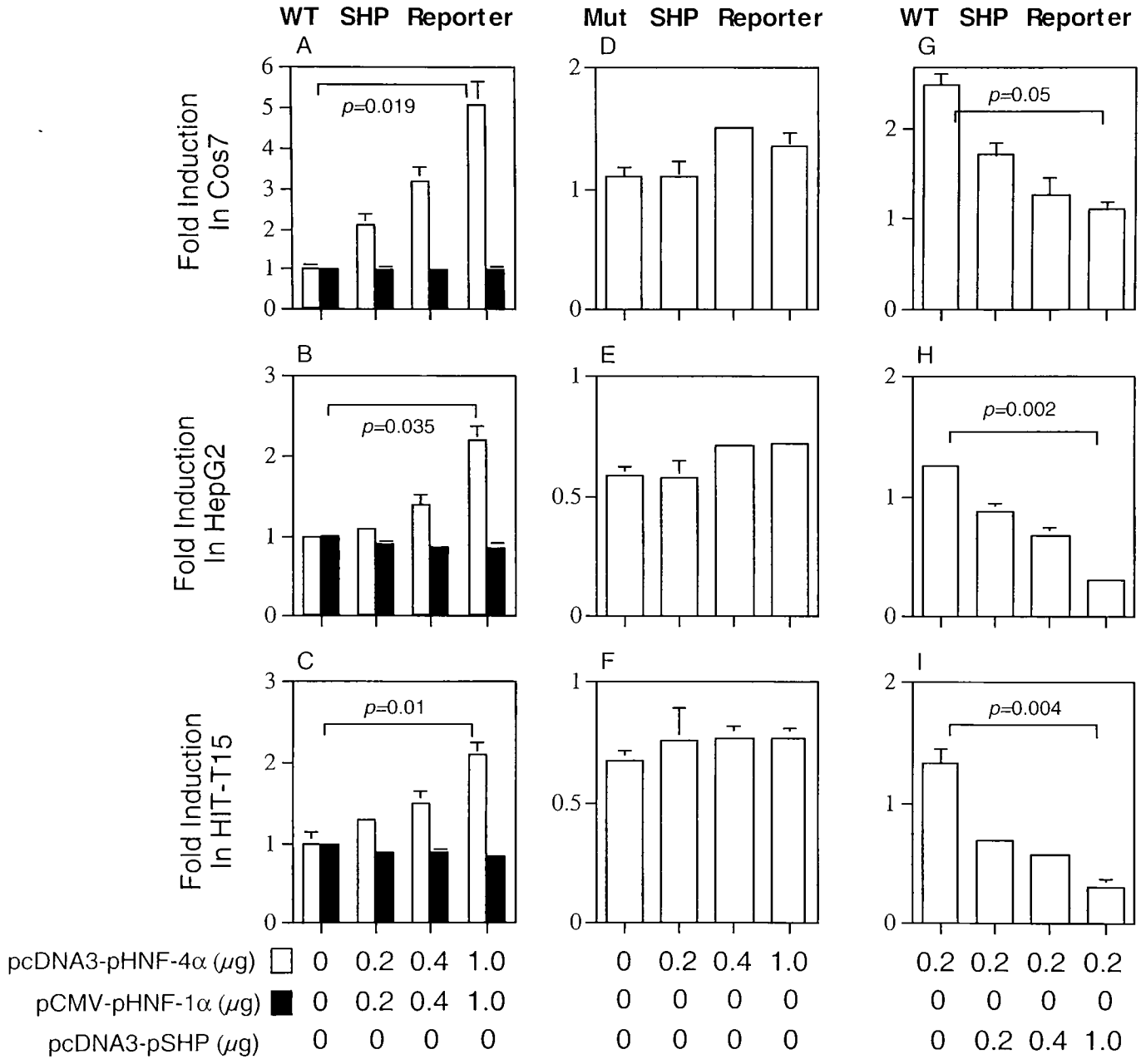

Figure 3-8. Hnf-4α transactivate the *SHP* reporter construct. The reporter construct pGL2-pSHP was cotransfected with pCMV-pHNF-4α or pcDNA3-pHNF-1α into Cos7, HepG2 and HIT-T15 cells (A-C). The HNF-4 binding site in the SHP promoter is mutated in pGL2-pSHPmut (D-F). G-I shows cotransfection in various cell types of pCMV-pHNF-4α and increasing amounts of pCMV-pSHP in the presence of reporter pGL2-pSHP Cells were harvested 48 hrs after transfections and assayed for luciferase and β-galactosidase activities. The average fold inductions from two independent transfections done in duplicates and normalized to β-galactosidase activity are shown. Error bars indicate SEM.

abolished (Fig. 3-8D-F), indicating that the HNF-4 binding site in the SHP promoter is functionally important for its expression.

In order to test if SHP can down-regulate its own transcriptional activation by inhibiting the function of HNF-4α, we co-transfected SHP expression vector pcDNA3-pSHP with constant quantities of pcDNA3-pHNF-4α and pGL2-pSHP into Cos7, HIT-T15 and HepG2 cells. Luciferase activity decreased in a dose-dependent manner when increasing amounts of pcDNA3-pSHP vector were co-expressed with constant amount of HNF-4α (Fig. 3-8G-I). These data suggest that SHP can inhibit its own transcription through a negative transcriptional feedback loop that is mediated by HNF-4α (Fig. 1-2).

Discussion

Nutrient metabolism starts with glycolysis and mitochondrial substrate oxidation in pancreatic β-cells to generate ATP. Mitochondrial ATP generation closes ATP-sensitive potassium channels and depolarizes the plasma membrane. Depolarization of the plasma membrane opens the voltage-dependent calcium channels which increase intracellular calcium concentration and consequently, insulin exocytosis. Previous studies have demonstrated that the insulin secretory responses to glucose are impaired in *Hnf-1α*$^{-/-}$ mice (41). Physiological studies have shown that ATP-sensitive K^+-currents (K_{ATP}) in β-cells of mutant mice are insensitive to suppression by glucose or glyceraldehyde but are normally sensitive to ATP. Flux of glucose through glycolysis in islets of mutant mice is reduced but mitochondrial substrates, such as methylpyruvate, can inhibit K_{ATP}, elevate $[Ca^{2+}]$, and restore the insulin secretion defect (40, 41). These results indicate that insulin secretion is impaired by a defect proximal to mitochondrial metabolism in the β-cell glycolytic signaling pathway. However, a recent *in vitro* study showed that

expressing a dominant negative form of Hnf-1α, HNF1α-P291fsinsC, in insulinoma INS-1 cells affects mitochondrial function by reducing the expression of Ogdh and increasing the expression of Ucp-2 (122). The net result of these expressing alterations is to impair mitochondrial function such as oxidation and ATP generation, and to dissipate the mitochondrial membrane potential, leading to decreased glucose stimulated insulin secretion. These inconsistent findings have not been resolved. In addition, the molecular basis by which *hnf-1α* deficiency causes impaired nutrient stimulated insulin secretion is poorly understood.

In this study, we investigated the transcriptional defects resulting from *hnf-1α* deficiency. We studied steady state mRNA levels in adult and newborn islets of genes that are critical β-cell function in the islets of *hnf-1α*$^{+/+}$ and *hnf-1α*$^{-/-}$ littermates. Gene transcript levels were also measured in the pancreata of newborn animals to control for secondary effects that hyperglycemia may have on gene expression profiles in *hnf-1α*$^{-/-}$ mice. Newborn *hnf-1α*$^{-/-}$ mice are normoglycemic (87 vs. 90 mg/dl in *hnf-1α*$^{+/+}$ and *hnf-1α*$^{-/-}$ newborn mice, respectively) and blood glucose levels of *hnf-1α*$^{+/-}$ females are indistinguishable from *hnf-1α*$^{+/+}$ female animals during the last week of pregnancy (118 vs. 121 mg/dl in *hnf-1α*$^{+/+}$ and *hnf-1α*$^{+/-}$ pregnant mice, respectively). This indicates that newborn islets of *hnf-1α*$^{-/-}$ mice were not exposed to chronic hyperglycemia. We found reduced expression of three genes involved in the glycolytic signaling pathway, namely Glut-2, Gck, and L-Pk in *hnf-1α*$^{-/-}$ mice (Fig. 3-1A). In addition, we also found diminished expression of Nbat, an amino acid transporter that transports both neutral and basic amino acids into the cell (Fig. 3-1A). Reduced expression of Glut-2, Gck and Nbat are likely to contribute to the defect in nutrient stimulated insulin secretion since mutant

mice lacking Glut-2 or Gck are hyperglycemic and hypoinsulinemic due to impaired glucose stiumlated insulin secretion (32, 128). The downregulation of Nbat may reduce the transport of basic and neutral amino acids into the β-cell and offers a molecular explanation for decreased cellular ATP production in response to leucine (122). In contrast, it is unlikely that decreased L-Pk expression levels contribute significantly to the β-cell defect in *hnf-1α*$^{-/-}$ mice because we did not observe a significant reduction in the overall enzyme activity of islet pyruvate kinase in *hnf-1α*$^{-/-}$ mice (Fig. 3-4C). Therefore, our findings agree with previous studies that indicated M2-Pk is the major pyruvate kinase isoform in pancreatic islets (125, 126). Our data suggest then, that the lack of Glut-2, Gck, and Nbat, which was not compensated for by increased expression levels of other glucose and amino acid transporters, may contribute to the diminished glucose or amino acid-stimulated insulin secretion rates in *hnf-1α*$^{-/-}$ animals.

To determine if *hnf-1α* deficiency also impairs the expression of genes that are critical for mitochondrial function, we measured mRNA levels of numerous mitochondrial genes including Ogdh and Ucp-2. Ogdh constitutes the rate-limiting enzyme in the mitochondrial TCA cycle and Ucp-2 uncouples respiration from oxidative phosphorylation and inhibits the efficiency of ATP synthesis. In contrast to a previous report (122), the expression of Ogdh and Ucp-2 were not changed in the absence of Hnf-1α (Fig. 3-3A). We also did not find the expression of other mitochondrial enzymes involved in the TCA cycle to be affected by Hnf-1α deficiency (Fig. 3-3A). Several reasons may account for these discrepancies. First, the previous study investigated the consequences of Hnf-1α deficiency by using a deoxycycline inducible dominant negative Hnf-1α. Doxycycline has been shown to be cytotoxic and thus, may alter gene expression

in treated cells (129, 130). Second, since Hnf-1α can either homodimerize, or heterodimerize with Hnf-1β, the dominant negative Hnf-1α used in the previous study may inhibit the function of both Hnf-1α and Hnf-1β (131). As a result, reduced Ogdh and increased Ucp-2 expression may also be due to impaired Hnf-1β function and not solely to Hnf-1α deficiency. Finally, the previous study was done in a transformed insulinoma cell line (INS-1) and differences between INS-1 cell line (132) and islets (used in the present study) exist that may explain the differences in Hnf-1α regulated genes in the mitochondria.

In addition to the transcriptional defect in genes regulating β–cell glycolytic signaling, we found the expression levels of several other transcription factors to be significantly reduced in mice with Hnf-1α deficiency. The steady-state mRNAs of Hnf-4α, Pdx-1, Nkx2.2, Nkx6.1, and Neuro-D1/Beta-2, as well as the dimerization cofactor Dcoh were reduced shortly after birth in islets of *hnf-1α*$^{-/-}$ mice, suggesting that these changes are caused by *hnf-1α* deficiency and are likely to contribute to the molecular defects in *hnf-1α*$^{-/-}$ islets. Decreased expression of several of these genes may be mediated directly by Hnf-1α. For instance, a functional Hnf-1 binding site has recently been identified in the *HNF-4α* promoter P2 that is located ≈46kb upstream of the hepatic (P1) promoter. Transcription from the P2 promoter is responsible for the expression of the most abundant HNF-4α isoform in pancreatic β-cells and HNF-1α is a potent activator of HNF-4α transcription from the P2 promoter *in vitro* (22). Our finding suggests that in pancreatic islets, Hnf-1α and Hnf-4α form an autoregulatory loop, and that a haploinsufficiency in either of these transcription factors causes an expression disequilibrium (see model proposed, Fig. 1-2). Mutations in HNF-4α in humans result in

a very similar β-cell phenotype to MODY3 patients (26, 28, 120), supporting the possibility that both are indeed involved in a common regulatory circuit that is present in pancreatic β-cells.

Interestingly, the expression of Pdx-1 was reduced in a dose-dependent manner in *hnf-1α*$^{+/+}$, *hnf-1α*$^{+/-}$ and *hnf-1α*$^{-/-}$ mice (Fig. 3-5). Pdx-1 is an essential transcription factor for pancreas development and β-cell function, and loss-of-function mutation in this gene causes MODY4 (7, 21, 54, 56). Expression levels of Pdx-1 in *hnf-1α*$^{-/-}$ islets were reduced 30-50% (Fig. 3-5). Since Pdx-1 is a transcriptional regulator of Gck, Glut-2, and insulin (56, 133-135), their down-regulation may also be due to diminished Pdx-1 expression levels in *hnf-1α*$^{-/-}$ mice. Functional Hnf-1α as well as Hnf-4α binding sites have been reported in evolutionarily conserved enhancer elements of the Pdx-1 promoter (57, 59). Therefore, decreased Pdx-1 expression in *hnf-1α*$^{-/-}$ islets may also be the result of reduced *hnf-1α* and *hnf-4α* gene expression. We also found that the mRNA levels of Neuro-D1, a helix-loop-helix transcription factor that can activate insulin gene transcription *in vitro* (136), were reduced 80% in *hnf-1α*$^{-/-}$ mice. Despite the reduced expression of Pdx-1 and Neuro-D1, mRNA levels of Ins-2 were indistinguishable in islets of in *hnf-1α*$^{+/+}$ and *hnf-1α*$^{-/-}$ mice (Fig. 3-3B). This finding is in agreement with other reports (40, 41) that did not find significantly reduced insulin mRNA levels in *hnf-1α*$^{-/-}$ mice and may be explained by compensation through other transcriptional activators of the insulin gene, such as Hnf-1β, Cdx2/3, Isl-1 and Pax4. In contrast, we found that Ins-1 expression was reduced ≈50% in islets of in *hnf-1α*$^{-/-}$ mice (Fig. 3-3B). This reduction is most likely a direct effect of Hnf-1α deficiency, mediated by an Hnf-1 binding element in the Ins-1 promoter that is lacking in the murine Ins-2 promoter (137).

It is worth noting that expression levels of other islet transcription factors that are important for β-cell metabolism, differentiation and insulin gene transcription, including Hnf-1β, -3α, -3β, -4γ, -6, Cdx-2, Isl-1, Pax4 and Pax6, were unchanged in *hnf-1α*$^{-/-}$ mice. Interestingly, the transcriptional control of this network and the regulation of downstream target genes are distinct in pancreatic islets and in the liver. For instance, the expression of Glut-2, Gck and L-Pk was normal or increased in the liver but significantly decreased in islets of *hnf-1α*$^{-/-}$ compared to wt littermates. These differences may be explained by compensatory upregulation of transcriptional regulators (e.g. Hnf-1β) in the liver, reduced expression of liver-enriched transcription factors absent in adult pancreatic islets (e.g. Hnf-6) or through differential regulation of transcription factors and downstream targets through tissue-specific promoters (e.g. Hnf-4α, Gck). These data indicate that the impairment in nutrient stimulated insulin release in *hnf-1α*$^{-/-}$ mice is likely to result from multiple pancreatic β-cell expression defects and support our hypothesis that loss of Hnf-1α function causes a pleiotrophic, but distinct defect in the β-cell transcriptional network that is essential to maintain glucose homeostasis. In addition, the observations that different Hnf-1α target genes have distinct tissue-specific requirement for Hnf-1α may be an explanation for MODY3 phenotype of pancreatic β-cell dysfunction without major extra-pancreatic abnormalities.

Finally, *in vitro* studies have suggested that Shp may heterodimerize with Hnf-4α and inhibit its transcriptional activity (84). Mutations in *SHP* have also been identified in humans and may be associated with mild obesity in Japanese subjects (138). Shp expression was markedly reduced in islets of *hnf-1α*$^{-/-}$ mice, suggesting that *it* may be regulated by Hnf-1α, Hnf-4α, Pdx-1, Nkx2.2, Nkx6.1 or Neuro-D. To better understand

the molecular basis of *shp* gene regulation, we studied its promoter. The 5'-regulatory sequence of *SHP* lacked binding sites for Hnf-1α, Pdx-1 and Neuro-D but contained a conserved and functional Hnf-4 site. The biochemical characterization of this site and *in vitro* transactivation studies indicate that Hnf-4α is a transcriptional activator of the *Shp* gene. The reduced Shp mRNA levels in pancreatic islets of *hnf-1α*$^{-/-}$ mice are likely due to the reduced expression of Hnf-4α in Hnf-1α-deficient islets. Furthermore, our data indicate that Shp may regulate its own expression by inhibiting Hnf-4α function, thus forming a negative feedback loop and indirectly (through Hnf-4α) regulate the activity of Hnf-1α, Pdx-1 and Neuro-D (Fig. 1-3). Shp may therefore serve as an important checkpoint to balance the activity of the islet transcriptional network. Further studies, including targeted mutagenesis of the *shp* gene in mice, are needed to shed light on the biological role of Shp in pancreatic islet function.

In summary, we have used a null mutant animal model as opposed to studies based solely on tissue culture systems to study impaired nutrient stimulated insulin secretion observed in MODY3 patients. We found that Hnf-1α mediates a distinct genetic program involving islet enriched transcription factors in pancreatic β-cells to decrease nutrient entry and reduce flux through glycolysis. Thus, the selective pancreatic β-cell dysfunction in the islets of *hnf-1α*$^{-/-}$ mice may be a molecular mechanism why human β-cells is particularly vulnerable to *hnf-1α* haploinsufficiency. However, it remains to be established whether the same tissue specific requirement for Hnf-1α function exists in MODY3 patients.

Chapter 4: Pancreatic β-Cell Defects in Mice with Combined Mutations in the Genes Encoding Pdx-1, Hnf-1α and Hnf-3β

Introduction

Type 2 diabetes (NIDDM) is a genetically determined metabolic disorder, affecting over 5% of the population in western countries (13). Numerous studies indicate that NIDDM is a polygenic disease, associated with peripheral insulin resistance and impaired pancreatic β-cell function. Although a majority of type 2 diabetic patients have insulin resistance in the muscle and the fat (tissues that are responsible for 90% of glucose disposal following a carbohydrate load) (139, 140), mice with muscle or adipose tissue specific deficiencies of the insulin receptor suggest that insulin resistance in these tissue alone is not enough to develop overt diabetes (141, 142). On the other hand, animals with targeted disruption of genes that impair insulin secretion in pancreatic β-cells invariably become diabetic, suggesting that impaired β-cell function by itself may be sufficient to develop clinical diabetes.

Genetic and biochemical studies in humans and mice have identified many key transcription factors that are involved in controlling pancreas development and β-cell function in the adult islet. Heterozygous mutations in a subset of these genes, including hepatocyte nuclear factor (*HNF*)-*4α*, *HNF-1α*, *PDX-1*, *HNF-1β*, and *BETA2*, are specifically associated with a form of type 2 diabetes, termed maturity-onset diabetes of the young (MODY), that is characterized by an early disease onset (usually <25 years) and a primary defect in insulin secretion. Interestingly, in contrast to humans, only

heterozygous *pdx-1* mutants but not *hnf-4α*, *hnf-1α*, *hnf-1β*, or *beta2* induce a diabetic phenotype in mice, presumably due to the direct importance of Pdx-1 in regulating glucose transporter-2 (Glut-2), glucokinase (Gck), and insulin expression. There is increasing evidence that these and other islet-enriched transcription factors (e.g. Nkx2.2, Nkx6.1, Pax-4, and Pax-6) form an integrated regulatory network in the β-cell that is critical for normal glucose-stimulated insulin secretion (143, 144).

The β-cell transcriptional network is organized in a hierarchical manner (Fig. 1-2). The upstream regulator of the network may be Hnf-3β, a protein in the forkhead transcription factor family. Although little is known about how Hnf-3β activates transcription in pancreatic β-cell development and function, it may promote transcription in a manner similar to its action in liver and initiate the opening of the chromatin and transcription complex assembly (79, 145). Hnf-3β and Hnf-1β regulates *hnf-4α* and *hnf-1α* gene expression in extra-pancreatic tissues (62, 63, 77), but it is unclear if this is also true in the pancreas. In β-cells, Hnf-3β and Hnf-1α may directly regulate *pdx-1* gene transcription (57-59, 146). In addition, HNF-1α and HNF-4α autoregulate each other's expression (25, 42). Collectively, Hnf-1α, Hnf-1β, Hnf-3β, Hnf-4α and Pdx-1 form crucial links in the cascade of transcription factors that control the appropriate expression of a number of key genes involved in glucose metabolism in the β-cell, including *glut-2*, *gck*, the liver pyruvate kinase isoform (*L-pk*), aldolase B (*aldo-B*), and insulin (147).

In spite of numerous gene targeting studies that characterized single gene mutations in islet enriched transcription factors, the effects of combined mutations on β-cell function has not been studied so far. To analyze the complex epistatic interactions between different components of the islet-enriched transcription factor network, we

created combined allelic mutations in genes encoding Pdx-1, Hnf-1α, Hnf-3α, Hnf-3β and Hnf-4α. Using this genetic approach, we show that Pdx-1 acts in concert with Hnf-1α and Hnf-3β to mediate a transcriptional program that control whole body glucose levels and maintain normal islet morphology.

Results

Generation of Mutant Mice

Mice carrying heterozygous mutations in of *hnf-1α*, *hnf-3α*, *hnf-3β*, *hnf-4α*, and *pdx-1* were bred into C57/Bl6 strain for at least 7 generations (2 years of breeding) and maintained in C57/Bl6 genetic background. The combined heterozygous *hnf-1α*$^{+/-}$*/hnf-4α*$^{+/-}$, *hnf-3β*$^{+/-}$*/hnf-4α*$^{+/-}$, *pdx-1*$^{+/-}$*/hnf-3β*$^{+/-}$, *pdx-1*$^{+/-}$*/hnf-4α*$^{+/-}$, and *pdx-1*$^{+/-}$*/hnf-1α*$^{+/-}$ mutant mice were generated by intercrossing mice heterozygous for each mutation. Except for *pdx-1*$^{+/-}$*/hnf-3β*$^{+/-}$, differentiation combination of the 5 mutations are born with expected Mendalian frequency with no significant difference between mouse growth rates. *Pdx-1*$^{+/-}$*/hnf-3β*$^{+/-}$ mice at weaning were less frequent than expected (16% actual versus 25% actual, n=126). This suggests that either a percentage of *pdx-1*$^{+/-}$*/hnf-3β*$^{+/-}$ are embryonic lethal or are dead before weaning. To differentiate between these possibilities, we determined the distributions of different genotypes during embryonic development and perinatal period. We found that *pdx-1*$^{+/-}$*/hnf-3β*$^{+/-}$ were born at expected frequency but a proportion (6% of all *pdx-1*$^{+/-}$*/hnf-3β*$^{+/-}$, n=103) died by 7 days after birth. The cause of death for these mice are unknown. However, the *pdx-1*$^{+/-}$*/hnf-3β*$^{+/-}$ mice that survived to weaning showed similar growth rates as mice with other mutations.

Development of Diabetes in *pdx-1*$^{+/-}$*/hnf-3β*$^{+/-}$ and *pdx-1*$^{+/-}$*/hnf-1α*$^{+/-}$ Mice

We first examined the metabolic consequences of mice carrying different

mutation combination by measuring glucose levels in the fasted and random-fed states. The effect of the combined mutants on serum glucose homeostasis was compared to *pdx-1*$^{+/-}$ to show the worsening of the *pdx-1*$^{+/-}$ diabetic phenotype. Only the *pdx-1*$^{+/-}$*/hnf-3*$\beta^{+/-}$ and *pdx-1*$^{+/-}$*/hnf-1*$\alpha^{+/-}$ mice exhibited progressive elevation in fasting and random-fed plasma glucose levels. *Pdx-1*$^{+/-}$*/hnf-1*$\alpha^{+/-}$ mice developed higher fasting and ad lib feeding serum glucose levels than *pdx-1*$^{+/-}$ mice at three month of age (136±11 and 188±10 vs. 94±4 and 167±5 mg/dl, p=0.04 and 0.03, respectively) (Fig. 4-1A, B). *Pdx-1*$^{+/-}$*/hnf-3*$\beta^{+/-}$ mice develop significant elevation in fasting and random-fed glucose levels after 4 month (Fig. 4-1C, D).

Intraperitoneal glucose tolerance tests (IPGTT) were performed on both male and female mice of the various genetic groups. Mice with combined allelic mutations in *pdx-1*$^{+/-}$*/hnf-4*$\alpha^{+/-}$, *hnf-1*$\alpha^{+/-}$*/hnf-4*$\alpha^{+/-}$, *and hnf-3*$\beta^{+/-}$*/hnf-4*$\alpha^{+/-}$ had indistinguishable blood glucose levels from the single haploinsufficienct mice over a six month interval (data not shown). *Pdx-1*$^{+/-}$*/hnf-1*$\alpha^{+/-}$ mice showed reduced glucose clearance levels when compared to the *pdx-1*$^{+/-}$ (Fig. 4-2). In addition, the IPGTT profile of *pdx-1*$^{+/-}$*/hnf-1*$\alpha^{+/-}$ mice deteriorated over time, whereas the *pdx-1*$^{+/-}$ mutants was non-progressing (Fig. 4-2). Male and female *pdx-1*$^{+/-}$*/hnf-3*$\beta^{+/-}$ mutant mice were phenotypically indistinguishable from *pdx-1*$^{+/-}$ animals at one month of age but developed a progressively decreased ability to clear glucose by 3 and 4 months (Fig. 4-3).

Eventhough a mutant *hnf-3*β allele worsens the diabetic phenotype of *pdx-1*$^{+/-}$ mice, their metabolic abnormalities are less severe than observed in *pdx-1*$^{+/-}$*/hnf-1*$\alpha^{+/-}$ mice. The glucose tolerance profile of *pdx-1*$^{+/-}$*/hnf-3*$\beta^{+/-}$ mice are milder and deteriorate at a later time than *pdx-1*$^{+/-}$*/hnf-1*$\alpha^{+/-}$ mice. *Pdx-1*$^{+/-}$*/hnf-1*$\alpha^{+/-}$ mice have an earlier onset

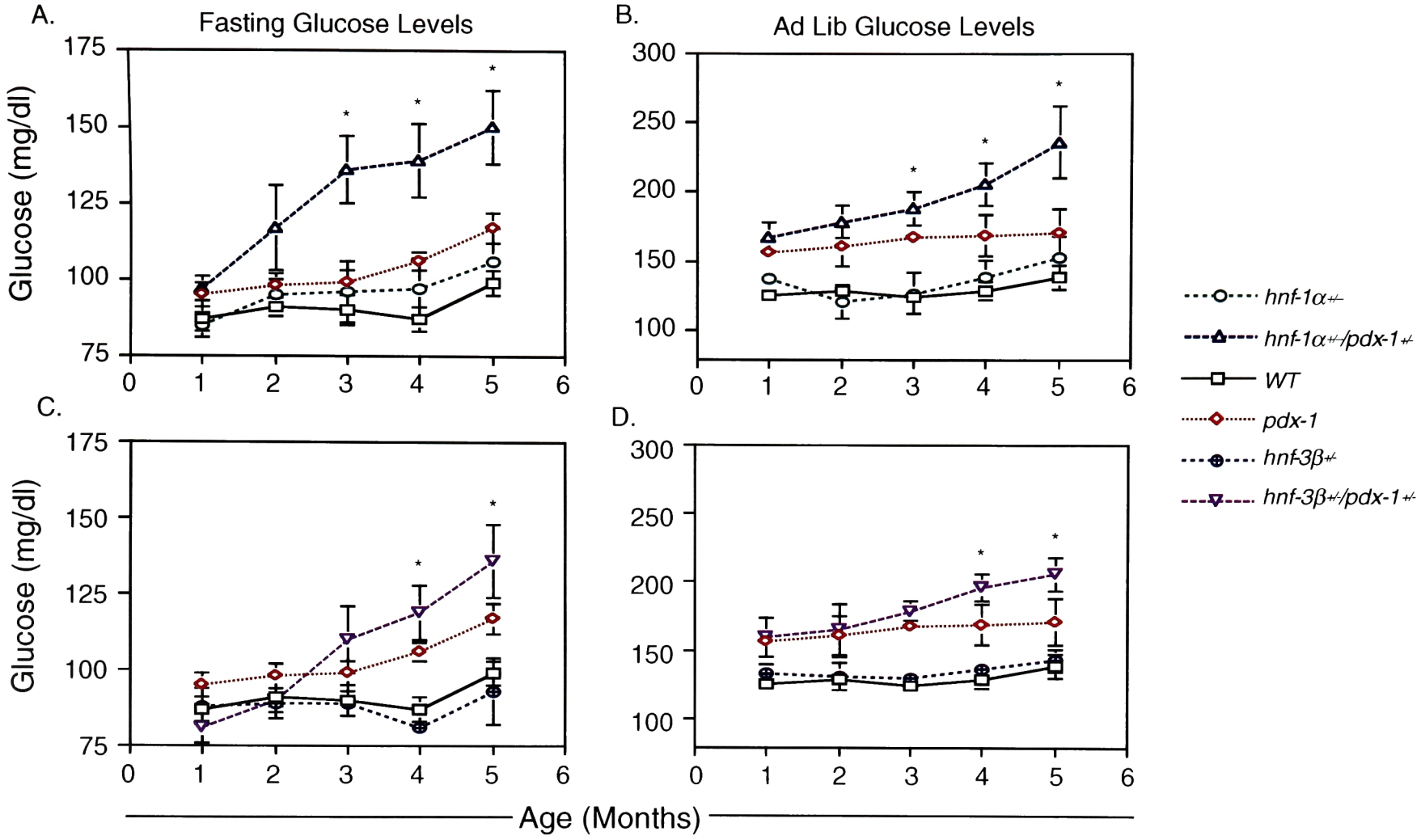

Figure 4-1. Development of diabetes in *hnf-1α*$^{+/-}$*/pdx-1*$^{+/-}$ and *hnf-3β*$^{+/-}$*/pdx-1*$^{+/-}$ mice. Blood glucose were measured either after a 12 hours fast (A, C) or ad lib (B, D). We observe that *hnf-1α*$^{+/-}$*/pdx-1*$^{+/-}$ (A, B) and *hnf-3β*$^{+/-}$*/pdx-1*$^{+/-}$ (C,D) develop progressively elevated fasting and ad lib plasma glucose levels. The results are the mean of at least 10 animals and the error bar represent SEM. *, $p<0.05$; **, $p<0.01$.

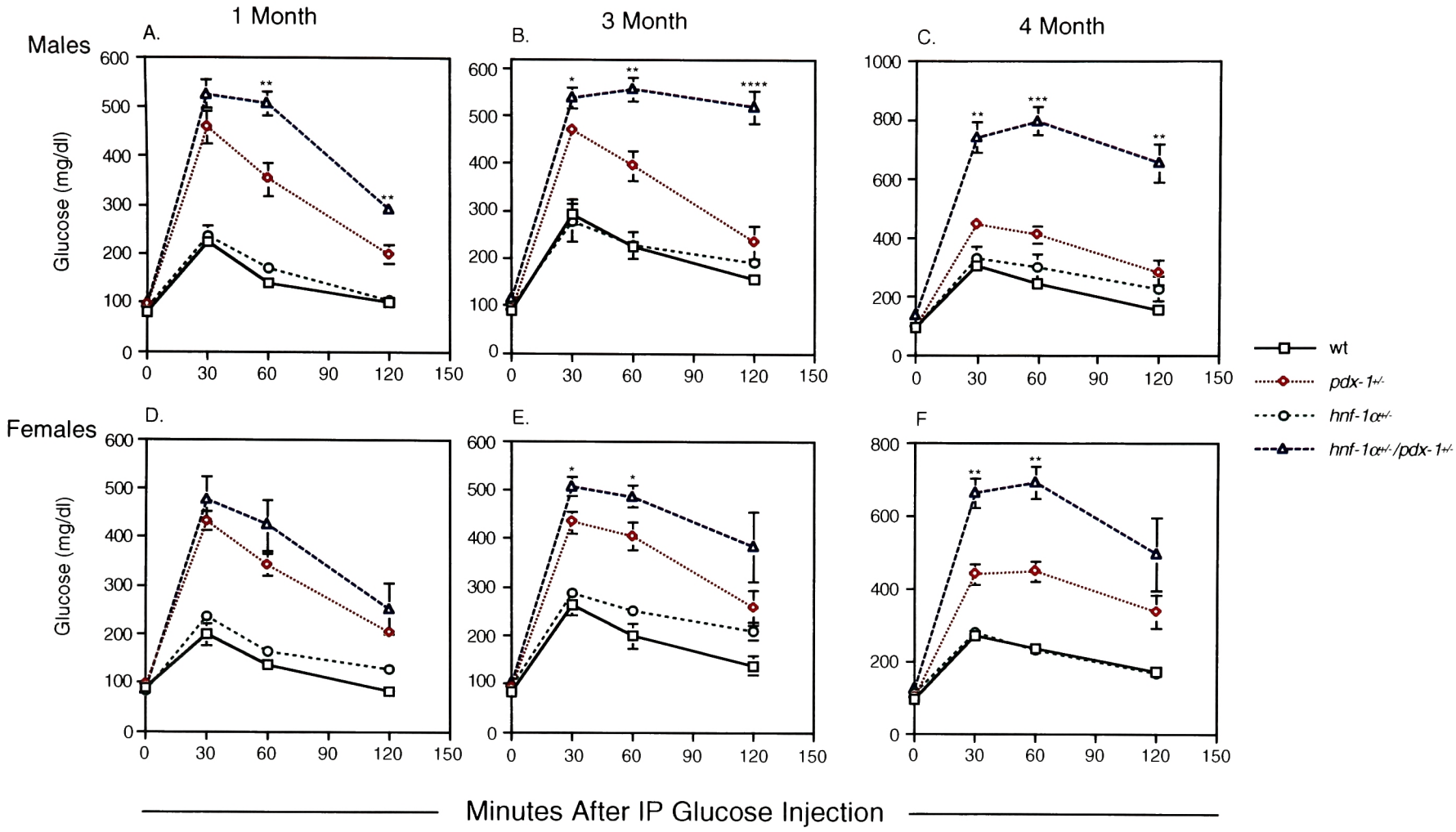

Figure 4-2: Impairment of glucose homeostasis in *pdx-1*$^{+/-}$*/hnf-1*$\alpha^{+/-}$ mice. IPGTT was performed in wildtype (*wt*) (black), *hnf-1*$\alpha^{+/-}$ (green), *pdx-1*$^{+/-}$ (red), and *pdx-1*$^{+/-}$*/hnf-1*$\alpha^{+/-}$ (blue) littermates at 1, 3 and 4 month of age. Significantly increased serum glucose concentrations were observed in male beginning at (first month) and female (at 3 month) of *pdx-1*$^{+/-}$*/hnf-1*$\alpha^{+/-}$ mice compared to *pdx-1*$^{+/-}$ A worsening of the glucose tolerance was seen in all double heterozygous animals. *: $p \leq 0.05$, **: $p \leq 0.01$, ***:$p \leq 0.005$, ****:$p \leq 0.0001$.

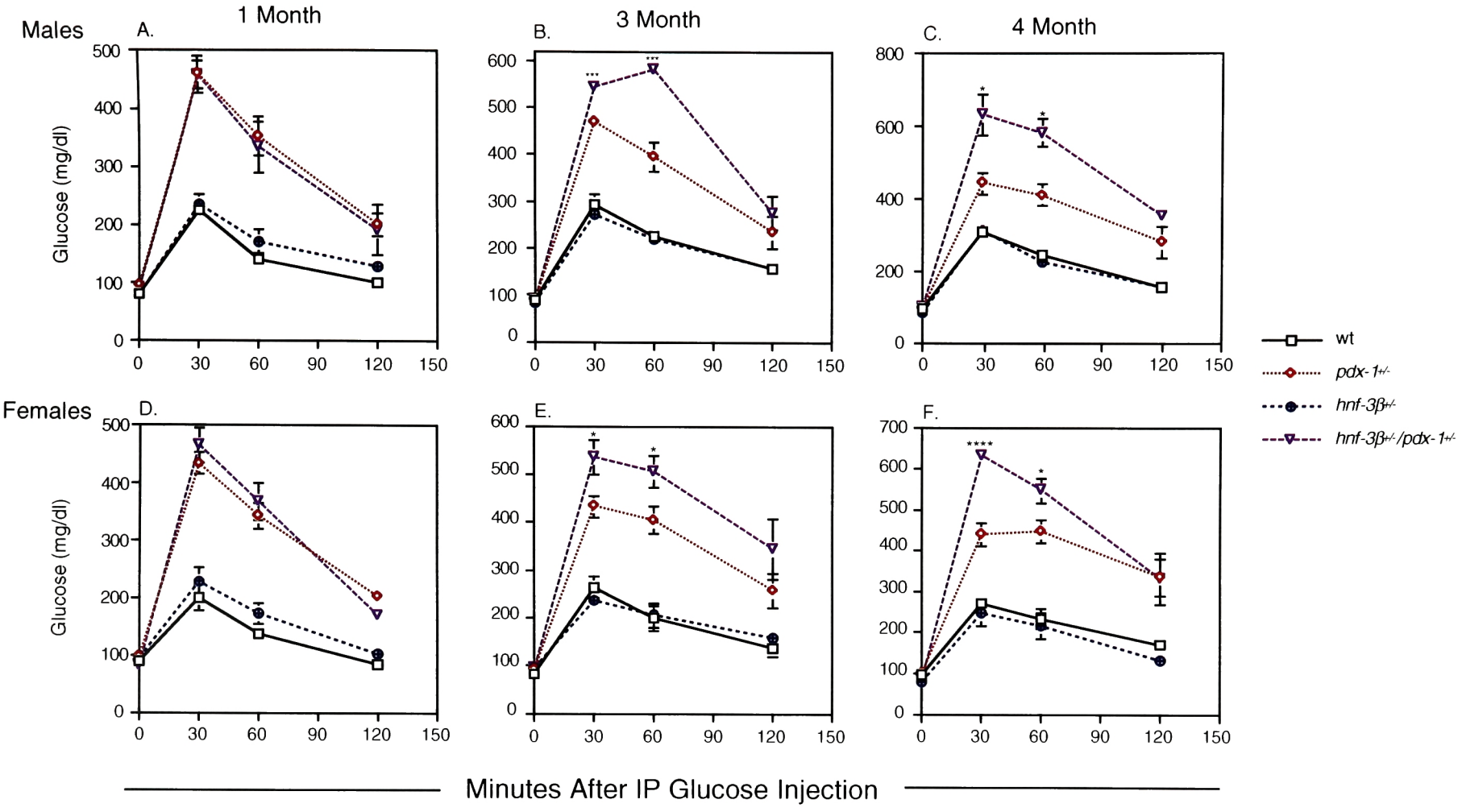

Figure 4-3: Impairment of glucose homeostasis in *pdx-1*$^{+/-}$*/hnf-3β*$^{+/-}$ mice. IPGTT was performed in wildtype (*wt*) (black), *hnf-3β*$^{+/-}$ (blue), *pdx-1*$^{+/-}$ (red), and *pdx-1*$^{+/-}$*/hnf-1α*$^{+/-}$ (purple) littermates at 1, 3 and 4 month of age. The IPGTT of *pdx-1*$^{+/-}$*/hnf-1α*$^{+/-}$ mice were indistinguishable from *pdx-1*$^{+/-}$ littermates at 1 month but blood glucose levels increased in male and female mice after 3 months. A worsening of the glucose tolerance was seen in all double heterozygous animals. *: $p \leq 0.05$, **: $p \leq 0.01$, ***:$p \leq 0.005$, ****:$p \leq 0.0001$.

of elevated fasting and ad lib plasma glucose levels than *pdx-1*$^{+/-}$*/hnf-3β*$^{+/-}$ animals. Despite the variability in the severity of the diabetic phenotype, both *pdx-1*$^{+/-}$*/hnf-3β*$^{+/-}$ and *pdx-1*$^{+/-}$*/hnf-1α*$^{+/-}$ mice exhibit an age-dependent progressive impairment in their ability to dispose of a glucose load. The worsening of the *pdx-1*$^{+/-}$ phenotype suggest that significant synergistic effects exist between Hnf-1α and Hnf-3β with Pdx-1, and that their interactions regulate glucose homeostasis.

Insulin Secretion Defects in *pdx-1*$^{+/-}$*/hnf-3β*$^{+/-}$ and *pdx-1*$^{+/-}$*/hnf-1α*$^{+/-}$ Mice

To further evaluate the synergistic interaction between Hnf-1α and Hnf-3β with Pdx-1, insulin release was measured in response to stimulation with glucose. Glucose-stimulated insulin release from *pdx-1*$^{+/-}$*/hnf-1α*$^{+/-}$ and *pdx-1*$^{+/-}$*/hnf-3β*$^{+/-}$ mice was compared to the *pdx-1*$^{+/-}$ animals to better assess the worsening of the diabetic phenotype. In both male and female controls (wt, *hnf-3β*$^{+/-}$, and *hnf-1α*$^{+/-}$), a three to six-fold increases in insulin levels were observed within two minutes after an intraperitoneal (IP) glucose injection (Fig. 4-4 and 4-5). Serum insulin levels in control mice remained higher than baseline values for up to 60 minutes, indicating an effective second phase insulin secretion response (Fig. 4-4 and 4-5). The *pdx-1*$^{+/-}$ mice exhibited a markedly impaired acute 1st and 2nd phase insulin secretion response. In spite of the secretion defect in *Pdx-1*$^{+/-}$ mice, insulin levels gradually rose, and by 120 minutes after glucose load, the insulin levels were not significantly different between *pdx-1*$^{+/-}$ and control mice. In contrast, the acute insulin response was virtually absent in *pdx-1*$^{+/-}$*/hnf-1α*$^{+/-}$ mice, and insulin secretion was reduced throughout the IPGTT when compared to *pdx-1*$^{+/-}$ mice (Fig. 4-4). Similarly, *pdx-1*$^{+/-}$*/hnf-3β*$^{+/-}$ mice also lost the first phase insulin response. However, insulin levels were not significantly different from the control mice at the two-hour point

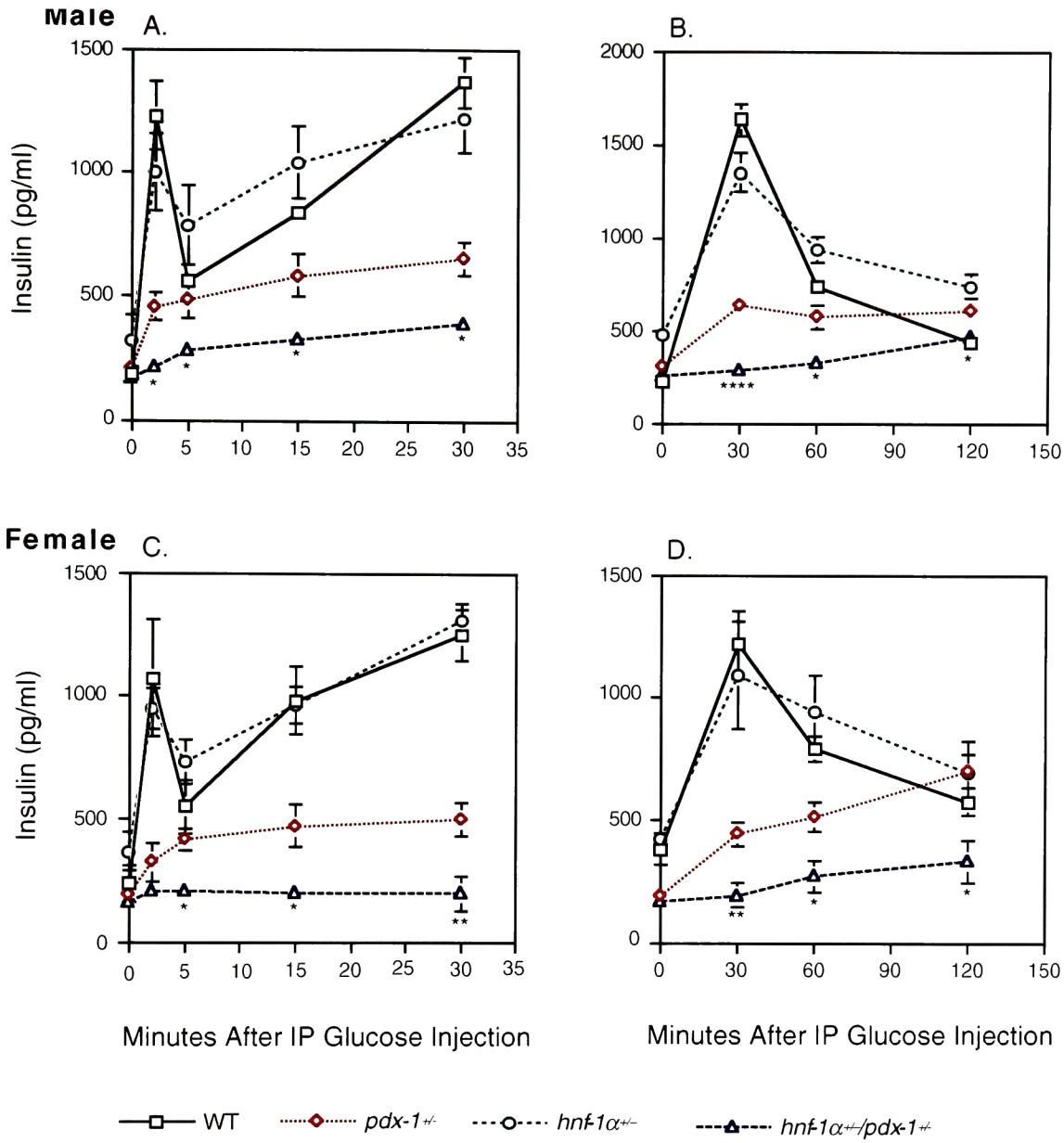

Figure 4-4: Insulin secretion defects in *pdx-1$^{+/-}$/hnf-1α$^{+/-}$* mice. Glucose (3 g/kg body weight) was injected intraperitonally to 5 month old male (A, B) and female (C, D) mice. The left panel (A, C) shows acute insulin secretion responses, the right panel (B, D) displays insulin levels after glucose challenge over a 2 hour period. The data of the left and right panels were collected independently and mice were allowed to recover for one week. Male and female *pdx-1$^{+/-}$/hnf-1α$^{+/-}$* mice show a complete loss of first phase insulin response and a blunted second phase insulin response compared to *pdx-1$^{+/-}$* littermates. *: $P \leq 0.05$, **: $p \leq 0.01$, ***: $p \leq 0.005$, ****: $p \leq 0.0001$.

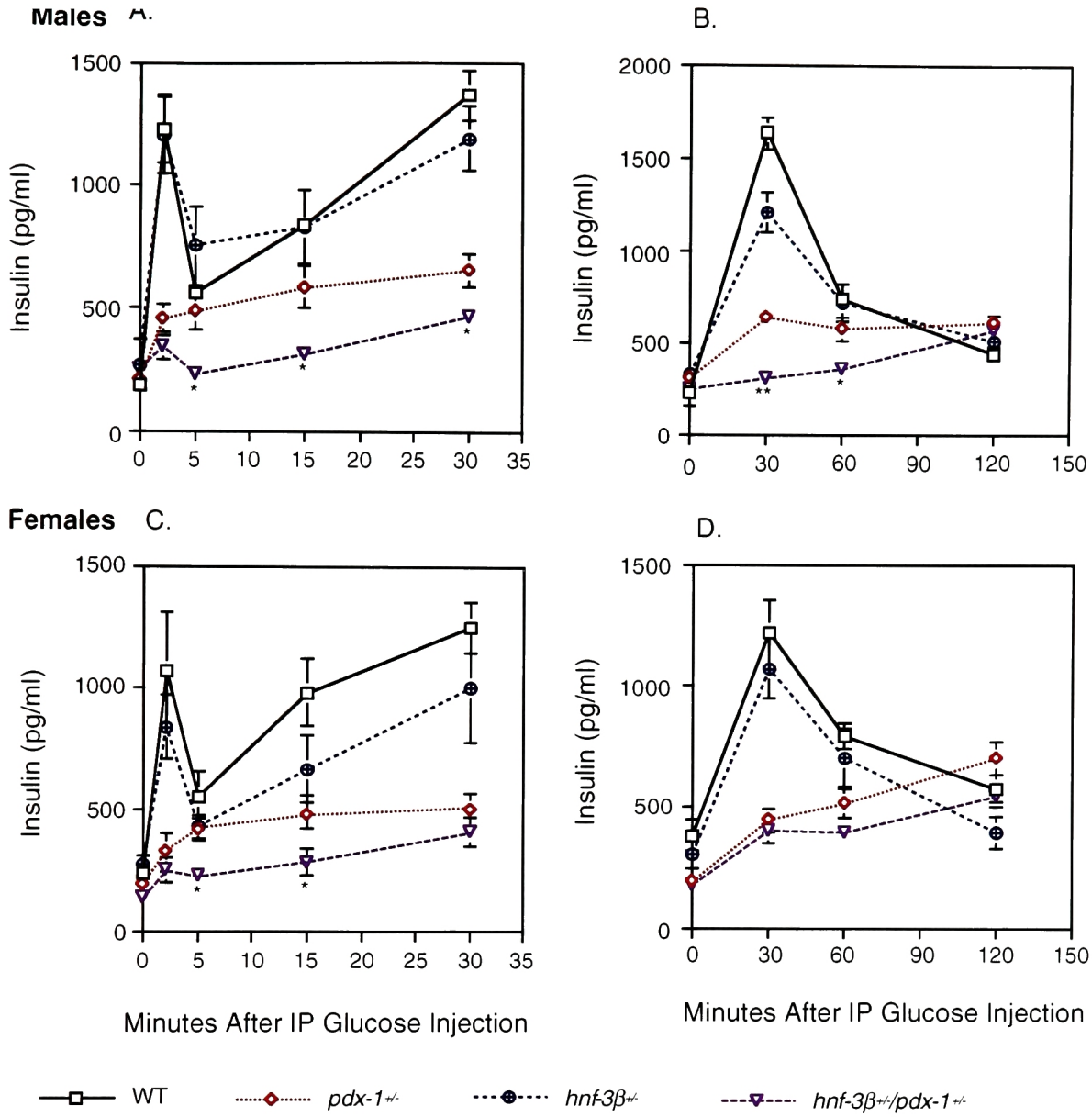

Figure 4-5: Insulin secretion defects in *pdx-1*$^{+/-}$*/hnf-3β*$^{+/-}$ mice. Glucose (3 g/kg body weight) was injected intraperitonally to 5 month old male (A, B) and female (C, D) mice. The left panel (A, C) shows acute insulin secretion responses, the right panel (B, D) displays insulin levels after glucose challenge over a 2 hour period. The data of the left and right panels were collected independently and mice were allowed to recover for one week. A significantly blunted first phase insulin secretion response was observed in male and female *pdx-1*$^{+/-}$*/hnf-3β*$^{+/-}$ mice as compared to compared to *pdx-1*$^{+/-}$ littermates. *: $P \leq 0.05$, **: $p \leq 0.01$, ***: $p \leq 0.005$, ****: $p \leq 0.0001$.

Table 4-1. Plasma Metabolic Parameters of 5 Month Old Mice

	Genotype						*p*					
	Wildtype	Pdx $^{+/-}$	HNF3 β	Pdx $^{+/-}$, HNF3 β	HNF1 α	Pdx $^{+/-}$, HNF1 α	Pdx $^{+/-}$/HNF3 β $^{+/-}$ vs.			Pdx $^{+/-}$, HNF1 α $^{+/-}$ vs.		
							Wildtype	Pdx $^{+/-}$	HNF3 β	Wildtype	Pdx $^{+/-}$	HNF1 α
n	6	6	5	5	5	5	-	-	-	-	-	-
Glucose (f) (mg/dL)	87.3±4.3	94.7±4.3	87.8±5.69	81.6±4.9	85.9±3.9	135.8±10.6	0.76	0.61	0.81	0.02	0.04	0.02
Glucose (p) (mg/dL)	125.7±4.0	167.4±4.5	133.4±7.2	196.1±13.6	138.6±2.5	188.6±9.9	0.01	0.02	0.01	0.02	0.03	0.02
Glucagon (pg/mL)	134.3±5.9	122.5±12.5	138.7±7.1	135.7±8.6	127.0±10.7	135.8±10.6	0.89	0.41	0.79	0.91	0.48	0.58
Fatty Acid (mMol/L)	0.3±0.02	0.4±0.02	0.3±0.03	0.3±0.02	0.3±0.01	0.4±0.02	0.27	0.46	0.43	0.19	0.87	0.23
Glycerol (mg/dL)	12.4±0.8	13.6±1.0	11.5±0.5	12.2±0.7	12.7±1.4	13.7±1.4	0.79	0.26	0.46	0.45	0.95	0.61
Triglyceride (mg/dL)	50.0±2.8	66.1±3.0	50.8±4.1	57.0±4.2	56.5±2.6	66.5±4.0	0.84	0.12	0.32	0.13	0.94	0.08
Choldesterol (mg/dL)	70.9±3.0	75.4±2.7	63.9±4.0	64.4±2.9	70.6±4.9	79.2±2.6	0.15	0.02	0.93	0.06	0.34	0.17
Bile Acid (uMol/ L)	3.9±0.7	3.9±0.5	3.5±0.6	3.9±0.5	4.2±0.3	4.2±0.2	0.99	0.99	0.56	0.75	0.66	0.99

The data represent mean ± SEM.
(f)= fasted, (p)= postprandial

(Fig. 4-5). These results suggest that synergistic interactions between Hnf-1α, Hnf-3β, and Pdx-1 profoundly affect insulin secretion and glucose homeostasis in mice.

Since Hnf-1α, Hnf-3β, and Hnf-4α are also expressed in liver and pancreatic α-cells, we investigated the levels of surrogate markers produced in these tissues that can influence glucose homeostasis. Serum glucagon, fatty acid, glycerol, cholesterol and bile acid levels in single and combined heterozygous mutant mice were indistinguishable from wt mice (Table 4-1). These data further support the notion that impaired glucose homeostasis in *pdx-1*$^{+/-}$*/hnf-1α*$^{+/-}$ and *pdx-1*$^{+/-}$*/hnf-3β*$^{+/-}$ mice is primarily due to a pancreatic β-cell defect.

Morphological Analysis of Pancreatic Islets

Several mechanisms could account for the observed deterioration of *pdx-1*$^{+/-}$ diabetic phenotype in *pdx-1*$^{+/-}$*/hnf-1α*$^{+/-}$ and *pdx-1*$^{+/-}$*/hnf-3β*$^{+/-}$ mice including changes in islet cell lineage allocation, alterations in islet architecture, and/or abnormalities in the expression of genes that mediate insulin secretion. Epistatic interactions between Hnf-1α and Hnf-3β with Pdx-1 could result in a decrease in insulin-producing β, thus reducing β-cell mass and altering α- to β- cell ratio. This possibility is relevant in light of recent Pdx-1 gene targeting experiment. Loss of Pdx-1 expression leads to pancreatic agenesis and β-cell specific abolition indicates that the Pdx-1 is required for late differentiation or maturation of the pancreatic β-cells (54-56). Therefore reducing the amount of Hnf-1α and Hnf-3b in Pdx-1 haploinsufficient state may lead to decreased β-cell mass.

To evaluate whether the alterations in islet function were associated with any changes in morphology, we carried out immunofluorescent analysis of pancreata from wt, *pdx-1*$^{+/-}$, *hnf-1α*$^{+/-}$, *hnf-3β*$^{+/-}$, *pdx-1*$^{+/-}$*/hnf-1α*$^{+/-}$ and *pdx-1*$^{+/-}$*/hnf-3β*$^{+/-}$ mice. Islet

Table 4-2. Morphometric analysis of pancreata of 5-month-old mice

	Genotype					
	Wildtype	**Pdx$^{+/-}$**	**Hnf-3β$^{+/-}$**	**Pdx$^{+/-}$, Hnf-3β$^{+/-}$**	**Hnf-1α$^{+/-}$**	**Pdx$^{+/-}$, Hnf-1α$^{+/-}$**
Avg. β-cell area (μm^2)	13792±1789	11437±2599 *P* = 0.7	12737±2681 *P* = 0.7	11845±2552 *P* = 0.5	13602±3147 *P* = 0.6	13346±2080 *P* = 0.6
Avg. α-cell area (μm^2)	1906±264	1534±288 *P* = 0.6	1699±281 *P* = 0.7	1814±323 *P* = 0.5	1640±365 *P* = 0.8	2070±265 *P* = 0.2
β-Cell:Total pancreas	0.0088	0.0099	0.011	0.010	0.012	0.0094
α-Cell:Total pancreas	0.0012	0.0013	0.0015	0.0016	0.0015	0.0015
Islets examined	32	27	28	27	21	33
α-Cell:β-Cell	0.138	0.134	0.133	0.153	0.121	0.155

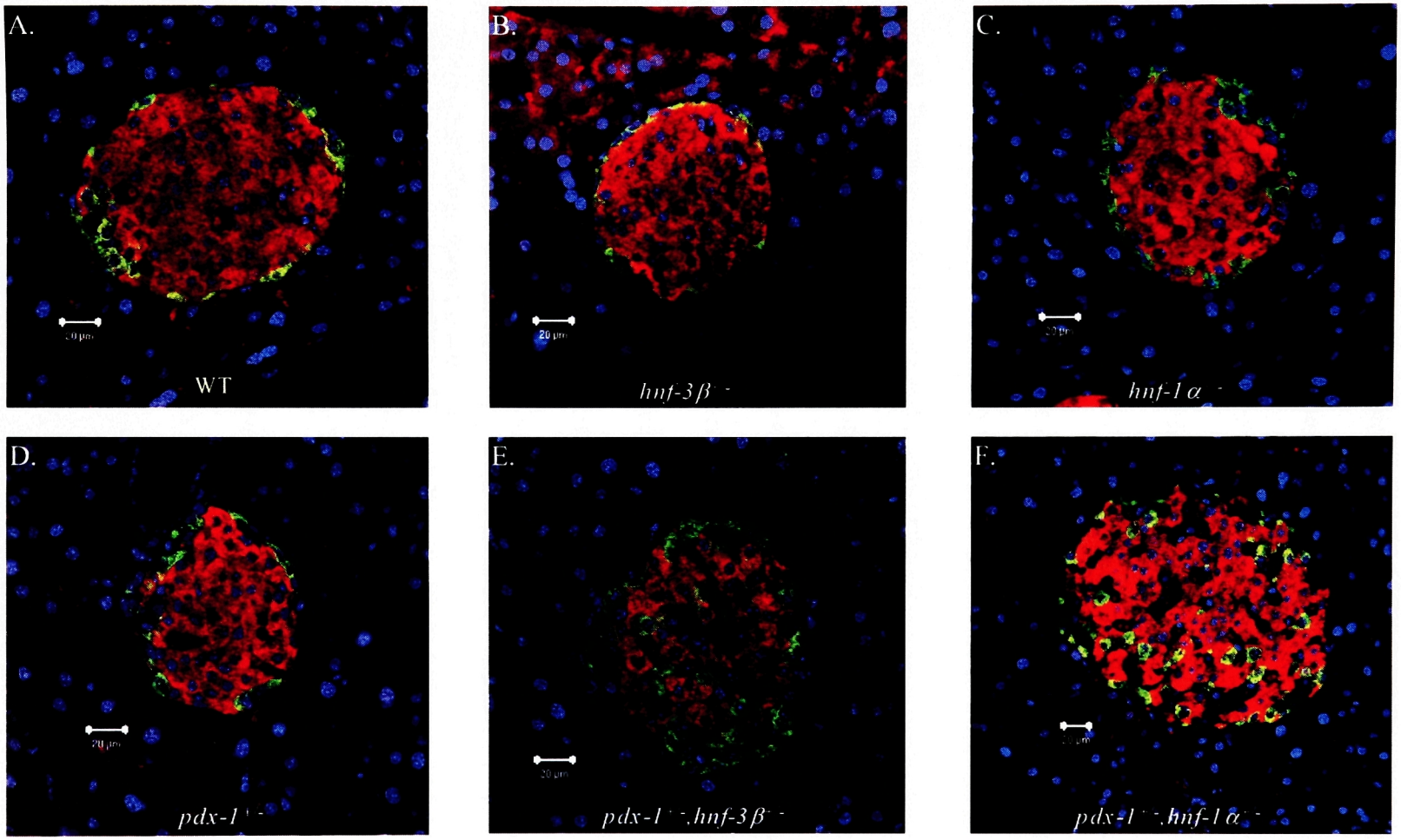

Figure 4-6: Islet morphology in *pdx-1* $^{+/-}$*/hnf-3* $\beta^{+/-}$ and *pdx-1* $^{+/-}$*/hnf-1* $\alpha^{+/-}$ mice. Immunofluorescent confocal microsopy of pancreatic islets of wildtype (A), *hnf-3* $\beta^{+/-}$ (B), *hnf-1* $\alpha^{+/-}$ (C), *pdx-1* $^{+/-}$ (D), *pdx-1* $^{+/-}$*/hnf-3* $\beta^{+/-}$ (E) and *pdx-1* $^{+/-}$*/hnf-1* $\alpha^{+/-}$ (F) mice. Insulin-expressing cells are shown in red, glucagon containing cells in green. Nuclei of respective cells are shown in blue. Islets from *pdx-1* $^{+/-}$*/hnf-3* $\beta^{+/-}$ (E) and *pdx-1* $^{+/-}$*/hnf-1* $\alpha^{+/-}$ (F) mice show scattered α-cells throughout the islets. Pancreatic islet size was not significantly different in the different mutant mice.

composition was assessed quantitatively by immunostaining with insulin and glucagon antibodies to visualize β- and α-cells, respectively. Morphometric analysis of pancreatic sections showed no apparent difference in total pancreatic islet area or in α- to β-cells ratio between wt and mutant islets (Table 4-2). Thus, it is unlikely that a reduction of β-cell size/number leads to the diabetic phenotype in double-mutant mice.

Wildtype, *pdx-1*$^{+/-}$, *hnf-1α*$^{+/-}$, and *hnf-3β*$^{+/-}$ mice display characteristic islet architecture where β-cells, the predominant cell type in the islets, form the core of the normal islet and are surrounded by α-cells which are confined to the periphery (Fig. 4-6A to D). In contrast, the characteristic islet architecture, specifically the confinement of α-cells to the periphery of islet, was disorganized in *pdx-1*$^{+/-}$*/hnf-3β*$^{+/-}$ and *pdx-1*$^{+/-}$*/hnf-1α*$^{+/-}$ mice (Fig. 4-6E, F). Even though the islet topology was disturbed, there was no inappropriate coexpression of islet hormones in any endocrine cells examined (i.e. no yellow cells were observed in the merged images), suggesting that islet cell lineage allocation was not impaired. These results indicate that the abnormal islet morphology could contribute to the phenotype of the combined heterozygous mutant mice.

Pancreatic Gene Expression

To determine more precisely why β-cell function was compromised *in pdx-1*$^{+/-}$*/hnf-3β*$^{+/-}$ and *pdx-1*$^{+/-}$*/hnf-1α*$^{+/-}$ mice, steady-state mRNA profiles of transcription factors, hormones, and components of the glucose-stimulated insulin secretion pathway that are essential for β-cell activity were generated by RT-PCR from wt and mutant islet RNA. Significant changes in expression from genes present in each effector category were identified in the combined heterozygous mutant mice (Fig. 4-7, Table 4-3).

Pdx-1 mRNA levels were moderately reduced in *hnf-3β*$^{+/-}$ mice (24%) and

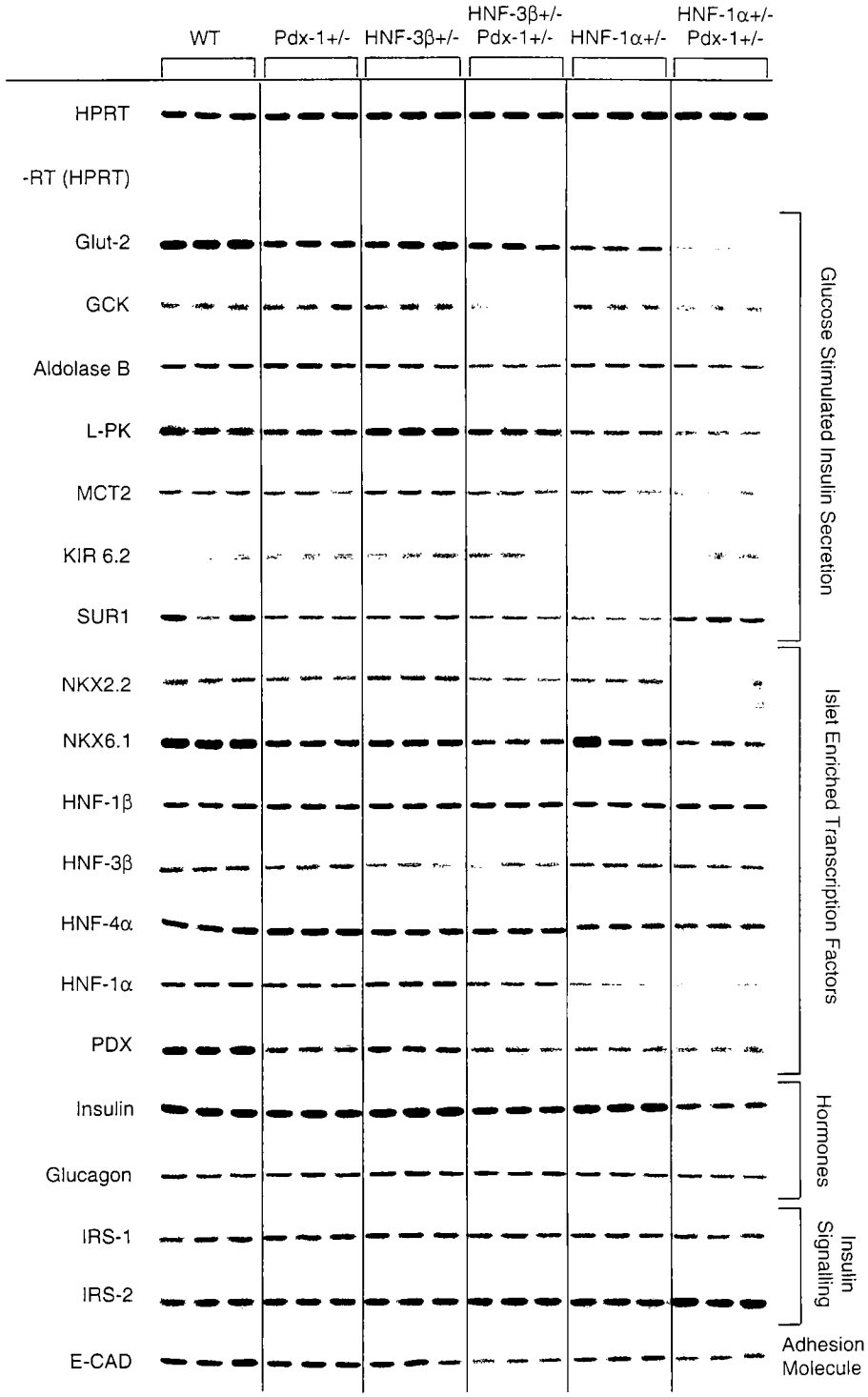

Figure 4-7. Pancreatic islet gene expression analysis. Steady-state mRNA levels of pancreatic islet enriched genes of wildtype, *pdx-1*$^{+/-}$, *hnf-3β*$^{+/-}$, *hnf-1α*$^{+/-}$, *pdx-1*$^{+/-}$*/hnf-3β*$^{+/-}$ and *pdx-1*$^{+/-}$*/hnf-1α*$^{+/-}$ mutant mice. The housekeeping gene hypoxanthine phosphoribosyltransferase (*Hprt*) was amplified to show that each sample contained similar amounts of mRNA. A lack of any amplification signal in reactions without reverse transcriptase (-RT) shows that genomic DNA did not contaminate the samples. Transcript levels were measured in 3 animals for each genotype by RT-PCR using [α-^{32}P]dCTP. PCR products were separated by PAGE, and bands were visualized by autoradiography.

	Genotype						*p*			
	Wildtype	Pdx-1$^{+/-}$	Hnf-3β$^{+/-}$	Pdx-1$^{+/-}$, Hnf-3β$^{+/-}$	Hnf-1α$^{+/-}$	Pdx-1$^{+/-}$, Hnf-1α$^{+/-}$	Pdx-1$^{+/-}$/Hnf-3β$^{+/-}$ vs.		Pdx-1$^{+/-}$/Hnf-1α$^{+/-}$ vs.	
							Pdx-1$^{+/-}$	Hnf-3β$^{+/-}$	Pdx-1$^{+/-}$	Hnf-1α$^{+/-}$
Hprt	5.0±0.1	5.1±0.1	5.1±0.2	5.0±0.1	5.1±0.2	5.1±0.1	0.288	0.567	0.725	0.999
Pdx-1	6.3±0.3	3.9±0.1	4.8±0.3	3.1±0.2	3.7±0.2	2.2±0.2	0.003	0.002	0.001	0.002
Hnf-1α	3.3±0.1	2.8±0.2	3.5±0.1	2.6±0.1	2.0±0.1	1.4±0.2	0.151	0.002	0.0003	0.006
Hnf-1β	4.0±0.3	4.0±0.1	4.2±0.2	4.0±0.2	3.7±0.1	3.8±0.2	0.999	0.281	0.221	0.496
Hnf-3β	3.1±0.2	2.9±0.2	2.5±0.3	2.4±0.2	3.0±0.3	2.8±0.1	0.024	0.461	0.387	0.264
Hnf-4α	5.1±0.2	5.5±0.1	5.0±0.2	4.9±0.2	4.5±0.2	4.3±0.3	0.006	0.252	0.013	0.337
Nkx2.2	2.3±0.2	1.7±0.1	2.5±0.1	1.5±0.1	1.6±0.2	1.1±0.1	0.071	0.0005	0.002	0.047
Nkx6.1	6.8±0.2	3.9±0.2	5.0±0.3	2.9±0.4	5.7±1.5	2.1±0.4	0.031	0.002	0.011	0.048
Glut-2	6.5±0.4	4.2±0.4	5.2±0.5	4.1±0.5	2.9±0.2	1.1±0.1	0.927	0.045	0.003	0.001
Gck	1.8±0.2	2.5±0.3	2.2±0.5	1.1±0.1	2.2±0.4	1.2±0.1	0.008	0.047	0.011	0.033
Aldo-B	3.1±0.1	3.6±0.3	3.1±0.4	1.8±0.2	2.8±0.1	1.8±0.3	0.002	0.012	0.001	0.011
L-Pk	4.8±0.3	4.8±0.3	5.3±0.2	4.6±0.2	2.5±0.1	1.7±0.1	0.251	0.004	0.002	0.002
Kir6.2	1.2±0.3	1.4±0.2	1.6±0.2	1.5±0.3	1.0±0.1	1.4±0.2	0.502	0.631	0.999	0.094
Sur1	4.0±2.0	2.5±0.2	2.6±0.2	2.1±0.3	1.8±0.1	2.9±0.6	0.115	0.054	0.384	0.087
E-Cad	5.0±0.3	4.8±0.2	4.5±0.6	2.6±0.4	4.0±0.1	2.8±0.4	0.071	0.0005	0.002	0.022
Ins	6.2±0.2	5.7±0.2	6.2±0.3	5.1±0.2	6.0±0.4	3.1±0.4	0.009	0.012	0.003	0.0006
Glucag	2.8±0.2	2.8±0.2	3.0±0.2	2.7±0.2	2.5±0.2	2.3±0.3	0.612	0.141	0.072	0.299

Table 4-3. Quantative measurement of expression alterations in combined haploinsufficiencies of Pdx-1 with either Hnf-1α or Hnf-3β. Quantitative measurements of gene expression were obtained by densitometry and the mean of measurements are shown ± STD. The levels of significance of the different comparisons (single vs. double heterozygous mutant) iare shown on the right.

decreased in *pdx-1*$^{+/-}$, *hnf-1α*$^{+/-}$, *pdx-1*$^{+/-}$*/hnf-1α*$^{+/-}$ and *pdx-1*$^{+/-}$*/hnf-3β*$^{+/-}$ animals by 38%, 41%, 65%, and 51%, respectively (Fig. 4-7, Table 4-3). These results are consistent with previous reports suggesting that Hnf-3β and Hnf-1α are regulators of *Pdx-1* gene expression (57-59, 146). Hnf-1α mRNA levels were only reduced in *hnf-1α*$^{+/-}$ and *pdx-1*$^{+/-}$*/hnf-1α*$^{+/-}$ mice whereas Hnf-1α mRNA levels were similar in all different genotypes (Fig. 4-7, Table 4-3). Hnf-4α expression levels were marginally reduced in *hnf-1α*$^{+/-}$ and *pdx-1*$^{+/-}$*/hnf-1α*$^{+/-}$ mice, indicating that the MODY1 gene may be regulated by Hnf-1α. Interestingly, Nkx6.1 expression was reduced in *pdx-1*$^{+/-}$ and *hnf-3β*$^{+/-}$ mice as well as in combined heterozygous *pdx-1*$^{+/-}$*/hnf-3β*$^{+/-}$ and *pdx-1*$^{+/-}$*/hnf-1α*$^{+/-}$ mice, but not in *hnf-1α*$^{+/-}$ animals, suggesting Nkx6.1 is regulated by Hnf-3β, Pdx-1 (Fig. 4-7, Table 4-3). Expression levels of Nkx2.2 were diminished in *pdx-1*$^{+/-}$ and in double heterozygous mutant mice, indicating that reduced Nkx2.2 expression is mainly mediated by Pdx-1 (Fig. 4-7, Table 4-3). Islet glucagon mRNA levels were similar in all mutants studied, supporting our immunohistological findings that indicated normal α-cell differentiation and similar α-cell to β-cell ratios between islets of wt and various mutants.

Decreased insulin transcript levels (11% and 46%, respectively) were detected in *pdx-1*$^{+/-}$*/hnf-3β*$^{+/-}$ and *pdx-1*$^{+/-}$*/hnf-1α*$^{+/-}$ mutants compared with *pdx-1*$^{+/-}$ (Fig. 4-7, Table 4-3), indicating that a reduction in insulin gene transcription may contribute to the insulin secretion defect in these mice. In addition, we found a number of changes in the expression of genes that are responsible for glucose-stimulated insulin secretion. The expression of Glut-2 was reduced in *pdx-1*$^{+/-}$ (35%, $p<0.05$), *hnf-1α*$^{+/-}$ (55%, $p<0.01$), *pdx-1*$^{+/-}$*/hnf-3β*$^{+/-}$ (37%, $p<0.05$) and *pdx-1*$^{+/-}$*/hnf-1α*$^{+/-}$ (83%, $p<0.001$) compared with wt animals, indicating that both Pdx-1 and Hnf-1α, but not Hnf-3β, are important regulators

of Glut-2 expression (Fig. 4-7, Table 4-3). There was a synergistic effect on Glut-2 expression in mice that were haploinsufficient for both *pdx-1* and *hnf-1α* genes. Liver pyruvate kinase mRNA levels were reduced in *hnf-1α*$^{+/-}$ animals and *hnf-1α*$^{+/-}$/*pdx-1*$^{+/-}$ mice and the expression pattern correlates best with this gene being under the transcriptional control of Hnf-1α. Expression levels of the gene encoding Gck, which operates at the rate-limiting step of glycolysis, were reduced in double heterozygous mutants compared with *pdx-1*$^{+/-}$ mice (56% and 52% for *pdx-1*$^{+/-}$/*hnf-3β*$^{+/-}$ and *pdx-1*$^{+/-}$/*hnf-1α*$^{+/-}$, respectively) (Fig. 4-7, Table 4-3).

To identify genes that may contribute to the abnormal islet morphology in the double heterozygous mice, we also investigated the expression levels of E-cadherin, a transmembrane domain glycoprotein that mediates cell-cell adhesion in the gastrointestinal tract and endocrine pancreas (148). Interestingly, expression levels of E-cadherin were significantly reduced in *pdx-1*$^{+/-}$/*hnf-1α*$^{+/-}$ and *pdx-1*$^{+/-}$/*hnf-3β*$^{+/-}$ animals (44% and 48%, respectively) (Fig. 4-7, Table 4-3), suggesting a possible role for E-cadherin in islet architecture of these mice.

As described above, compound heterozygous of *pdx-1*$^{+/-}$/*hnf-4α*$^{+/-}$, *hnf-3β*$^{+/-}$/*hnf-4α*$^{+/-}$ and *hnf-1α*$^{+/-}$/*hnf-4α*$^{+/-}$ mice do not have a worsened phenotype than is seen in single-mutant mice alone. These findings were surprising since heterozygous inactivation of *HNF-4α*, like *HNF-1α*, in humans is associated with the development of MODY. To study the possible mechanism(s) that confer(s) relative protection to the development of diabetes on an *hnf-4α*$^{+/-}$ genetic background we assayed gene expression in pancreatic islets of mice with one or two functional *hnf-4α* alleles. We did not detect a significant down regulation in the expression of any transcription factor including Hnf-4α, or gene

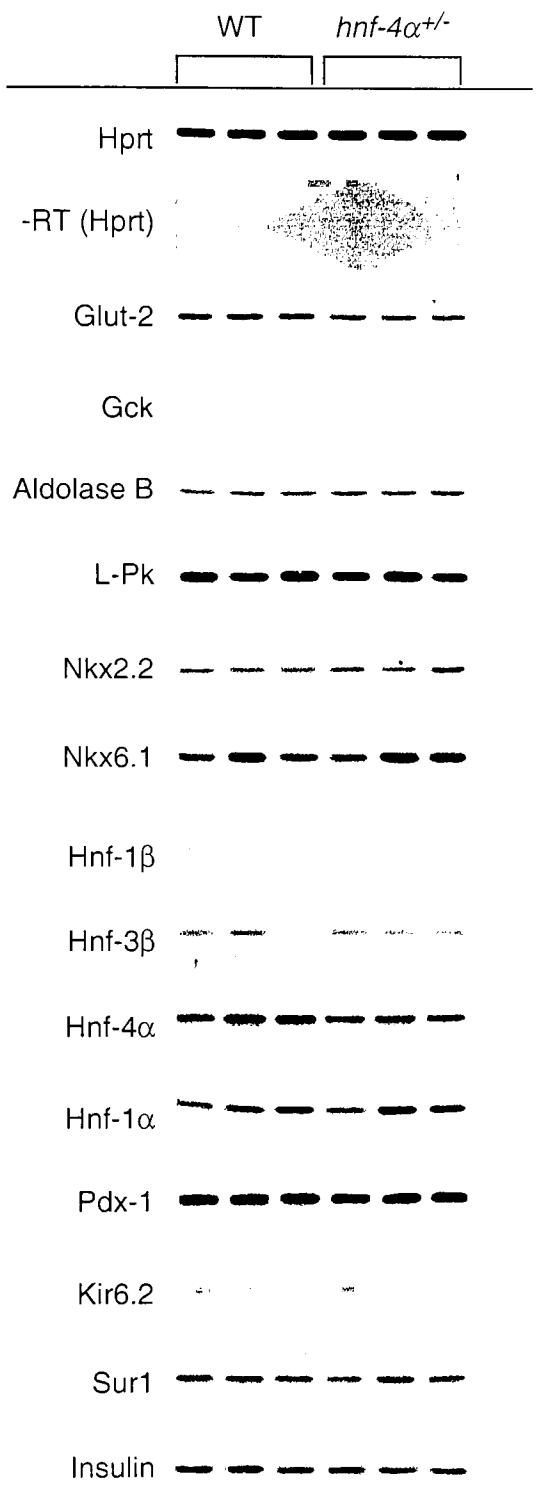

Figure 4-8. Gene expression profile of *hnf-4α*$^{+/-}$ islets. Steady-state mRNA levels of pancreatic islet enriched genes of wildtype and *hnf-4α*$^{+/-}$ mutant mice. The housekeeping gene hypoxanthine phosphoribosyltransferase (Hprt) was amplified to show that each sample contained similar amounts of mRNA. A lack of any amplification signal in reactions without reverse transcriptase (-RT) shows that genomic DNA did not contaminate the samples. Transcript levels were measured in 3 animals for each genotype by RT-PCR using [α-^{32}P]dCTP. PCR products were separated by PAGE, and bands were visualized by autoradiography.

that is involved in glucose-stimulated insulin secretion, such as Glut2, Gck, L-Pk and aldolase B (Fig. 4-8). Moreover, known target genes of Hnf-4α such as aldolase B and Hnf-1α were not reduced in *hnf-4α*$^{+/-}$ mice compared to wt animals. This is in contrast to our findings in *hnf-1α*$^{+/-}$ mice, which displays reduced levels of Glut-2, L-Pk, Hnf-4α, Hnf-1α and Pdx-1 mRNA. Our results therefore suggest that, in mice, Hnf-4α can compensate for allelic loss by up-regulating the expression of its remaining functional allele.

Discussion

Type 2 diabetes is a polygenic disease and genetic predisposition to this condition is likely due to changes in expression and/or activity of proteins important in insulin sensitivity and normal pancreatic islet function. However, a mutation in a susceptibility gene often does not result in diabetes unless present in combination with another, which together result in impaired glucose homeostasis. Such gene-gene interactions within the insulin-signaling pathway have been shown upon combining specific inactivating gene mutations in mice that are predisposed to insulin resistance (149-151). For instance, plasma insulin levels increased by almost 50-fold in mice with combined haploinsufficiencies in the insulin receptor (ir) and insulin receptor substrate-1 (*irs-1*) genes, with approximately 40% of the *ir*$^{+/-}$*/irs-1*$^{+/-}$ mice becoming overtly diabetic at 4-6 months of age (149). Interestingly, islet mass was greatly expanded in these diabetic mice as means of producing more insulin to aid in glucose clearance. Although the islet has clearly been shown to have a central role in regulating glucose homeostasis, little is known about how this process is influenced by epistatic interactions between factors critical for pancreatic β-cell function. In this study, we have shown that a combination of

heterozygous deletions in certain subsets of the islet transcription factor network can act synergistically to cause diabetes.

Allelic loss of *hnf-1α* and *hnf-3β*, athough having no effect on glucose homeostasis as single mutants, markedly worsened the diabetic phenotype in *pdx-1*$^{+/-}$ mice. Pdx-1 is a key effector of glucose sensing due to its action on Glut-2, insulin, and Gck expression. Insulin secretion and blood glucose levels were compromised in both female and male double mutant mice. These results are consistent with recent findings showing that Hnf-3β and Hnf-1α directly activate *pdx-1* transcription (39, 57-59, 146). In contrast, allelic loss of function of Hnf-3α or Hnf-4α with Pdx-1 haploinsufficiency revealed no synergism between these genes and did not alter the phenotype of *pdx-1*$^{+/-}$ mice. Furthermore, *hnf-1α*$^{+/-}$*/hnf-4α*$^{+/-}$ and *hnf-3β*$^{+/-}$*/hnf-4α*$^{+/-}$ mutant mice have similar blood glucose levels as littermates with single mutations. Together, our *in vivo* data suggest that Hnf-3β, Hnf-1α and Pdx-1 are key components of a common pathway that is essential for normal glucose-induced insulin secretion.

To gain insight into the molecular mechanisms by which β-cell function was impaired in *pdx-1*$^{+/-}$*/hnf-1α*$^{+/-}$ and *pdx-1*$^{+/-}$*/hnf-3β*$^{+/-}$ mice, pancreatic islet gene expression profiles were generated in the individual and combined mutants. Target genes of Hnf-1α and Pdx-1, such as *glut-2*, were significantly reduced in the individual mutants. *L-pk*, a target gene of Hnf-1α, was also reduced in *hnf-1α*$^{+/-}$ mice. In addition, there was a modest reduction in Pdx-1 expression levels in the phenotypically normal *hnf-3β*$^{+/-}$ and *hnf-1α*$^{+/-}$ mice. Interestingly, the *pdx-1*$^{+/-}$*/hnf-1α*$^{+/-}$ and *pdx-1*$^{+/-}$*/hnf-3β*$^{+/-}$ mice exhibited decreased mRNA expression of specific factors involved in regulated islet gene transcription (Pdx-1, Nkx2.2, and Nkx6.1) and glucose-stimulated insulin secretion

signaling (Glut-1, Gck, L-Pk, and aldol-B) (Fig. 4-7). Insulin message was also significantly decreased in the double-heterozygous mutant mice in which Pdx-1 mice was reduced by ≥ 50%. A reduction in Pdx-1 expression of ≥ 50% seems to be a critical threshold for causing a decrease in insulin gene mRNA levels. The insulin mRNA levels found in *pdx-1*$^{+/-}$ islets (i.e. normal) and islets wherein Pdx-1 was selectively removed also support our data (56). Together our findings illustrate that significant synergism exists between the Hnf-3β, Hnf-1α, and Pdx-1 transcription factors in regulating insulin gene transcription and expression of genes involved in glucose-stimulated insulin secretion.

Expression profiling of different mutants revealed that cooperative interactions exist between Hnf-3β and Hnf-1α with Pdx-1 to maintain the genetic program for proper glucose homeostasis. Particularly important are their regulation on islet enriched transccription factors and GSIS signaling components. The islet transcription factors Nkx2.2, Nkx6.1, and Pdx-1 were previously shown to be important for pancreatic β-cell function and their inactivation all lead to severe diabetes in mice (54-56, 144, 152). The components of glucose stimulated insulin secretion regulate various functions of β-cells such as glucose sensing, stimulus-secretion coupling, insulin biosynthesis and processing, and exocytotic machinery. We found that glucose sensing is further impaired when Hnf-3β or Hnf-1α haploinsufficiencies are combined with *pdx-1*$^{+/-}$ mice. Particularly important for glucose sensing are Gck and Glut-2. The low affinity, high capacity glucose transporter Glut-2 transport glucose with the Michaelis-Menten constant (Km) of 18 mM (153). The low affinity Gck then phosphorylates glucose with a Km of 10 mM (153). The physiological ranges of glucose are 5-7 mM. Since Km is defined as the substrate

concentration at which the reaction velocity is half-maximal, the Km of Glut-2 and Gck would enable glucose uptake and phosphorylation when blood glucose is elevated (after a meal), thus serve as glucose sensor of the pancreatic β-cells. However the maximal reaction velocity (Vmax) is dependent on the concentration of the catalysts (Glut-2, and Gck). As a result, if the expression of Glut-2 and Gck are decreased, then the Vmax for the eventual ATP generation would also be decreased, thus compromising glucose sensing and GSIS in *pdx-1*$^{+/-}$*/hnf-1α*$^{+/-}$ and *pdx-1*$^{+/-}$*/hnf-3β*$^{+/-}$ mice.

To begin to address why β-cell function was not compromised in *pdx-1*$^{+/-}$*/hnf-4α*$^{+/-}$, *hnf-4α*$^{+/-}$*/hnf-1α*$^{+/-}$, or *hnf-4α*$^{+/-}$*/hnf-3β*$^{+/-}$ mice, gene expression profiles were generated with islet RNA from wt and *hnf-4α*$^{+/-}$ mice. Interestingly, in contrast to the *hnf-1α*, *hnf-3β* or *pdx-1* haploinsufficiency, the loss of an *hnf-4α* allele did not significantly affect Hnf-4α mRNA expression levels as compared to the wt. In addition, we did not find reduced expression of Pdx-1 or known targets of Hnf-4α (e.g. L-Pk, Hnf-1α, and Aldo-B). These results suggest that mechanism(s) exist(s), possibly through an autoregulatory feedback loop that can compensate for the loss of one *hnf-4α* allele. Furthermore, our results also suggest that factors that do not significantly reduce Pdx-1 gene expression, like *hnf-4α*$^{+/-}$*/hnf-1a*$^{+/-}$ and *hnf-3β*$^{+/-}$*/hnf-4α*$^{+/-}$ (data not shown), are less likely to affect β-cell activity.

To study if allelic variation in *pdx-1*, *hnf-3β* and *hnf-1α* affected islet development, a detailed morphological analysis was performed. We did not detect differences in islet size although marked alterations in architecture were revealed by immunohistological analysis, with α-cells no longer confined to the islet periphery. However, the α-cells in double heterozygous mutant mice appeared to be functional (no

differences in plasma glucagon levels were observed in mice of various genotypes) and present at the same relative ratio to β-cells as in wt. As a change in islet morphology has also been noted in *nkx2.2*, *nkx6.1* and *hnf-3β*-deficient mice (97, 144, 152), the reduced expression levels of these genes in *pdx-1*$^{+/-}$*/hnf-3β*$^{+/-}$ and *pdx-1*$^{+/-}$*/hnf-1α*$^{+/-}$ mice may therefore contribute to this phenotype. In addition, the double heterozygous mice had reduced expression of E-cadherin. E-cadherin is important to regulate adhesion between all pancreatic endocrine cells and to maintain correct islet topology (148, 154). Furthermore, the cell-to-cell contacts mediated by E-cadherin have been shown to be required for insulin secretion in response to nutrient stimuli (155). Therefore, the reduced E-cadherin levels observed in the islets of double mutant mice may not only lead to disorganized islets, but may also contribute to impaired glucose tolerance.

In conclusion, we have created novel polygenic models for progressive pancreatic β-cell failure. Our results provide new molecular insights of how subclinical, genetically predisposing defects in the pancreatic islet transcription network can synergize to develop progressive β-cell failure. Furthermore, these mutant mice provide unique models to dissect the epistatic interactions among different genes in complex pathways that regulate islet morphology and function, and to design specific therapeutic approaches that prevent β-cell failure.

Chapter 5: The Role of Islet-Enriched Transcription Factors in the Development of Pancreatic β-Cells *in vitro*

Introduction

Both type 1 and type 2 diabetes mellitus result from an insufficient pancreatic β-cell mass. Type 1 diabetes mellitus (IDDM) is caused by a polygenic autoimmune disease that leads to the self-destruction of insulin producing pancreatic β-cells. In type 2 diabetes mellitus (NIDDM), the inadequate functional β-cell mass is due to impaired islet function and/or increased insulin demand often caused by insulin resistance. Strict glycemic control through intensive drug (glitazones, sulphonylureas) and/or insulin therapy can significantly retard the morbidity and mortality associated with diabetes (156, 157). However, patient compliance to strict treatment regimen is often poor and thus normoglycemia is not maintained in the majority of cases. In principle, diabetes should be curable by maintaining sufficient β-cell mass through reduction of autoimmune destruction, transplantation of exogenous β-cells, and/or regeneration of islet cells. However, the success of these approaches are limited by the following obstacles: (1) immunosuppressive therapy used to treat autoimmune disease and to reduce graft rejection often themselves lead to diabetogenic side effects (158); (2) prolonged treatment with immunosuppressive agents are associated with several undesirable complications such as development of malignancies and susceptibility to infections; (3) islet transplantation is further limited by the shortage of purified islets from cadaveric donors; (4) the neogenic factor(s) necessary for *in vivo* islet regeneration remained to be identified.

The limitations of the above approaches along with the increased epidemic of diabetes demand a search for alternative source of islet cells. A promising approach to increase functional β-cell mass is to use pluripotent embryonic stem (ES) cells to generate an unlimited supply of insulin producing cells. ES cells are non-transformed cells with normal karyotype, are capable of unlimited, undifferentiated proliferation *in vitro*, have the capacity to regenerate themselves, and can differentiate to generate all of the cell types in an organism (159). ES cells have also been used to study the differentiation of various cell types and tissues *in vitro*, such as neuronal cells (160, 161), hematopoietic lineages (162), and cardiomyocytes (163). Furthermore, these cells have been successfully transplanted into animals, where morphological and functional integration was demonstrated (163, 164). Recently, promising results have been reported for the generation of insulin producing cells from undifferentiated ES cells (165, 166). However, these initial advances suffer from several shortcomings that remain to be conquered. One major limitation is that the current stem cell differentiation protocol resulted in a mixture of cell types and that the percentage of cells expressing insulin at best reached 15% (165, 166). A recent report used cell trapping strategy to increase the functional consistency in the differentiated ES cells (167). However, this method resulted in possibility transformed cells that may have malignant potential. Despite the limitations, these results demonstrated that ES cells can give rise to different cell types of the endocrine pancreas. Furthermore, pure populations of insulin producing cells with the desired phenotypes may be obtained with more elaborate selection and differentiation schemes that are compatible with normal β-cell development. This will most likely require similar patterning, inductive, and cell intrinsic signals that are important for *in*

vivo pancreas development.

The endocrine and exocrine pancreas are derived from the endodermal cells of the upper duodenal region of the foregut (fig. 5-1) (168). The gut epithelium that will become the future dorsal pancreatic bud is initially in direct contact with the notochord (169). At the 13-somite stage around embryonic day 8.5 (E8.5), the notochord secretes a variety of potent signaling molecules such as the TGF-β family member activin-β and fibroblast growth factor (FGF)-2. These two inductive factors have been implicated in the repression of two members of the hedgehog family of signaling molecules, sonic hedgehog (Shh) and indian hedgehog (Ihh), in the presumptive dorsal pancreatic endoderm and thus, allow the formation of the dorsal pancreatic bud and expression of pancreatic marker pdx-1 (170-172). In contrast, the exclusion of Shh and Ihh expression from the ventral pancreatic epithelium may be achieved by a notochord-independent mechanism. The budding of the dorsal and ventral pancreas occurs on E9 and E10.5 respectively (173). The growth, morphogenesis, and differentiation of the dorsal pancreatic bud require the function of two homeobox transcription factors, pancreatic and duodenal homeobox gene-1 (Pdx-1) and homeobox gen-9 (Hlxb9), whereas the function of Hlxb9 is dispensable for the ventral bud (54, 55, 174). A few insulin-expressing cells appear within a day after bud formation, and these early insulin-expressing cells often co-express glucagon (175). Fully differentiated β-cells first appear around E13 at the start of a massive wave of β-cell proliferation and differentiation named the secondary transition (176). Fusion of the dorsal and ventral pancreatic bud occurs around E16/17 (177). The specification of endocrine and exocrine fate utilizes the Notch signaling pathway and lateral specification analogous to mammalian neurogenesis (fig. 5-1) (178, 179). Cells

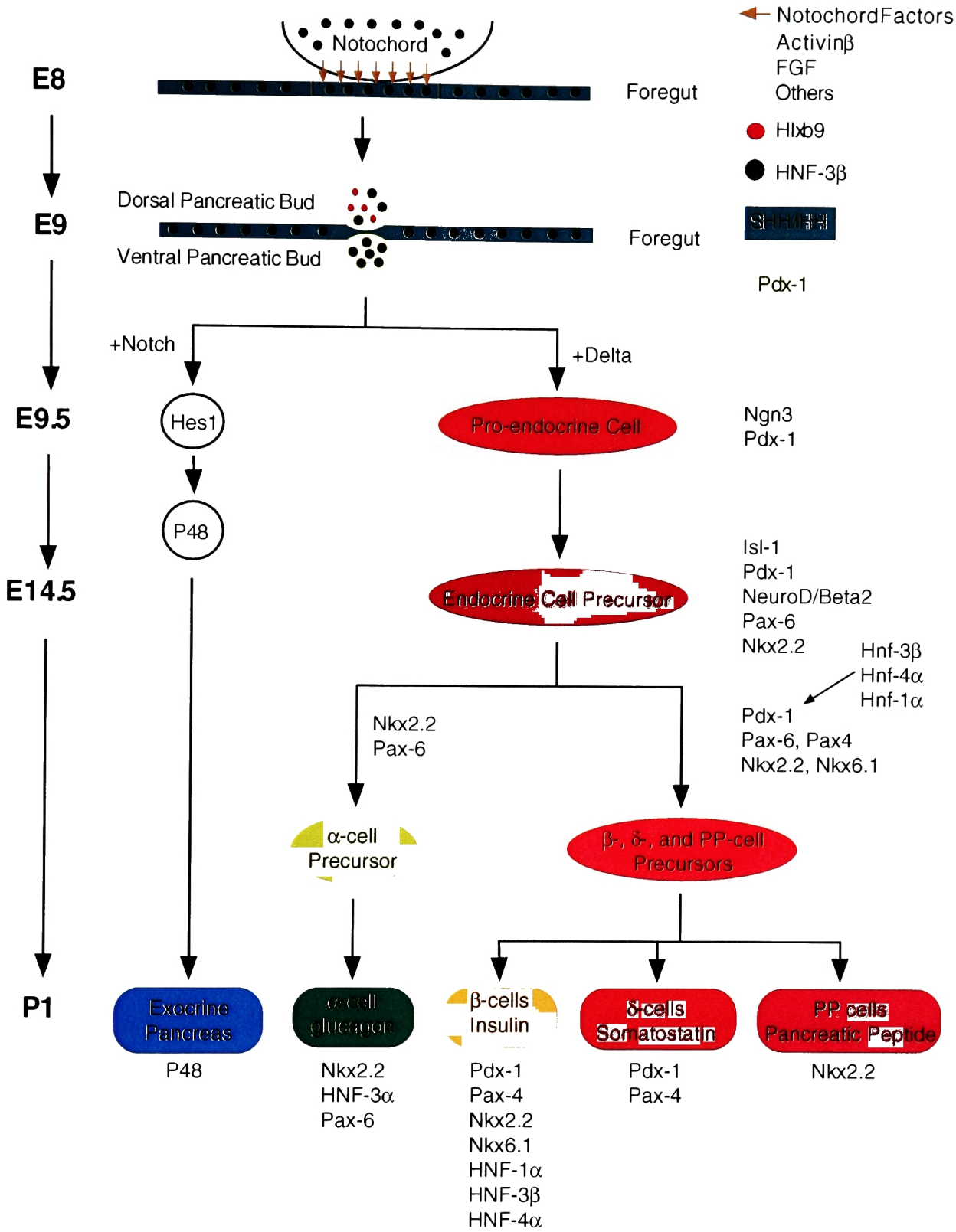

Figure 5-1. Proposed model for pancreatic cell differentiation. This diagram shows the cell extrinsic and intrinsic factors that are vital for pancreatic development. The numbers on the left (E8-P1) indicate the approximate time in the requirement of these factors.

with active Notch-signaling express the bHLH class transcription factor P48, which is required for the generation of exocrine pancreas. In contrast, cells that lack Notch-signaling express the transcriptional factor neurogenin (Ngn) 3 and adopt an endocrine fate (178, 180, 181). The endocrine cells subsequently migrate to the adjacent mesenchyme where they aggregate and form typical architecture of mature islets with insulin expressing cell in the center and non-insulin-producing cells in the periphery at about E18.5 (175). In late embryogenesis and early postnatal life, as the wave of β-cell neogenesis that initiated with the secondary transition starts to wane, the proliferation of pre-existing β--cells produce a further increase in β-cell number (182). The endocrine pancreas develops the ability to sense glucose and regulate insulin secretion only after birth (175, 183).

Mouse genetic studies have uncovered an emerging developmental pathway controlled by several transcription factors that are essential for the development of the endocrine and exocrine pancreas (184). The transcription factors Pdx-1, hepatocyte nuclear factor (Hnf)-3β, Ngn3, and Hlxb9 are required for the early stages of pancreas development (fig. 5-1). For example, mice that are deficient for the Pdx-1 lack a pancreas (54, 55, 174). Hnf-3β is temporally expressed earlier than Pdx-1 and has been shown to bind to conserved regulatory elements in the mouse and human *pdx-1* promoters and activate their transcription (57, 59). Ngn3 null mice fail to generate any pancreatic endocrine cells and die postnatally from diabetes (181). Finally, Hlxb9 deficient mice selectively ablate the dorsal pancreas (185, 186). In addition to the above transcription factors, late pancreatic differentiation requires the function of islet 1 (Isl1), NK homeobox (Nkx) 2.2, Nkx6.1, paired box gene (Pax) 4, Pax6, neurogenic differentiation

1 (NeuroD1), Hnf-1α, and Hnf-3α (36, 37, 42, 71, 123, 144, 152, 187-190). Disruption of these transcription factors affect the differentiation state, proportion, and/or function of the different endocrine cell types, indicating that they act in various combinations to ensure the correct endocrine differentiation during late pancreatic ontology.

The development of the pancreas shares many similarities to neuronal cells. Analogous to the central nervous system (CNS), the process of lateral specification mediated by the Notch signaling pathway specifies endocrine and exocrine cell fate from a homogenous field of cells. Furthermore, the pancreas and the CNS share many cell intrinsic factors that are vital for their proper differentiation such as Isl1, NeuroD1, Pax4, Pax6, Nkx2.2, and Hnf-3β. In this study, we describe a differentiation scheme that would direct the differentiation of ES cells into pancreatic endocrine cells based on the similarities between islet and neuronal cell development. We also establish the use of fluorescence-activated cell-sorting (FACS) to quantitate the proportion of endocrine precursors that were generated at various stages of the differentiation protocol and to isolate these precursors to over 90% purity. In addition, the function of different cell intrinsic factors in pancreatic development were studied by generating *pdx-1*$^{-/-}$ ES cells and differentiating these cells along with *hnf-3α*, *hnf-3β*, and *hnf-4α* null ES cells. The roles of these transcription factors in development were analyzed by gene expression profiling and by their ability to secrete insulin in response to glucose and other secretagogues. Finally, a mouse transgene was constructed in which enhanced green fluorescent protein (EGFP) is driven by the *Pdx-1* promoter. We determined that mice carrying this transgene express EGFP in insulin producing β-cells and in islet periductal cells (putative adult pancreatic stem cells). This transgenic mouse will be used in future

studies to study pancreatic development, β-cell neogenesis, and expansion and transdifferentiation of pancreatic duct cells *in vivo*.

Results:

Differentiation of ES Cells into Pancreatic Endocrine Cells

The differentiation protocol was divided into 4 stages (Fig. 5-2). In stage 1, ES cells were grown on gelatin-coated plates in the absence of mouse embryonic fibroblasts (MEF) and leukemia inhibitory factor (LIF). This stage is to initiate differentiation and to reduce the number of MEF in the culture. To induce embryoid bodies (EB) formation (stage 2), ES cells were grown in suspension on non-adherent petri dishes. Generation of EB is important because they provide many of the conditions (polarized cell contact, production of growth factors, cell-cell interactions, etc...) necessary to produce cells of different lineages. Cells at the end of stage 1 and 2 were stained with primary anti-insulin and anti-glucagon antibodies, however, no insulin or glucagon positive cells were detected (data not shown).

Recent studies have shown that nestin, an intermediate filament protein, is a marker for precursor cells of certain lineages including neuronal cells and hormone negative pancreatic endocrine precursors (160, 191-193). Nestin expressing cells were selected by growing EB in serum free medium supplemented with insulin, transferrin, selenium, and fibronectin (ITSF) supplement (stage 3). The nestin positive cells were then expanded by using 2 mitogens, basic fibroblast growth factor (bFGF) and nerve growth factor (βNGF), that were shown to maintain the expression of *pdx-1* and promote the development of pancreas (60, 170, 194-197). Cells at the end of this stage are morphologically heterogeneous. Neuronal cells are the largest with long cellular

Stage 1: Initial Differentiation of ES Cells

ES cells are grown on gelatin coated tissue culture plate in the absence of MIF and LIF until they are sub-confluent.

↓

Stage 2: Differentiation of Embroid Bodies (EB)

EB are generated by culturing the ES cells in suspension without LIF on petri dishes for 3 days. Differentiation must be restarted if EB are not metabolically active, ie, media do not turn yellow everyday.

↓

Stage 3: Selection and Expansion of Endocrine/Neural Progenitor Cells

Phase 1- Dissociated EB are cultured on tissue culture plates coated with gelatin, poly-D-lysine, and fibronectin until they are subconfluent. (If less than 50% of the dissociated EB attach onto tissue culture plates, differentiation must be restarted.)

Phase 2- Nestin positive cells are selected by culturing dissociated EB in serum free media with ITSF supplement until 20% of the cells are left.

Phase 3- Nestin postive ES cells are expanded in the presence of ITSF supplement, βNGF, bFGF, B27, and nicotinamide to enrich endocrine/neural progenitors for 6 days. If the cells do not aggregate at the end of this stage, differentiation must be restarted.

↓

Stage 4: Terminal Differentiation of Endocrine Progenitors

Phase 1- Immature endocrine cells are cultured in the presence of βNGF, B27, nicotinamide and 12.5 mM glucose for 2 days.

Phase 2- Cells are differentiated further by withdrawing bNGF and lower the glucose concentration to 6 mM for 4 days.

Figure 5-2. General outline for the differentiation of ES cells. A flow chart is shown describing the differentiation of undifferentiated ES cells into pancreatic hormone producing clusters with islet like topology. A more detailed procedure with the exact concentrations of the reagents used can be found in materials and methods.

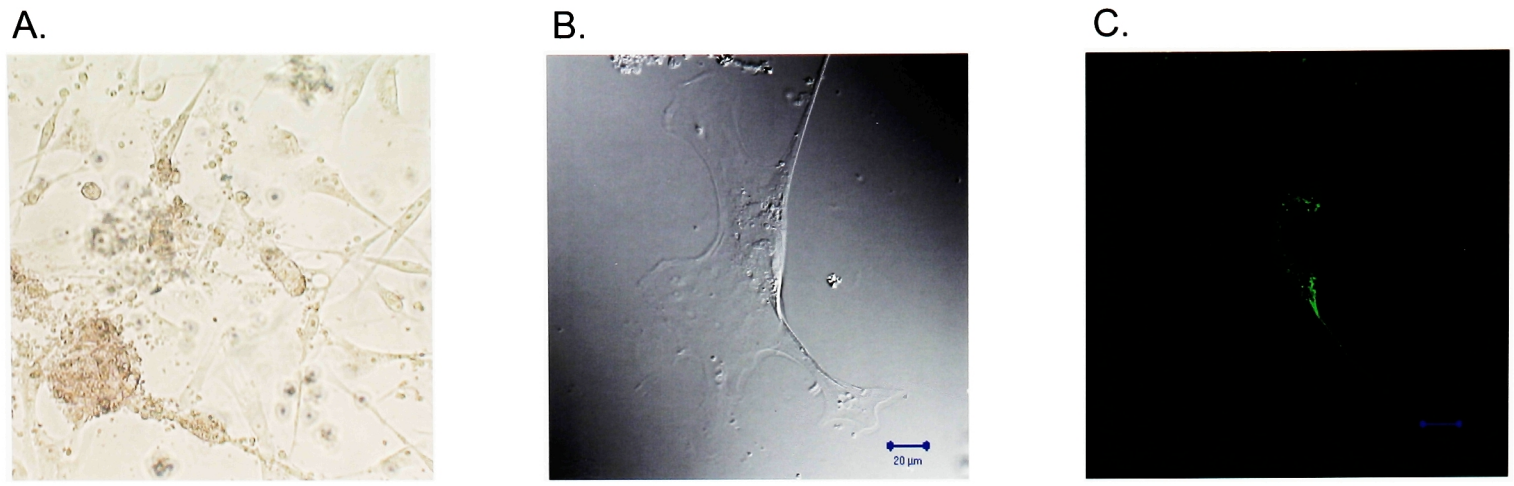

Figure 5-3. Cell morphology at the end of differentiation stage 3. Wildtype cells at the end of stage 3 differentiation are visualized by differential interference contrast (A, B). (A) Representative view of cell morphology at the end of stage 3, showing small rounded cells forming aggregates and large neuronal cells with long cellular extensions. Occasionally, some neurons express glucagon (B, C). Glucagon is stained green.

extensions, and grow as separated cells (Fig. 5-3A, B). Occasionally we observed a few neurons in the culture express glucagon (Fig. 5-3B, C). Many smaller and rounded cells are also present and aggregate into clusters (Fig. 5-3A and Fig. 5-4A, B). To determine if these cell aggregates express any of the pancreatic hormones, we stained them using primary anti-insulin (red) and anti-glucagon (green) antibodies to visualize β- and α-cells respectively. We found that both hormones were generated in the clusters and that numerous cells co-express insulin and glucagon (yellow) (Fig. 5-4E, F arrow). In addition, cells in these clusters appeared to be polarized with the majority of insulin or double positive cells surrounded by glucagon expressing cells (Fig. 5-4E, F). This is reminiscent of pancreatic islet morphology.

In stage 4 of the differentiation protocol, these endocrine cells were grown under low glucose with the addition of nicotinamide and B27. The cells continued to aggregate themselves into clusters (Fig. 5-5A, B). These hormone positive clusters proceed to organize into pancreatic islet like topology with a majority of glucagon producing cells forming a mantle around insulin and double positive cells (Fig. 5-5E, F). At the end of this stage, fewer cells were stained with both insulin and glucagon (Fig. 5-5E, F). In addition, we observed that insulin positive cells were increased and glucagon positive cells were decreased relative to stage 3 differentiation (compare Fig. 5-5E, F with Fig. 5-4E, F). These results show that the differentiation protocol generates cells that express pancreatic hormones and that they organize into islet like cell clusters.

Role of Pdx-1 in pancreatic endocrine development *in vitro*

The phenotypes observed in the β-cell specific and complete inactivation of the mouse *pdx-1* gene indicate that Pdx-1 is important for initial pancreas development as

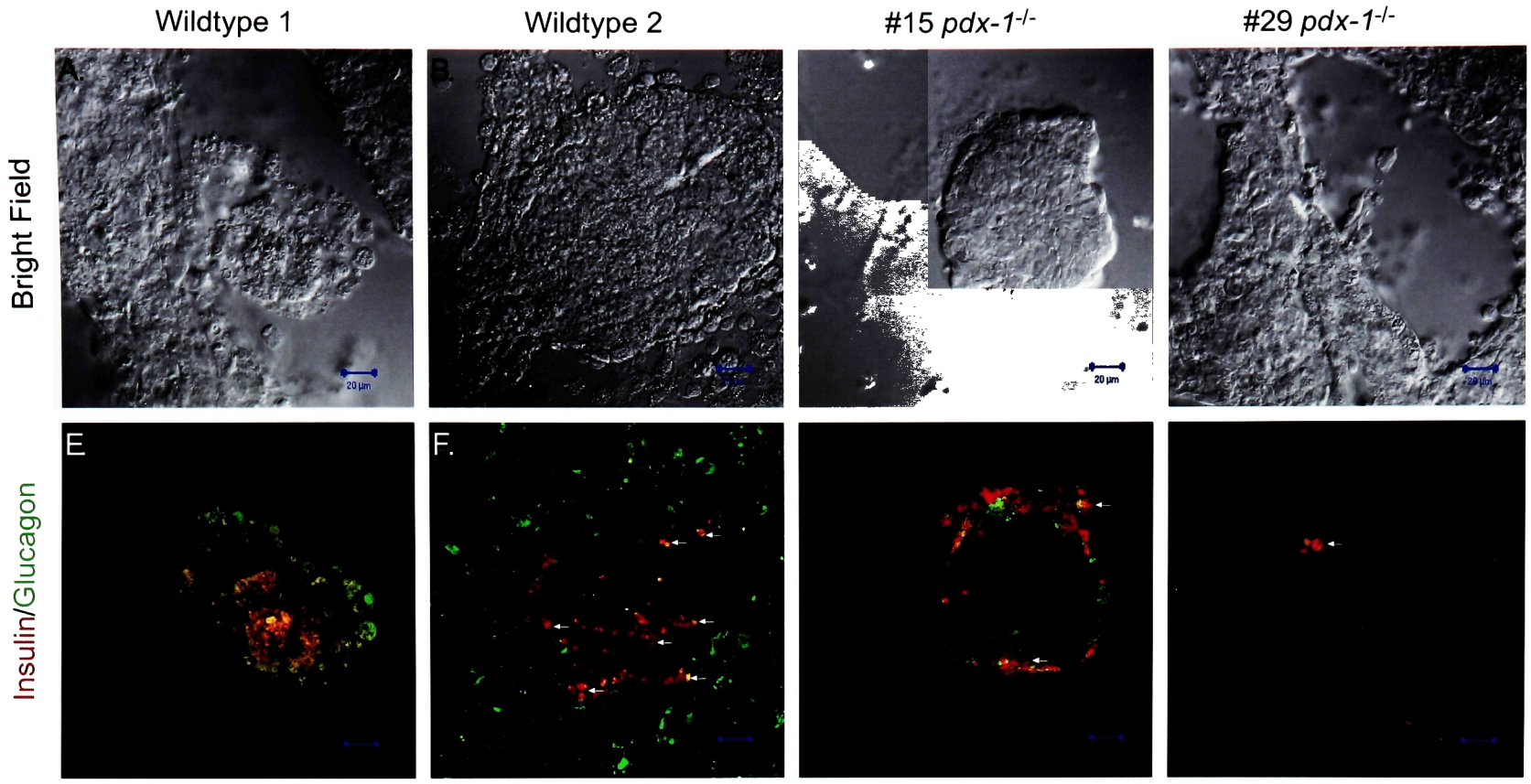

Figure 5-4. Imaging analysis of wildtype and *pdx-1*$^{-/-}$ cells at stage 3. Wildtype (wt) and *pdx*-1$^{-/-}$ ES cells at the end of stage 3 differentiation are visualized by differential interference contrast (A-D) or dual fluorescence using insulin (red) and glucagon (green) antibodies (E-H). Insulin and glucagon co-expressing cells appear yellow/orange. WT hormone producing cells organize topologically into pancreatic islet like structures with insulin expressing cells surrounded by the glucagon positive cells (E and F). The number of hormone positive cells are drastically decreased in Pdx-1 deficient mutants (G and H). Insulin and glucagon co-expressing cells are frequently seen in differentiated WT (E and F, marked by arrow) and *pdx*-1$^{-/-}$ ES cells (G and H, marked by arrow). Scale bar, 20 um.

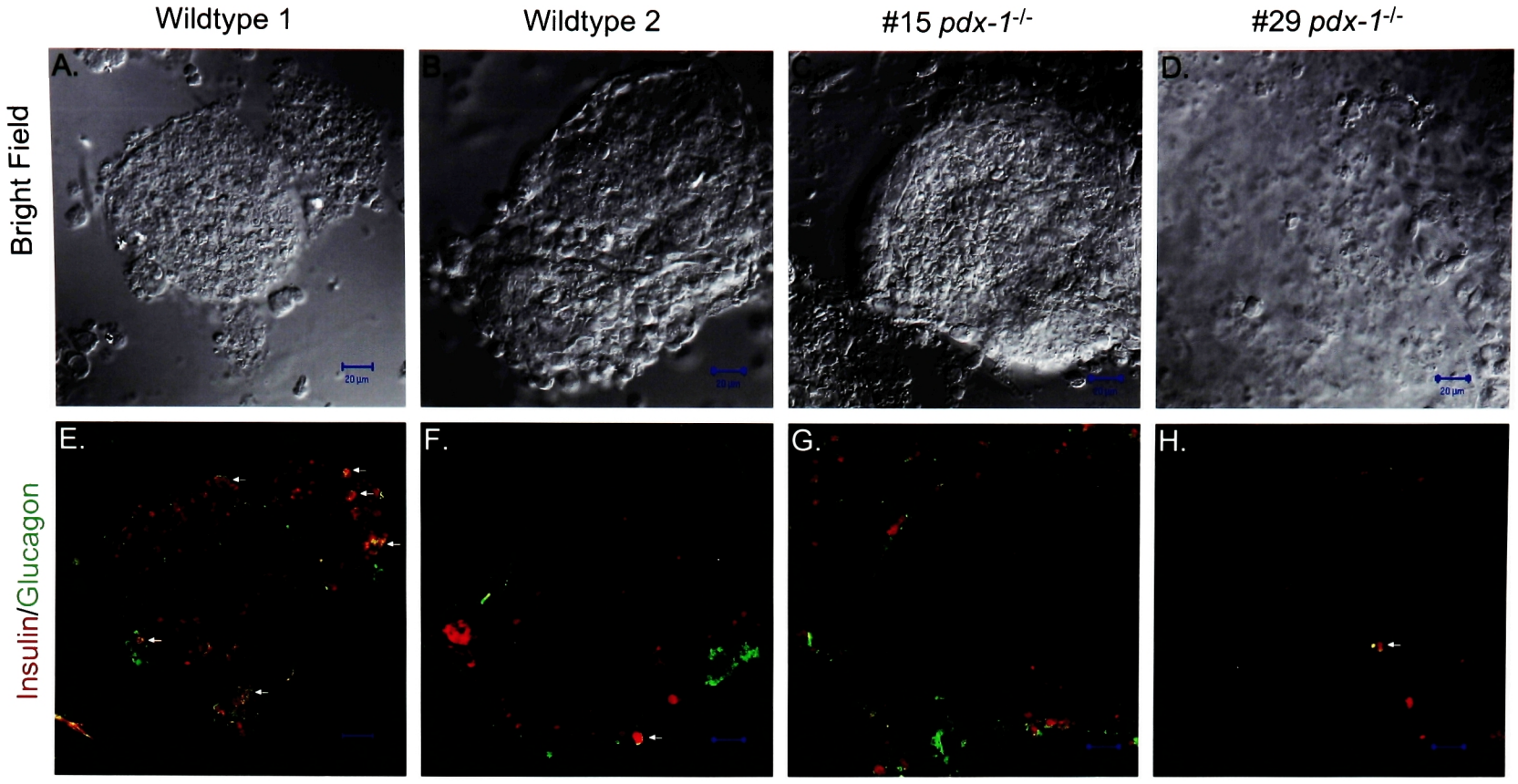

Figure 5-5 Imaging analysis of wildtype and *pdx-1*$^{-/-}$ cells at stage 4. Wildtype (wt) and *pdx-1*$^{-/-}$ ES cells at the end of stage 4 differentiation are visualized by differential interference contrast (A-D) and double immunofluorescence (E-H) using insulin (red) and glucagon (green) antibodies. Cells that express both insulin and glucagon appear yellow/orange. WT hormone positive cells continue to organize into pancreatic islet like structures with glucagon producing cells forming a mantle around insulin producing cells (E and F). In contrast to WT, there are reduced hormone positive cells in *pdx-1*$^{-/-}$ mutants. Cells that co-express both insulin and glucagon are also seen in both WT and *pdx-1*$^{-/-}$ mutants at this stage (G, and E, F, H marked by arrow), but the co-expressing cells appear to be fewer in number in the wt. Scale bar, 20 um.

well as in β-cell differentiation and function. To study the role of *pdx-1* in differentiating ES cells, we generated three independent *pdx-1* null ES cell lines by culturing the *pdx-1*$^{+/-}$ ES cells (*pdx-1* is disrupted by a *lacZ* knockin) in high concentrations of G418 medium (55). The frequency in generating *pdx-1* null ES cells were: 0/200 at 1.0 mg/ml G418, 2/200 at 1.5 mg/ml G418, and 1/200 at 2.0 mg/ml G418. The genotypes of these clones were analyzed by Southern blot analysis, which confirmed the precise targeting of the remaining *pdx-1* allele without DNA rearrangement and gene duplication (Fig. 5-6A). They were also additionally confirmed by Western blot analysis showing that no functional PDX were produced in *pdx-1* null ES cells (Fig. 5-6B).

The different *pdx-1*$^{-/-}$ ES cell lines were differentiated and analyzed by immunofluorescent staining for insulin and glucagon at the end of stage 1, 3, and 4. Similar to the WT, we did not detect insulin or glucagon positive cells at stage 1 and 2 (data not shown). The *pdx-1* null ES cells also begin to aggregate in stage 3 (Fig. 5-4C, D). However, these pancreatic precursors contained much less hormone positive cells than WT and that majority of these cells were localized to the periphery of the cluster (compare Fig. 5-4G with 5-4E, F). A few insulin, glucagon, and double positive cells were detected in isolation away from other hormone positive cells (Fig. 5-4H).

In stage 4 of the differentiation protocol, the cultures that contained *pdx-1* deficient cells were observed to have more neuronal structures than WT cultures (data not shown). The morphology of various cell types was examined by differential interference contrast (DIC) microscopy, however no differences between wt and *pdx-1*$^{-/-}$ cells or the structures that they form were detected (Fig. 5-5A-D, data not shown). In contrast to wt, the number of hormone positive cells were drastically reduced in *pdx-1*$^{-/-}$ cells and

A.

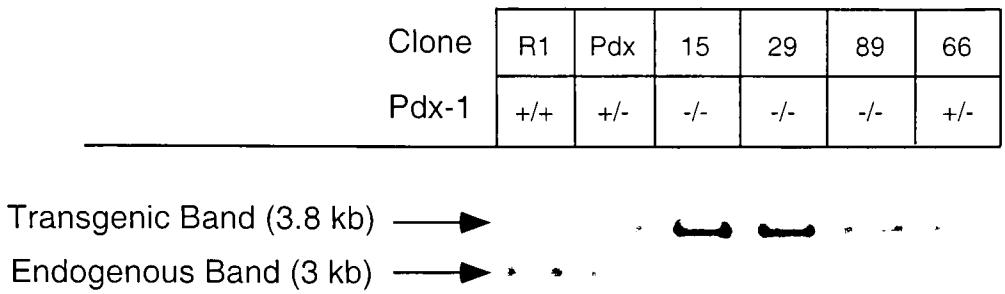

B.

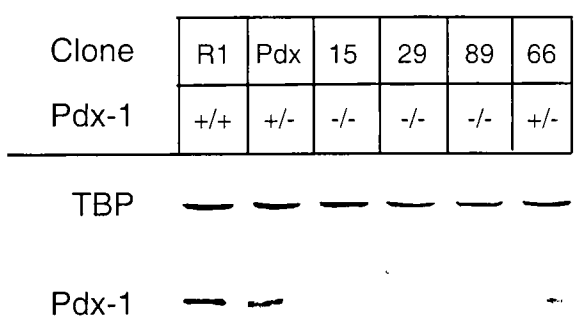

Figure 5-6. Generation of *pdx-1*$^{-/-}$ ES cells. *pdx-1*$^{-/-}$ ES cells were produced by selection of *pdx-1*$^{+/-}$ ES cells in high concentration of G418. (A) Southern blot analysis of DNA samples digested with *Eco*RI from wildtype, *pdx-1* heterozygous, and *pdx-1* null ES cells. *pdx-1* targeted band is 3.8 kb and endogenous *pdx-1* band is 3 kb (B) Western blot analysis of nuclear extracts generated from differentiated ES cells showing that no Pdx-1 proteins were produced in the null cell lines. TBP is the nuclear extract loading control showing equal loading in each sample.

typically surrounded by hormone negative cells in the cluster (compare Fig. 5-5G to 5-5E, F). In addition, cells that express insulin, glucagon, or both were scattered among hormone negative cells (Fig. 5-5H). These results revealed that the homeodomain transcription factor Pdx-1 is critically involved in organizing cells into clusters with islet like topology *in vitro*. Furthermore, Pdx-1 plays an important role in either generating pancreatic endocrine cells or maintaining their phenotype.

Role of Pdx-1 in pancreatic endocrine cell function *in vitro*

To assess the physiological effects of various cell intrinsic factors that are important for islet development, we differentiated wt, *pdx-1*$^{+/-}$, *pdx-1*$^{-/-}$, *hnf-3*$\alpha^{-/-}$, *hnf-3*$\beta^{-/-}$, and *hnf-4*$\alpha^{-/-}$ ES cells. Their insulin contents and secretory responses to different insulin secretagogues such as glucose, glucagon-like peptide (GLP)-1, and tolbutamide were determined. At the end of stage 3, only the insulin content of *pdx-1*$^{-/-}$ cells were significantly lower than wt (28.9±4.4 vs. 53.1±3.5 ng/mg, p=0.003) (Fig. 5-7). Even though cells of various genotypes at the end of stage 3 produced insulin, they were not responsive to any of the insulin secretagogues (Fig. 5-8, data not shown).

The total insulin content at the end of stage 4 increased over stage 3 for wt and all mutants except for Pdx-1 null cells (wt 2.0 fold increase, *pdx-1*+/- 1.9 fold increase, *hnf-3*$\alpha^{-/-}$1.7 fold increase, *hnf-3*$\beta^{-/-}$ 1.9 fold, and *hnf-4*$\alpha^{-/-}$ 2.0 fold) (Fig. 5-7). The intracellular insulin content of *pdx-1*$^{-/-}$ cells were significantly lower than wt (36.4±2.3 vs. 108.4±8.6 ng/mg, p=0.002) (Fig. 5-7). We did not observe any significant differences in total insulin levels between other mutants and wt. We found that wt cells could secrete insulin in response to different stimuli at the end of stage 4 (tolbutamide 2.4 fold increase, GLP-1 1.8 fold increase, and glucose 2.3 fold increase) (Fig. 5-9). In addition,

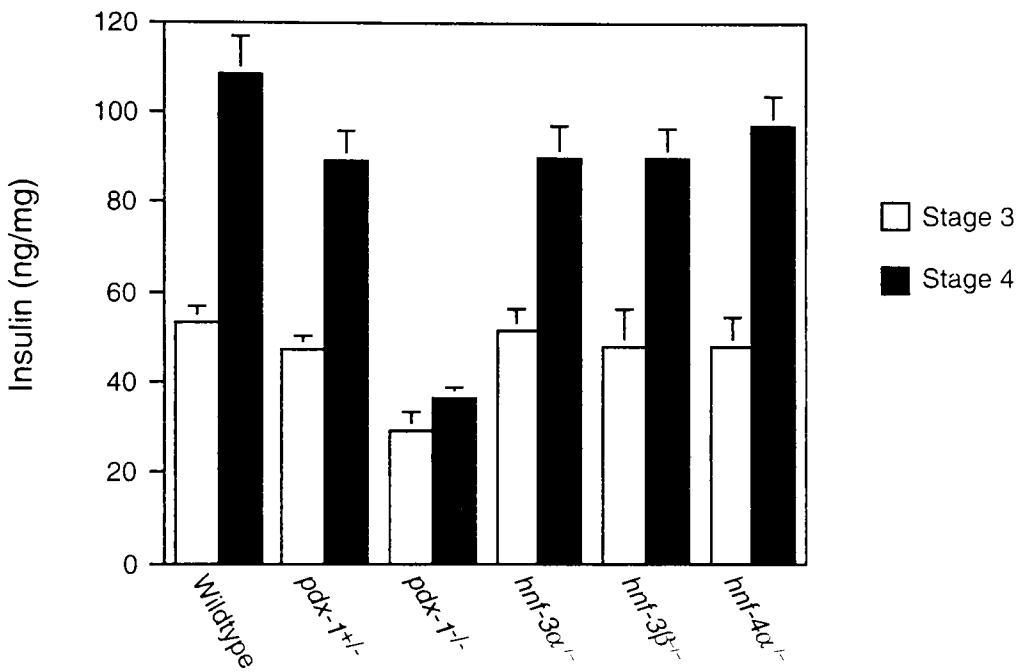

Figure 5-7. Loss of Pdx-1 reduces insulin production. Wildtype, *pdx-1*$^{-/-}$, *hnf-3α*$^{-/-}$, *hnf-3β*$^{-/-}$, and *hnf-4α*$^{-/-}$ increased total intracellular insulin content with progressive differentiation. In contrast, *pdx-1* null ES cells have diminished insulin content. Grey and black bars represent insulin content measured at stage 3 and 4, respectively. The results were reproduced in at least 3 independent experiments for the wildtype and *pdx-1*$^{+/-}$ cells. At least 2 independent null clones for each genotype were used. Insulin values for the differentiated null cells were measured in 2 independent experiments in duplicates.

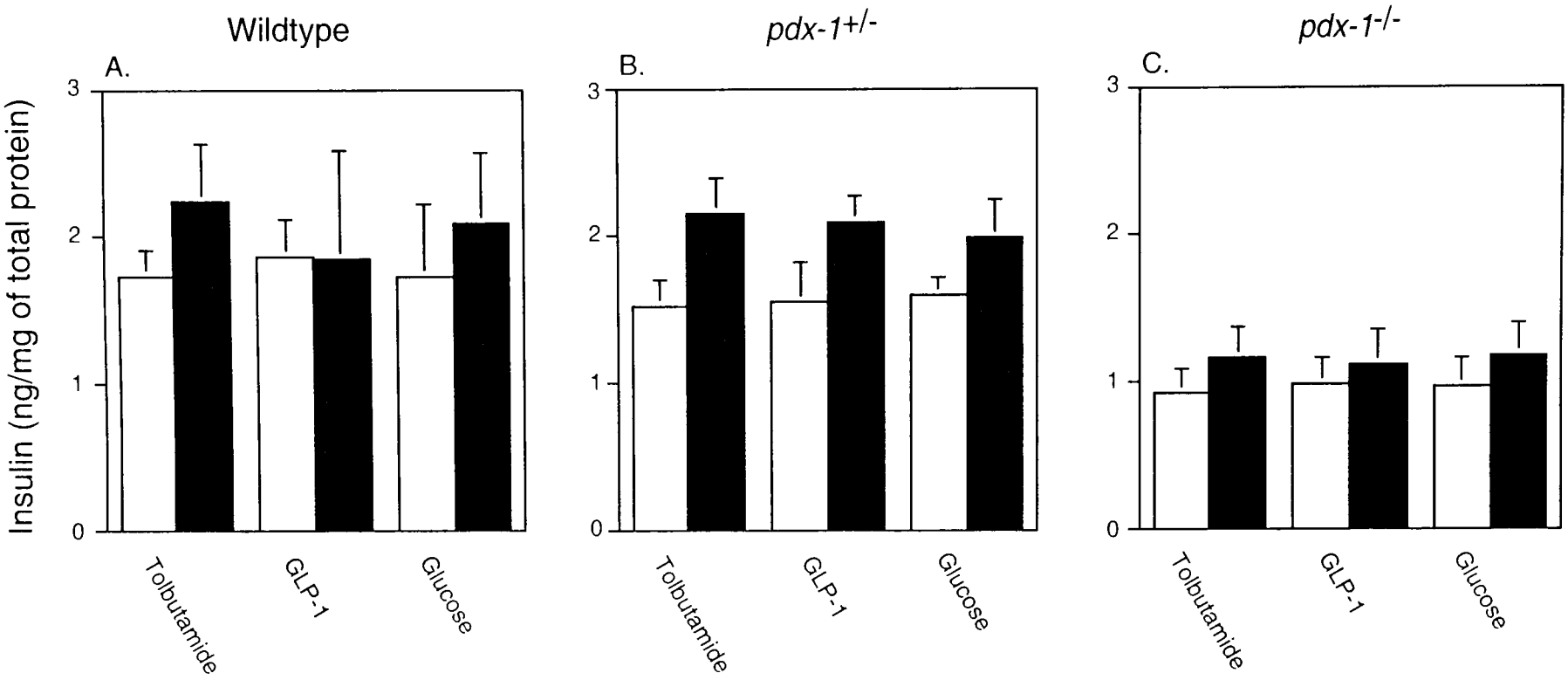

Figure 5-8. Impaired insulin secretion of cells at the end of stage 3. Insulin release in response to glucose (16.6 mM), GLP-1 (100 nM), and tolbutamide (500 μM) were measured at baseline (grey bars) and 30 minutes after induction (black bars). No significant induction of insulin release in response to different secretagogues was observed. The results for wildtype and *pdx-1*$^{+/-}$ cells were done in 3 independent experiments (A, B). 3 different *pdx-1* null clones were used, and the induction experiments were done in duplicates (C).

with the exception of *pdx-1* null mutants, cells of various other genotypes also showed secretagogue-induced insulin secretion (Fig. 5-9). However, wt exhibited better insulin secretory response relative to cells with gene disruptions in *pdx-1*, *hnf-3α*, and *hnf-3β* (Table 5-1).

Insulin content and glucose stimulated insulin secretion (GSIS) were measured in isolated pancreatic islets and compared to insulin producing cells generated *in vitro*. We found that the total intracellular insulin content for pancreatic islets, of which 90% are insulin producing, was 115 μg/mg. Wt cells at the end of stage 4 contain 0.1 μg/mg of insulin, however not all of them are insulin producing. Using flow cytometry, we determined that approximately 20% of all cells at stage 4 express Pdx-1 (Fig. 5-12). Assuming that 50% of the Pdx-1 positive cells also express insulin, the total insulin producing cells is 10% of all cells at the end of stage 4. Since insulin producing cells account for only 10% of all cells, the actual insulin content per insulin producing cell may be 1.0 μg/mg. This would mean that the insulin producing cells at the end of stage 4 have approximately 100 times less insulin than pancreatic islets (1.0 μg/mg vs. 115 μg/mg). GSIS was compared between pancreatic islets and insulin producing cells generated *in vitro*. We found that islets increased insulin secretion by 37.9 fold in response to glucose (Fig. 5-10), in contrast, wildtype cells at the end of stage 4 increased insulin secretion by 2.4 fold (Fig. 5-9).

Our physiological assessments revealed that insulin positive cells undergo significant maturation between stage 3 and 4. We found that insulin content increased approximately 2 fold from stage 3 to stage 4 and that the insulin positive cells developed a machinery to secrete insulin in response to different secretagogues. The physiological

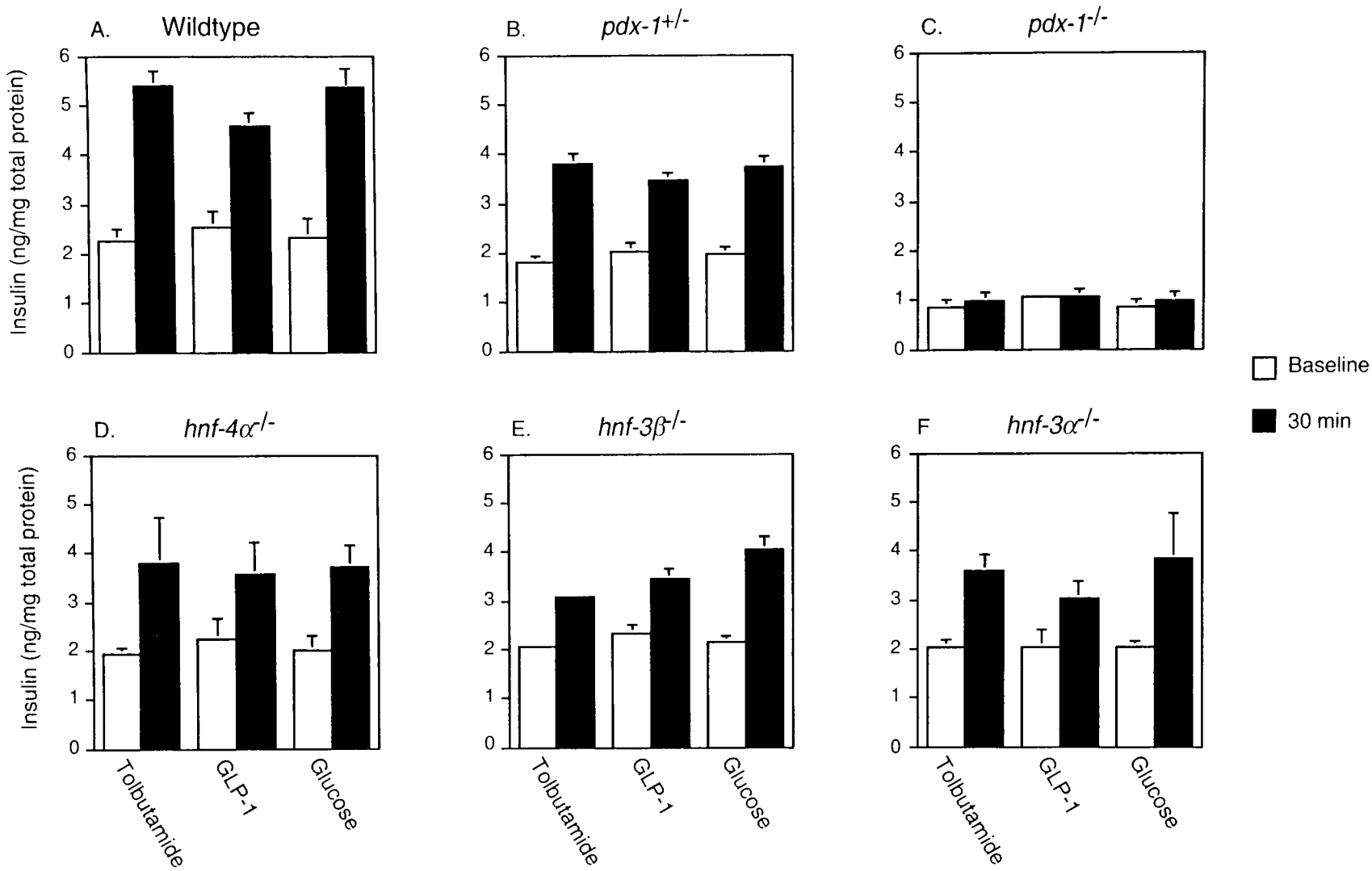

Figure 5-9. Insulin secretory function of cells at the end of stage 4 differentiation. Insulin release in response to glucose (16.6 mM), GLP-1 (100 nM), and tolbutamide (500 μM) were measured at baseline (grey bars) and 30 minutes after induction (black bars). At the end of stage 4 wildtype (A), *pdx-1*$^{+/-}$ (B), *hnf-4α*$^{+/-}$ (D), *hnf-3β*$^{-/-}$ (E), and *hnf-3α*$^{-/-}$ (F) can release insulin in response to different stimuli using normal pancreatic mechanisms. In contrast, *pdx-1* null cells are unresponsive to all of the insulin secretagogues used (C). Data are the mean ± SEM of at least 3 independent experiments (A, B) and of at least 2 different clones done in duplicates (C-F).

	Insulin Levels (ng/mg)			*p* values		
	Tolbutamide	GLP-1	Glucose	Tolbutamide	GLP-1	Glucose
Wildtype	5.39±0.31	4.57±0.28	5.36±0.63	1	1	1
***hnf-3α*$^{-/-}$**	3.59±0.27	3.01±0.31	3.82±0.75	0.017	0.038	0.233
***hnf-3β*$^{-/-}$**	3.07±0.17	3.42±0.45	4.05±0.54	0.004	0.021	0.129
***hnf-4α*$^{-/-}$**	3.81±0.76	3.57±0.53	3.72±0.36	0.249	0.265	0.087
***pdx-1*$^{+/-}$**	3.81±0.21	3.47±0.15	3.73±0.23	0.007	0.019	0.077
***pdx-1*$^{-/-}$**	0.98±0.18	1.08±0.13	0.98±0.18	7.00E-5	2.00E-4	0.004

Table 5-1. Insulin secretion response of cells at the end of stage 4. Insulin contents in cells 30 minutes after induction with glucose (16.6 mM), GLP-1 (100 nM), and tolbutamide (500 μM) were measured and shown. Baseline insulin levels in different mutants were not significant and values are not shown. Data are the mean ± SEM of at least 3 independent experiments for wildtype and *pdx-1* heterozygotes done in duplicates. Data for *hnf-3α*$^{-/-}$, *-3β*$^{-/-}$, *-4α*$^{-/-}$, and *pdx-1*$^{-/-}$ were collected from at least 2 different clones and in at least 2 independent experiment done in duplicates.

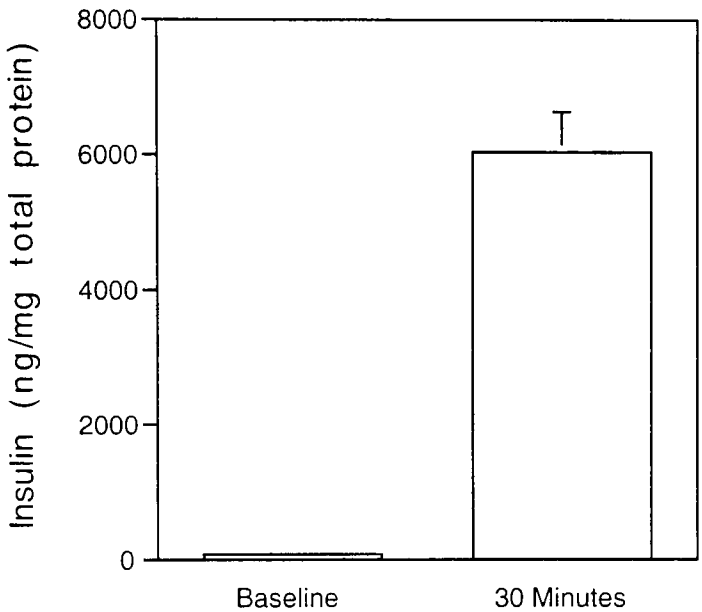

Figure 5-10 Glucose stimulated insulin secretion in isolated pancreatic islets. Insulin release in response to glucose challenge (16.6 mM) was measured 30 minutes after induction in static incubations. Islets increased insulin secretion by 37.9 fold in response to glucose, approximately 15 times more responsive than wildtype differentiated cells at stage 4. Results were the average of 4 independent experiments. Data are shown as mean ± SEM.

effects of various cell intrinsic factors that are important for pancreatic β-cell development and function were also assessed in our *in vitro* system. We found that insulin production and secretion is critically dependent upon the homeodomain transcription factor, Pdx-1. In contrast, deficiencies in Hnf-3α and Hnf-3β only mildly impaired insulin secretory responses but not insulin production. Finally, insulin producing cells generated by *in vitro* differentiation were compared to pancreatic islets. We showed that the insulin positive cells generated in this system contained about 1% of insulin compared to pancreatic β-cells. In addition, differentiated ES cells were less efficient in releasing insulin in response to glucose challenge.

Role of Pdx-1 in pancreatic endocrine cell formation *in vitro*

The temporal and spatial expression patterns of the *pdx-1* gene indicate that it is an ideal marker to identify pancreatic endocrine cells. Consequently, *pdx-1*$^{+/-}$ and *pdx-1*$^{-/-}$ ES cells (generated by the LacZ gene knocked into the *Pdx-1* locus) can be used as reporter cells to study pancreatic development *in vitro*. After differentiation of these reporter cells, β-galactosidase (β-gal) should be expressed in all the pancreatic cell lineages. A vital fluorogenic substrate for LacZ, 5-chloromethylfluorescein di-β-D-galactopyranoside (CMFDG), was used to label pancreatic endocrine cells. In LacZ positive cells, CMFDG is converted to a bright green fluorescent product. Because loading with CMFDG is based on osmolar shock, propidium iodide (PI) was used to identify dead cells by labeling them with a red nuclear fluorescence. These labeled pancreatic endocrine cells could then be quantitated by flow cytometry.

pdx-1$^{+/-}$ and *pdx-1*$^{-/-}$ ES cells were differentiated and stained with CMFDG at the end of stage 2, 3, and 4, and the proportion of LacZ/Pdx-1 positive cells was determined

by flow cytometry. Figure 5-11 shows the typical controls that were done for each flow cytometric measurement. We found that about 40% of the cells survived the CMFDG loading procedure as indicated by PI negative staining (Fig. 5-11A). Only live cells (PI negative) were used to determine the percentage of cells that stained with CMFDG (fluorescein positive). The background fluorescein level was determined by using cells not stained with CMFDG and was used to set the region to detect LacZ/Pdx-1 positive cells. Less than 0.064% of the unstained cells were in the fluorescein positive interval (Fig. 5-11B). In wt cells (without the *lacZ* transgene), less than 0.87% of the cells are stained with CMFDG (Fig. 5-11C). To confirm that the LacZ/Pdx-1 positive cells were stained with CMFDG, we collected fluorescein positive and negative cells by fluorescence-activated cell-sorting (FACS) and analyzed them by microscopy and gene expression. We determined that fluorescein positive and negative cells were green and unstained respectively, under fluorescent microscope (Fig. 5-11E, F, and data not shown). In addition, there was selective enrichment of LacZ and/or Pdx-1 expression in fluorescein positive cells (Fig. 5-14).

Figure 5-12 shows the representative CMFDG staining profiles of *pdx-1*$^{+/-}$ and *pdx-1*$^{-/-}$ cells at the end of differentiation stages 2, 3, and 4. The percentages of LacZ/Pdx-1 positive cells representing pancreatic endocrine cells (fluorescein positive/PI negative) were determined. We found that the proportions of LacZ/Pdx-1 positive cells at the end of stage 2 were similar between ES cells with one or no functional copies of *pdx-1* (fig. 5-12A, D, G). The number of *pdx-1*$^{+/-}$ cells that were fluorescein positive and PI negative increased approximately 4-fold from stage 2 to stage 3 (Fig. 5-12A, B). In contrast, this cell population only increased about 2-fold from stage 2 to stage 3 in cells without any

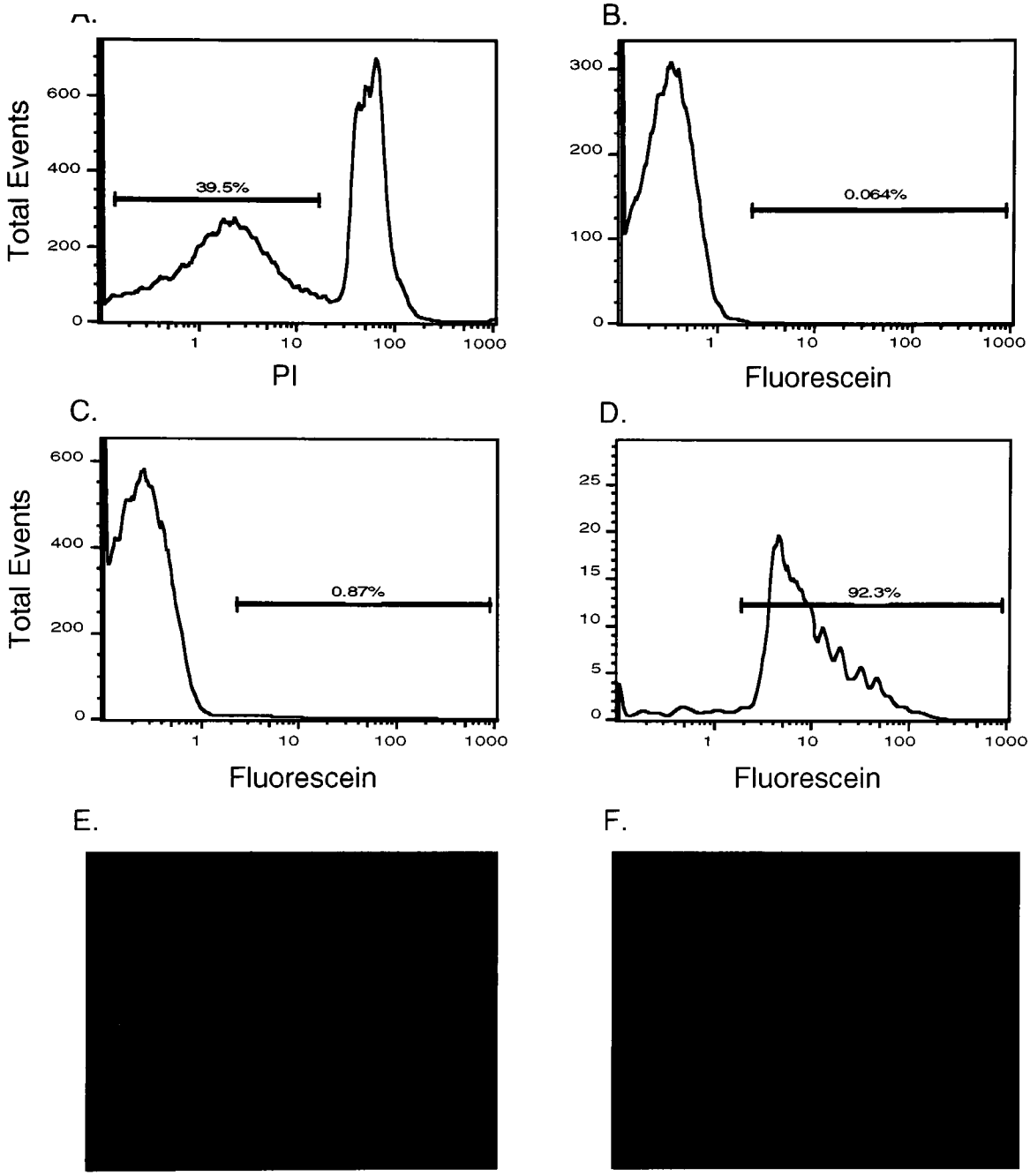

Figure 5-11 Flow cytometry controls to isolate lacZ+/Pdx-1+ population. (A) The propidium iodide (PI) negative cells represent the live cells and approximately 40% of the cells are PI negative after staining with the vital fluorogenic substrate for lacZ, 5-chloromethylfluorescein di-β-D-galactopyranoside (CMFDG). The PI negative population was gated and their fluorescein content (representing lacZ expression) was determined. (B) This figure shows the fluorescein intensity of unstained cells. Typically, less than 0.064% of the unstained cells exhibit fluorescein stain. (C) In wildtype cells (without the lacZ transgene), less than 0.87% of the cells were stained with CMFDG. (D) The purity of the fluorescein containing cells were determined at the conclusion of the cell sort. Typically, about 90% purity was achieved from the sorting protocol. (E) & (F) Cells after sorting for fluorescein were examined by microscopy under transmission light in (E) and UV light in (F).

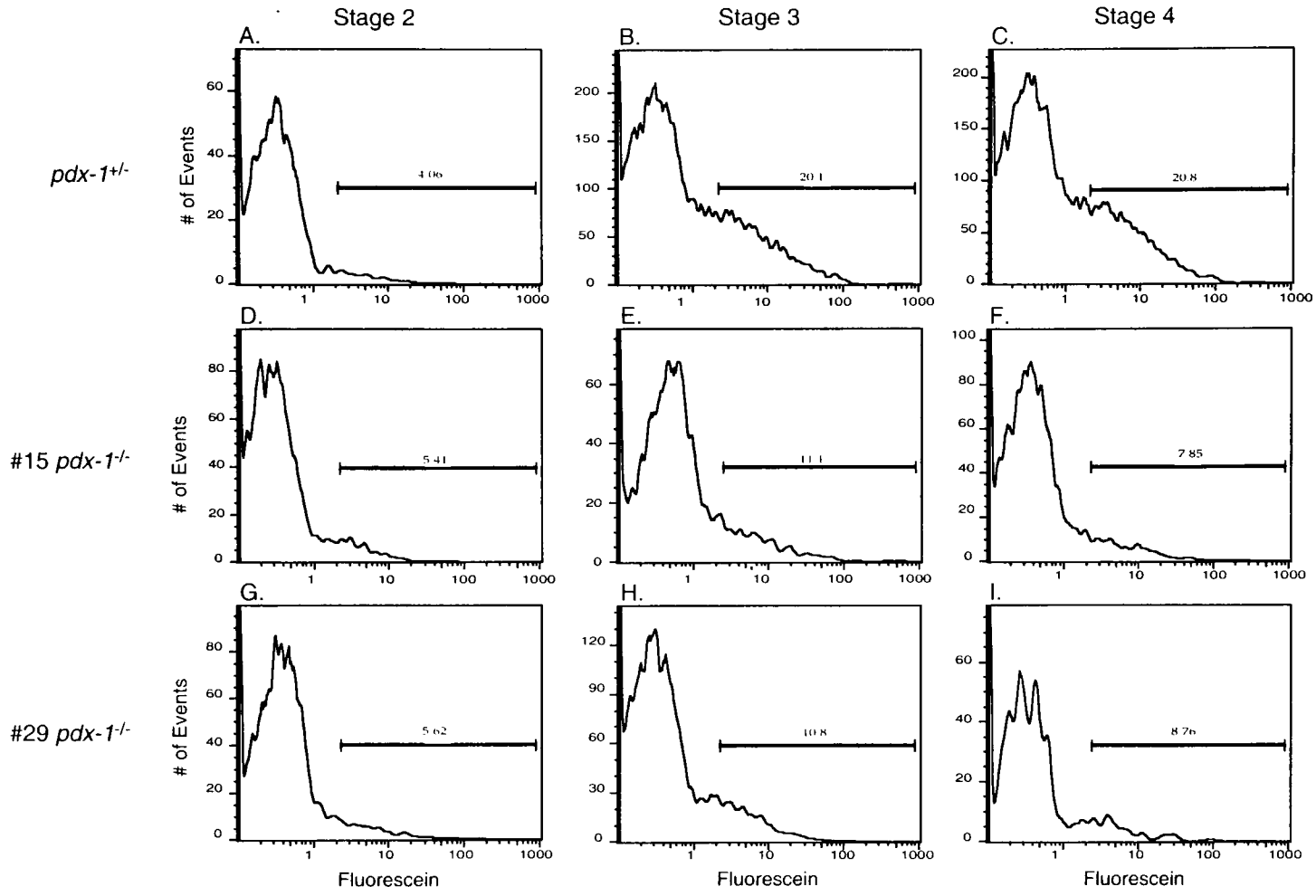

Figure 5-12. Loss of Pdx-1 leads to a decrease in the number of LacZ/Pdx-1 positive cells. *pdx-1*$^{+/-}$ and *pdx-1*$^{-/-}$ ES cells were differentiated and stained with CMFDG at the end of stage 2, 3, and 4, and the proportion of LacZ/Pdx-1 positive cells was determined by flow cytometry. The percentages of LacZ/Pdx-1 positive cells representing pancreatic endocrine cells (fluorescein positive/PI negative) were determined. The Y-axis represent the number of events counted and the X-axis denotes staining intensity for fluorescien. Fluorescein positive means that the cells are LacZ/Pdx-1 positive and may represent endocrine cells and/or cells fated to become endocrine cells. Only live cells (PI negative) are gated and used to determine the percentage of LacZ/Pdx-1 positive cells. We found that in *pdx-1*$^{+/-}$ cells, the percentage of LacZ/Pdx-1 population increased from stage 2 to stage 3 but stabilized from stage 3 to stage 4 (A-C). At stage 2, there is no difference in the amount of LacZ/Pdx-1 positive population between *pdx-1*$^{+/-}$ and *pdx-1*$^{-/-}$ cells (A, D, G). However at stage 3 and 4, the LacZ/Pdx-1 positive population is decreased in *pdx-1*$^{-/-}$ cells as compared to *pdx-1*$^{+/-}$ cells at equivalent differentiation stages (B, C, E, F, H, I). The results were reproduced in two independent experiments.

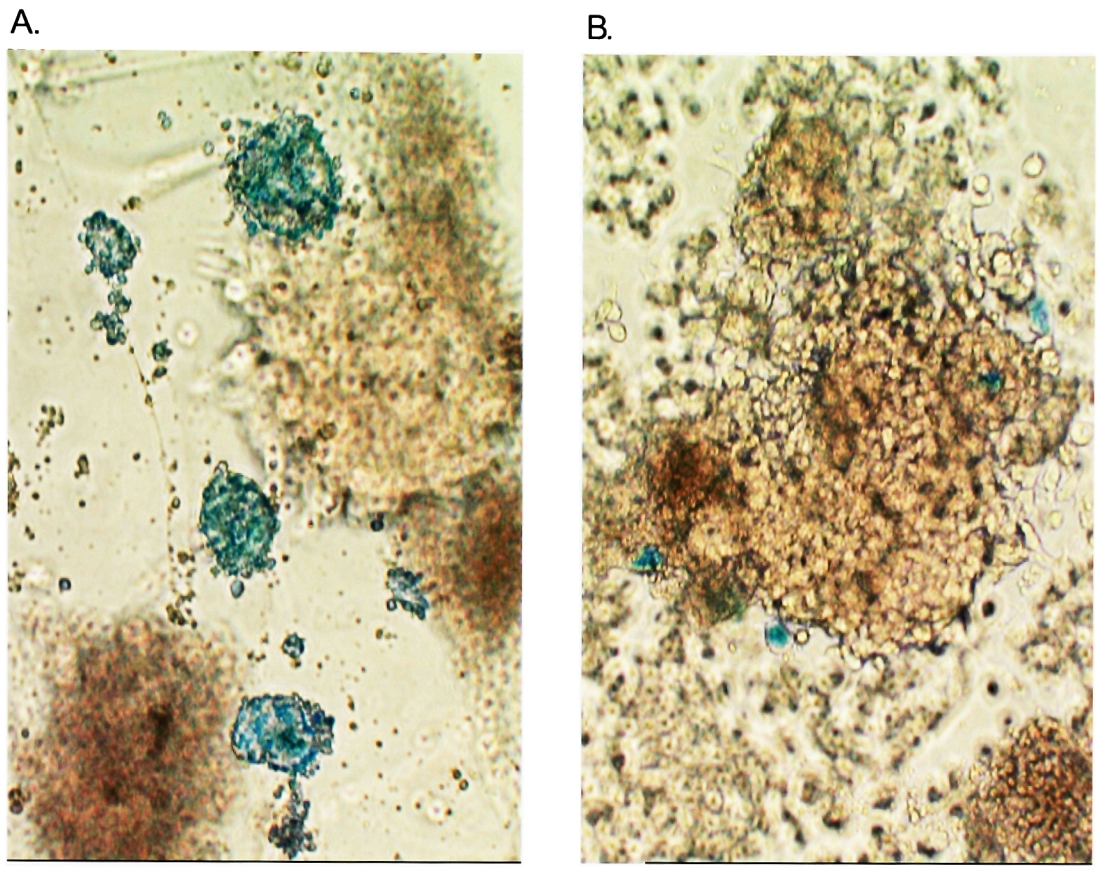

Figure 5-13. X-gal stain of *pdx-1*$^{+/-}$ and *Pdx-1*$^{-/-}$ differentiated ES cells. *pdx-1*$^{+/-}$ (A) and *pdx-1*$^{-/-}$ (B) ES cells were differentiated and stained with X-gal at the end of stage 4. Numerous X-gal positive (blue) cells (representing endocrine cells, LacZ/Pdx-1 positive) were observed in hormone positive cell clusters of differentiated *pdx-1*$^{+/-}$ cells (A). In contrast, few X-gal positive cells were detected scattered among X-gal negative cells (B).

functional Pdx-1 protein (Fig. 5-12D, E, G, and H). The percentage of this population remained stable from stage 3 to stage 4 in both the *pdx-1*$^{+/-}$ and *pdx-1*$^{-/-}$ cells (Fig. 5-12B, C, E, F, H, and I). The decreased number of LacZ/Pdx-1 positive population in differentiated *pdx-1*$^{-/-}$ cells were also confirmed by X-gal staining (Fig. 5-13A, B).

Overall, these results showed that the homeodomain transcription factor Pdx-1 is important to generate cells committed to the pancreatic fate. In addition, differences in the rate of proliferation and apoptosis during phase 3 of stage 3 differentiation were ruled out as possible mechanisms that caused decreased pancreatic population in *pdx-1*$^{-/-}$ cells.

Isolation and Molecular Characterization of LacZ/Pdx-1 Positive Cells

By staining *pdx-1*$^{+/-}$ and *pdx-1*$^{-/-}$ cells with the vital fluorescent β-gal substrate CMFDG and analyzing by flow cytometry, we identified a population of cells (fluorescein positive) that may have committed into pancreatic fate. Furthermore, in the absence of Pdx-1, there were less putative pancreatic cells and that they had significantly lower total insulin content along with an inability to secrete insulin in response to secretagogues. To study the molecular mechanisms that are responsible for these differences, we isolated these putative pancreatic cells by fluorescence-activated cell sorting (FACS) and analyzed their steady-state mRNA levels.

At least 200,000 LacZ/Pdx-1 positive cells were isolated from *pdx-1*$^{+/-}$ and *pdx-1*$^{-/-}$ cells at the end of stage 2, 3, and 4 for expression analysis. In addition, LacZ/Pdx-1 negative cells were also isolated and used as controls. At the end of each FACS experiments, we determined the purity of our isolated cells. Only isolated cells with over 90% purity were used for gene expression profiling (Fig. 5-11D). The cDNA of *pdx-1* heterozygous cells were generated from two independent differentiations and the *pdx-1*$^{-/-}$

cDNAs were synthesized from two different *pdx-1* null clones. We measured expression of different pancreatic developmental markers as well as genes shown to be important for pancreatic development and function in order to characterize LacZ/Pdx-1 positive cells from with one or no functional *pdx-1* allele.

Hypoxanthine phosporibosyltransferase (Hprt) expression levels were determined to show that each sample contained equivalent amounts of mRNA (Fig. 5-14). No products were amplified in the absence of reverse transcriptase (Hprt-RT), indicating the absence of genomic DNA in the mRNA samples. The expression of LacZ and Pdx-1 were additional controls confirming the genotype and the enrichment of the desired population (Fig. 5-14). The expression pattern of nestin showed that nestin positive cells were indeed selected during stage 3 and that as differentiation progressed (stage 4), downregulation of nestin occurs (Fig. 5-14). We observed that LacZ/Pdx-1 positive cells expressed many pancreatic markers including Ngn-3, Hnf-3β, P48, Isl-1, NeuroD1, Nkx2.2, Nkx6.1, Pax6, Pax4, insulin, and glucagon. These pancreatic markers can be subdivided based upon their requirement in the pathway of pancreatic development (Fig. 5-1). We observed that the expression of Hnf-3β in *pdx-1*$^{+/-}$ cells was decreased with differentiation. In contrast, the expression of Hnf-3β was maintained in *pdx-1*$^{-/-}$ cells. mRNA levels of the pro-endocrine gene, Ngn3, increased with differentiation and was not regulated by Pdx-1. The expression of P48, the pro-exocrine gene, was not regulated by Pdx-1 but its expression was enriched in LacZ/Pdx-1 cells. These results indicate that Pdx-1 does not affect early pancreatic development and specification of exocrine and endocrine fates *in vitro*.

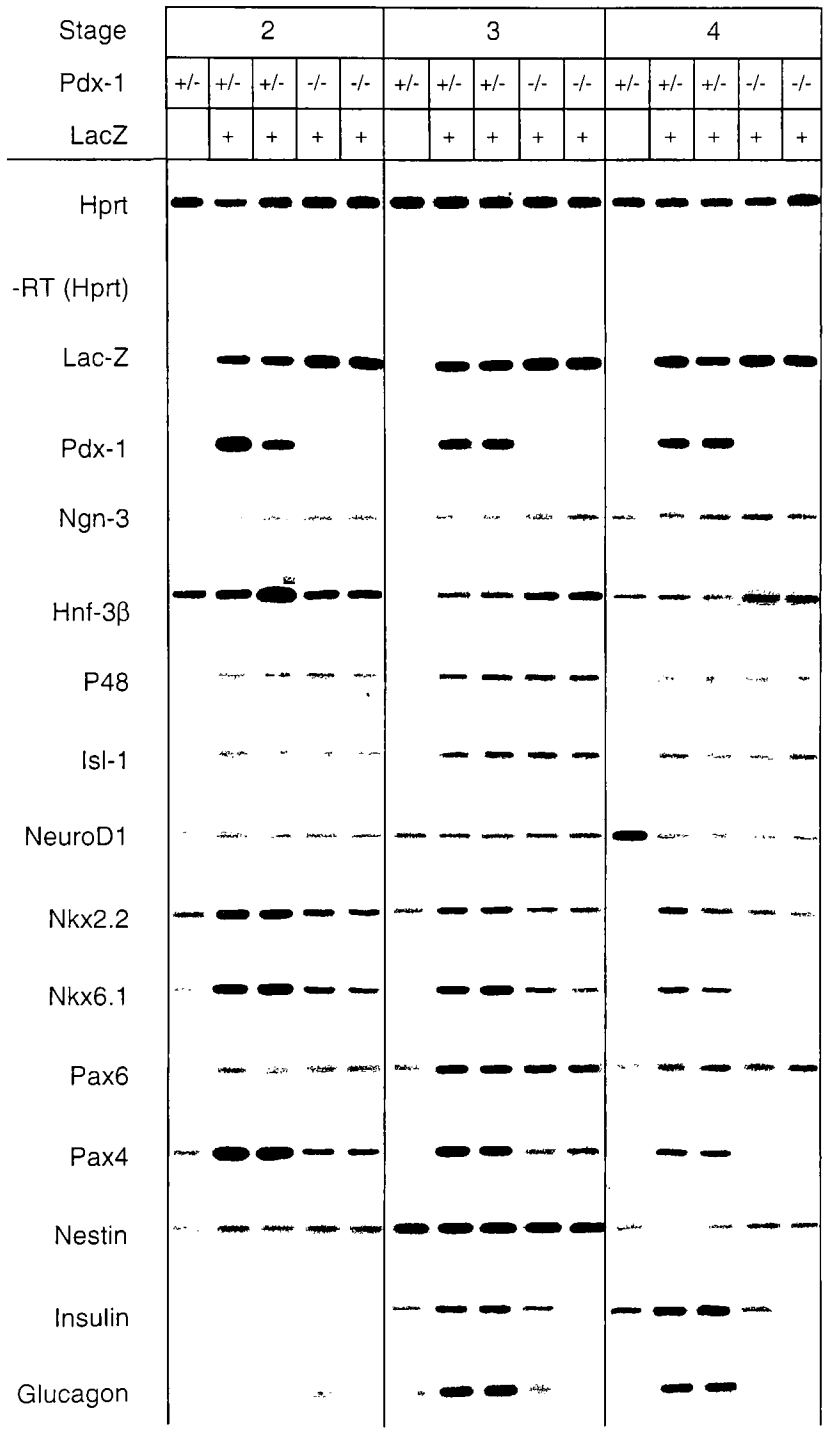

Figure 5-14. Gene expression profile of isolated pancreatic endocrine cells. RT-PCR analysis of pancreas developmental markers and genes important for pancreatic function was performed on LacZ/Pdx-1 positive cells isolated by FACS. cDNAs were made from at least 200,000 LacZ/Pdx-1 positive cells isolated from *pdx-1*$^{+/-}$ and *pdx-1*$^{-/-}$ cells at the end of stage 2, 3, and 4. Each differentiation stage contained the following samples: one sample of LacZ/Pdx-1 negative population from *pdx-1*$^{+/-}$ cells, two samples of LacZ/Pdx-1 positive population from *pdx-1*$^{+/-}$ cells from 2 independent isolations, and finally 2 samples of LacZ/Pdx-1 positive population from 2 different *pdx-1*$^{-/-}$ clones. Transcript levels were measured in the isolated cell population by RT-PCR using [α-^{32}P]dCTP. PCR products were separated by PAGE, and bands were visualized by autoradiography.

We observed that Pdx-1 is critically important for the subsequent differentiation of pancreatic endocrine cells after the initial fate specification. Pdx-1 regulated the expression of several transcription factors that are important to determine the lineage of islet cells including Nkx2.2, Nkx6.1, Pax6, and Pax4 (Fig. 5-14). Lack of Pdx-1 function does not affect the expression of Isl-1 and NeuroD1 (Fig. 5-14), suggesting that in *pdx-1*$^{-/-}$ cells, the arrest of pancreatic differentiation occurred after the requirement for Isl-1 and NeuroD1. As expected, the expression of insulin and glucagon were drastically reduced in the absence of Pdx-1.

Overall, our results showed that pancreatic endocrine cells can be generated *in vitro* and be isolated to over 90% purity by FACS. In addition, we showed that the phenotypic defects in *pdx-1*$^{-/-}$ cells might be caused by an arrest of pancreatic endocrine development downstream of the requirement for Isl-1 and NeuroD1.

Generation of pdx-1-EGFP Transgenic Mice.

To generate an *in vivo* mouse model to study pancreatic β-cell development, a mouse transgene was constructed in which the *pdx-1* promoter drives enhanced green fluorescent protein (EGFP). A transgenic approach was selected because an EGFP knocked into the *pdx-1* locus would result in diabetic mice and may compromise pancreatic development and gene expression in these mice. During murine embryogenesis, Pdx-1 is initially expressed throughout the pancreas and parts of the stomach and duodenum. Its expression becomes progressively restricted to pancreatic β-cells by birth. Therefore both pancreatic precursors as well as β-cell of the transgenic mice can be selected by the presence of EGFP and studied subsequently.

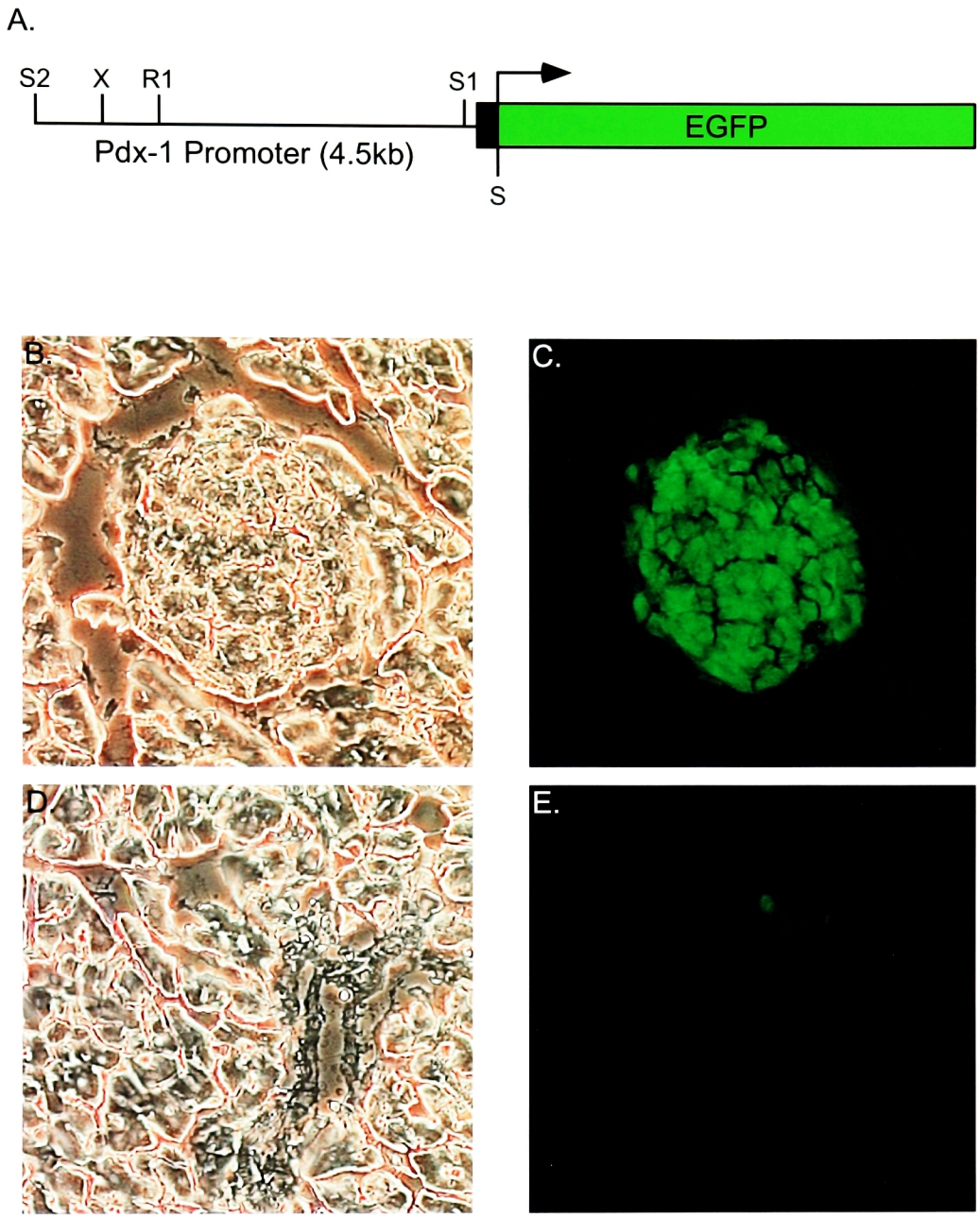

Figure 5-15. Generation of Pdx-EGFP Transgenic Mouse. (A) A schematic diagram showing the pPdx-1-pEGFP transgenic construct. In mice carrying this transgene, the expression of GFP was found in the adult pancreatic islets (B and C) as well as in periductal cells (D and E).

The *pdx-1* promoter was isolated by screening a mouse genomic library. A 4.5 kb *pdx-1* promoter was cloned upstream of the EGFP to generate the mouse transgene (Fig. 5-15A). This transgene was transfected in an insulinoma cell line HIT-T15 and functionally confirmed that EGFP is expressed (data not shown). The pPdx-1-pEGFP construct was used to generate 19 founder mice. The pancreas from the progeny of these founders were examined and only one exhibited EGFP expression in pancreatic β-cells (Fig. 5-15B-E). In addition, we observed that isolated cells next to pancreatic ducts expressed EGFP (Fig. 5-15D, E), which may represent adult endocrine precursor cells or ductal cells (198). We are currently checking whether the transgenic EGFP expression exactly mimics Pdx-1 expression both spatially and temporally during development.

We have generated mice carrying EGFP under the control of *pdx-1* promoter. In the adult, we found EGFP expression in pancreatic β-cells as well as in periductal cells which may be adult endocrine precursors. This transgenic mouse is an important reagent for the lab in the future.

Discussion:

Despite the minute size of the pancreatic islets, the endocrine pancreas is a critical organ for maintaining glucose homeostasis and plays a key role in the etiology of type 1 and type 2 diabetes mellitus. Diabetes is one of the most costly chronic disease of children, adolescents, and adults and frequently lead to microvascular and macrovascular complications (1). Replacement of functional pancreatic β-cell mass through islet transplantation may be a cure for type 1 and in some cases type 2 diabetes mellitus. However, problems such as paucity of doners and immunosuppressive therapy limited the

success of islet transplantation. Therefore, a major goal in the treatment of diabetes is to generate alternative sources of β-cells that can maintain glucose homeostasis in transplanted host. Because ES cells are capable of both self-renewal and can differentiate into a variety of lineages, they may represent one such unlimited source of pancreatic β-cells. We utilized the developmental similarities between neurons and islets to generate insulin producing cells from ES cells. Even though the pancreas (endoderm) and neurons (ectoderm) are derived from different embryonic germ layers and are functionally distinct, comparable signaling pathways, inductive molecules, and cell intrinsic factors control their development and function. These similarities suggest that methods that were used to generate neurons could also be adopted to produce pancreatic endocrine cells. Recently, promising results have demonstrated that pancreatic hormone producing cells can be generated from ES cells *in vitro* by using strategies that were established for neural differentiation (160, 166). To generate cells expressing insulin and other pancreatic islet specific markers, we have adopted a modified neural differentiation protocol and developed a differentiation scheme that would direct the differentiation of ES cells into pancreatic endocrine cells. Figure 5-2 summarizes the differentiation scheme.

There are several critical steps in the differentiation protocol. The first important step is in the generation of EB. EB may be the first *in vitro* differentiated structure to contain cells from different germ layers (ie endoderm) and to provide conditions such as polarized cell contact, cell-cell interactions, and production of growth factors necessary to generate and maintain cells of different lineages. To achieve this state, EB must be metabolically active and as a result, the media should turn quite yellow everyday. Since

differentiation is promoted in less than optimal growth conditions (ie upon growth factor withdrawal and in limiting resources), media is changed at most once a day. If EB are not metabolically active, then differentiation should be restarted.

Stage 3 contains several critical steps in the differentiation procedure. In phase 1 of stage 3, at least 50% of dissociated EB should attach to tissue culture plates to ensure that the cells which have initiated into pancreatic fate are selected and enriched in subsequent steps of differentiation. We have tested different coating reagents including laminin, collagen, fibronectin, gelatin, poly-D-lysine, and poly-L-lysine and found that tissue culture plates coated with the combination of poly-D-lysine, fibronectin, and gelatin are the most favorable for cell adherence. Recent studies have shown that there are pluripotential stem cells in the brain that are capable of differentiating into neuronal cells (160, 193, 199). These cells have in common with hormone negative pancreatic endocrine precursors in that they both express nestin, an intermediate filament protein (191, 200). The nestin-positive hormone negative cells isolated from adult pancreas can differentiate *ex vivo* into insulin and glucagon expressing cells (192). We therefore hypothesized that pancreatic endocrine cells may be generated *in vitro* by first differentiating ES cells into nestin positive cells. This is achieved by growing dissociated EB in serum free ITSF medium to select for nestin positive cells (160, 166). Pancreatic ductal cells, which may represent adult pancreatic stem cells, are also differentiated into insulin positive cells by culturing in serum free ITSF medium (198, 201). The resulting nestin positive cells are then expanded and directed into pancreatic fate using bFGF, βNGF, nicotinamide and B27. bFGF and βNGF were used as mitogens over other growth factors because they were shown both *in vitro* and *in vivo* to be essential for pancreas

development (60, 170, 194-197). Nicotinamide and B27 supplement were used because they were shown *in vitro* to promote the generation of pancreatic endocrine cells (166, 167, 202, 203). Despite the "propancreatic" reagents used for differentiation, the cells at the end of stage 3 differentiation are morphologically heterogeneous, although 2 major cell types predominate: small rounded cell clusters and large neuronal cells. Consistent with a previous report that used a similar differentiation strategy, the cell clusters formed at the end of this stage express insulin and glucagon (166). The hormone producing cells in the cluster organize into islet-like topology with majority of glucagon positive cells located at the periphery of the cluster. In contrast to the report by Lumelsky et. al., we found that there are numerous insulin and glucagon double positive cells. Although not conclusive, our data suggest that β- and α- cells arise from a common progenitor *in vitro*.

Differentiated cells at the end of stage 3 were tested for their ability to use physiological signaling pathways to regulate insulin release. The insulin secretagogues used are glucose, tolbutamide, and GLP-1. Glucose targets the first step of GSIS and is used to check if the insulin positive cells developed machinery for glucose sensing. Tolbutamide an anti-diabetic drug that targets the sulphonylurea receptor (Sur1) induces the closure of ATP sensitive potassium channel which leads to membrane depolarization and insulin release (204). GLP-1 stimulates insulin secretion by an ATP-sensitive potassium channel-independent pathway by targeting cAMP/protein kinaseA (205). We found that the insulin positive cells at the end of stage 3 are unable to secrete insulin in response to these secretagogues, suggesting that *in vitro*, cells committed to the panceatic β-cell fate produce insulin before developing machinery that would couple physiological signal to insulin secretion.

The pancreatic hormone producing cells undergo a maturation process during stage 4. Growth factors are withdrawn to induce further differentiation. In addition, glucose levels are gradually lowered from 25 mM to 6 mM in the culture medium. Low glucose concentration is used at stage 4 because elevated glucose level alters gene expression and the phenotype of pancreatic β-cells *in vitro* (167, 206, 207). Recently, chronic hyperglycemia was shown to trigger loss of β-cell differentiation in a rat model of diabetes (208). The morphology of cells at the end of stage 4 is similar to that at stage 3 with numerous large neurons and small, rounded cells that aggregated into clusters. The hormone positive clusters continue to organize into structures with islet-like topology with insulin or insulin/glucagon double positive cells surrounded by glucagon expressing cells. Even though cells that co-express insulin and glucagon were also observed in stage 4, the proportion of double positive cells are less than in stage 3. In contrast, the number of insulin positive cells increased in stage 4 suggesting that differentiation of double positive precursors into insulin producing cells had occurred. The functional characteristics of stage 3 and 4 islet like clusters were compared by their insulin content and their insulin secretory response. We found that the total cellular insulin content is increased. Furthermore, stage 4 cells are responsive to different insulin stimuli indicating that significant functional maturation also occurred between stage 3 and 4.

The "holy grail" in ES cell transplantation for treating diabetes is to reconstitute all of the biochemical, molecular, and physiological functions of pancreatic β-cells in differentiated ES cells. Morphologically, we have generated islet like structures that express pancreatic hormones. A series of experiments were performed to compare the functional characteristics of stage 4 islet like clusters and pancreatic islets. We found that

the insulin content of *in vitro* hormone positive cells is 1% of pancreatic islets. In four independent experiments with 25 islets each, we found that stage 4 cells were about 15 times less efficient in their GSIS response than pancreatic islets (2.4 fold induction vs. 37.9 fold induction). These data showed that although the *in vitro* cells have similar insulin secretory response to physiological cue as pancreatic islets, the signaling pathways to regulate insulin release may not be fully developed. The hormone positive cells generated by our procedure may represent pancreatic endocrine precursors and that additional refinements in culturing condition are necessary to further differentiate and/or mature these cells to have the same functional capabilities as pancreatic islets. Additional conditions may be to culture cell clusters from stage 4 on Matrigel, a commercial preparation of murine basement membrane, with keratinocyte growth factor (KGF), and GLP-1 since these components were required to differentiate pancreatic ductal tissue into glucose responsive islet tissue *ex vivo* (201, 209).

Spatial and temporal modifications of gene expression by different cell intrinsic and extrinsic factors direct the process of development from endoderm precursors to differentiated β-cells *in vivo*. To determine if ES cells in combination with our differentiation protocol can be used as a model system to study endocrine development, we differentiated WT, *pdx-1*$^{+/-}$, *pdx-1*$^{-/-}$, *hnf-3α*$^{-/-}$, *hnf-3β*$^{-/-}$ and *hnf-4α*$^{-/-}$ ES cells and compared their functional efficacy with respect to insulin content and physiologically relevant insulin secretion pathways. Three classes of phenotype can be catagorized: (1) reduced insulin content and complete lack of insulin secretion response (*pdx-1*$^{-/-}$), (2) impaired insulin secretion response (*pdx-1*$^{-/-}$, *hnf-3α*$^{-/-}$, *hnf-3β*$^{-/-}$), and (3) similar functional response as differentiated WT cells (*hnf-4α*$^{-/-}$). Based upon the observed

defects, the function of Pdx-1 may lie upstream of Hnf-3α, Hnf-3β, and Hnf-4α in the *in vitro* pathway of pancreas development. Differentiated *pdx-1*$^{+/-}$, *hnf-3α*$^{-/-}$, and *hnf-3β*$^{-/-}$ cells exhibited milder defect than *pdx-1* null cells and may represent endocrine precursors unable to complete functional maturation. The phenotype of Hnf-4α suggests that it may either be dispensible or lie downstream of Hnf-3α and Hnf-3β in the pathway of *in vitro* pancreas development.

Since Pdx-1 deficiency severely impairs the development and/or function of insulin producing cells *in vitro*, *pdx-1*$^{-/-}$ cells were further characterized by microscopy and flow cytometry. We observed that although the morphology of differentiated cells are similar, there are significantly less insulin producing cells in *pdx-1*$^{-/-}$ cell clusters. Furthermore, cells in the middle of the *pdx-1*$^{-/-}$ islet like clusters are hormone negative suggesting that these cells may have lost their pancreatic endocrine phenotype. Flow cytometry quantitatively confirmed our microscopy results. The mechanism of decreased pancreatic endocrine cells was addressed by measuring the rate of proliferation and apoptosis during expansion phase of stage 3. Stage 3 was selected because the quantitative difference in pancreatic precursors occurred during this period. No differences in proliferation or apoptosis were observed between WT or *pdx-1*$^{-/-}$ pancreatic endocrine cells. However, an increased rate of apoptosis and/or decreased rate of proliferation in may still be one of the mechanisms that lead to reduced proportion of *pdx-1*$^{-/-}$ pancreatic endocrine cells since only one time point in stage 3 were checked. Alternatively, Pdx-1 may be required to sustain its own expression either directly or indirectly by maintaining the differentiation state of pancreatic endocrine cells. Such an

autoregulatory role in sustaining expression is a common feature shared with other transcription factors involved in differentiation (80, 210-213).

To gain insight into the characteristics of pancreatic endocrine/Pdx-1 positive cells and well as to study the molecular mechanisms of *pdx-1*$^{-/-}$ phenotypes, we isolated these putative pancreatic precursors by FACS and analyzed their steady-state mRNA levels. Markers of pancreatic development such as Ngn-3, Hnf-3β, P48, Isl-1, NeuroD1, Nkx2.2, Nkx6.1, Pax6, Pax4, insulin, and glucagon are expressed in these cells, suggesting that the endocrine precursors generated *in vitro* developed molecular characteristics of an islet. The expression profiling results further support the notion that these islet-like clusters use physiological signaling pathways to regulate insulin release.

Previous reports have shown that development and differentiation of the pancreas requires the coordinate activation of different cell intrinsic as well as cell extrinsic factors. The pancreatic markers that were used for expression analysis can be grouped by their requirement in development. The function of Hnf-3β and Pdx-1 may be required the earliest followed by Ngn-3 for endocrine fate and P48 for exocrine fate (54, 55, 91, 92, 94, 178, 180, 181). Isl-1, NeuroD1, Pax-6, and Nkx2.2. lie more upstream than the homeobox genes Pax4 and Nkx6.1 in the development of endocrine pancreas (71, 144, 152, 187-189). Insulin and glucagon are differentiated markers for β- and α- cells respectively. PDX-1 deficiency does not lead to reduced expression of Hnf-3β, Ngn3, P48, Isl-1, and NeuroD1. These results suggest that lack of Pdx-1 function does not affect the early steps of *in vitro* pancreas development such as specification of endocine vs. exocrine fate. In contrast, the expression of Nkx2.2, Nkx6.1, Pax4, Pax6 are drastically decreased in the absence of Pdx-1. Since the function of Nkx2.2 is required more

upstream in endocrine development (144, 152, 188, 189), arrest of pancreatic development in *pdx-1*$^{-/-}$ cells caused by decreased Nkx2.2 expression may also contribute to decreased Nkx6.1, Pax6, and Pax4 expression. Nkx2.2 is a member of the NK2 homeobox transcription factor that is expressed in α-, β-, and PP- cells of the islet (214). In Nkx2.2 deficient mice, there is an arrest in the development of the endocrine pancreas that results in a large population of islet cells that do not produce any of the four endocrine hormones (152). Interestingly, the phenotype observed in *nkx2.2* KO mice share a remarkable similarity to *pdx-1*$^{-/-}$ islet-like clusters *in vitro*. Together, our results show that *in vitro*, Pdx-1 is important in the specification or maintenance of different pancreatic endocrine cell types and its deficiency may not lead to a block in cell type differentiation (since insulin and glucagon positive cells are present, but at reduced numbers). In addition, the phenotypes observed in *pdx-1*$^{-/-}$ cells may be due to a block in pancreas development at the stage when the function of Nkx2.2 is required.

We have demonstrated the feasibility of isolating pancreatic precursor cells by FACS. Purifying insulin producing cells is critical since a mixed cell population is not suitable for transplantation. The disadvantage of our system is that we used a reporter gene inserted into the *pdx-1* locus. Disruption of even one allele of *pdx-1* was shown in both in human and mice to impair glucose homeostasis. Therefore, a better method to mark pancreatic cells must be established. One such way is to put the reporter gene under the control of a β-cell specific enhancer element (ie. pdx-1 promoter or insulin promoter). We have cloned a 4.5 kb pdx-1 enhancer element and shown in transgenic mouse that this element mediates β-cell and periductal cell specific expression. A reporter construct

using the pdx-1 promoter is therefore a viable way to mark ES cells that have committed into the pancreatic endocrine fate for isolation.

Another major problem in transplantation therapy to treat diabetes is host versus graft disease (HVGD). Immunosuppressants such as glucocorticoids and steroids can minimize HVGD, however it also lead to many unwanted side effects (158, 215, 216). Nuclear transfer technology may be used in combination with ES cells to reduce HVGD in transplantated β-cells. The transfer of the nucleus into an enucleated donor oocyte will result in a clone with the same genetic information as the donor. This technique was used to clone dolly the sheep (217). Recently, the feasibility of nuclear transfer technology has been demonstrated in ES cells (218). In theory, customized ES cells can be generated to carry the genetic material of any diabetic patient. Our differentiation protocol can then be adopted to differentiate the customized ES cells and the resulting insulin producing cells isolated by FACS. Thus, another potential advantage of an ES cell based differentiation system is that insulin producing cells with a patient's own genetic information can be generated to avoid graft rejection and immunosuppressive therapies.

It is generally assumed that all islet cell types develop from a common endocrine precursor that undergo progressive stages of differentiation to give rise to different endocrine cell types (152). However, due to the complexity in studying pancreas development *in vivo*, no endocrine precursor cells have been identified nor are their molecular properties characterized. In addition, no direct lineage tracing has been done in the pancreas to follow the development of various islet cell types. ES cells represent a genetically tractable model system to study pancreas development. Null mutation in different cell intrinsic or inductive factors can be generated in ES cells and its effect

studied. We showed that *pdx-1*$^{-/-}$, *hnf-3α*$^{-/-}$, *hnf-3β*$^{-/-}$, and *hnf-4α*$^{-/-}$ cells arrest at distinct stages of pancreatic endocrine development *in vitro*. These cells may represent various intermediate endocrine precursors and its molecular characteristics can be studied and compared. Similar studies can be done with other factors involved in pancreas development. The information gathered from these studies may contribute to our understanding of pancreatic development *in vivo* and may one day generate a molecular fate map where each step of pancreatic development can be identified by a particular set of gene expression code.

In summary, we have developed an ES cell system to generate pancreatic islet like clusters that expresses insulin as well as physiological signaling pathways to regulate its release. Using FACS, we were able to isolate the pancreatic endocrine cells to over 90% purity. Purified endocrine cells represent a much safer mean for transplantation purposes. Finally, the feasibility of using an ES cell based system as a model to study pancreas development were illustrated by differentiating *pdx-1*$^{-/-}$, *hnf-3α*$^{-/-}$, *hnf-3β*$^{-/-}$, and *hnf-4α*$^{-/-}$ ES cells. Similar studies can be done with other factors that are known to be important for pancreas development. The data from these studies may one day lead to a molecular blueprint where scientists can engineer sufficient amounts of functional insulin producing cells for cell replacement therapy in both type 1 and type 2 diabetes mellitus.

Chapter 6: Hepatocyte Nuclear Factor 1α is an Essential Regulator of Bile Acid and Plasma Cholesterol Metabolism.

Introduction

Hepatocyte nuclear factor 1α (HNF-1α, TCF1) is a homeodomain containing transcription factor that is critical for diverse metabolic functions in pancreatic islets, liver, intestine and kidney (115). Mutations in *TCF1* cause maturity-onset diabetes of the young type 3 (MODY3) that is characterized by an autosomal dominant mode of inheritance, an age of onset usually before 25 years of age and defects in insulin secretion (5). In chapter 4, we showed that mice with null mutations in *tcf1* have multiple metabolic abnormalities including defects in glucose and amino acid homeostasis. Loss of Tcf1 function in mice also results in hypercholesterolemia but normal plasma triglycerides levels (36, 37). The role of Tcf1 in cholesterol homeostasis has not been elucidated.

Cholesterol homeostasis is achieved through the coordinated regulation of dietary cholesterol absorption, *de novo* biosynthesis, and disposal in the form of bile acids (summarized in Fig. 6-1). Within the intestinal lumen, dietary cholesterol is presented to the brush border of mucosal enterocytes as a micelle formed by the action of bile salts, cholesterol, and fatty acids. Cholesterol is principally absorbed in the duodenum and jejunum, whereas bile acids are absorbed in the ileum via specific bile acid transporters at the apical surface that include apical sodium-dependent bile acid transporter (Asbt, Slc10a2) and organic anion-transporter polypeptide (Oatp3, Slc21a7). The secretion of

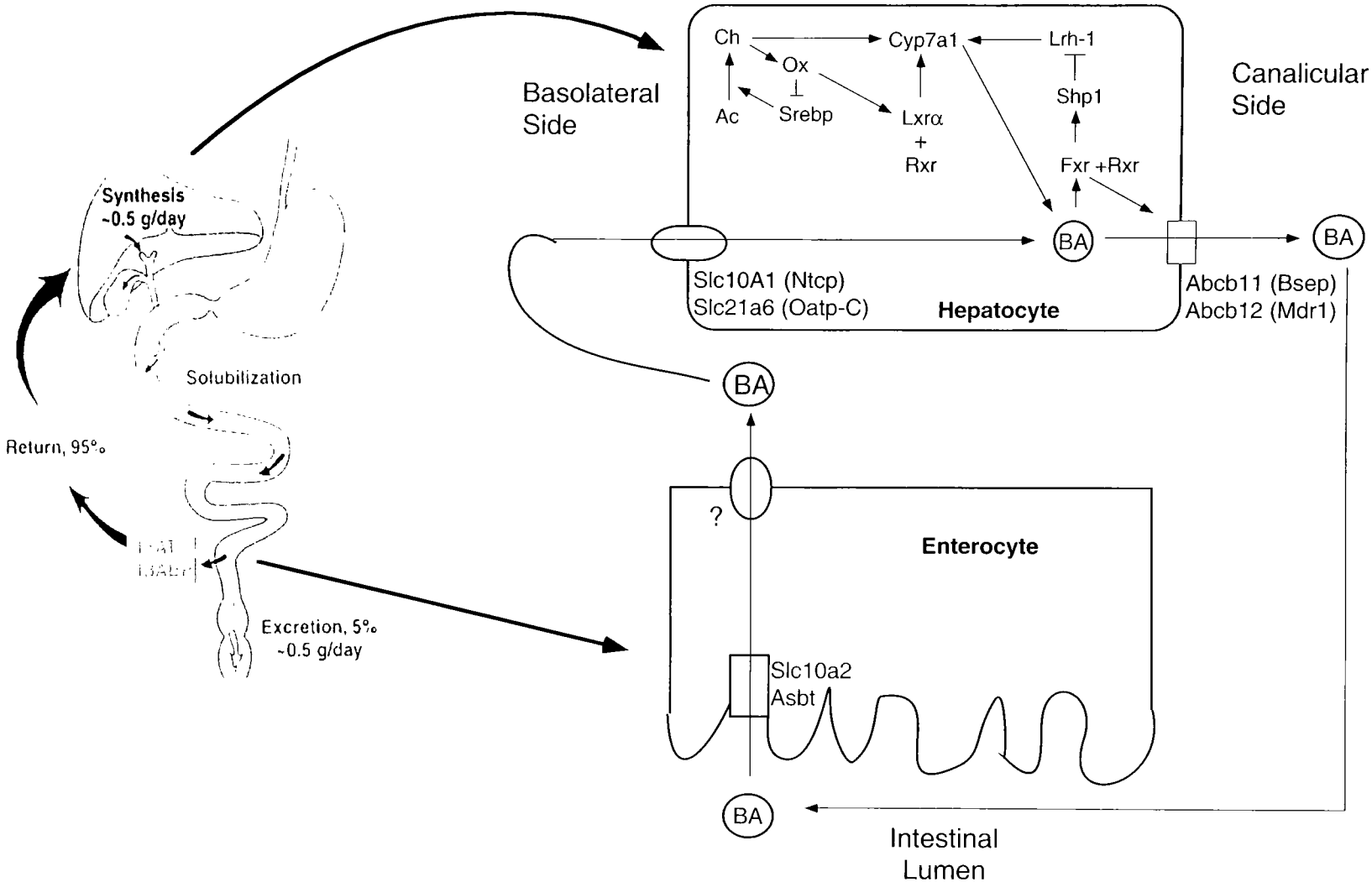

Figure 6-1. Overview of bile acid and cholesterol metabolism. BA, bile acid; Ch, cholesterol; Ox, oxysterols; Oatp, Organic anion transporter polypeptide; Asbt, apical sodium-dependent bile acid transporter; Ntcp, sodium taurocholate cotransporting polypeptide; Srebp, sterol regulatory element binding proteins; Shp, small heterodimer protein; Lrh, liver receptor homologue 1; Lxr, liver X receptor; Cyp7a, cholesterol 7α-hydroxylase; Rxr, retinoid X receptor.

bile salts from the basolateral surface of enterocytes into the portal circulation has been attributed to an anion-exchange protein (219), however the transporter is yet unknown. Circulating bile acids are taken up from portal blood by 2 major class of hepatic basolateral transportes: sodium-dependent and sodium-independent organic anion transporter polypeptide family of transporters. At the apical surface of hepatocytes, conjugated bile acids are actively extruded into the canalicular space by members of the ATP-binding cassette (ABC) superfamily of proteins (220) that include bile salt export pump (Bsep, Abcb11) and multidrug resistance proteins (MRP) –1 (Abcc1). Elevated intracellular bile acid levels in the hepatocyte activate the nuclear receptor Fxr and modulates further bile acid uptake by decreasing the levels of influx bile acid transporter (Slc10a1) and increasing the level of efflux transporter (Abcb11). Bile acids are then transported in the canalicular space to the gall bladder where they are concentrated against a 1000-fold concentration gradient. About 5% of the bile acid pool (0.5g/day) are lost and are excreted in the stool. The lost bile acids are replaced by *de novo* synthesis in the liver.

The conversion of cholesterol into bile acids and the biliary excretion of cholesterol are important mechanisms for the removal of cholesterol from the body. The degradation of cholesterol occurs principally by conversion to bile acids in the liver through two main pathways: the classic pathway and the acidic pathway (221). The classic pathway, responsible for ≥50% of biosynthesis of bile acids, starts with a 7α-hydroxylation of cholesterol by the cytochrome P450 hydroxylase Cyp7a1 and occurs only in the liver. The transcription of Cyp7a1 is subject to both feedforward and feedback regulation (222). Expression of *cyp7a1* is activated by the orphan receptor Lrh-1. In

addition, feedforward activation by oxysterols, mediated by the liver X receptor α (Lxrα, NR1H3) along with its dimerization partner retinoid X receptor (Rxr) also regulate the expression of Cyp7a1 (223, 224). Feedback repression of *cyp7a1* is mediated by the farnesoid X nuclear receptor (Fxr) through a complex molecular mechanism that involves the coordinated regulation of several liver-enriched nuclear receptors. Bile acids are physiological ligands of Fxr, and its binding to Fxr leads to the transcription of small heterodimer partner (*shp, NR0B2*) (225, 226). Shp then heterodimerizes with Lrh-1 and inhibit its activity, which leads to promoter-specific repression of *cyp7a1* (227-230).

The acidic pathway starts with a 27 hydroxylation of cholesterol by the cytochrome P450 hydroxylase Cyp27a1 to generate oxysteroids. Since all the primary bile acids carry a 7α-hydroxyl group, this group is added to the oxysteroids by a specific hydroxylase Cyp7b1 at a later step in bile acid formation. Cyp7b1 is completely specific for oxysterols and has no significant activity for cholesterol. Humans with mutations in the *cyp7b1* have severe neonatal cholestasis, cirrhosis, and liver failure even though the *cyp7a1* gene is intact (231), thus highlighting the importance of the acidic pathway in early life.

In this study we used Affymetrix® oligonucleotide microarrays to identify Tcf1-regulated genes involved in cholesterol and bile acid metabolism. We then studied the physiological consequences of these molecular defects in $tcf^{-/-}$ mice. We show that Tcf1 is a key regulator of multiple pathways that are essential for the maintenance of normal plasma cholesterol levels, including bile acid synthesis, bile acid uptake by the liver, intestines and kidney, and HDL-cholesterol metabolism.

Results

Liver Gene Expression in *tcf1*$^{-/-}$ Mice

To study the molecular basis of hypercholesterolemia in *tcf1* null mice, we used the murine Affymetrix® oligonucleotide microarrays to compare gene expression between *tcf1*$^{-/-}$ and wildtype (wt) littermate animals. Gene expression was measured in the liver, the principal organ that regulates cholesterol homeostasis. Several distinguishable clusters of genes involved in lipid, glucose, and amino acid metabolism, as well as detoxifying enzymes, transporters, secreted proteins and transcription factors were differentially expressed (Table 6-1). Of the 37,820 gene sequences surveyed, 165 known genes and 279 EST sequences displayed a greater than two-fold decrease in expression in *tcf1*$^{-/-}$ and 415 genes were increased in *tcf1*$^{-/-}$ compared to wt livers. Upregulation of genes in adult *tcf1*$^{-/-}$ mice are most likely secondary events and were not found in newborn mice, an observations that is in agreement with Tcf1 being a transcriptional activator (115).

Regulation of Bile Acid Transporter Genes by Tcf1

Genes involved in bile acid metabolism and cholesterol synthesis were identified. In the liver, we found that the steady state mRNA of *slc10a1* (*ntcp*), the gene encoding the principal sodium-dependent bile acid transporter for conjugated bile acids (232, 233), and *slc21a6* (*oatp-C*), *slc21a11* (*oatp-D*) and *slc21a5* (*oatp2*), three distinct genes of the sodium-independent organic ion transport family (234-236), were either absent or markedly downregulated in *tcf1*$^{-/-}$ mice (Fig. 6-2A). All proteins encoded by these genes are known to mediate the uptake of bile acids across the basolateral (sinusoidal) membrane of hepatocytes. Protein levels were also studied in crude membrane extracts of

Acc.#	Fold change	Gene name	Function
Steroid Metabolism			
D45850	-16 8	estradiol 17-beta-dehydrogenase (A-specific)	steroid hormone metabolism
NM_009040	-7 3	retinol dehydrogenase	steroid hormone metabolism
Y09517	-3 6	17-beta-hydroxysteroid dehydrogenase type II	steroid hormone metabolism
AB006361	-3 4	prostaglandin D synthetase	prostaglandin D biosynthesis
X07888	*12 6*	*3-hydroxy-3-methylglutaryl coenzyme A reductase (Hmgcr)*	*cholesterol biosynthesis*
L23754	*7 9*	*cholesterol alpha-7-hydroxylase (Cyp7a1)*	*bile acid metabolism*
AF057368	*3 1*	*7-dehydrocholesterol reductase*	*cholesterol synthesis*
D29016	*2 2*	*squalene synthase*	*cholesterol synthesis*
D42048	2 0	squalene epoxidase	cholesterol synthesis
AF090317	2 0	sterol 12-alpha hydroxylase	bile acid biosynthesis
Lipid Metabolism			
AI648067	-39 0	hydroxyacid oxidase 3	oxidation of 2-hydroxy fatty acids
AB037540	-21.5	leukotriene B4 omega-hydroxylase	leukotriene metabolism
Y14660	*-11 6*	*fatty acid binding protein*	*intracellular transfer of fatty acids*
X58426	*-3 4*	*hepatic lipase (Lipc)*	*lipoprotein catabolism*
Msa 294360	*-3 1*	*high affinity bile acid binding protein (Akr1c2)*	*bile acid storage*
U48403	-2 2	glycerol kinase	fatty acid and glucose metabolism
NM_008509	*14 6*	*lipoprotein lipase*	*lipoprotein catabolism*
D30666	9 1	brain acyl-CoA synthtase II	triacylglycerol biosynthesis
U28960	5 6	phospholipid transfer protein	phospholipid metabolism
M20497	*4.3*	*adipose fatty acid binding protein*	*intracellular transfer of fatty acids*
X85983	3 5	carnitine acetyltransferase	fatty acid catabolism
AB033887	3 3	acyl-CoA synthetase 4 variant2	triacylglycerol biosynthesis
X13135	*2 9*	*fatty acid synthetase*	*fatty acid biosynthesis*
M65034	*2 6*	*fatty acid binding protein intestinal*	*intracellular transfer of fatty acids*
AJ011864	2 4	L-specific multifunctional beta-oxdiation protein	fatty acid catabolism
Glucose Metabolism			
AF080469	-3 6	glucose-6-phosphate transporter	glycogenolysis
J02652	6 1	malate NADP oxidoreductase	TCA cycle
D63764	*4 5*	*pyruvate kinase*	*glycolysis*
L09192	*3 2*	*pyruvate carboxylase*	*TCA cycle and gluconeogenesis*
AB027012	*2 7*	*galactokinase*	*carbohydrate catabolism*
U05809	2 3	transketolase	hexose monophosphate pathway
Secreted Protein			
U51017	-72 3	kallistatin	kallikrein inhibitor
AJ011080	*-60 5*	*alpha-albumin*	*carrier protein*
U66900	-52 4	insulin-like growth factor binding protein, acid labile subunit	carrier protein
X13588	-18 3	C-reactive protein	acute phase reactants
X76066	-14 3	insulin like growth factor binding protein 4	growth factor
D10071	-12 5	coagulation factor XIII	coagulation factor
XM_003476	-5 3	coagulation factor XI	coagulation factor
X04480	*-2 5*	*insulin-like growth factor 1*	*growth factor*
J04766	*-2.1*	*plasminogen*	*coagulation factor*
AF002719	10 1	secretory leukoprotease inhibitor	serine protease inhibitor
U34277	8 4	PAF acetylhydrolase	pro-inflammatory autacoid
M25529	7 6	alpha-1-antitrypsin	serine protease inhibitor
M75720	2 6	serine protease inhibitor 1-3	serine protease inhibitor

Acc.#	Fold change	Gene name	Function
Detoxification			
L11333	-314 1	carboxyesterase	xenobiotic metabolizing enzyme
M13506	-69 4	UDP-glucuronosyltransferase	xenobiotic metabolizing enzyme
X83202	*-29 5*	*11beta-hydroxysteroid dehydrogenase/carbonyl reductase*	*xenobiotic metabolizing enzyme*
AF026075	-19 5	sulfotransferase	sulfate conjugation
U96746	-6 8	thiol peroxidase	antioxidant enzyme
AJ000413	-3 0	glutathione S-transferase class M5	xenobiotic metabolizing enzyme
U13705	-2 7	glutathione peroxidase 3	antioxidant enzyme
U00937	7 8	gadd45	DNA repair
AF241240	6 9	SNM1	DNA repair
U66322	6 2	dithiolethione-inducible gene-1	xenobiotic metabolizing enzyme
U86108	3	nicotinamide N-methyltransferase	xenobiotic metabolizing enzyme
AF037044	2 6	thiopurine S-methyltransferase	xenobiotic metabolizing enzyme
D87896	2 5	glutathione peroxidase 4	antioxidant enzyme
J04696	2 1	glutathione S-transferase class mu	xenobiotic metabolizing enzyme
Transporters			
AB031959	*-55 6*	*liver-specific organic anion transporter-1 (Slc21a6)*	*organic anion transporter*
NM_006632	-24 7	solute carrier family 17 (slc17a3)	sodium phosphate transporter
U29881	-8 0	low affinity Na-dependent glucose transporter	glucose transporter
Y19035	-5 0	amiloride-sensitive Na+ channel	sodium channel
AB002693	*-4 2*	*ileal bile acid transporter (Slc10A2)*	*bile acid transporter*
U20973	-3.2	solute carrier family 12 (Nkcc2)	Na-K-Cl cotransporter
AF058054	-3 1	monocarboxylate transporter 2	pyruvate transporter
U61085	-2 9	thiazide-sensitive Na-Cl cotransporter	Na-Cl cotransporter
X70060	-2 7	gamma subunit of sodium potassium ATPase	Na-K channel
AF018952	-2 6	aquaporin-8	water/urea channel
AJ249198	-2 4	glycoprotein-associated amino acid transporter	amino acid transporter
AF081499	4 5	type IIb Na/phosphate-cotransporter	sodium phosphate transporter
L03290	2 2	amino acid transporter, cationic 2	amino acid transporter
Transcription Factor			
L76567	*-5 7*	*small heterodimer partner (Nr0b2, Shp-1)*	*nuclear receptor, inactivates Lrh-1*
Msa 66110 0	*-2 5*	*Dimerization cofactor of HNF-1α*	*Activates Tcf1*
U44752	*-2.2*	*hepatocyte nuclear factor 3 alpha*	*forkhead transcription factor*
U20282	-2	stromelysin PDGF responsive element binding protein	nuclear Factor
U09416	*-2*	*farnesoid receptor RIP14 (Fxr)*	*nuclear receptor, activates Shp-1*
U10374	*6.1*	*peroxisome proliferator activator receptor gamma*	*nuclear receptor*
U19118	4 9	lipopolysaccharide inducible transcription factor LRG-21	Homology to ATF3, LRF-1
U20735	2 9	transcription factor JunB	activating protein 1 transcription factor
Amino Acid Metabolism			
AB021968	-89 4	carboxypeptidase R	protein turnover
AA675075	-52 5	proline oxidase 1	proline degradation pathway
X51942	*-23 7*	*phenylalanine hydroxylase*	*tyrosine biosynthesis*
X63349	-12 6	tyrosinase-related protein-2	melanin pigment biosynthesis
U74683	-2.2	cathepsin C	protein turnover
AJ242663	-2.1	cathepsin Z	protein turnover
U38940	3 5	asparagine synthetase	asparagine biosynthesis

Table 6-1. Gene expression changes in livers of adult *tcf1*$^{-/-}$ and wildtype littermates. GeneBank accession numbers are listed under "Acc. No." Accession numbers in italics indicate that the expression of the corresponding gene was independently confirmed by semiquantitative RT-PCR analysis. A more comprehensive list that includes unknown genes is available (See Web Table A).

livers using western blot analysis. The expression of Slc10a1 was reduced to 4% of wt animals in *tcf1*$^{-/-}$ mice. Furthermore, we were unable to detect Slc21a6 protein in the livers of *tcf1*$^{-/-}$ mice (Fig. 6-3B).

Since *tcf1*$^{-/-}$ mice develop hepatomegaly and central lobular hypertrophy at 5-7 weeks of age which may lead to secondary changes in hepatic gene expression, we studied mRNA levels in newborn animals with no morphological or biochemical evidence of liver diseas (36, 37). We found that the decrease in gene expression of basolateral bile acid transporters was already apparent shortly after birth, suggesting that loss of Tcf1 function rather than chronic liver disease is the primary cause of the defect (Fig. 6-2A). Together, these results indicated that Tcf1 is essential for bile acid transport across the basolateral (sinusoidal) hepatocyte membrane.

Regulation of Bile Acid biosynthesis by Tcf1

Conjugated bile acids exist as anions at physiological pH and consequently, require carrier for transport across the membranes of enterohepatic tissues. Efflux of bile acids at the apical surface of the hepatocytes is mainly mediated by ATP-binding cassette (ABC) superfamily of proteins that include including Abcb11 (Bsep), Abcc2 (Mrp2), Abcb1 (Mdr1), and Abcb4 (Mdr2) (220). ABC proteins share common structural motifs including a conserved intracellular domain that binds ATP and couples primary active, unidirectional export of a broad range of compounds (xenobiotics, bile acids, etc) to ATP hydrolysis.

To investigate whether Tcf-1 similarly regulates bile acid transporters that are located at the apical (canalicular) membrane, we measured mRNA levels of transporters that are responsible for the efflux of bile acids. In contrast to the basolateral bile acid

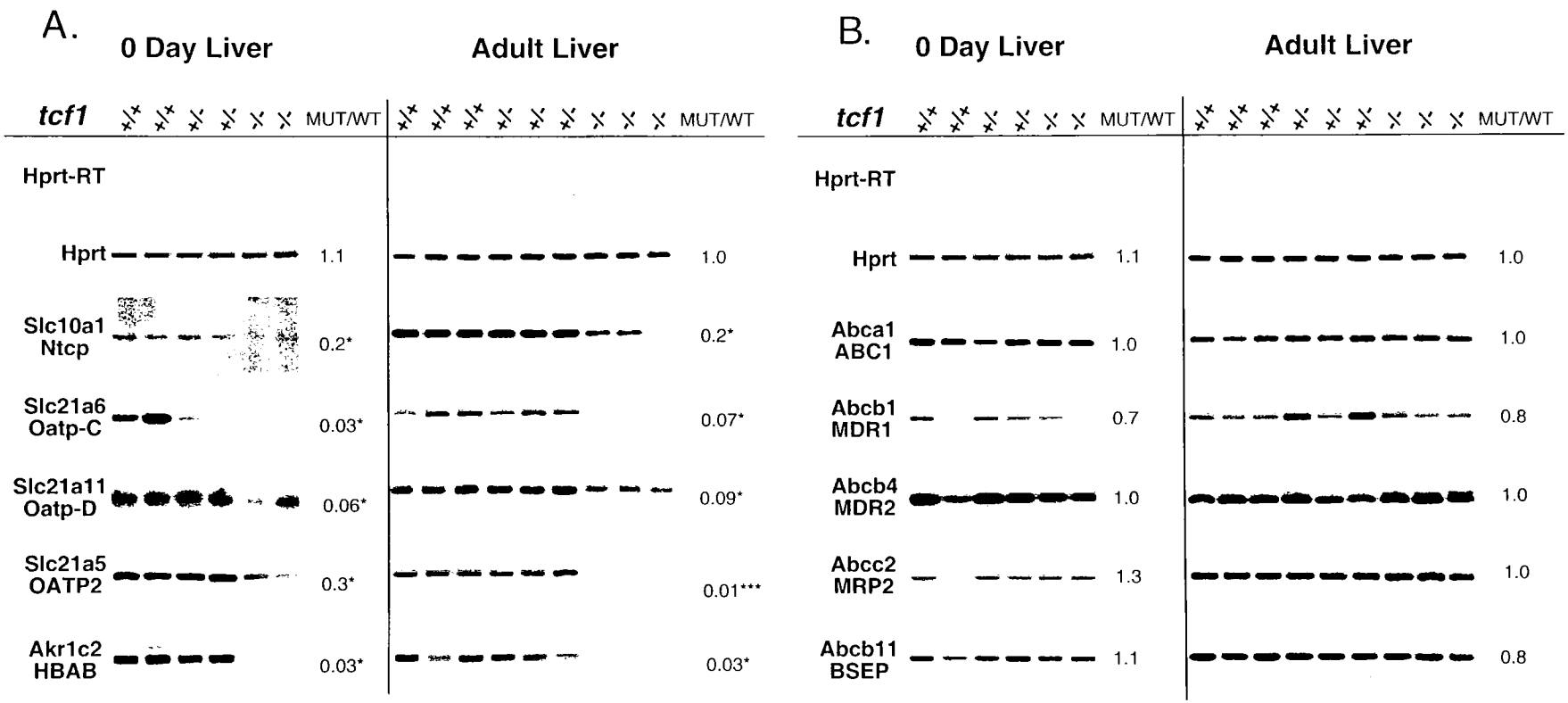

Figure 6-2. Regulation of bile acid transporters by Hnf-1α. Expression of bile acid transporters that are located exclusively at the basolateral (A) and canalicular (B) membrane was measured by reverse-transcription-PCR using [α-^{32}P]dCTP. Gene expression was measured in three to six animals for each genotype (only two and three animals/genotype are shown for newborn and adult livers, respectively). Quantitative measurements were obtained by densitometry. MUT/WT indicates the ratio of expression levels of the means of null (*tcf1*$^{-/-}$) mice and wildtype (*tcf1*$^{+/+}$)(n=3-5). *:$P \leq 0.05$; **: $P \leq 0.005$; ***: $P \leq 0.001$. Hprt: hypoxanthine phosporibosyltransferase; Slc10a1: (basolateral) sodium-taurocholate cotransporting polypeptide (NTCP); Slc21a6, Slc21a11and Slc21a5: (sodium-independent) organic anion transporter (Oatp-C, -D and -2, respectively); Abca1 (Abc1), Abcb1 (Mdr1), Abcb4 (Mdr2): ATP-(multidrug-resistance) binding cassette proteins; Abcc2 (Mrp2, Moat): multiorganic anion transporter; Abcb11 (Bsep): (ATP-driven canalicular) bile salt export pump; Akr1c2: bile acid binding protein,

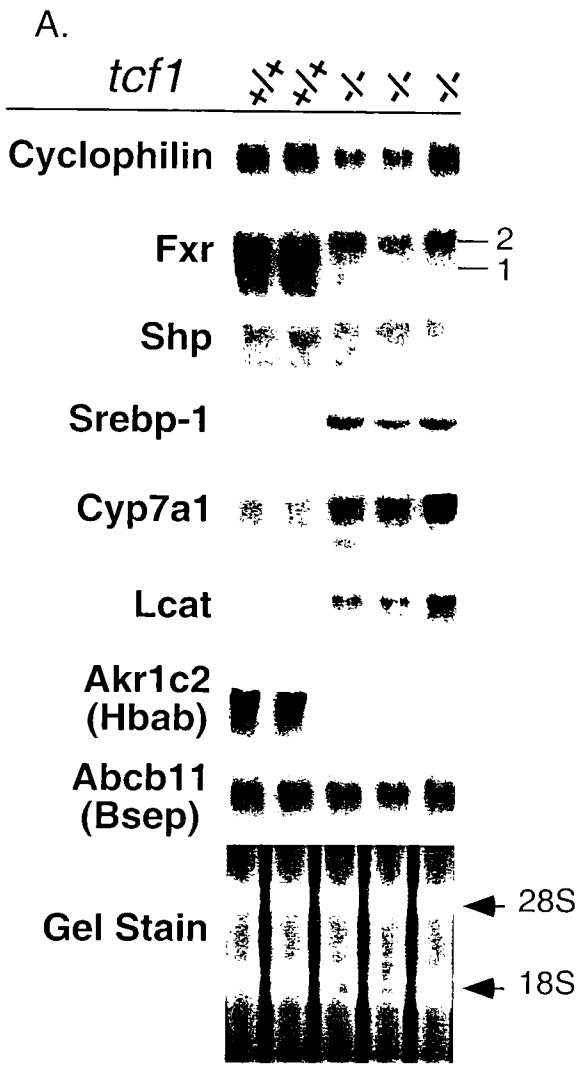

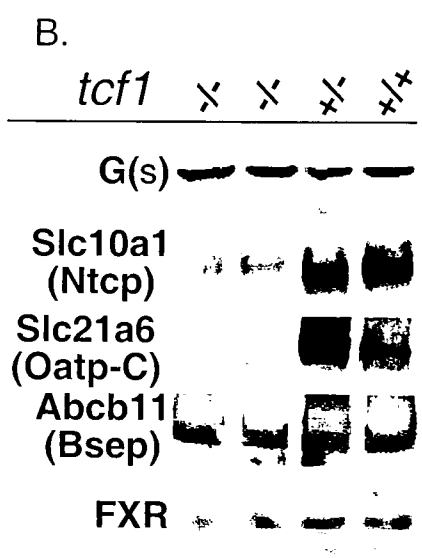

Figure 6-3. Northern and Western blot analysis of genes involved in bile acid and cholesterol metabolism in Tcf-1 deficient mice. (A) Northern blot analysis of genes involved in bile acid and cholesterol metabolism in livers of two *tcf1*$^{+/+}$ (left two lanes) and three *tcf1*$^{-/-}$ (three lanes on right) animals. Cyclophilin was used as a control for RNA loading. The two Fxr isoforms are indicated with an arrow. (B) Western blot analysis of bile acid transporters and farnesoid X receptor (Fxr) in liver protein extracts. The expression of Slc10a1 (Ntcp), Slc21a6(Oatp-C) and Fxr was reduced to 12%, 4.2%, and 50%, respectively. Abcb11 (Bsep) situated at the canacular membrane is not regulated by Tcf-1. GTP binding stimulatory protein (Gs) was used as loading control.

transporters, the expression of bile acid carriers such as Abcb11, Abcc2 and Abcb1, that are located at the canalicular membrane of the hepatocytes, were indistinguishable between *tcf1*$^{+/+}$ and *tcf1*$^{-/-}$ animals (Fig. 6-2B, 6-3). The expression of Abcb4 (Mdr2), a transporter protein that is mutated in progressive familial intrahepatic cholestasis (PFIC) (237, 238), is also normal in *Tcf1* null mice (Fig. 6-2B).

Regulation of Bile Acid Biosynthesis by Tcf1

To study the role of Tcf1 in bile acid biosynthesis, we determined the steady-state mRNA levels of genes that are involved in the classical and the acidic pathway of cholesterol catabolism in *tcf1*$^{-/-}$ mice. Gene expression studies showed that the expression of cholesterol 7α-hydroxylase (Cyp7a1), but not oxysterol 7α-hydorxylase (Cyp7b1), was increased in adult *tcf1*$^{-/-}$mice. Furthermore, the biochemical measurement of Cyp7a1 activity showed a 5-fold increase in *tcf1*$^{-/-}$ mice (35.1 vs 177.5 pmol/mg microsomal protein/min *tcf1*$^{+/+}$ vs. *tcf1*$^{-/-}$, respectively, n=10, P <0.001) (Fig. 6-3A, 6-4A, B). To study the molecular basis of the upregulation in bile acid synthesis, we analyzed the expression levels of Lxr-α, Lrh1, Shp-1, and Fxr in the liver. Lxrα, Rxr, and Lrh1 expression levels did not differ significantly in wt and *tcf1*$^{-/-}$ mice (Fig. 6-4A). In contrast, the DNA array data and northern blot analysis revealed a significant decrease in Shp-1 and Fxr expression, due to the loss of the Fxr-1 specific isoform (Table 6-1, Fig. 6-3A). Two Fxr-isoforms, Fxr-1 and Fxr-2, exist in mice and differ in their 5'-untranslated and coding regions. These transcripts are expressed in approximately equimolar quantities in liver and intestine (Fig. 6-3A). The selective loss of expression of the Fxr-1 isoform was confirmed in adult and newborn livers of *tcf1*$^{-/-}$ mice by RT-PCR analysis using specific primers (Fig. 6-4A). This result indicated that the increase in Cyp7a1 expression in *tcf1*$^{-/-}$

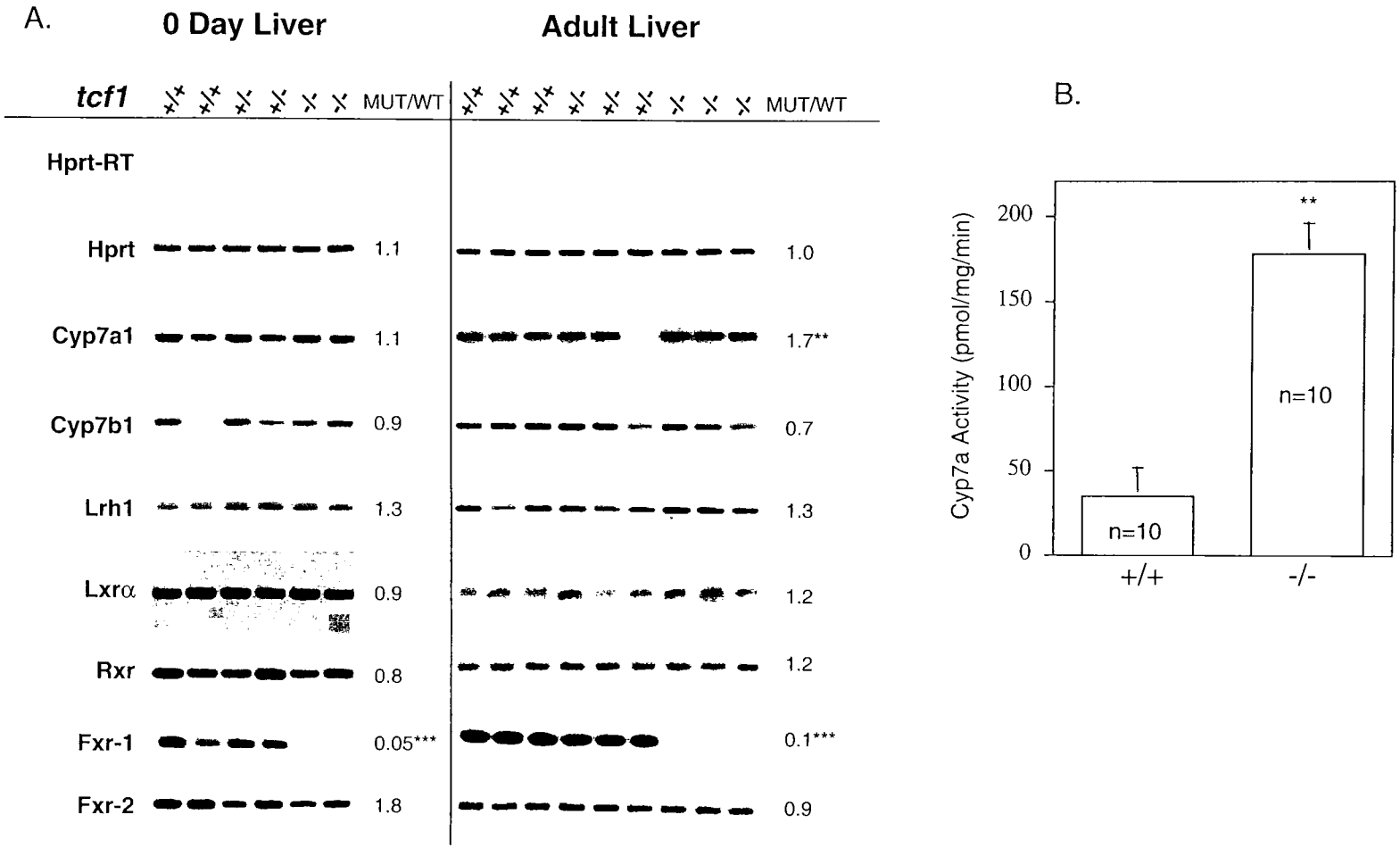

Figure 6-4. The activity of Cyp7a1 is increased in *tcf-1*$^{-/-}$ mice. (A). RT-PCR analysis steady state mRNA of genes involved in bile acid biosynthesis. Gene expression was measured in three to six animals for each genotype (only two and three animals/genotype are shown for newborn and adult livers, respectively). Quantitative measurements were obtained by densitometry. MUT/WT indicates the ratio of expression levels of the means of null (*tcf1*$^{-/-}$) mice and wildtype (*tcf1*$^{+/+}$)(n=3-5). (B) The activity of Cyp7a1 is detemined in isolated hepatic microsomes. Enzymee activity is expressed as pmol of 7α–hydroxycholesterol formed per mg protein/min. *:$P \leq 0.05$; **: $P \leq 0.005$; ***: $P \leq 0.001$. Hprt: hypoxanthine phosporibosyltransferase; Cyp7a1: cholesterol 7α-hydroxylase; Cyp7b1: oxysterol 7α-hydroxylase; Lrh1: liver receptor homolog-1; Lxrα: liver X receptor α; RXR: retinoid X receptor; Fxr: farnesoid X nuclear receptor.

mice is the result of decreased feedback repression of Fxr, mediated by reduced expression of Shp1 and possibly diminished intracellular bile acid concentrations.

To further study the transcriptional regulation of Fxr by Tcf1, we cloned 0.7 kb of the 5'-flanking promoter region of the murine*fxr* gene and linked it to a luciferase reporter gene (pGL2-pFxr-1). Cotransfection of this reporter plasmid with a Tcf1 expression vector (pcDNA3-pHNF-1α) showed an approximately six-fold dose-dependent activation of the Fxr-1 promoter (Fig. 6-5A). Sequencing analysis of the Fxr-1 promoter identified a high affinity Tcf1 binding site at –201 to -217 bp. Electrophoretic mobility shift assays were performed with mouse liver nuclear extracts to study the binding properties of this Tcf1 binding site. A major DNA/protein complex was detected with a ^{32}P-labeled oligonucleotide that contained the Tcf1 binding site (Fig. 6-5B, lane 2). This binding activity could be competed by an unlabeled excess of an oligonucleotide containing a known high-affinity Tcf1 binding site of the insulin growth factor binding protein-1 (*igfbp1*) promoter (239) (Fig. 6-5B, lane 3). To test directly for the interaction of Tcf1 with the oligonucleotide probe, we analyzed whether a Tcf1-specific antibody affected the protein-DNA complex. A supershift of the complex was observed after preincubation of extracts with Tcf1 antiserum, but not with anti-STAT-1 antibodies, demonstrating that Tcf1 can bind to the Tcf1 site in the Fxr-1 promoter (Fig. 6-5B, lane 4 and 5). Together, these data indicate that Tcf1 is a transcriptional activator of Fxr-1 and that loss of Tcf1 function reduces the feedback inhibition of ligand-activated Fxr target genes, and thereby activating bile acid synthesis.

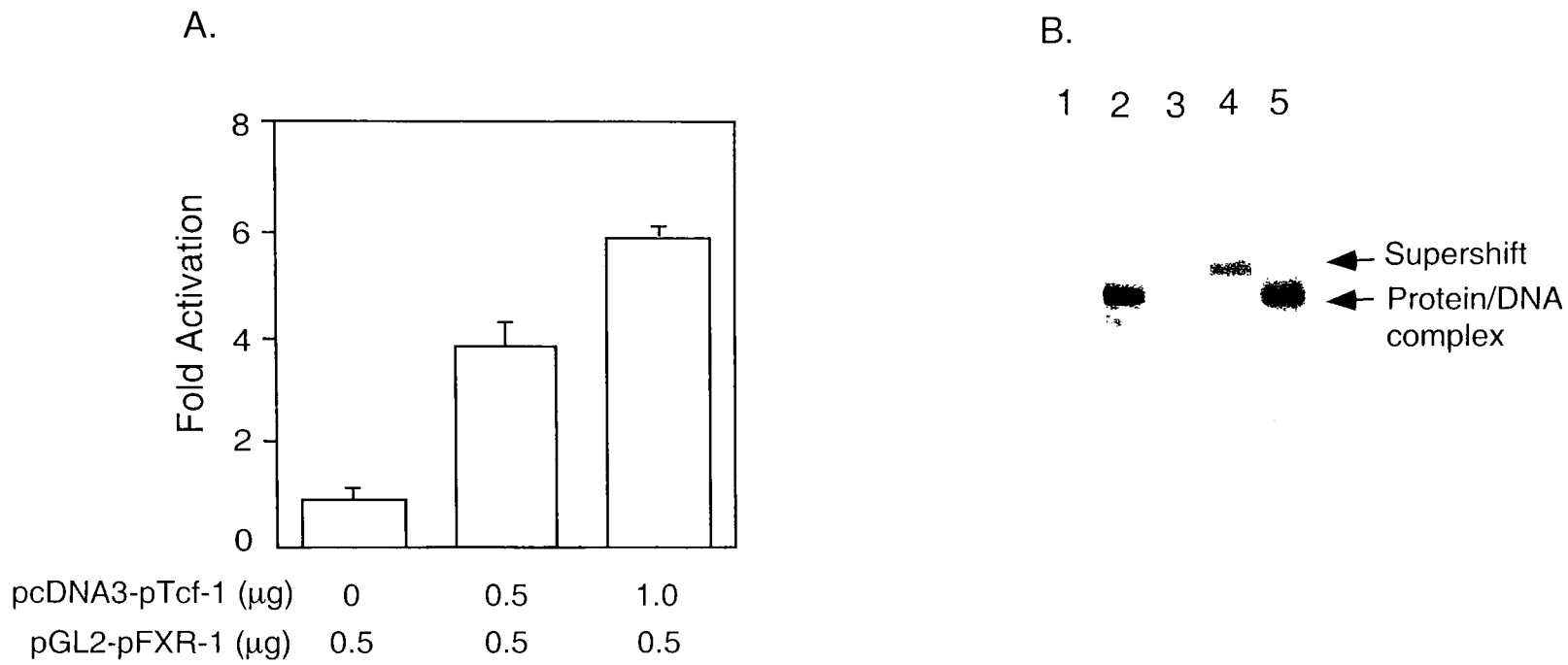

Figure 6.5. Analysis of Fxr-1 promoter. (A) Cotransfection of Tcf1 expression vector and pGL2-pFxr-1 in HepG2 cells. The average-fold inductions of two independent transfections, performed in duplicates and normalized to ß-galactosidase activity, are shown. Error bars indicate standard error of the mean. (B)Tcf1 binds to the Tcf1 binding site in the Fxr-1 promoter. EMSA analysis of DNA binding activity of liver nuclear extracts and a ^{32}P-labeled double-stranded oligonucleotide containing the Tcf1 binding site of the Fxr-1 promoter. Lanes 1: probe alone (signal on bottom of gel, not seen in this picture), 2: probe + nuclear extract, 3: probe + nuclear extract + 20x cold competitor (Tcf1 binding site of Igfbp1 promoter), 4: probe + nuclear extract + anti- Tcf1 antibody, 5: probe + nuclear extract + anti-STAT1 antibody.

Ileal and Renal Bile Acid Absorption in *tcf1*$^{-/-}$ Mice

We next investigated the physiological effects resulting from the impaired expression of genes encoding hepatic bile acid uptake and the enhanced *de novo* synthesis of bile acids in the liver. From our expression data, we predicted that bile acids in the serum may be elevated and that *de novo* synthesized bile acids would be secreted normally into the canalicular system and ultimately into the intestine. Serum bile acid levels in *tcf1*$^{-/-}$ mice were indeed elevated to ≈250 μmol/L and five-fold higher than in WT control littermates (Fig. 6-6A). Interestingly, fecal bile acid concentrations were approximately six-fold elevated in the stool of mice that lacked expression of Tcf1 compared to normal littermates (Fig. 6-6B). We also found increased bile acid concentrations in the urine of *Tcf1* null mice (Fig. 6-6C).

The incomplete absorption of bile acids from the distal ileum and the renal proximal tubule of *tcf1*$^{-/-}$ mice suggested that Tcf1 might also be a transcriptional activator of genes involved in intestinal and renal bile acid uptake. The apical sodium dependent bile acid transporter (Slc10a2, Asbt, Ibat) is expressed at the apical surface of enterocytes in the terminal ileum and on the apical membrane of the renal tubule and biliary epithelia (240, 241). Measurements of steady state mRNA of *slc10a2* by RT-PCR in the terminal ileum and kidney showed that expression was practically absent in *tcf1* null mice (Fig. 6-7A, B). Furthermore, we were not able to detect any Slc10a2 expression in *tcf1*$^{-/-}$ mice of intestinal protein extracts using immunoblot analysis or in tissue sections of the terminal ileum using immunohistochemistry (Fig. 6-7C and D, respectively).

To study whether Tcf1 is a direct activator of *slc10a2* gene transcription, we cloned the *slc10a2* promoter and identified a single high-affinity Tcf1 binding site in its

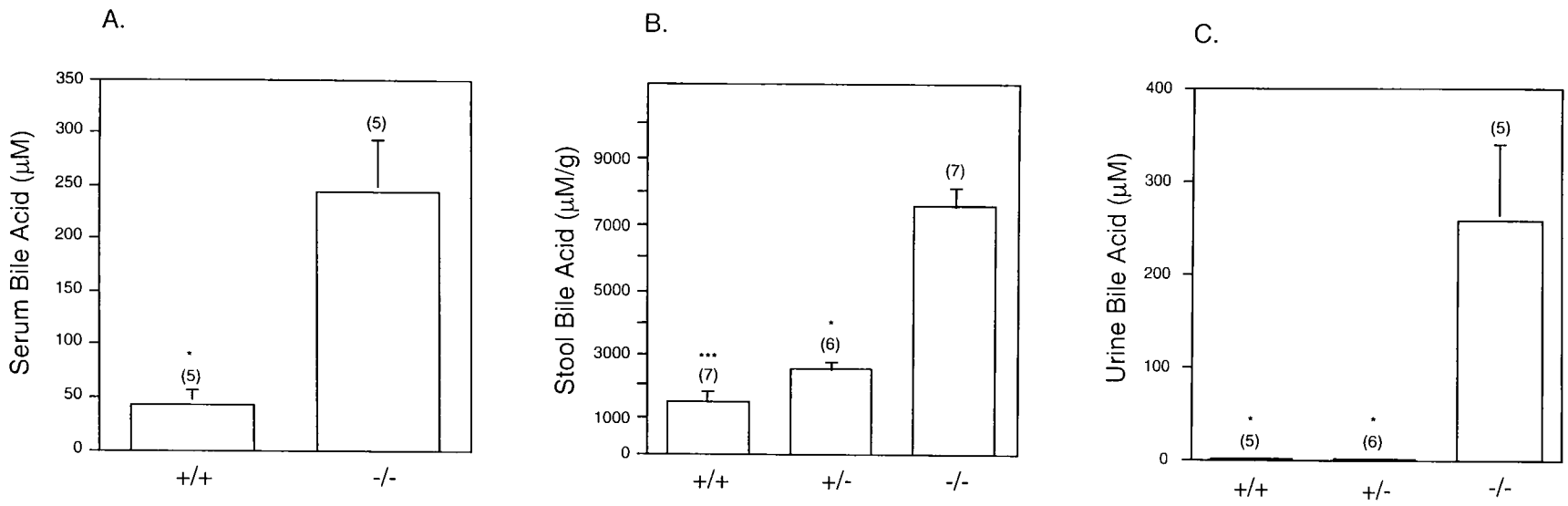

Figure 6-6. Physiological characterization of bile acid levels in *tcf1*$^{-/-}$ mice. (A) Serum bile acid measurements in wildtype (*tcf1*$^{+/+}$) and mutant (*tcf1*$^{-/-}$) mice. (B) Bile acid measurements in the stool of wildtype (*tcf1*$^{+/+}$), heterozygous (*tcf1*$^{+/-}$) and null (*tcf1*$^{-/-}$) mice. (C) Bile measurements in the urine of wildtype (*tcf1*$^{+/+}$), heterozygous (*tcf1*$^{+/-}$) and null (*tcf1*$^{-/-}$) mice. Numbers in brackets indicate the number of animal studied. *: $P \leq 0.05$; **: $P \leq 0.005$; ***: $P \leq 0.0005$.

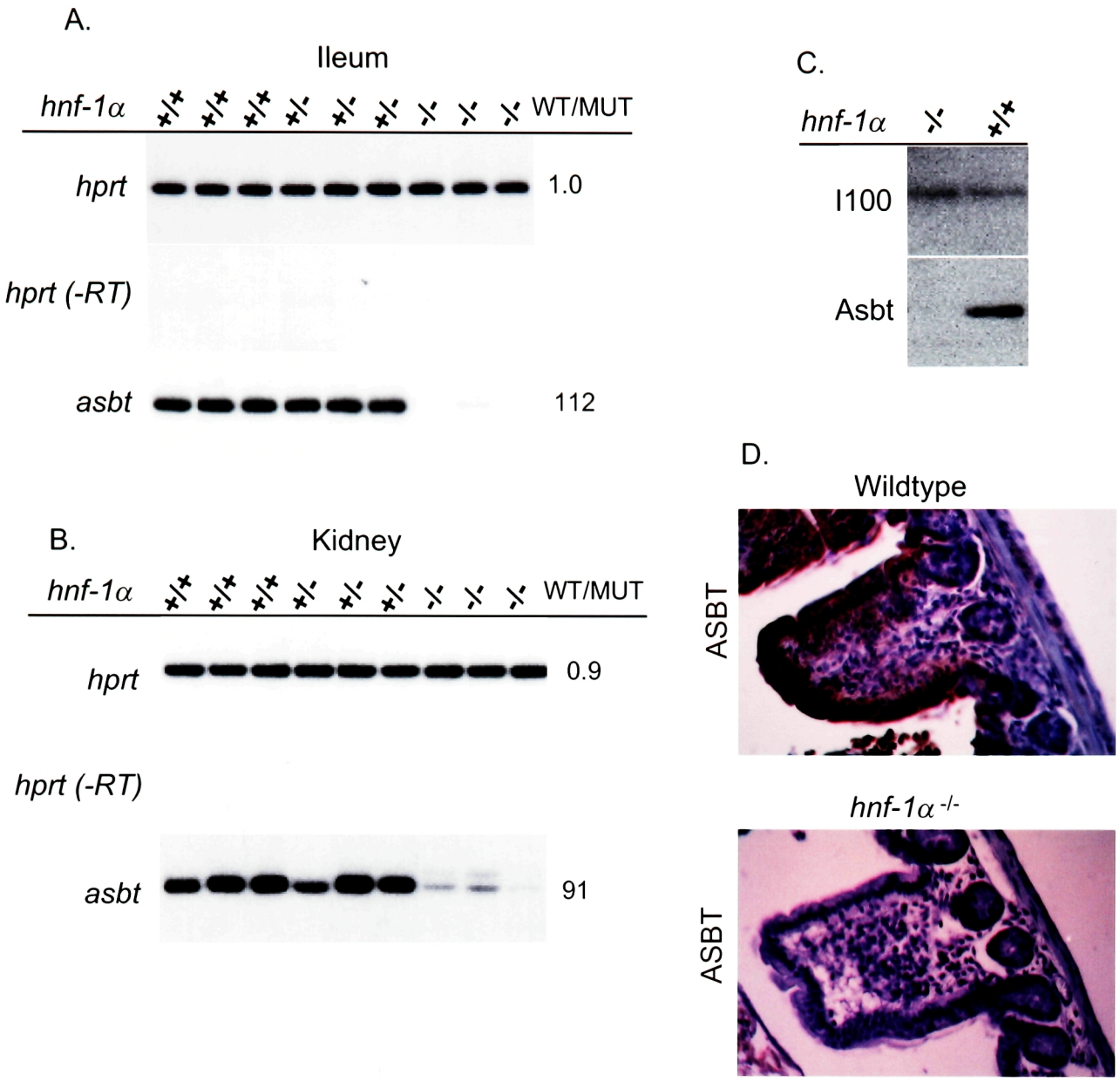

Figure 6-7. Tcf1 is a transcriptional activator of the apical sodium-dependent bile acid transporter gene. RT-PCR analysis of *asbt* gene expression in the terminal ileum (A) and in the kidney (B) of wildtype, $tcf1^{+/-}$, and $tcf1^{-/-}$ mice. Hprt was used as a control and shows that equal amounts of RNA samples were used for the analysis. WT/MUT indicates the ratio of expression levels of the means of three wildtype and three mutant ($tcf1^{-/-}$) mice. (C) Immunoblot analysis of crude brush border membrane proteins from the terminal ileum of wildype ($tcf1^{+/+}$) and null ($tcf1^{-/-}$) mice. Anti-Naaladasel (I100) antibody recognizes an enterocyte-specific peptidase (*Naaladasel*) and was used to control for equal loading. (D) Normal intestinal morphology but defective immunostaining for Asbt protein in $tcf1^{-/-}$ mice. Sections from the terminal ileum were stained with a polyclonal antibody against Asbt. Asbt was detected on the apical membrane of enterocytes in wildtype, but not in mutant ($tcf1^{-/-}$) mice.

regulatory region. An 1854 bp promoter region was cloned upstream of a luciferase reporter and cotransfected with a Tcf1 expression vector. Transient cotransfections of Tcf1 with the *slc10a2* promoter led to a dose-dependent 40-fold activation of luciferase activity (Fig. 6-8A). When the Tcf1 site in the *slc10a2* promoter was selectively mutated, transcriptional activation was reduced 50-80% (Fig. 6-8A). Gel mobility shift assays were performed using double stranded ^{32}P-labeled oligonucleotides containing the wt and mutated Tcf1 binding site using mouse liver nuclear extracts. A DNA-protein complex was detected (Fig. 6-8B, lane 2). The specificity of protein binding to this site was determined by competition assays using cold wt and Tcf1-binding defective oligonucleotides. The competitor wt sequence, but not the mutant binding site, effectively competed for protein-DNA complex formation (Fig. 6-8B, lanes 3 and 4). Furthermore, Tcf1 antiserum supershifted the DNA-protein complex, demonstrating that Tcf1 protein is a component of the binding activity (Fig. 6-8B, lane 5). These data suggest that Tcf1 is a potent activator of *slc10a2* transcription *in vivo* and *in vitro*.

Cholesterol Metabolism in *tcf1*$^{-/-}$ Mice

Mice lacking Tcf1 expression have normal cholesterol levels at birth but develop hypercholesteremia (≈300 mg/dl) at 6 to 8 weeks of age (Fig. 6-9A). We examined the cholesterol distribution in plasma lipoproteins of *tcf1*$^{-/-}$, wt, and LDL receptor knockout animals (*ldlr*$^{-/-}$ mice accumulate cholesterol predominantly in LDL particles) (242). Fasting plasma lipoprotein composition was analyzed following FPLC fractioning. As shown in figure 6-9B in the *ldlr*$^{-/-}$ mice, cholesterol was eluted mainly in the LDL but was also present in the VLDL and HDL fractions (Fig. 6-9B; the positions at which VLDL, LDL, and HDL elute are indicated). In contrast, almost all of the cholesterol in the

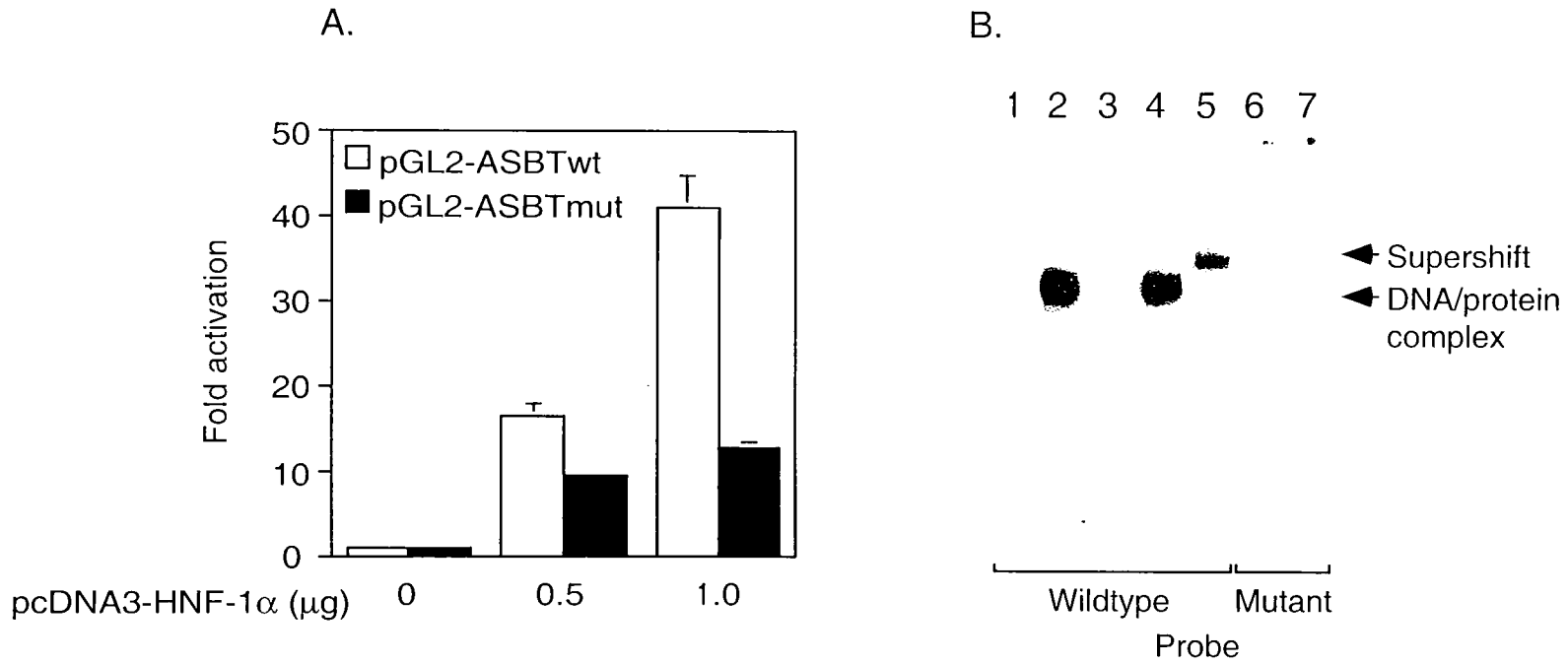

Figure 6-8. The *asbt* promoter is activated by Tcf1. (A) Cotransfection assays in HIT-T15 cells demonstrate that Tcf1 can activate the *asbt* promoter in a dose-dependent fashion. This activation was impaired when the Tcf1 binding site of the *asbt* promoter was mutated (pGL2-pASBTmut). (B) Tcf1 binds to the Tcf1 binding site in the *asbt* promoter. The DNA binding activity of liver nuclear extracts and a 32P-labeled double stranded oligonucleotide containing the Tcf1 binding site of the *asbt* promoter (probe) was studied in gel mobility shift assays. Lanes 1: gel shift mobility assay of probe alone (signal on bottom of gel, not seen in this picture); 2: probe + nuclear extract, 3: probe + nuclear extract + 20x cold competitor probe, 4: probe + nuclear extract + 20x cold, binding defective, competitor (mutated Tcf1 binding site of *asbt* promoter), 5: probe + nuclear extract + anti- Tcf1 antibody, 6: mutant probe alone (signal on bottom of gel, not shown); 7: mutant probe + nuclear extract.

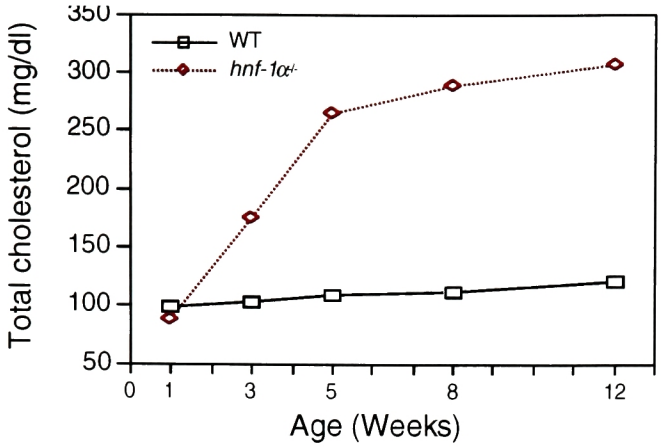

B.

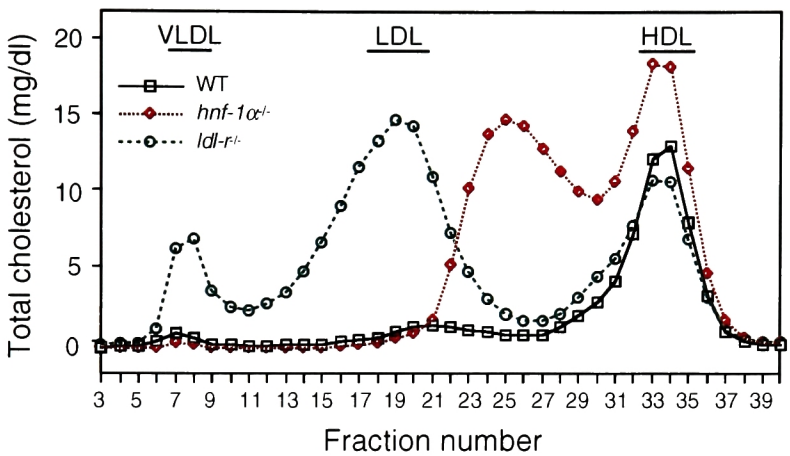

C.

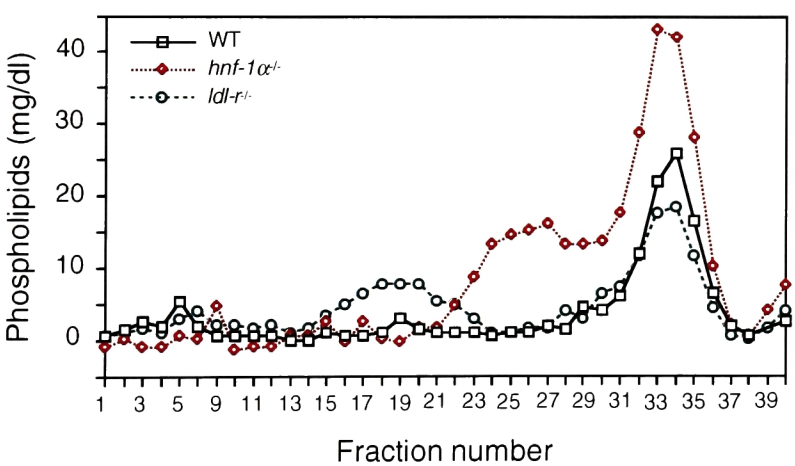

Figure 6-9. Serum lipoprotein profiles of control and *hnf-1α*$^{-/-}$ mice. (A) Hnf-1α deficient mice have normal cholesterol levels at birth but develop progressive hypercholesteremia. (B) and (C) Plasma (0.5 ml) from wt, *hnf-1α*$^{-/-}$ and low-density lipoprotein receptor-deficient (*ldlr*$^{-/-}$) mice were separated by FPLC, which was run with PBS as elutant. The fractions (0.5ml) of the eluate were assayed for Cholesterol (B) and Phospholipids (C). An "abnormal" lipoprotein particle with intermediate buoyancy between HDL and LDL peaks is seen in *hnf-1α*$^{-/-}$ mice.

plasma of *tcf1*$^{-/-}$ mice was carried by the HDL fraction and an "abnormal fraction" with intermediate buoyancy between HDL and LDL peaks (Fig. 6-9B, fractions 23 to 29). Phospholipids in the plasma of *tcf1*$^{-/-}$ mice was also carried mainly by the HDL fraction and by the "abnormal" lipoprotein particle (Fig. 6-9C).

Three lipoprotein particles may account for this abnormal lipoprotein fraction: Lp-X, small dense LDL or large HDL (HDL_c). Lp-X is a lamellar particle that contains mainly unesterified (free) cholesterol (FC) and has been identified in the plasma of patients with obstructive jaundice and in familial lecithin cholesterol acyltransferase deficiency (243-247). Small dense LDL is a spherical particle that contains mainly esterified cholesterol (EC) (248). Large HDL has been described in mice lacking hepatic lipase or increased activity of Lcat and may be caused by a defect in HDL phospholipids hydrolysis or increased choesterol esterification, respectively (249, 250). To distinguish between the three possibilities, we characterized the abnormal lipoprotein fractions in the plasma of *tcf1* null mice. The analysis of the cholesterol content in the abnormal lipoprotein fraction by gas liquid chromatography revealed that this particle contains mostly esterified cholesterol (62% EC vs. 38% FC) and in that respect was similar to that of LDL of *ldlr*$^{-/-}$ mice (62%EC vs. 38% FC). To further rule out the existence of Lp(X) in the plasma of *tcf1*$^{-/-}$ mice, we examined these particles by electron microscopy (Fig. 6-9A). Negatively stained samples revealed structures with diameters ranging from 40-100 nm. The abnormal lipoprotein particles from *tcf1*$^{-/-}$ mice were smaller than LDL particles of *ldlr*$^{-/-}$ mice and lacked the lamellar (hollow spherical) structures that characterize Lp-X (Fig. 6-10A) (246). We also determined the concentrations of Apo A1 and Apo B48/100, markers of HDL and LDL particles, respectively, using western blotting and

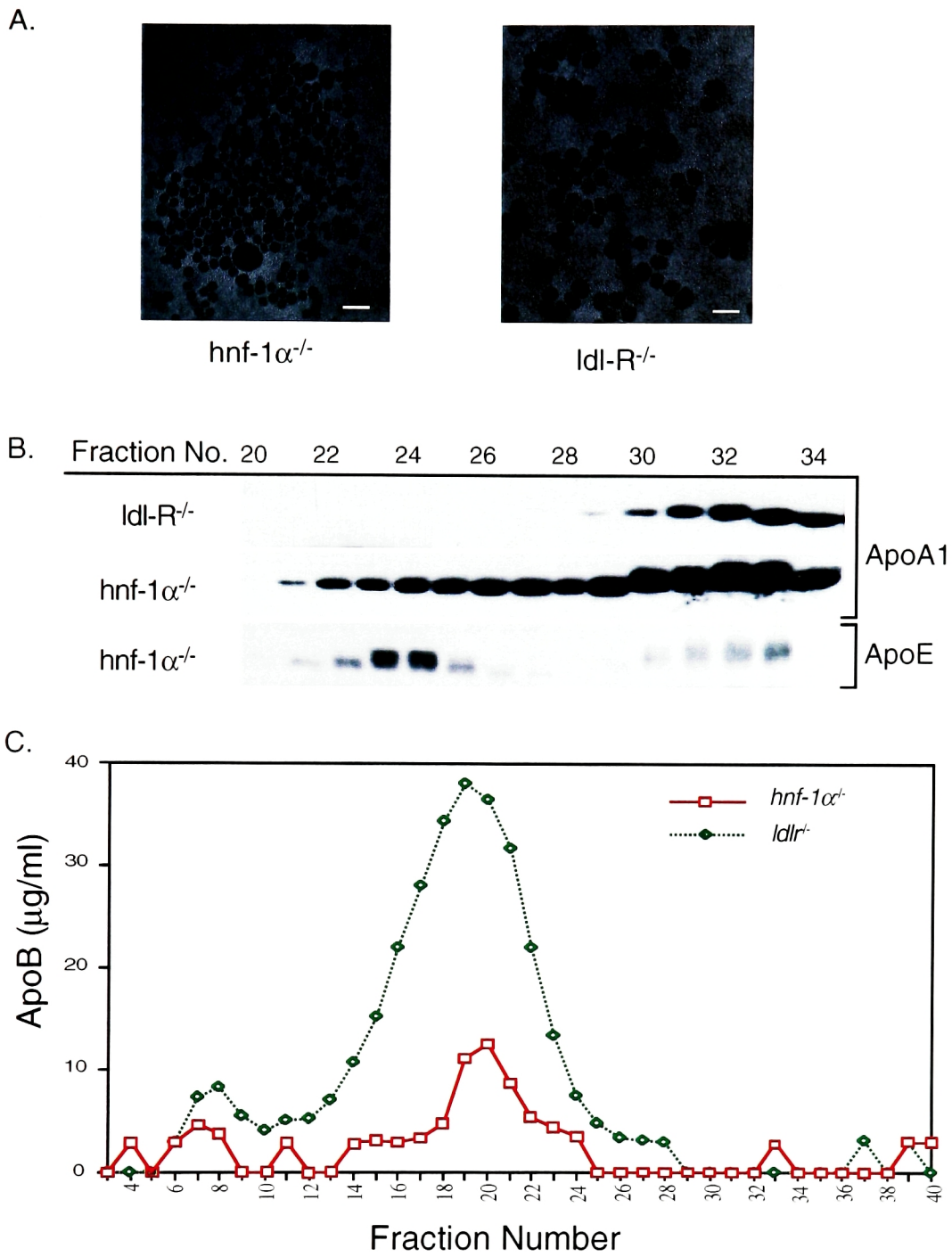

Figure 6-10. Characterization of large buoyant HDL in *hnf-1α*$^{-/-}$ mice. (A) Electron microscopy is shown of the abnormal lipoprotein and LDL factions in the plasma of Hnf-1α deficient and Ldlr deficient mice. Negative staining of a sample from fractions 16 and 17 of *ldlr*$^{-/-}$ mice and fractions 23 and 24 of *hnf-1α*$^{-/-}$ mice. The particles in *hnf-1α*$^{-/-}$ mice lacked lamellar discoid structures that are typical of Lp-X. Bar, 200 nm. (B) Measurements of ApoA1 (top) and ApoE levels (bottom) in fractions 20 to 34 of *hnf-1α*$^{-/-}$ and *ldlr*$^{-/-}$ mice using immunoblot analysis. (C) Immunoturbitrometric measurements of ApoB48/100 concentrations in FPLC gel filtration fractions of *ldlr*$^{-/-}$ (green line) and *hnf-1α*$^{-/-}$ (red line) mice.

immunoturbometric analysis. In *tcf1*$^{-/-}$ mice the abnormal fraction contained ApoA1 (Fig. 6-10B, fractions 21-27). In contrast, apolipoproteins B48/B100 were detected mainly in the LDL fractions (14 to 24), and were only seen in small amounts at the beginning of the abnormal lipoprotein peak (fractions 21-24)(Fig. 6-10C). These findings strongly suggest that the abnormal lipoprotein fraction consist mainly of large HDL particles. Large ApoE-enriched HDL particles have been shown in high cholesterol fed animals (251). We therefore measured the ApoE levels in the FPLC fractions and found ApoE enriched in the buoyant HDL fractions (21-27) of *tcf1*$^{-/-}$ mice (Fig. 6-10B). These results suggest that the abnormal lipoprotein fraction is similar to HDL_C.

To begin to investigate the molecular mechanisms for the formation of large, buoyant HDL in *tcf1*$^{-/-}$ mice, we measured the mRNA levels of HDL modifying enzyme including lecithin:cholesterol acyl transferase (*lcat*), sterol acyltransferase (*soat1* and *soat2*) and hepatic lipase (*lipc*) genes. Previous reports have shown that transgenic mice overexpressing lcat and lipc-deficient animals have moderately elevated plasma cholesterol levels and large HDL (249, 250). We did not find down regulation of Soat1 or Soat2. However, consistant with the animal models that exhibit large buoyant HDL particles, we found that the expression of lcat is significantly increased in adults and that of lipc is reduced in newborn and adult *tcf1*$^{-/-}$ mice (Fig. 6-11A). Moreover, Lipc activity was reduced in *tcf*$^{+/-}$ and *tcf1*$^{-/-}$ mice compared to wt animals (Fig. 6-11B). These findings suggest that *tcf1*$^{-/-}$ mice may have enhanced HDL cholesterol esterification and impaired HDL phospholipids hydrolysis that may account for the large HDL particles in the plasma of these animals.

Finally, the content of free cholesterol in the livers of *tcf1*$^{-/-}$ animals was lower

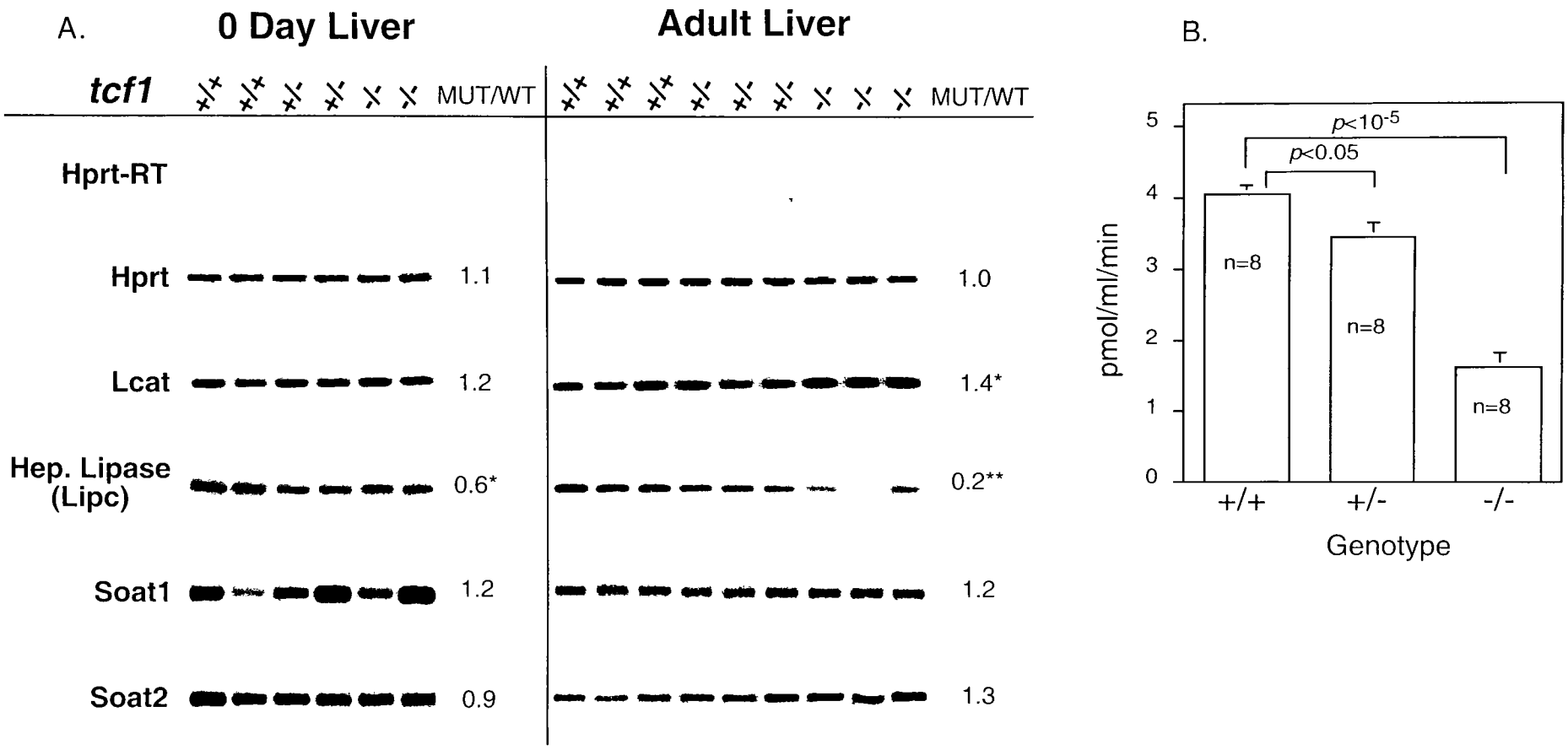

Figure 6-11. Characterization of HDL metabolism in *tcf-1*$^{-/-}$ mice. (A). RT-PCR analysis of steady state mRNA of genes involved in HDL metabolism. Gene expression was measured in three to six animals for each genotype (only two and three animals/genotype are shown for newborn and adult livers, respectively). Quantitative measurements were obtained by densitometry. MUT/WT indicates the ratio of expression levels of the means of null (*tcf1*$^{-/-}$) mice and wildtype (*tcf1*$^{+/+}$)(n=3-5). (B) The activity of Lipc is detemined in the plasma of control and *tcf1*$^{-/-}$ mice. Enzymee activity is expressed as pmol of pyrene fluorescence detected per ml of plasma/min. *:$P \leq 0.05$; **: $P \leq 0.005$; ***: $P \leq 0.001$. Hprt: hypoxanthine phosporibosyltransferase; Lcat: of lecithin:cholesterol acyl transferase.

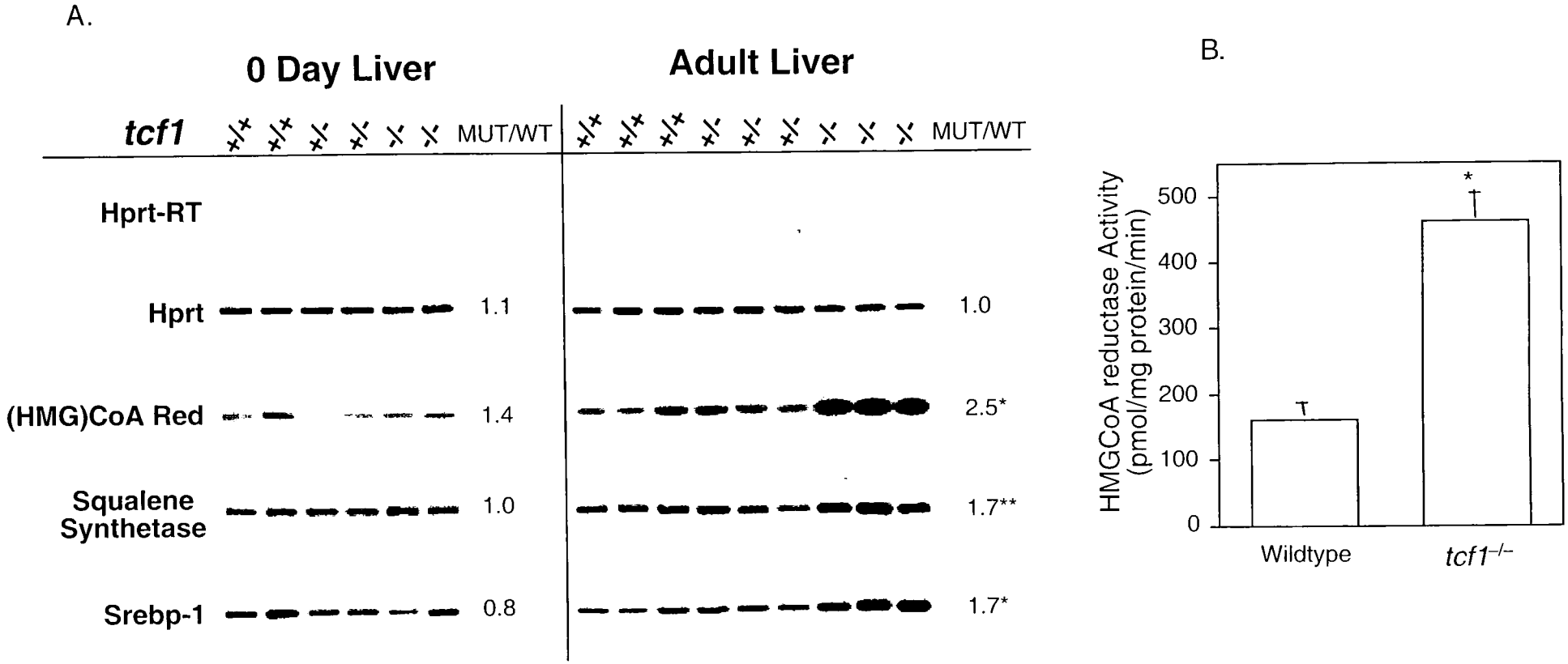

Figure 6-12. Increased cholesterol synthesis in *tcf-1*$^{-/-}$ mice. (A). RT-PCR analysis of genes involved in cholesterol biosynthesis. The rate limiting enzymes of cholesterol biosynthesis (HMGCoA reductase and squalene synthetase) as well as SREBP-1, the transcriptional activator central to cholesterol homeostasis, are increased in the adult liver of *tcf1*$^{-/-}$ mice. Quantitative measurements were obtained by densitometry. MUT/WT indicates the ratio of expression levels of the means of null (*tcf1*$^{-/-}$) mice and wildtype (*tcf1*$^{+/+}$)(n=3-5). (B) The activity of (HMG)CoA reductase is detemined in the isolated hepatic micorsomes. Enzymee activity is expressed as pmol of mevalonolactone formed per mg protein of microsome protein/min. *:$P \leq 0.05$; **: $P \leq 0.005$; ***: $P \leq 0.001$.

than in wt mice (1.61 vs 1.87 mg/g, respectively, n=12, p=0.01) and was associated with increased expression of key regulators and enzymes of cholesterol synthesis, including Srebp1, squalene synthase (fdft1), and (HMG)-CoA reductase (hmgcr) (Fig. 6-12A). The activity of this Hmgcr, the rate limiting enzyme of cholesterol synthesis, was also increased ≈3-fold in livers of tcf1–/– vs. tcf1+/+ animals (460 vs. 162 pmol/mg microsomal protein/min, respectively, n=10, P <0.001), indicating that cholesterol synthesis is increased in mutant tcf1 mice (Fig. 6-12B). However, it is important to note that increased expression of these genes is absent immediately after birth and develops only secondary to chronic intestinal bile acids malabsorption (Fig. 6-12A).

Discussion

The presence of functional consensus recognition sites for Tcf1 in the promoters of numerous genes encoding metabolic enzymes suggests that Tcf1 fulfill an essential role in cellular metabolism. Consistant with this notion, we found that Tcf1 is indispensable for the expression of several key genes involved in bile acid and cholesterol metabolism. Tcf1 deficiency in mice leads to profound bile acids loss in the stool and urine, increase in bile acids levels in the plasma, increase in cholesterol and bile acid synthesis, and formation of large buoyant HDL particles.

Our results demonstrate that Tcf1 regulates bile acid metabolism and cholesterol homeostasis by at least three mechanisms: First, Tcf1 appears to be a transcriptional activator of bile acid transporters that are located at the apical plasma membrane of ileal enterocytes and renal tubule cells as well as the basolateral side of the hepatocyte. The entry of bile acids into hepatocytes at the basolateral surface (in contact with the blood sinusoids) occurs by two processes. The major uptake system is sodium-dependent and

driven by the transmembrane Na+ gradient maintained by Na+/K+-ATPase. The major member in this transporter family for bile acid influx into hepatocytes is Slc10a1, a glycoprotein of 362 amino acid residues (233). A second sodium-independent uptake system in the liver is mediated by several members of the organic anion transporter polypeptide (OATP) family of transporters, which function as anion exchangers. In the liver, the sodium independent bile acid uptake is predominantly mediated by Slc21a6 and to a lesser extent by Slc21a11 and Slc21a5 (234, 236, 252, 253). Impaired Tcf1 function leads to reduced expression of the major sodium dependent (Slc10a1) and sodium independent (Slc21a6, Slc21a11, and Slc21a5) transporters resulting in marked elevation in plasma bile acid levels. Some bile acid up-take probably occurs in *tcf-1* deficient animals by bile acid transporters not regulated by Tcf-1 including Slc21a3. Slc21a3 is not sufficient to compensate for the decreased expression of other bile acid transporters in *tcf1*$^{-/-}$ mice because it is expressed at low levels and have low affinity for bile acids (Km of Slc21a3 and Slc21a6 for taurocholate are 60 mmol/l and 14mmol/l, respectively) (252-254). An efficient intestinal re-uptake of bile salts and delivery to the portal blood for re-entry at the basolateral surface of hepatocytes is important to maintain bile acid homeostasis. Reabsorption mechanisms exist mainly in the distal ileum which expresses a sodium-dependent carrier, Slc10a2, for the re-uptake of both primary and secondary conjugated and unconjugated bile acids (255). Unlike its liver counterpart Slc10a1 which is expressed basolaterally, Slc10a2 is expressed at the apical surface in the ileum. Mutations in SLC10A2 that result in a clinical syndrome of diarrhoea, malabsorption of fat and malnutrition and primary bile acid malabsorption have been identified in humans (256), further underscore the importance of this ileal bile acid transporter. The absence of

Slc10a2 in the enterocytes of the terminal ileum is responsible for reduced bile acid reabsorption and fecal loss in *tcf1*$^{-/-}$ mice. In the kidney, downregulation of the same transporter is responsible for impaired reabsorption in the proximal and distal renal tubules and loss of bile acids in the urine.

Second, Tcf1 is a transcriptional activator of Fxr-1. Intracellular and extracellular cholesterol and bile acid levels are tightly maintained within a narrow physiological range by a transcriptional control network. In the liver, Lxr-α and Lrh-1 are the 2 major transcriptional activator of *cyp7a1*, the rate-limiting step in bile acid synthesis. Expansion of the bile acid pool activates the nuclear receptor Fxr. Fxr mediates bile acid-dependent repression of the *cyp7a1* gene by inducing the transcription of *shp* (225, 257). Elevated Shp protein levels inactivate Lrh-1 by forming a complex that leads to the repression of *cyp7a1* (228, 229). Therefore, impaired Fxr-1 expression in *tcf1*$^{-/-}$ mice results in decreased levels of Shp, leading to increased Cyp7a1 activity and bile acid synthesis. In addition, the absence of the hepatic bile acid binding protein (Akr1c2) (258) in *tcf1*$^{-/-}$ mice suggests a role for Tcf1 in determining the intracellular bile acid pool that may contribute to defective sensing of the bile acid stores in hepatocytes.

Third, Tcf-1 is involved in HDL metabolism. A number of epidemiological studies have shown that serum HDL-cholesterol levels are negatively correlated with the incidence of coronary heart disease (259). Furthermore, patients with a genetic deficiency of HDL are often accompanied by atherosclerotic cardiovascular diseases (260). Thus, HDL plays an essential role in the protection of blood vessels from atherosclerosis. HDL serves as a shuttle, delivering excess cholesterol from peripheral tissues to the liver for excretion into the bile. This pathway was named "reverse cholesterol transport" (261).

Plasma HDL particles are continuously modulated by various enzymes including cholesterol ester transfer protein (Cetp), Lcat, and hepatic lipase. Hypercholesteremia and the accumulation of large buoyant HDL in the plasma of *tcf1*$^{-/-}$ animals probably reflect a combined increase in HDL cholesterol esterification by Lcat and decreased hepatic lipase expression with decreased HDL phospholipid hydrolysis. Finally, the marked upregulation in Srebp1, (HMG)-CoA reductase, and squalene synthase expression and the increased activity of (HMG)-CoA reductase suggests increased hepatic *de-novo* cholesterol biosynthesis. This is most likely secondary to impaired cholesterol absorption from the intestines and/or stimulated bile acid synthesis in the liver.

Cholesterol homeostasis is maintained by a series of complex transcriptional program including Fxr that control the acquisition of cholesterol from endogenous and exogenous sources and elimination cholesterol through conversion to bile acids and biliary excretion. In this study we have identified Tcf1 as a novel regulatory pathway for bile acids and cholesterol homeostasis in addition to its role in pancreatic β-cells to maintain glucose metabolism as shown in chapter 4. In the pancreas, it is part of an islet enriched transcription factor network that controls the expression of genes involved in glucose stimulated insulin secretion. In extra-pancreatic tissues however, it is a key player in the control of many aspects of cholesterol homeostasis including bile acid re-uptake, bile acid and cholesterol biosynthesis, and HDL metabolism. In addition, Tcf-1 is a major *in vivo* regulator of Fxr, a nuclear receptor that was shown to integrate multiple pathways for cholesterol homeostasis. In view of the profound physiological implications of bile acid metabolism in man and its link to cholesterol homeostasis, further analysis of this model that may identify novel molecular mechanisms that govern these process and

may uncover new target for pharmacological interventions in a variety of metabolic disease.

Chapter 7: Genotype/Phenotype Relationships in HNF-4α/MODY1 and HNF-1α/MODY3 Diabetes:

Associations with Reduced Apolipoprotein and Triglyceride Levels

Introduction

The MODY1 gene is encoded by HNF-4α, a transcription factor that belongs to the steroid/thyroid hormone receptor superfamily. It was first identified by its interaction with cis-regulatory sequences of liver-specific gene promoters (262). HNF-4α plays a critical role in development, cell differentiation, and metabolism and is essential for the normal functioning of visceral endoderm, liver, intestine, kidney, and pancreatic β-cells (24, 25, 77). HNF-4α also regulates the expression of transcription factor HNF-1α, thereby defining a transcriptional hierarchy responsible for these phenotypically indistinguishable forms of early-onset type 2 diabetes (29, 80, 120).

The first HNF-4α/MODY1 mutation was found to be a nonsense mutation in codon 268, Q268X (4). This mutation generates a truncated protein containing an intact DNA binding domain but lacking part of the AF2 region. Functional studies of this mutation have shown that the cause of diabetes is a loss-of-function mutation, rather than by a dominant-negative or gain-of-function mechanism (25).

Clinical studies have shown that *HNF-4α* and *HNF-1α* mutations are associated with impaired pancreatic β-cell function characterized by abnormal insulin secretion (27, 29, 120). These studies indicate that MODY is a primary genetic disorder of the β-cells and that the MODY genes form crucial links in the cascade of islet enriched transcription

network that control the appropriate expression of β-cell specific genes. However, with the exception of the insulin gene, target genes of both HNF-4α and HNF-1α are also expressed in other tissues including the liver, kidney, and intestine. Therefore, mutations in the MODY1 and MODY3 genes could result in pleiotropic phenotypes such as impairment in cholesterol and lipoprotein metabolism in the liver. Recently, a mutation in the *HNF-4α* gene has been shown to affect triglyceride metabolism (263). Patients with *HNF-1α* mutation have a reduction in the renal threshold for glucose, resulting in glucosuria, which suggests that kidney function may be abnormal in MODY3. Mice that are deficient for either Hnf-1α or Hnf-4α also exhibit extra-pancreatic abnormalities. Hnf-1α null mice have renal Fanconi-like syndrome, glycogen storage disease 1b and defects in bile acid and plasma HDL-cholesterol metabolism (Chapter 6) (36-39). Mice with targeted inactivation of the *hnf-4α* gene specifically in the liver accumulate lipid in the liver, exhibited greatly reduced serum cholesterol and triglycceride levels, and increased serum bile acid concentrations (264). Together, these data suggest that HNF-1α and HNF-4α are also major *in vivo* regulators of genes involved in liver function.

The liver is a major organ that performs many functions that are essential for metabolic homeostasis including plasma protein synthesis and cholesterol metabolism. Apolipoproteins are plasma proteins synthesized by the liver that are important for cholesterol and lipid homeostasis. In blood, apolipoproteins form lipoprotein particles that are composed of a nonpolar lipid core (containing cholesterol ester and triglycerides) surrounded by relatively polar coat that consist of phospholipid, free cholesterol, and apolipoproteins (265). The major plasma lipoprotein particles are defined according to the densities at which they are isolated and include: chylomicrons, very low density

lipoproteins, low density lipoprotiens, and high density lipoproteins. Lipoproteins function both to keep lipids soluble as they transport them in the plasma, and to provide an efficient mechanism for delivering their lipid contents to the tissues. The apolipoproteins associated with lipoprotein particles perform a number of diverse functions including serving as structural components of the particles, providing recognition sites for cell-surface receptors, and serving as cofactors for enzymes involved in lipoprotein metabolism (265). The presence of HNF-4α and HNF-1α binding sites in the promoters of apolipoproteins have been identified (265). In addition, several apolipoproteins are down-regulated in Hnf-4α deficient mouse livers (264). These data suggest that HNF-1α and HNF-4α may regulate several key plasma proteins synthesized in the liver that are involved in lipid transport and metabolism and thus, may contribute to MODY3 and MODY1 phenotypes respectively.

To gain a better understanding of the physiological consequences of *HNF-1α* mutations, we followed up on Hnf-1α target genes in the liver that were identified through Affymetrix® oligonucleotide microarrays (see chapter 6). In particular, we have begun to characterize a recently identified apolipoprotein, apoM, that is associated with high density lipoprotein (266). In addition, we used a genetic screen to identify liver-secreted target genes of HNF-4α in genetically manipulated embryonic stem (ES) cells. We then measured the serum levels of these proteins in subjects with HNF-4α haploinsufficiency and control groups. Our results indicate that a reduction in HNF-4α activity in humans manifests as a unique gene expression profile, affecting apolipoprotein and triglyceride concentrations.

Results

Hnf-1α is an Essential Transcriptional Regulator of Apolipoprotein M

In the previous chapter, we demonstrated that Hnf-1α is an essential regulator of bile acid and cholesterol homeostasis, and HDL metabolism. In view of the profound physiological implications of these metabolic defects and its possible association with the MODY3 phenotype, we are currently investigating expression sequence tags (ESTs) that are regulated by Hnf-1α identified from Affymetrix® oligonucleotide microarrays. Characterization of Hnf-1α regulated ESTs may identify new molecular components of existing metabolic pathways as well as novel pathways that may govern cholesterol homeostasis. These ESTs may also provide surrogate markers that could be used for the diagnosis MODY3.

Six ESTs (Accession #: ai256288, aa866766, ai645500, ai574068, ai527381, aa791426, aa655303) that were regulated more than 10 fold by Hnf-1α were reconfirmed by RT-PCR (data not shown). We also hybridized these ESTs in a Northern blot analysis of multiple tissues and shown that they are indeed enriched in the liver (data not shown). During the course of our analysis, one of the ESTs (aa655303) was identified as a novel HDL associated apolipoprotein, ApoM. In light of the abnormalities of HDL metabolism in *hnf-1α*$^{-/-}$ mice, we have begun to further characterize this apolipoprotein.

Hybridization of apoM probe on a multiple tissue Northern blot revealed an approximately 750 bp message that is enriched in the liver and the kidney (Fig. 7-1A). Rabbit antibodies were raised against 2 synthetic ApoM peptides 113-132 and 140-159. These antisera were used to reconfirm the tissue expression pattern on Western blot (Fig. 7-1B) and were also used to analyze the distribution of the protein amoung the various

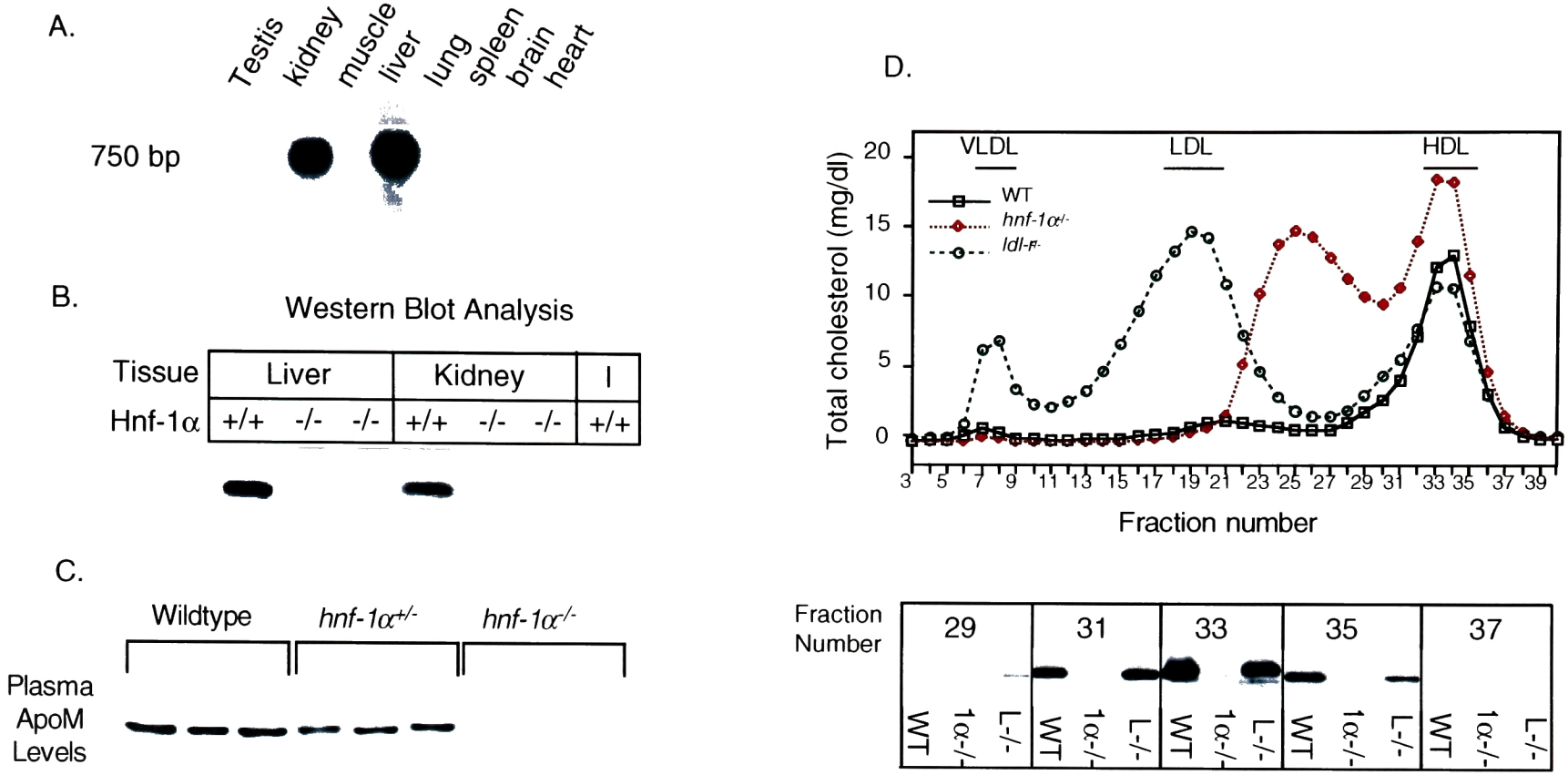

Figure 7-1. Expression analysis of ApoM. (A) Multiple Tissue Northern Blot showing tissue enriched expression of ApoM in the liver and the kidney. (B) Western blot analysis showing the absence of ApoM protein in Hnf-1α deficient liver and kidney. I, intestine. (C) Western blot analysis showing that plasma ApoM expression level is directly correlated with the hnf-1α genotype. (D) Top, FPLC plasma profile showing the fraction at which VLDL, LDL, and HDL elutes for wildtype, LDL-receptor KO (*ldlr*$^{-/-}$) and *hnf-1α*$^{-/-}$ mice. Bottom, measurements of ApoM levels in fractions 31 to 36 of wildtype (wt), *hnf-1α*$^{-/-}$ (1α-/-) and *ldlr*$^{-/-}$ (L-/-) mice using immunoblot analysis.

lipoprotein classes (Fig. 7-1D). Consistent with the previous observation (266), we found that ApoM is predominately associated with the HDL particle (Fig. 7-1C, data not shown). In addition, ApoM is completely absent in the HDL fractions of *hnf-1α*$^{-/-}$ mice (Fig. 7-1C).

Using the Celera database, we analyzed the promoter of ApoM to study its transcriptional regulation. We identified a consensus Hnf-1α binding element at position –117 to –131 bp in the mouse ApoM promoter. This binding site was also evolutionary conserved at similar location in the human ApoM promoter (Fig. 7-2A). Electrophoretic mobility shift assays (EMSA) were performed to determine if the Hnf-1α binding site is functional. A major DNA/protein complex was detected with a ^{32}P-labeled oligonucleotide that contained the Hnf-1 binding site (Fig. 7-2A, lane 2). This binding activity could be competed by an unlabeled excess of cold Hnf-1 binding oligonucleotide (Fig. 7-2A, lane 3). Furthermore, a supershift of the complex was observed after pre-incubation of extract with a polyclonal anti-Hnf-1α antiserum, but not with anti-STAT-1 antibodies (Fig. 7-2A, lanes 4 and 5) demonstrating that Hnf-1α can bind to the Hnf-1 site in the *apoM* promoter.

Next, we addressed the question whether Hnf-1α can act as a direct transcriptional activator in co-transfection assays by cloning a 610 bp of the 5'- murine *apoM* promoter containing the putative HNF-1 binding site and linked it to a luciferase reporter gene (pGL2-pAPOM). Co-transfection of pGL2-pAPOM with a Hnf-1α expression vector (pcDNA3-pHNF-1α) showed an approximately 3- and 27- fold dose-dependent activation of the *apoM* promoter in HepG2 (liver) and Cos7 (kidney) cells, respectively (Fig. 7-2B). To confirm that Hnf-1α can directly activate the *apoM*

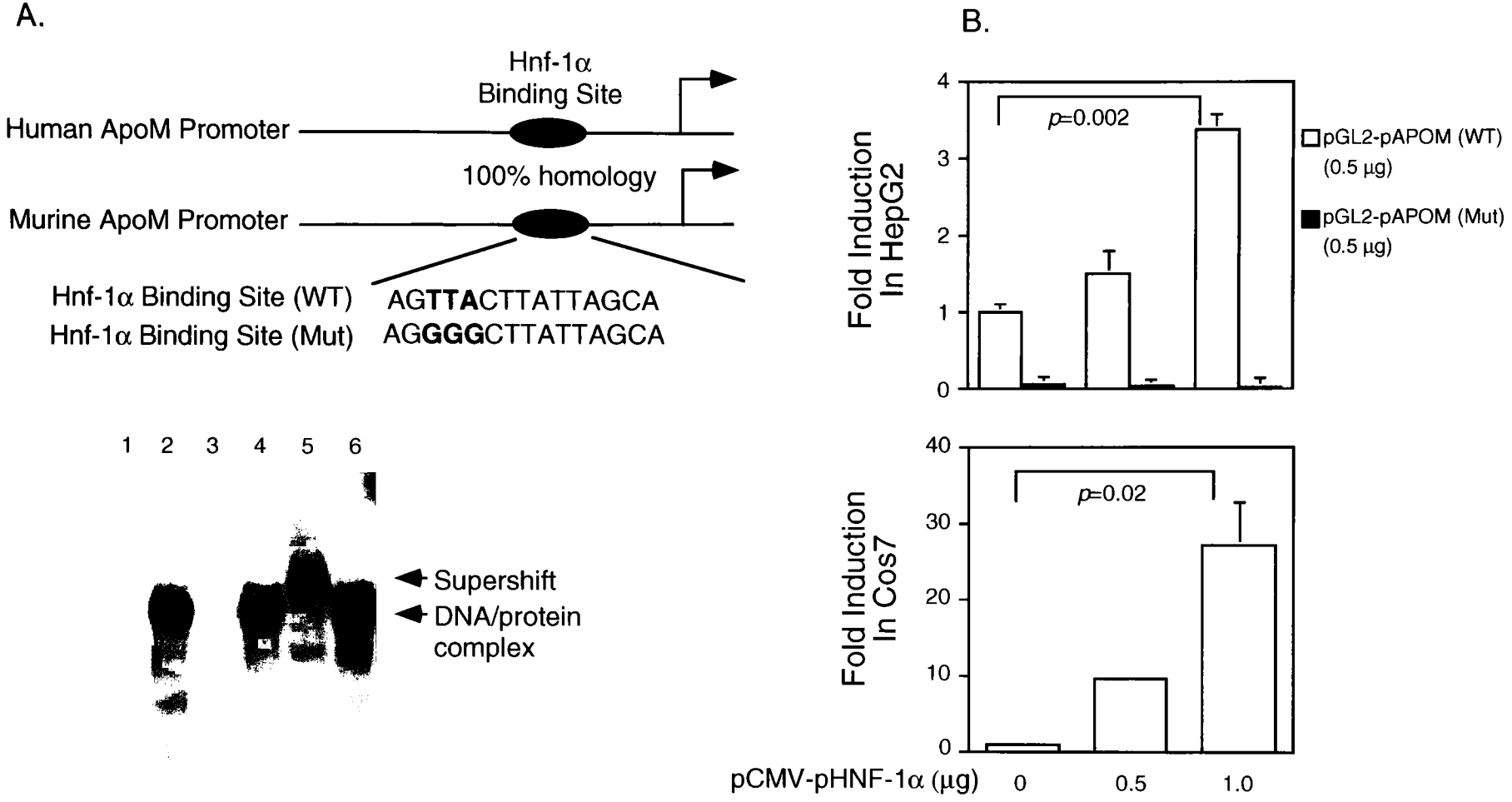

Figure 7-2. The *apoM* promoter is activated by Hnf-1α. (A) Comparison of human and murine apoM promoter shows an evolutionary conserved Hnf-1 binding site. The wildtype (wt) and mutant (mut) sequences of the Hnf-1 binding site is shown. The DNA binding activity of liver nuclear extracts and a ^{32}P-labeled double stranded oligonucleotide containing the Tcf1 binding site of the *apoMt* promoter (probe) was studied by EMSA. Lanes 1: probe alone (signal on bottom of gel, not seen in this picture); 2: probe + nuclear extract, 3: probe + nuclear extract + 20x cold competitor probe, 4: probe + nuclear extract + 20x cold, mutated Hnf-1 binding site, 5: probe + nuclear extract + anti-Hnf-1 antibody, 6: probe + nuclear extract + anti-STAT-1 antibody. (B) Cotransfection assays in HepG2 and Cos7 cells demonstrate that Hnf-1α can activate the *apoM* promoter in a dose-dependent fashion. This activation was impaired when the Hnf-1 binding site of the *apoM* promoter was mutated (pGL2-pAPOMmut).

promoter, we mutated the Hnf-1 binding site in the reporter plasmid pGL2-pApoM (Fig. 7-2B). The basal transcription activity of pGL2-pApoMmut is 95% lower than pGL2-pApoMwt in HepG2 cells (HepG2 cells have endogenous Hnf-1α expression). In addition, the transcriptional activation of HNF-1α on the pGL2-pApoMmut was abolished (Fig. 7-2B), indicating that the HNF-1 binding site in the ApoM promoter is functionally important for its expression.

We have shown that Hnf-1α is an important transcriptional regulator of ApoM expression. In the absence of Hnf-1α, apoM is essentially missing in liver, kidney, and blood. To determine if Hnf-1α haploinsufficiency reduces ApoM expression, we determined plasma ApoM levels in wt, *hnf-1α*$^{+/-}$, and *hnf-1α*$^{-/-}$ mice. We showed that Hnf-1α has a dose-dependent effect on plasma ApoM levels in mice (Fig. 7-1C). Therefore it represent a strong candidate surrogate marker for the early diagnosis of MODY3.

Identification of Liver-Enriched HNF-4α Target Genes

To gain a better understanding of a possible extra-pancreatic defect in *HNF-4α* haploinsufficient (MODY1) patients, we used a genetic screen to identify HNF-4α target genes in the liver. At the time of this study, only the complete knock-out of *hnf-4α* mice were generated. *Hnf-4α* null mice die during development prior to formation of the liver and cannot be used to identify Hnf-4α regulated genes. Heterozygous *hnf-4α* mutant mice have normal glucose tolerance and do not mirror the human MODY1 disease. We therefore studied the loss of Hnf-4α function on target gene expression in embryoid bodies (EBs) that were derived from embryonic stem cells *in vitro* (267). EBs contain

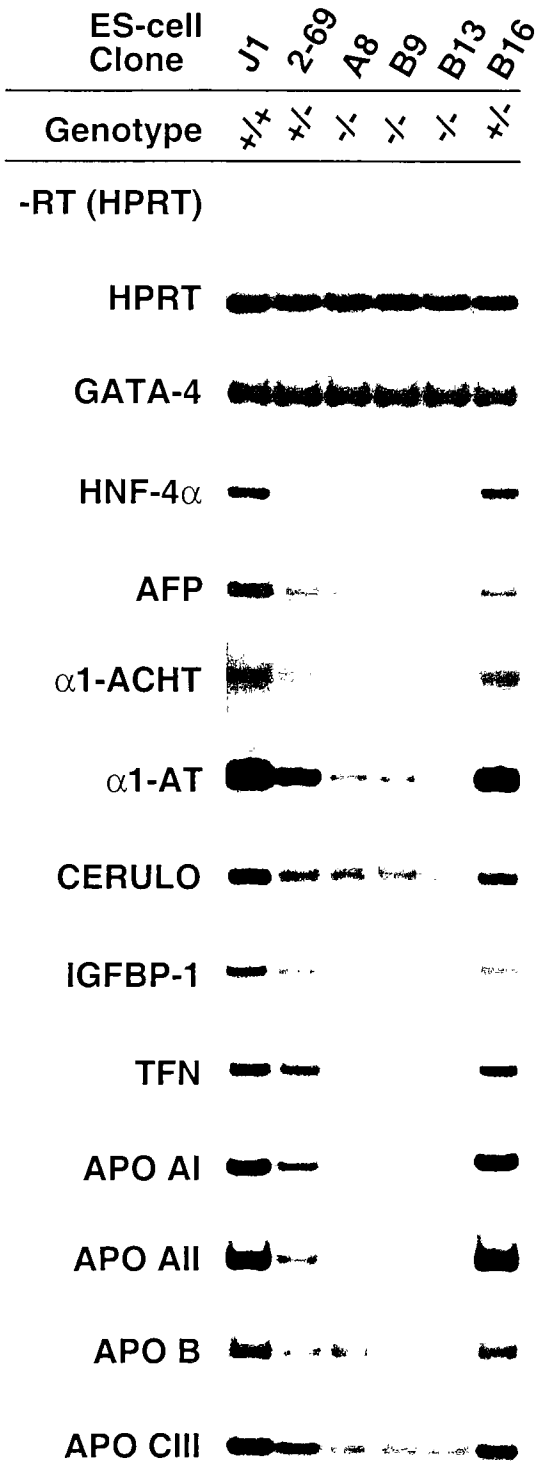

Figure 7-3. Regulation of liver-specific genes by Hnf-4α in embryoid bodies. Hnf-4α target genes were identified using genetically manipulated EBs. They included α1-antitrypsin (α1-AT), α1-antichymotrypsin (α1-ACHT), alpha fetal protein (AFP), ceruloplasmin (CERULO), insulin growth fator binding protein (IGFBP-1), transferrin (TFN), and apolipoproteins (APO) AI, AII, B, and CIII. RT-PCR analysis of Hnf-4α regulated genes in wildtype, *hnf-4α*$^{+/-}$, and *hnf-4α*$^{-/-}$ EBs shows that steady state mRNA levels of these genes are either reduced or absent in *hnf-4α* null EBs.

visceral endoderm (VE), a tissue that displays many characteristics of the liver, including the expression of hepatocyte nuclear factors and their target genes (25, 267).

A candidate gene approach in which genes that are primarily synthesized and secreted by hepatocytes were analyzed in EBs containing two, one or no functional *hnf-4α* allele. Using this approach, we identified alpha fetal protein (AFP), insulin growth factor binding protein-1 (IGFBP-1), α1-antitrypsin (α1-AT), α1-antichymotrypsin (α1-ACHT), ceruloplasmin (CERULO), transferrin (TFN), and apolipoproteins (apo) AI, AII, B, and CIII (Fig.7-3).

Genotype/Phenotype Analysis in HNF-4α/MODY1 Diabetes

Hnf-4α is a key regulator of hepatocyte-specific gene expression. Therefore, it might be anticipated that loss of function by *hnf-4α* mutations could manifest in a pleiotropic MODY1 phenotype that results not only in pancreatic islets but also liver dysfunction. To test this hypothesis, we obtained serums of the RW/MODY1 family. MODY1 in the RW diabetic individuals is caused by Q268X mutation in the *HNF-4α* gene (4). This mutation results in a truncated HNF-4α protein with no transcriptional activity (25). Our study groups were composed of 12 diabetic patients with *HNF-4α* mutation (D-HNF4+/-), 6 non-diabetics with HNF-4α mutation (N-HNF-4+/-), 12 normal matched controls (N-HNF4+/+), and 12 matched diabetic (MODY-X) patients (D-HNF4+/+). These study subjects were matched with respect to ethnicity, gender, age, and body mass index (BMI). The clinical characteristics of the different study groups are shown in table 7-1.

Table 7-1

Clinical Characteristics of Study Groups

Phenotype/ Genotype	n	M:F	Age (yrs)	Age of Diagnosis (yrs)	BMI (kg/m^2)	Fasting Glucose (mg/dL)	HgbA1c %	Fasting Insulin (ng/ml)
HNF4 α +/-	18	10:8	32±3		24.0±1.0	92.2±4.9	6.0±0.3*	0.11±0.01
D	12	6:6	37±4	14±1	24.3±1.3	93.3±7.1	6.4±0.5*	0.13±0.02
N	6	4:2	23±4		23.3±1.8	90.0±4.8	5.3±0.3*	0.09±0.01
HNF4 α +/+	24	12:12	35±2		24.6±0.7	124.8±10.3	5.9±0.4	0.40±0.10
D	12	6:6	38±3	21±3	25.2±1.2	160.3±14.0	6.9±0.7	0.64±0.17
N(unrl)	6	2:4	38±2		24.1±0.8	91.3±3.5	4.5±0.1	0.20±0.01
N(fam)	6	4:2	28±5		24.2±1.6	87.2±4.8	4.8±0.2*	0.11±0.01

D: Diabetic

N: Normal Glucose Tolerance

Unrl: unrelated individuals

Fam: RW family members

*Total HgbA was measured in members of the RW family and was adjusted for HgbA1c

We measured the protein levels of HNF-4α-regulated genes in the study subjects' serum including α1-antitrypsin, ceruloplasmin, transferrin, IGFBP-1, and apo AI, AII, B, CIII and Lp(a). In addition, we also measured total triglyceride serum concentrations. The results of our measurements are shown in table 7-2. Serum concentrations of α1-AT, ceruloplasmin, transferrin, and apo AI, and B showed no significant or consistent differences among the various study groups. However, we found that subjects who carry a *HNF-4α* mutation have a significant reduction in serum ApoAII (26.9 ± 1.4 vs. 37.4 ±1.6 mg/dL; p=1.3E-5), ApoCIII (19.8±1.5 vs. 26.5±2.0; p=0.01), Lp(a) (12.1±3.5 vs. 45.2± 6.3 mg/dL; p=5.9E-5), and triglyceride levels (72.1±6.3 vs. 124.2±7.3 mg/dL; p=3.1E-6) when compared to individuals without the *HNF-4α* mutation (Table 7-2). (In 1989, mean serum concentrations of triglycerides for 14 diabetic subjects of the RW pedigree (D-HNF4+/-) was 77.7±7.3 mg/dl). Moreover, no significant differences were observed when diabetic and nondiabetic subjects with or without the MODY1 mutation were compared (D-HNF4+/- vs N-HNF-4+/- and D-HNF-4+/+ vs. N-HNF4+/+, respectively) (Table 7-2, Fig.7-4). This indicates that HNF-4α haploinsufficiency rather than secondary effects due to impaired glucose homeostasis is the primary cause of decreased serum ApoAII, ApoCIII, Lp(a), and triglyceride concentrations. To exclude the possibility that the reductions we observe could be due to genetic (other than HNF-4α) or environmental factors, we compared serum factors of HNF-4α$^{+/+}$ individuals from the RW-family and unrelated control subjects ($N_{fam.}$ vs $N_{unrl.}$). No significant differenes between these two groups were observed, indicating that familial aggregation of modifiers does not contribute to the reductions of these serum proteins (Table 7-2).

Table 7-2
Serum Concentrations of Liver-Specific Proteins in MODY1 Subjects

Phenotype/Genotype								*p*			
	HNF4+/-	HNF4+/- D	HNF4+/- N	HNF4+/+	HNF4+/+ D	HNF4+/+ N(unrel)	HNF4+/+ N (fam)	+/- vs. +/+	D vs. N	D vs $N_{unrl+fam}$	N_{unrl} vs N_{fam}
n	10	12	6	24	12	6	6	-	-	-	-
α1-AT(mg/dl)	157.8±8.8	170.9±10.0	131.7±11.5	129.0±7.1	140.1±10.6	117.7±9.1	124.3±15.6	0.015	0.024	0.120	0.494
Cerulo (mg/dl)	35.2±1.9	37.1±2.4	31.5±2.8	45.5±3.2	51.0±5.6	43.3±5.1	58.7±9.5	0.009	0.150	0.089	0.188
TFN (mg/dl)	290±11.6	281±13.8	310±20.0	265±10.6	255±16.0	274±18.6	274±23.2	0.104	0.261	0.380	0.991
IGFBP-1 (ng/ml)	70.4±6.1	76.3±6.2	59.6±12.3	47.3±6.5	54.5±11.4	47.3±12.1	34.1±6.9	0.013	0.262	0.287	0.368
Apo (A1) (mg/dl)	115.2±6.9	119.3±7.9	105.6±14.1	119.1±7.0	126.8±10.9	131.5±11.6	91.2±5.6	0.697	0.430	0.276	0.014
Apo (AII) (mg/dl)	26.9±1.4	26.5±1.6	27.8±2.7	37.4±1.6	37.8±2.8	39.7±3.2	34.3±1.3	0.00001	0.683	0.803	0.156
Apo (B) (mg/dl)	79.4±5.8	82.3±8.0	72.4±3.0	97.3±6.0	104.2±9.0	102.3±13.2	78.3±6.4	0.037	0.268	0.256	0.138
Apo(CIII) (mg/dl)	19.8±1.5	18.9±1.6	19.6±1.0	26.5±2.0	29.3±0.7	25.5±2.2	22.2±2.7	0.010	0.730	0.188	0.345
Lp (a) (mg/dl)	12.1±3.5	13.5±4.8	8.6±3.9	45.2±6.3	57.7±8.6	29.5±9.6	35.8±14.2	0.00006	0.441	0.045	0.715
Triglyceride (mg/dl)	72.1±6.3	73.8±8.4	68.7±9.1	124.2±7.3	136.8±9.1	108.3±9.2	114.9±20.6	0.000003	0.686	0.084	0.775

Data are means±SEM. α1-AT, α1-antitrypsin; D, diabetic; fam, RW family members; N, normal glucose tolerance; TFN, transferrin; unrl, unrelated individuals.

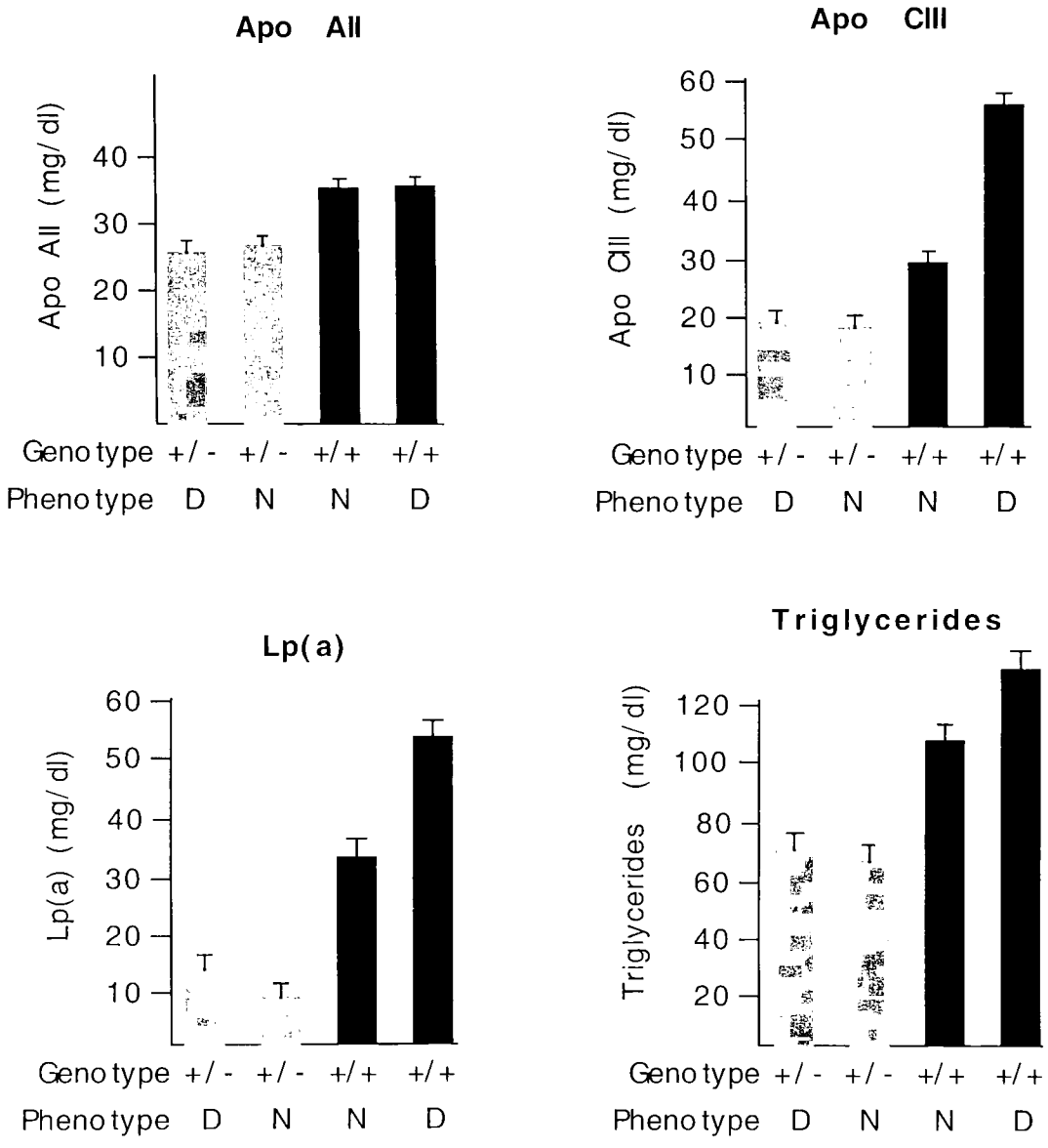

Figure 7-4. *HNF-4α* haploinsufficiency reduces serum levels of apolipoprotein (Apo) AII, ApoCIII, lipoprotein(a), and triglyceride. Serum concentrations of ApoAII (A), ApoCIII (B), Lp(a) (C), and triglycerides (D) in nondiabetic individuals and subjects with *HNF-4α* mutations. D, diabetic individuals; N, nondiabetic individuals.

Discussion

To identify novel pathways that may contribute to the MODY3 and MODY1 phenotype, we performed genetic screens to identify Hnf-1α and Hnf-4α target genes in the liver. ApoM was initially identified from Affymetrix® oligonucleotide microarrays as a strong target gene of Hnf-1α. To better understand the molecular basis of *apoM* gene regulation, we studied its promoter. The 5'-regulatory sequence of *apoM* contained an evolutionary conserved Hnf-1α binding site. Biochemical characterization of this site and *in vitro* transactivation studies indicate that Hnf-1α is a direct transcriptional activator of the *apoM* gene. *In vivo* expression studies revealed that Hnf-1α is necessary for the expression of ApoM and that its expression is directly correlated with the allelic dose of Hnf-1α. These properties make ApoM an ideal candidate as a plasma surrogate marker for the possible diagnosis of MODY3. We are currently studying serum ApoM levels in MODY3 patients and control subjects. We are also developing an ELISA assay for high throughput measurement of serum ApoM levels.

The function of ApoM remains to be determined. ApoM is hypothesized to be linked to the HDL assembly and secretion from the liver (266). This possibility is unlikely since HDL particles are found in *hnf-1α*$^{-/-}$ mice that does not express ApoM. Hnf-1α deficient mice however have abnormal HDL metabolism by accumulating large buoyant HDL. Accumulation of large buoyant HDL in the plasma of *hnf-1α*$^{-/-}$ mice probably reflects a combined increase in HDL cholesterol esterification and decreased HDL phospholipid hydrolysis (39). In light of these findings, ApoM may be involved in the formation of large buoyant HDL by serving as activators or coenzymes for enzymes involved in lipoprotein metabolism. To better characterize the function of ApoM, we

have generated transgenic mice carrying the ApoM gene under the control of ApoA1 promoter (ApoA1-ApoM). We will characterize the cholesterol and lipid profile of the ApoA1-ApoM mice as well as crossing them into Hnf-1α deficient mice.

HNF-4α is a transcription factor of the steroid hormone receptor superfamily that has an important role as a key regulator of pancreatic islet and hepatic gene expression. Genetic studies have shown that mutations in HNF-4α result in an autosomal dominant form of non-insulin-dependent diabetes mellitus characterized by defects in pancreatic β-cell function and glucose- and arginine-stimulated insulin release. Liver function has not been thoroughly assessed MODY1 patients.

We have performed a genetic screen to identify hepatocyte enriched genes that are regulated by HNF-4α. We used the visceral endoderm (VE) of embryoid bodies that were derived from wt and *hnf-4α* null ES cells as a model system to identify HNF-4α target genes. The VE is functionally related to the liver and shares many molecular characteristics including the components of the hepatocyte nuclear factor network and their targets (25, 77, 267). This model also allows the analysis of transcriptional regulation of HNF-4α targets genes on a genomwide scale and in the context of native chromatin. Nine proteins that are encoded by genes that are predominantly expressed in the liver and secreted into the blood were strongly dependent on the expression levels of Hnf-4α in visceral endoderm (Fig. 7-3). We therefore tested if the serum concentrations of these proteins were reduced in subjects with HNF-4α haploinsufficiency as compared to normal control individuals and, thereby, serve as serum markers for MODY1. In order to differentiate between changes in gene expression that are caused by the genotype and effects that are due to the phenotype of the study participants, we included 4 groups in

our study design: 1. diabetic patients with HNF-4α mutations (D-HNF4+/-), 2. non-diabetic subjects with HNF-4α mutations (N-HNF4+/-), 3. normal matched controls (N-HNF4+/+) and 4. matched, early-onset diabetic subjects that do not have defects in the MODY1-5 genes (D-HNF4+/+).

We found that subjects who carry a *HNF-4α* mutation have a significant reduction in serum apoAII, apoCIII, Lp(a), and triglyceride levels when compared to normal controls. We also observed that this reduction still holds when various genotypic and phenotypic comparisons were made, indicating that HNF-4α haploinsufficiency rather than confounding effects due to family aggregation or diabetes is the primary cause of the defect in lipoprotein metabolism. Our findings are in agreement with a recent study (263) that observed a significant reduction of triglyceride plasma levels in individuals carrying a MODY1 mutation. In contrast to two other reports (268, 269), we found that the serum levels of apoAII and Lp(a) were significantly decreased in individuals with a heterozygous HNF-4α mutation. We believe that one of these discrepancies can be explained by the fact that the HNF4(R127W) mutation in these individuals is not a functional mutation but rather a rare polymorphisms and therefore does not lead to altered HNF-4α-dependent gene expression (269, 270). The other study, reporting a family with a HNF-4(R154X) mutation found elevated Lp(a) and no significant differences in ApoAII, CIII and triglyceride levels (268). However, this study used a small sample size, including only two normal control individuals that were not well matched with regards to age and BMI. Another explanation for the difference in Lp(a) levels may be confounding factors that were not ruled out. For example, Lp(a) shows wide quantitative variation among individuals, the variations in concentration are

heritable and the LPA gene itself accounts for almost all genetic variability in plasma Lp(a) levels (271, 272). Differences in Lp(a) concentrations between *HNF-4α*$^{+/+}$ and *HNF-4α*$^{+/-}$ individuals may therefore also be due to genetic variation in the LPA gene itself.

The serum levels of some HNF-4α-regulated genes including TFN, α1AT, IGFBP-1, ApoAI and ApoB were not decreased in subjects with HNF-4a mutations. Several reasons may account for this finding. Insulin and glucose levels per se can alter gene expression and this effect may be stronger and mask differences between genotypes. For example, IGFBP-1 gene expression is known to be markedly upregulated in diabetic subjects and this may account for the elevated IGFBP-1 serum levels in D-HNF-4+/- subjects (273). The lack of reduction in other HNF4-regulated serum factors may also be explained by compensatory posttranscriptional mechanisms. Lastly, differences in gene expression of HNF-4α target genes between human and mice may exist.

The mechanisms by which HNF-4α regulates expression of the above genes are unknown but are likely to be both direct and indirect. Some of these genes, including Apo AII and ApoCIII, are known to contain HNF-4α binding site and therefore may be directly regulated by HNF-4α (262, 274). HNF-4α may also mediate its regulation of these target genes through a transcriptional cascade involving HNF-1α (77, 80). However, there may be a subset of genes that is regulated by HNF-4α but not by HNF-1α since the expression of the glycolytic gene aldolase B is decreased in the absence of HNF-4α but not in the absence of HNF-1α (25, 36). Such a subset of genes could in theory serve as a molecular marker to be used to differentiate between MODY1 and MODY3.

Our data suggests that the decrease in apoAII, apoCIII, Lp(a) are caused by impaired transcriptional activation of these genes due to HNF-4α haploinsufficiency. These transcriptional changes in the liver lead to a decrease in the serum levels of these factors. Lowered triglyceride concentrations may be due to an increased lipoprotein lipase (LPL) activity since apoCIII is an inhibitor of LPL-activity *in vitro* (275) and transgenic mice overexpressing human apoCIII have elevated triglyceride levels in plasma due to the presence of enlarged triglyceride-rich lipoproteins with increased apoCIII levels (276). Low apoII levels may also contribute to decreased triglyceride levels since overexpression of apoII in transgenic mice leads to hypertriglyceridemia (277), and apoAII deficiency in knockout mice are associated with low free fatty acid (278). However, a 25% decrease in apoAII levels are unlikely to have a major effect on lipid metabolism, since human deficiency of apoAII has little influence on either lipid and lipoprotein profiles or the occurrence of cardiovascular disease (279). Subjects with HNF-4α mutations may have a slightly lower risk of developing cardiovascular complications since Lp(a) and triglycerides, two independent risk factors for cardiovascular diseases, are reduced. Our finding here were later corroborated by *hnf-4α* liver specific knock-out mice which also showed an atheroprotective serum lipid profile (264).

Our data suggest that HNF-4α is a central regulator of glucose and lipid metabolism and that the development of HNF-4α-agonists and antagonists may be powerful drugs for the treatment of insulin secretion defects or dyslipoproteinemias, respectively. Ideally, any future therapeutic drug development that targets HNF-4α to improve ß-cell function should increase HNF-4α activity and exhibit pancreatic β-cell

tissue specificity whereas selective improvement of lipoprotein metabolism may be achieved with HNF-4α-antagonists in the liver and intestine.

In summary, genotype/phenotype relationship studies can dissect primary and secondary defects of pancreatic β-cell dysfunction and lipid/lipoprotein metabolism. Altered hepatocyte gene expression contributes to the phenotype of HNF-4α/MODY1 diabetes. HNF-4α haploinsufficiency causes primary defects in lipoprotein metabolism and is independent of altered glucose metabolism. HNF-4α-dependent serum protein profiles may in the future serve as molecular markers that can be used for the differential diagnosis of MODY1 diabetes from type 2 diabetes or other forms of MODY.

Chapter 8: Materials and Methods

Vectors.

The sequences of all the clones were confirmed by dideoxynucleotide sequencing at the Protein/DNA Technology Center (Rockefeller University, NY).

pCMV-pHNF4α: The construction of expression vector pcDNA3-pHNF4α was generated by cloning a *Eco*RI *hnf-4α* fragment from pCMV-pHNF-4α (25).

pcDNA3-pHNF-1α: The vector pcDNA3-pHNF-1α was generated by cloning a 2.8 kb *Not*1/*Bam*H1 fragment from pBJ5-pHNF-1α (a gift from G. Crabtree)(80) containing the entire rat HNF-1α coding sequence into pcDNA3.

pCDNA3-pSHP: The pCDNA3-pSHP expression vector was constructed by PCR amplification of an 850 bp mouse Shp fragment that contained the entire open reading frame using mouse liver cDNA as a template. This fragment was cloned into the *Eco*R1 site of pcDNA3.

pGL2-pSHP: The reporter plasmid pGL2-pSHP was constructed by PCR amplification of the human SHP-1 promoter (Genebank accession no. AF044316), using oligonucleotides SHP-Pm-1 (5' TCCTAGACTGGACAGTGGGCA-3') and SHP-Pm-2 (5' CTTCCAGCTCTCTG GCTCTGT-3") and subsequent cloning of the 582 bp fragment into plasmid pPCR2.1. A *Kpn*1/*Xho*1 fragment from this plasmid was then subcloned into the pGL2, inserting the SHP promoter upstream of the luciferase reporter gene.

pGL2-pSHPmut: Vector pGL2-pSHPmut was generated by PCR using oligonucleotides SHPmut-F (5'-TCCTAGACTGGACAGTAA AAAAAGCCT-3') and SHP-Pm-2, and

pGL2-pSHP as a template. This fragment, containing a mutated HNF-4 binding site, was cloned into pPCR2.1 prior to insertion into pGL-2.

pGL2-pASBT: The reporter plasmid pGL2-pASBT was constructed by PCR amplification of the human SCL10A2 promoter using oligonucleotides ASBT1 (5'-GGTTGCCCTGGAAGGAAATGG-3') and ASBT2 (5' GCCCTGGCTCTGCTGCTGGTTG-3') and subsequent cloning of the 1854 bp fragment into plasmid pCR2.1. A *SpeI/Eco*RV fragment from this pPCR2.1-pASBT was then subcloned into the pGL2 (pPGL2-pASBT), inserting the SCL10A2 promoter upstream of the luciferase reporter gene.

pGL2-pASBTmut: Vector pGL2-pASBTmut was generated by PCR using oligonucleotides ASBTmut1A3 (5'-CAAACCCTCGAGGACAGGGGACAT-3') and ASBT2, using pCR2.1-pASBT as a template. This 308 bp fragment, containing a mutated Tcf1 binding site, was cloned into pCR2.1. A 0.3 kb *Xho*I fragment from this plasmid was inserted into pGL2-pASBT *Xho*I fragment to create pGL2-pASBTmut.

pBS-pFxr-1: To identify the Fxr-1 promoter, we screened a mouse (Sv129) genomic library in lambda Fix II (Stratagene). Three identical phage clones were identified that contained the Fxr-1 promoter. A 1.2 kb *Eco*RI Fxr promoter fragment containing the transcription start site was subcloned into pBluescript KSII to generate pBS-pFxr-1.

pGL2-pFxr-1: pBS-pFxr-1 was used as a template to PCR amplify the Fxr-1 promoter using oligonucleotides T7 and FXR 1promR (5' GAGAAGGACTCGAGGTAAGAAGCGACAGG-3'). The PCR product was blunt-ended with Klenow and then digested with *Xho*I, prior to cloning into a blunted *Sac*1 and a *Xho*1 site of pGL2. The resulting plasmid was named pGL2-pFxr-1.

HNF-3α Targeting Construct.

The *hnf-3α* gene was isolated from a λFIXII murine 129/Sv genomic library (Stratagene, CA). *hnf-3α* was mutated by targeted deletion of the DNA binding domain and the C-terminal transcriptional transactivation domains by homologous recombination in ES cells. To generate the *hnf-3α* targeting vector, an approximately 2.0 kb *Xho*I/*Alf*III fragment (5' short arm) containing the first exon, intron, and part of exon 2 was inserted into the modified targeting vector pPNT with an in-frame fusion of the E.coli *lacZ* gene (93). The 3'-end of the targeting vector was generated by cloning an 8.0 kb *Nhe*I/*Sac*I fragment downstream of the neomycin resistance gene (Fig. 2-1).

Generation of pPdx-1-pEGFP Transgenic Mice.

To identify the *pdx-1* promoter, we screened a mouse (Sv129) genomic library in lambda Fix II (Stratagene, CA). Two identical phage clones were identified that contained the *pdx-1* promoter. A 4.5 kb *pdx-1* promoter was cut using *Sac*II and *Sma*I (position 245 bp in the first exon) sites and was cloned into pBluescript KSII to generate pBS-pPdx-1. The promoter was then cloned into pEGFP-1 (Clontech, CA) to generate pPdx-1-pEGFP. A 5.8 kb pPdx-1-pEGFP fragment was cut out using *Sac*II and *Dra*III and injected into pronucleus (The Rockefeller University Transgenic Service Facility, NY). Mice containing the transgene were confirmed by Southern blot and by PCR using the primers GFP-3, GGGGGTGTTCTGCTGGTAGTGGTC and GFP-5, ATGGTGAGCAAGGGCGAGGAG.

Animals and Genotyping.

The mice used for chapters 2, 3, and 6 were in a mixed background. The mice used in chapters 4 and 5 were bred and maintained in C57/B6 background and were

housed in Laboratory of Animal Research Center (LARC), a pathogen-free animal facility at the Rockefeller University. The animals were maintained on a 12 hours light/dark cycle and fed a standard rodent chow. Genotyping was performed on DNA isolated from 3 weeks old mice by PCR. The primer sequences of the wildtype and mutant alleles are available upon request.

MODY Subjects.

HNF-4α$^{+/-}$ (Q268X) and non-affected individuals of the RW pedigree were previously identified by sequencing analysis (4). 12 diabetic patients with *HNF-4α* mutations (D-HNF4$^{+/-}$), six non-diabetics with HNF-4a mutations (N-HNF4$^{+/-}$), 12 normal matched controls (N-HNF4$^{+/+}$) and 12 matched early-onset diabetic (MODY-X) patients (D-HNF4$^{+/+}$) were included in the study. The N-HNF-4$^{+/+}$ control group consisted of six N-HNF-4$^{+/+}$ RW relatives and six nonrelated N-HNF-4$^{+/+}$ matched control subjects. MODY-X patients and unaffected controls were of European descent and the majority of these subjects were referred to the Rockefeller University GCRC. Clinical diabetes was defined according to the new guidelines of the expert committee on the diagnosis and classification of diabetes mellitus (10). Individuals were classified as MODY-X when their pedigrees were consistent with an autosomal dominant form of inheritance, at least two subjects in a given pedigree were diagnosed ≤ 35 years of age, in the absence of overt obesity, and in the absence of mutations in the genes encoding MODY1-5. Study groups were matched for gender, age and BMI. Fasting blood glucose and insulin levels in MODY-X subjects (D-HNF-4α$^{+/+}$) was significantly higher than than the other groups. This is most likely due to the different ascertainment procedure of these subjects (see

above) and continued insulin treatment. The clinical characteristics of the four study groups are shown in Table 7-1.

Mutation Analysis.

MODY-X patients were screened for mutations in the *HNF-4α*, *GCK*, *HNF-1α*, *PDX-1* and *HNF-1β* genes by single strand conformational polymorphism (SSCP) analysis as described (280). In addition, haplotype analysis was performed in the majority of families using markers in the MODY1-5 gene locations. Abnormal SSCP conformers were reamplified and sequenced using an Applied Biosystem DNA sequencer, model 373A, a didioxynucleotide-cycle-sequencing protocol and fluorescent labeled dideoxynucleotide terminators as described by Applied Biosystems.

Biochemistry Assays

Plasma for insulin, glucagon, and cortisol measurements were obtained by collecting whole blood in heparinized capillary tubes, immediate centrifugation, and storage at -20°C. Insulin and glucagon levels were measured using radioimmunoassay (RIA) kits with rat insulin and glucagon standards (Linco, MO). Glucocorticoid levels were measured with a cortisol RIA kit (Diagnostic Systems Laboratories, TX). Growth hormone was assayed by using a ^{125}I-GH assay system with magnetic separation (Amersham Pharmacia, NJ). Total catecholamine was measured by using catecholamines [^{3}H] radioenzymatic assay (Amersham Pharmacia, NJ). Glucose was measured using an enzymatic (glucose oxidase) assay (Sigma, MO). Serum triglyceride levels were analyzed using colorimetric test (Sigma, MO). Liver glycogen contents were measured after homogenization in ice cold perchloric acid and glycogen hydrolysis with amyloglucosidase as described previously (281). Quantitation of amino acids were performed on a Beckman Model 6300 ion-exchange instrument.

Bile acid concentrations in feces were determined as previously described (282, 283). In short, bile acids were extracted from each fecal sample with 80% methanol and chloroform-methanol. The two extracts were combined and taken to dryness. The extract was resuspended in 80% methanol by sonication and stored at –20 °C. [^{14}C] cholic acid (New England Biolabs) was added to determine the relative recoveries of bile acids throughout the procedure. Plasma was obtained by collecting whole blood in EDTA treated 1ml syringe, immediately centrifuging, and storing at –20 °C. Bile acid content from stool, serum, and urine were determined enzymatically using Sigma Diagnostics Bile Acid reagents (Sigma, MO). Lipoprotein cholesterol profiles of control, *Tcf1*$^{-/-}$ and Ldlr$^{-/-}$ mice were determined by on line post-column analysis of Superose 6 gel-filtered mouse plasma (284). Samples (0.2 ml) of the Superose-column filtered LDL and HDL peaks were extracted and analyzed for total, free and esterified cholesterol using gas liquid chromatography as previously described (285). ApoB levels were measured by an automated immunoturbidimetric assay for mouse apoB (coefficient of variation: <5%) (286). Cyp7a1 and (HMG)-CoA reductase activities were measured as describes previously (285). Hepatic lipase activity was measured by a continuous fluorometric hepatic lipase select test (Progen): the kinetic increase in fluorescence intensity is measured at 342 nm excitation and 400 nm emission for 10 min using luminescence spectrometer LS50B (Perkin Elmer).

Concentrations of Lp(a), apoAI and apoB were determined with immunoturbidimetric assays from (Roche Diagnostics, Germany) using a Hitachi 917 autoanalyser. ApoC-III was quantified with a commercially available electroimmunoassay (Hydragel LpA-I, Sebia, Paris, France). The coefficient of variance

(CV(%)) of of Lp(a) and apoB are <6.4 and 2.7, respectively. ApoA-II was determined independently by the use of an immunoturbidimetric test from Immuno (Vienna, Austria) with a Cobas Bio analyzer (Roche Diagnostics, Germany) and an ELISA test. For the latter, mouse anti-human apo AII monoclonal antibody (PerImmune), diluted 1:100 in bicarbonate buffer, was applied to wells of Nunc Maxisorb ELISA plates and incubated overnight at 4°C. All subsequent incubations were performed at room temperature with gentle agitation. Wells were washed with PBS and blocked with casein blocker (Pierce) for one hour. Serum standards (Kamiya Biomedical) and serum samples, diluted 1:30,000 in buffer A (casein blocker/0.5% tween20), were applied to the wells for 1 hour. Plates were washed with buffer B (PBS/0.5% Tween 20) and a biotinylated goat anti-human apoA-II polyclonal antibody (Biodesign), diluted 1:1000 in PBS/1% BSA, was applied for 1 hour. After washing, streptavidin-HRP (Pierce), diluted 1:1000, was applied for 1 hour. HRP enzyme was detected by incubation with TurboTMB substrate (Pierce). The reaction was terminated with 1M sulfuric acid, and the absorbance was measured at 450 nm on a SpectraMax plate reader (Molecular Devices). The CV(%) of this test was <7. Serum concentrations of a1-antitrypsin, ceruloplasmin, and transferrin were determined by rate nephelometry on a Beckman Array 360 (Beckman-Coulter, Brea, CA) using specific antibodies to each analyte. The system measures the intensity of light as it is scattered by particles in suspension when a beam of light is passed through a flow cell. The resulting antigen-antibody reaction is converted to a peak rate signal and is proportional to sample antigen (analyte) concentration. CV(%) were 4.2, 3.4 and 2,7, respectively. Serum triglyceride concentrations were determined using an enzymatic, colorimetric assay (GPO-Trinder, Sigma, MO). The coefficient of variance of this test is

<5%. Serum IGFBP-1 concentrations were measured by using an immunoradiometric assay and antibodies specific for human IGFBP-1 (DSL).

Measurements of Pyruvate Kinase Activity.

Pyruvate kinase enzyme activity was measured in extracts of islets isolated from four mice. Following overnight culture in RPMI 1640 containing 11.6 mM glucose, islets were hand picked, washed twice in PBS and transferred to a homogenization buffer consisting of 200 mM mannitol, 70 mM sucrose, 5 mM potassium HEPES buffer, pH 7.5 and 1 mM dithiothreitol. The islets were washed twice in buffer containing 1 mM EGTA and then twice in the buffer without EGTA. The islets were then sonicated (Ultrasonics Sonicator Cell Disrupter, Model W 185 F, Heat Systems, Inc. Plainview, NY) and centrifuged at 105,000 x g for 60 minutes at 4C. The protein content of the islet extracts was measured (Biorad, #500-0006) and the activity was measured in equivalent amounts of protein from the different mice. Pyruvate kinase enzyme activity was measured in a reaction buffer consisting of 80 mM triethanolamine chloride buffer, pH 7.5, 5 mM $MgSO_4$, 100 mM KCl, 2.5 mM ADP, 0.14 mM NADH, 1 mM dithiothreitol and 7 mM phosphoenolpyruvate and 2.5 U of lactic dehydrogenase (all reagents were purchased from Sigma, St Louis, MO). Each reaction was carried out in a final volume of 1 ml and was started by the addition of the islet extract. NADH levels were measured as fluorescence emitted at 448 nm in response to excitation at 340 nm for ten minutes. The rates of consumption of NADH were similar *in hnf-1*$\alpha^{+/+}$ (n=4), *hnf-1*$\alpha^{+/-}$ (n=5), and *hnf-1*$\alpha^{-/-}$ (n=4) mice.

Generation of *pdx-1*$^{-/-}$ ES Cells.

pdx-1 null ES cells were generated by culturing the *pdx-1*$^{+/-}$ ES cells (55) in either 1.5 mg/ml or 2.0 mg/ml of G418 in ES medium. DNA from resistant ES cell clones were digested with *Eco*RI and the Southern blots were hybridized with the 3' external probe (55). The 3 kb and 3.8 kb bands on the Southern blot represent endogenous and targeted *pdx-1* locus respectively.

Maintenance of Undifferentiated ES Cells *in vitro*.

ES cells were grown on 0.1% gelatin-coated tissue culture plates in ES cell medium supplemented with 1,000 units ml^{-1} of ESGRO (Chemicon International, CA) over a primary embryonic fibroblast feeder layer. ES cell media is composed of Dulbecco's Modified Eagle's Medium (DMEM) (Specialty Media, NJ) supplemented with 25 mM glucose, 15% fetal bovine serum (FBS) (Atlanta Biologicals, GA), non-essential amino acids (NEAA), 110 mg/L sodium pyruvate, 365 mg/L L-glutamine, and 0.55 mM β-mercaptoethanol (BME).

Differentiation of ES Cells into Insulin-Producing Cells

The differentiation protocol is composed of 4 stages. It begins with culturing ES cells on gelatin-coated tissue culture plates in ES cell media in the absence of primary embryonic fibroblast feeder layer and ESGRO to sub-confluency (stage 1). To induce embryoid bodies (EB) formation (stage 2), cells were dissociated in trypsin/EDTA (Life Technologies, NY) and plated onto non-adherent bacterial culture dishes at a density of 2-3x10^4 cells cm^{-1} in ES cell medium and cultured for 3 days. Differentiation must be restarted if EB are not metabolically active; media must turn yellow every day. Selection and expansion of endocrine/neural progenitor cells comprised stage 3 differentiation. It was initiated by trypsinizing EB for ≤ 5 min and plated onto tissue culture dishes coated

for 3 hours (hrs) with 0.1% gelatin (Sigma, MO), 0.1% poly-D-lysine (Sigma, MO), and 1 μg/ml fibronectin (Life Technologies, NY) dissolved in PBS. Differentiation must be restarted if less than 50% of the dissociated EB attach. The cells were maintained in ES medium until they grow to sub-confluence (≤ 3 days), after which the selection of endocrine/neural precursors were initiated by using serum-free ITSF medium. ITSF medium is composed of DMEM/F12 (Rockefeller Tissue Culture Service, NY), supplemented with 25mM glucose, NEAA, 55 mg/L sodium pyruvate, 365 mg/L L-glutamine, 0.55 mM BME, ITSX (Life Technologies, NY), and an additional 45mg/L transferrin (Life Technologies, NY). After the cells were reduce to approximately 20% confluent, cell expansion was initiated by culturing in ITSF medium supplemented with B27 (Life Technologies, NY), 10 ng/ml basic fibroblast growth factor (bFGF) (R&D Systems, MN), and 100 ng/ml β nerve growth factor (NGF) (R&D Systems, MN). They were expanded until sub-confluent. If cells do not aggregate at the end of this stage, differentiation must be restarted. Terminal differentiation (stage 4) was comprised of 2 phases. It started by culturing the cells in differentiation medium with 100 ng/ml βNGF and 12.5 mM glucose for 2 days, and then with 6 mM glucose for 4 days. Differentiation medium was composed of RPMI medium supplemented with 2.5% FBS, NEAA, 110 mg/L sodium pyruvate, 365 mg/L L-glutamine, B27, and 10mM nicotinamide (Sigma, MO).

Detecting β-galactosidase Activity in Living Cells.

The presence of β-galactosidase (β-gal) was detected in LacZ/Pdx-1 positive cells by the vital fluorescent β-gal substrate, 5-chloromethylfluorescein di-β-D-galactopyranoside (CMFDG) following manufacture's instructions with minor

modifications (Molecular Probes, OR). Briefly, cells were dissociated from the surface of tissue culture dishes by trypsin/EDTA. These cells were washed in medium and pelleted for 5 min at 500G. 50 million cells were gently resuspended (by tapping only) in 1 ml of loading medium containing 1 mM CMFDG and 50 μM verapamil and incubated at 37°C for 10 mins. 150 ml of hypotonic lysis medium (6 parts medium without serum and 4 parts deionized water) was added to the cell suspension, mixed by gentle inversion, and incubated at RT for 1 minutes. Cells were pelleted for 1.5 mins at 500G and resuspended in 50 ml of growth medium containing 1.5 μM propidium iodide to facilitate the identification of dead cells incurred during the procedure. These cells were incubated at 37°C for 30 minutes before examination. Data for flow cytometry was acquired on FACSCalibur™ (Becton Dickinson, CA). For FACS experiments, LacZ/Pdx-1 positive cells were isolated using Coulter Altra Cell Sorter™ (Beckman Coulter, CA), Cornell Sort-Stat Sort Stabilization Device© (Weill Medical College of Cornell University, NY) and a Coulter Sort Sense quartz flow cell tip (Beckman Coulter, CA) by C. Colon at the Cornell Weill Flow Cytometry Core Facility. Excitation of fluorescein and propidium iodide was accomplished with a Coherent Enterprise™ Argon laser 15 mw at 488nm. Sheath fluid used was Coulter Isoflow (Coulter, CA).

Data for both flow cytometry and FACS were analyzed using FlowJo software (Tree Star, Inc., CA).

BrdU Labeling and Staining for Flow Cytometry.

BrdU staining was performed by using the BrdU Flow Kit (BD Pharmingen, CA) and following the manufacturer's protocol. Briefly, cells during day 2 phase 3 of differentiation stage 3 exposed for 6 hours to 0.01 mM BrdU and chased for 12 hours

with tissue culture media. Cells were then loaded with CMFDG (Molecular Probes, OR). Fixation and permeabilization was done with Cytofix/Cytoperm Buffer (BD Pharmingen, CA) for 30 minutes at room temperature and were washed in Perm/Wash Buffer (BD Pharmingen, CA). Cells were refixed in Cytofix/Cytoperm Buffer for 5 minutes at room temperature and washed again in Perm/Wash Buffer. Cells were then treated with 30 μg of Dnase for every 1 million cells and incubated for 1 hours at 37°C. Cells were washed in Perm/Wash Buffer and stained with anti-BrdU antibodies for 20 minutes at room temperature. Data were acquired on FACSCalibur™ (Becton Dickinson, CA) and analyzed using FlowJo software (Tree Star, Inc., CA).

Annexin V-PE Labeling and Staining for Flow Cytometry.

Annexin V staining were performed using Annexin V-PE apoptosis detection kit I (BD Pharmingen, CA) following manufacture's instructions. After loading the cells with CMFDG (Molecular Probes, OR), the cells were resuspended in Annexin V binding buffer and stained with 1 test unit of Annexin V conjugated to the fluorochrome Phycoerythrin (PE) and 1 test unit of 7-amino-actinomycin D (7-AAD) (BD Pharmingen, CA) for every 1 X 10^5 cells. The cells were then incubated for 15 minutes at room temperature in the dark. Data were acquired on FACSCalibur™ (Becton Dickinson, CA) and analyzed using FlowJo software (Tree Star, Inc., CA).

Tissue Culture, Transient Transfections and Luciferase Assay.

Cos7 and HepG2 cells were grown on MEM supplemented with 10% fetal calf serum and DMEM supplemented with 15% fetal calf serum, respectively. HIT-T15 cells were grown in DMEM supplemented with 5% fetal calf serum and 10% horse serum. MIN cells were grown in ES cell media (See maintenance of undifferentiated ES cells *in*

vitro). A modified calcium phosphate precipitation procedure using calcium phosphate transfection system (Life Technologies, NY) was used for transient transfections. In short, 0.5 ml of the precipitate, containing 1 μg of CMV-LacZ, 0.5 μg of luciferase reporter construct, the indicated amount of expression vectors and carrier DNA (up to 10 μg), were added per 60 mm dish. Luciferase was normalized for transfection efficiency by the corresponding β-galactosidase activity (287).

Nuclear Extract Preparation.

In vitro cultured cells: cells were lysed in hypotonic buffer (20 mM Hepes, pH7.9, 10 mM KCl, 0.1 mM Na_3VO_4, 1mM EDTA, 10% Glycerol, 1X complete protease inhibitor (Roche, Germany), 20 mM NaF, and 1 mM DTT) with 0.2% NP40 on ice for 10 minutes. After centrifugation at 4°C (1200 G) for 2 minutes, the supernatants were collected as cytoplasmic extracts. The crude nuclei (pelleted) was washed in hypotonic buffer before resuspending in hypertonic buffer (hypotonic buffer with 20% glycerol and 420 mM NaCl), rocked for 30 minutes at 4°C, and the supernatants were collected after centrifugation at 4°C (1200 G) for 10 minutes.

Animal Tissues: Tissues were removed and dounce-homogenized 15 times in 100:1 (v:v) of buffer A (10 mM KCl, 1.5 mM $MgCl_2$, 10 mM Hepes pH 7.9, 1 mM DTT, 1 mM $NaVO_4$, 1x complete TM protease inhibitor (Roche, Germany). After centrifugation at 2,000x*g* for 10 min at 4 °C, the pellet was resuspended in 4 volumes of the same buffer, dounced 10 times and centrifuged again at 2,000x*g*. The nuclei containing pellet was resuspended in 2 volumes of buffer B (420 mM NaCl, 10 mM KCl, 20 mM Hepes pH 7.9, 20% glycerol, 1 mM DTT, 1 mM $NaV0_4$, 1x complete TM protease inhibitor) and extracted for 30 min at 4 °C on a shaking rotor. After centrifugation at 16,000x*g*, the

supernatant was diluted 10 fold in buffer C (10 mM KCl, 20 mM Hepes pH 7.9, 20% glycerol, 1 mM DTT, 1 mM $NaV0_4$, 1x complete TM protease inhibitor) and centrifuged for 15 min at 16,000x*g*. The supernatant was loaded onto a Biomax-50 filter unit (Millipore) and centrifuged for 2 h at 4,000x*g* at 4 °C. The protein concentration of the concentrated and desalted sample was determined by Bradford assay (BIO-RAD).

Whole Cell Extract Preparation.

Whole cell lysates were prepared in RIPA buffer (1X PBS, 1% NP40, 0.5% sodium deoxycholate, 0.1% SDS, and 1X complete protease inhibitor) and rocked for 4°C for 30 minutes, and supernatants were collected after centrifugation at 4°C (1200 G) for 10 minutes. Protein concentrations were determined using Bicinchoninic Acid Protein Assay Kit (Sigma, MO).

Western Blot Analysis.

20 μg of nuclear extract, total cell extract, or total tissue extract was separated by 10% SDS-PAGE and transferred onto a nitrocellulose membrane (Schleicher&Schuell, NH) by electroblotting (30 min, 15 V). Expression of organic anion transporter proteins on the basolateral (Slc10a1, Oatp1) and canalicular (Abcb11) membranes of liver was analyzed in crude liver membranes (100,000 x g pellet) of WT, *hnf-1*$\alpha^{+/-}$ or *hnf-1*$\alpha^{-/-}$ mice. The preparation of liver membranes have been described previously (288, 289).

Pdx-1 was detected with rabbit anti-Pdx-1 antiserum (1:500).

Tcf1 was detected with rabbit anti-Tcf1 (1:300) polyclonal antibody (Geneka Biotechnology Inc., Canada).

Fxr was detected with goat anti-FXR (1:1000) polyclonal antibody (Santa Cruz, CA).

Slc10a2 was detected with rabbit anti-Slc10a2 (1:2000) antibody.

Slc21a3 was detected with rabbit anti-Slc21a3 (1:1000) antibody.

Slc10a1 was detected with rabbit anti-Slc10a1 (1:1000) antibody.

Abcb11 was detected with rabbit anti–Abcb11 (1:2500) antibody.

ApoA1 was detected with mouse anti-ApoA1 (1:1000) antibody (Biodesign International).

GTP binding stimulatory protein (Gs) was detected with rabbit anti-Gs (1:1000) antibody (generous gift of T. Sakmar).

Tbp was detected with rabbit anti-TBP (1:3000) antibody (generous gift of M. Teichmann).

Goat anti-rabbit IgGs conjugated to HRP (Santa Cruz, CA) was used at 1:10,000.

All antibodies were dissolved in 5% milk in TBS with 0.5% Tween-20. The blots were washed 3 times 15 min each between each antibody incubation. All the primary antibodies were incubated over night at 4°C and the secondary antibody incubation were done at RT for 1 hr. For visualization, the Renaissance chemiluminescence substrate (NEN, MA.) was used.

Electrophoretic Mobility Shift Analysis.

In vitro translated proteins, total cell extracts, or nuclear cell extracts were incubated with ^{32}P-labeled ds-stranded oligonucleotide probes containing the transcription factor binding sites. The 15 μl reaction mixture contained 20 mM Hepes buffer pH 7.9, 40 mM KCl, 1mM $MgCl_2$, 0.1 mM EGTA, 0.5mM DTT, 4% Ficoll and 2 μg poly(dIdC) at 25°C for 20 min. Supershift analysis was performed by incubating the antibody with the protein or nuclear extracts for 5 min on ice before adding the probe. The reaction mixture was loaded on a 6% non-denaturating polyacrylamide gel

containing 0.25 x TBE buffer (0.023 M Tris-borate, 0.5 mM EDTA) and run at 4°C. The list of transcription factor binding site is listed below:

Hnf-4α binding site in SHP promoter: sequences: 5' TGGACAGTGGGCAAAGTCC-TCCC-3' and 5'-TGGACAGTAAAAAAAGTCCT CCC-3', respectively.

Tcf1 binding sites in the Slc10a2 promoter: sequences: 5'-AGGACATTAAACATTAA-CGTGGCTC-3' and 5'-AGGACAGGGGACATTAACGTGGCTC-3', respectively.

Tcf1 binding site in the Fxr-1 promoter: sequence: 5'-GATGGGGGTTAATCAAGT-AAACCACAC-3'.

Tcf1 binding site in the insulin growth factor binding protein: sequence: 5'-ACTGGTTAATGATTGGCATGC-3' (239).

Immunohistochemistry and Immunofluorescence Analysis.

Immunofluorescent analysis was performed on differentiated ES cells grown on fibronectin coated coverslips (Becton Dickinson, CA). Cells were fixed for 30 minutes with 4% paraformaldehyde, washed with 10mM glycine in PBS, and permeabilized with 0.1% Triton X (if detecting cytoplasmic protein). Cells were blocked for 30 min with 5% normal donkey serum in PBS. Primary antibodies used were guinea pig anti-insulin (1:600) (Linco, MO), rabbit anti-glucagon (1:300) (Linco, MO), and rabbit-anti-Pdx-1 antibody (1:300). Secondary antibodies used were Rhodamine Red conjugated donkey anti-guinea pig (Jackson Immunoresearch, PA) and Alexa Fluor 488 conjugated donkey anti-rabbit (Molecular Probes, OR) at a dilution of 1:100 and 1:600 in PBS respectively. Hybridization with primary antibodies was done at 4°C overnight in a humidified chamber. Hybridization with secondary antibodies was done at room temperature for 1

hour. Sections or ccells were washed three times in PBS between each step and were mounted using Prolong Antifade Kit (Molecular Probes, OR).

Glut 2 immunofluorescence was performed on 5 μm sections from 6 weeks old *hnf-1α*$^{+/+}$, *hnf-1α*$^{+/-}$, and *hnf-1α*$^{-/-}$ mice which were prepared as previously described (41). Sections were blocked for 30 min with normal rabbit serum at a concentration of 1:100, in PBS. Sections were stained with rabbit anti-mouse Glut2 antibody (Chemicon International Inc., Temecula, CA) in PBS at a dilution of 1:200. The secondary antibody, a TRITC-labeled guinea pig anti-rabbit IgG, was applied at a concentration of 1:100 in PBS. Sections were washed twice in PBS between each step and after the application of the secondary antibody, and were mounted in PBS:glycerol, 1:9.

For Slc10a2 immunohistochemistry, mice were perfused with 4% paraformaldehyde through the heart and ileum was post fixed in 4% paraformaldehyde for 15 min, dehydrated, and embedded in paraffin. Seven micrometer sections were cut, deparaffinized, rehydrated, and permeabilized in 0.2% TritonX-100 for 20 min, blocked with 0.3% H_2O_2 for 20 min, and 4% normal goat serum for 1 h. Sections were stained with rabbit anti-Slc10a2 antibody in PBS at a dilution of 1:200 for 1 hr (289). The slides were washed with PBS before incubation with a secondary biotinylated anti-IgG antibody. Sections were developed using the ABC kit and DAB substrate (Vector Laboratories) and counterstained with hematoxylin (Sigma, MO).

Image analysis were performed using Zeiss LSM 510 confocal laser scanning microscope (Zeiss, Germany) with three detectors, differential interference contrast (DIC), and an argon-krypton (Ar/Kr) laser for simultaneous scanning of two different

fluorochromes and DIC microscopy. Images were acquired using LSM 510 software package (Zeiss, Germany).

Morphometric Analysis

The pancreata were fixed in paraformaldehyde and stained for insulin and glucagon as described above. Sections (7 μm) through the entire pancreas were taken, and every sixth section was used for morphometric analysis. At least 288 nonoverlapping images (pixel size 0.88 μm) were scanned using a confocal laser scanning microscope (Zeiss LSM 510, Germany). The morphometry parameters were analyzed by using the METAMORPH software package (Universal Imaging, PA). The areas covered by cells stained by insulin or glucagon were integrated by using stained objects that are greater than 3 pixels in size.

Cryostat Sections.

For cryostat sections, the animal were perfused in 4% paraformaldehyde, the tissue of interest were post-fixed in 4% paraformaldehyde for 30 minutes at room temperature, washed 3 times for 15 minutes each in PBS, and incubated overnight in 30% sucrose in PBS. Embryos were then mounted in Tissue-Tek (Miles Scientific, Naperville, IL). 7 μm sections were cut in a cryostat, collected in Superfrost slides (Fisher, PA), and stored in -80°C until examination.

X-gal Staining.

Differentiated ES cells grown on fibronectin coated coverslips (Becton Dickinson, CA) were fixed in 0.2% gluteraldehyde, 5 mM EGTA, 2 mM magnesium chloride in sodium phosphate buffer (pH. 7.3) for 5 minutes. Cells were washed 3 times, 5 minutes each in wash buffer (2.5 mM magnesium chloride, 0.01% deoxycholate, 0.02% Nonidet-

P40 in sodium phosphate buffer pH. 7.3) and stained overnight in 1mM 5'-bromo-4-chloro-3-indolyl-β-D-galactopyranoside (X-gal) (Roche, Germany) in wash buffer.

Electronmicroscopy

For negative staining, the fractions were mixed with an equal volume of a 2% Na-phosphotungstate solution at neutral pH. Samples were adsorbed onto a formvar-carbon-coated 400-mesh grid for one minute. Excess fluid was removed with a torn filter paper and air-dried. Samples were studied and photographed in a JOEL 100CX at an accelerating voltage of 80 kV. Pictures were taken at magnifications ranging from x50,000 to x100,000.

Isolation of Pancreatic Islets and Newborn Pancreata.

Pancreatic islets were isolated from 4 to 6 week-old mice. We used collagenase digestion and differential centrifugation through Ficoll gradients, with a modification of procedures previously described (290). Islets were cultured overnight in RPMI1640 medium supplemented with 10% fetal calf serum and 11.1 mM glucose. Islets were then double hand picked the next day and then used for subsequent analysis. Whole pancreata were removed from newborn mice and immediately snap frozen in liquid nitrogen or homogenized in TRIzol reagent (Life Technologies, NY).

Measurement of Total Intracellular Insulin Content.

Insulin was extracted from pancreatic islets or differentiated cells with acid ethanol (10% flacial acetic acid in absolute ethanol), sonicated for 1 minute, and centrifuged 2 times at 4°C at 12,000 G for 10 minutes. Supernatants are collected and stored in -20°C for insulin determination by Ultra Sensitive Insulin Elisa Kit (Crystal Chem, IL).

Measurement of Insulin Release.

For static measurements of insulin release: 20 size-matched islets or differentiated cells grown on 6 well plate were washed twice in D-PBS/BSA/HEPES (Dulbecco's PBS, supplemented with 2g/l bovine serum albumin and 20mM HEPES (pH7.4)). They were then preincubated in 1ml of D-PBS/BSA/HEPES with 3.3mM (for glucose and sulphonylurea induction) or 6.6mM glucose (for GLP-1 induction) at 37°C for 30min. D-PBS/BSA/HEPES are collected at the end of pre-incubation for baseline values. After preincubation, islets or differentiated cells were washed twice in D-PBS/BSA/HEPES and incubated in 1ml of D-PBS/BSA/HEPES with 16.7mM glucose (for glucose induction), 3.3mM glucose and 500μM tolbutamide (for sulphonylurea induction) (Sigma, MO), or 6.6mM glucose and 100nM hGLP-1(7-36) (for GLP-1 induction) (Sigma, MO) at 37°C for 30min. After incubation, media was collected and kept at -20°C for insulin ELISA assay (Crystal Chem, IL).

For *in vivo* measurement of insulin release: For *in vivo* insulin release, glucose (3 g/kg body weight) was injected IP. Venous blood was collected at 0, 2, 5, 15, 30, 60, 120 min in heparinized tubes, centrifuged, and the plasma stored at –20°C. Insulin levels were measured with an ultrasensitive ELISA assay (Crystal Chemical, IL).

Glucose Tolerance Test

On 3 days old mice: Glucose tolerance tests were performed by intraperitoneal or subcutaneous glucose injection (2g/kg body weight). Whole blood was obtained from 2-3 days old mice by decapitation 1 hr after glucose injection. Blood glucose was measured using an enzymatic assay (Sigma, MO).

On adult Mice: Mice were fasted overnight for 12 hr followed by intraperitoneal (IP) glucose injection (2 g/kg body weight). Venous blood was obtained from the tail vein at 0, 15, 30, 60, and 120 min after the injection. Blood glucose was measured using an automated glucometer (Encore, Bayer).

Selective Amplification via Biotin- and Restriction-Mediated Enrichment (SABRE).

SABRE subtraction was performed as described previously (291). Double stranded cDNA is produced from oligo(dT) purified mRNA and digested with Sau3AI. Linkers were annealed to the digested overhangs containing an BamHI restriction site. "Tester" cDNA, in which differential messages are to be detected, was PCR reamplified with a biotinylated primer containing the *Bam* HI site. "Driver" or reference cDNA was amplified with a non-biotinylated primer containing a mutant *Bam* HI site. 33-fold excess of driver was hybridized to biotin-labeled tester, after which tester-tester homohybrides (representing differentially expressed genes) are purified by paramagnetic beads and digestion with *Bam* HI (292). Three rounds of subtraction were completed to enrich differentially expressed cDNAs.

Gene Expression Analysis using Affymetrix Oligonucleotide Arrays

i. Preparation of hybridization samples.

Newborn and four-week-old *tcf1* wildtype and null mutant mice were sacrificed by CO_2 asphyxiation and total RNA was isolated from livers using Trizol® (Life Technologies, NY). RNA was pooled from five animals of each genotype for each experiment. RNA sample integrity was assessed by running denaturing formaldehyde gels. cDNA synthesis was completed with 30 μg of total RNA cleaned with RNeasy columns (Qiagen). cDNA synthesis was be carried out according to the Superscript

Choice cDNA Synthesis Protocol (Life Technologies, NY), except an HPLC purified T7-Promoter-dT30 primer (Genset) was used to initiate the first-strand reaction. Biotin labeled cRNA was synthesized from T7-cDNA using the RNA transcript labeling kit, Bio Array (Enzo), supplemented with biotin 11-CTP and biotin-16-UTP (Enzo) as specified in the Affymetrix technical manual. The sample was cleaned with RNeasy columns (Qiagen) to remove free nucleotides and quantitated spectrophotometrically. Biotin labeled cRNA was fragmented in 40 mM Tris pH 8.1, 100 mM KOAc, 30 mM MgOAc for 30 min at 94 °C. Hybridization samples were prepared according to the Affymetrix manual with a final concentration of fragmented cRNA of 0.05 $\mu g/\mu l$.

ii. Hybridization, washing, staining, and scanning of probe arrays.

Affymetrix Genechip® Mu11K and Mu19K probe arrays were prehybridized with 100 mM MES (Sigma) pH 6.6, 1M[Na^+], 20 mM EDTA, and 0.01% Tween-20 (Sigma) for 10 min at 45 °C. Hybridization samples were heated to 99 °C for 5 min, equilibrated to 45 °C for 5 min and centrifuged at 14,000 x *g* for 5 min to sediment any particulate matter. The prehybridization solution was removed and the sample was added to the probe array and allowed to hybridize for 16 h, rotating at 60 rpm at 45 °C. Probe arrays were subsequently washed and stained according to the Affymetrix technical manual in an Affymetrix fluidics station. The arrays were scanned using a Hewlett Packard confocal laser scanner and visualized using Affymetrix Genechip 3.1 software (Affymetrix).

iii. Control experiments

Messenger RNA levels of differentially expressed genes were studied independently using semiquantitative RT-PCR (See next section).

RNA Extraction and RT-PCR.

Total RNA was extracted using TRIzol reagent (Life Technologies, NY) and following the manufacturer's instructions. Contaminating genomic DNA was removed using 10U of RNase free DNase-I (Boehringer Mannheim, Germany) per 5μg of RNA. cDNAs were synthesized using Moloney murine leukemia virus reverse transcriptase with dNTPs and random hexamer primers (Stratagene, CA). The cDNAs provided templates for polymerase chain reactions (PCRs) using specific primers at annealing temperatures ranging between 60 and 65°C in the presence of dNTPs, [α-^{32}P]dCTP, and Taq DNA polymerase. PCR synthesis for each primer pair was quantified at 15, 20, 25, and 30 cycles in a test reaction to ensure that the quantitative PCR amplification was in the linear range. The primer sequences used for PCR are available upon request.

Statistical Analysis.

Data are means ± SEM unless otherwise indicated. The statistical analysis was performed using the Microsoft Excel 98 statistical package (Microsoft Inc., WA). Student's *t* -test for 2 tailed analysis and unequal variance as parameters was used to assess statistical significance and the null hypothesis was rejected at the 0.05 level.

References:

1. Saltiel, A. R. (2001) *Cell* **104,** 517-29.
2. Taylor, S. I. (1999) *Cell* **97,** 9-12.
3. Fajans, S. S., Bell, G. I. & Polonsky, K. S. (2001) *N Engl J Med* **345,** 971-80.
4. Yamagata, K., Furuta, H., Oda, N., Kaisaki, P. J., Menzel, S., Cox, N. J., Fajans, S. S., Signorini, S., Stoffel, M. & Bell, G. I. (1996) *Nature* **384,** 458-60.
5. Yamagata, K., Oda, N., Kaisaki, P. J., Menzel, S., Furuta, H., Vaxillaire, M., Southam, L., Cox, R. D., Lathrop, G. M., Boriraj, V. V., Chen, X., Cox, N. J., Oda, Y., Yano, H., Le Beau, M. M., Yamada, S., Nishigori, H., Takeda, J., Fajans, S. S., Hattersley, A. T., Iwasaki, N., Hansen, T., Pedersen, O., Polonsky, K. S. & Bell, G. I. (1996) *Nature* **384,** 455-8.
6. Stoffers, D. A., Zinkin, N. T., Stanojevic, V., Clarke, W. L. & Habener, J. F. (1997) *Nature Genetics* **15,** 106-10.
7. Stoffers, D. A., Ferrer, J., Clarke, W. L. & Habener, J. F. (1997) *Nature Genetics* **17,** 138-9.
8. Horikawa, Y., Iwasaki, N., Hara, M., Furuta, H., Hinokio, Y., Cockburn, B. N., Lindner, T., Yamagata, K., Ogata, M., Tomonaga, O., Kuroki, H., Kasahara, T., Iwamoto, Y. & Bell, G. I. (1997) *Nature Genetics* **17,** 384-5.
9. Malecki, M. T., Jhala, U. S., Antonellis, A., Fields, L., Doria, A., Orban, T., Saad, M., Warram, J. H., Montminy, M. & Krolewski, A. S. (1999) *Nature Genetics* **23,** 323-8.
10. (1997) *Diabetes Care* **20,** 1183-97.
11. Bach, J. F. & Chatenoud, L. (2001) *Annu Rev Immunol* **19,** 131-61.

12. Tisch, R. & McDevitt, H. (1996) *Cell* **85,** 291-7.

13. Harris, M. I. (1998) *Diabetes Care* **21 Suppl 3,** C11-4.

14. Harris, M. I., Flegal, K. M., Cowie, C. C., Eberhardt, M. S., Goldstein, D. E., Little, R. R., Wiedmeyer, H. M. & Byrd-Holt, D. D. (1998) *Diabetes Care* **21,** 518-24.

15. LeRoith, D., Taylor, S. I. & Olefsky, J. M. (2000) *Diabetes mellitus : a fundamental and clinical text* (Lippincott Williams & Wilkins, Philadelphia, Pa.).

16. Kahn, C. R., Vicent, D. & Doria, A. (1996) *Annu Rev Med* **47,** 509-31.

17. Weir, G. C., Laybutt, D. R., Kaneto, H., Bonner-Weir, S. & Sharma, A. (2001) *Diabetes* **50 Suppl 1,** S154-9.

18. Froguel, P., Zouali, H., Vionnet, N., Velho, G., Vaxillaire, M., Sun, F., Lesage, S., Stoffel, M., Takeda, J. & Passa, P. (1993) *New England Journal of Medicine* **328,** 697-702.

19. Ledermann, H. M. (1995) *Diabetologia* **38,** 1482.

20. Matschinsky, F. M. (1990) *Diabetes* **39,** 647-52.

21. Stoffers, D. A., Stanojevic, V. & Habener, J. F. (1998) *Journal of Clinical Investigation* **102,** 232-41.

22. Thomas, H., Jaschkowitz, K., Bulman, M., Frayling, T. M., Mitchell, S. M., Roosen, S., Lingott-Frieg, A., Tack, C. J., Ellard, S., Ryffel, G. U. & Hattersley, A. T. (2001) *Hum Mol Genet* **10,** 2089-97.

23. Zhong, W., Mirkovitch, J. & Darnell, J. E., Jr. (1994) *Mol Cell Biol* **14,** 7276-84.

24. Chen, W. S., Manova, K., Weinstein, D. C., Duncan, S. A., Plump, A. S., Prezioso, V. R., Bachvarova, R. F. & Darnell, J. E. (1994) *Genes & Development* **8,** 2466-77.

25. Stoffel, M. & Duncan, S. A. (1997) *Proceedings of the National Academy of Sciences of the United States of America* **94,** 13209-14.

26. Byrne, M. M., Sturis, J., Fajans, S. S., Ortiz, F. J., Stoltz, A., Stoffel, M., Smith, M. J., Bell, G. I., Halter, J. B. & Polonsky, K. S. (1995) *Diabetes* **44,** 699-704.

27. Herman, W. H., Fajans, S. S., Smith, M. J., Polonsky, K. S., Bell, G. I. & Halter, J. B. (1997) *Diabetes* **46,** 1749-54.

28. Shih, D. Q., Dansky, H. M., Fleisher, M., Assmann, G., Fajans, S. S. & Stoffel, M. (2000) *Diabetes* **49,** 832-7.

29. Byrne, M. M., Sturis, J., Clement, K., Vionnet, N., Pueyo, M. E., Stoffel, M., Takeda, J., Passa, P., Cohen, D. & Bell, G. I. (1994) *Journal of Clinical Investigation* **93,** 1120-30.

30. Njolstad, P. R., Sovik, O., Cuesta-Munoz, A., Bjorkhaug, L., Massa, O., Barbetti, F., Undlien, D. E., Shiota, C., Magnuson, M. A., Molven, A., Matschinsky, F. M. & Bell, G. I. (2001) *N Engl J Med* **344,** 1588-1592.

31. Glaser, B., Kesavan, P., Heyman, M., Davis, E., Cuesta, A., Buchs, A., Stanley, C. A., Thornton, P. S., Permutt, M. A., Matschinsky, F M. & Herold, K. C. (1998) *New England Journal of Medicine* **338,** 226-30.

32. Grupe, A., Hultgren, B., Ryan, A., Ma, Y. H., Bauer, M. & Stewart, T. A. (1995) *Cell* **83,** 69-78.

33. Velho, G., Petersen, K. F., Perseghin, G., Hwang, J. H., Rothman, D. L., Pueyo, M. E., Cline, G. W., Froguel, P & Shulman, G. I. (1996) *Journal of Clinical Investigation* **98,** 1755-61.

34. Hattersley, A. T., Beards, F., Ballantyne, E., Appleton, M., Harvey, R. & Ellard, S. (1998) *Nature Genetics* **19,** 268-70.

35. Pearson, E. R., Velho, G., Clark, P., Stride, A., Shepherd, M., Frayling, T. M., Bulman, M. P., Ellard, S., Froguel, P. & Hattersley, A. T. (2001) *Diabetes* **50 Suppl 1,** S101-7.

36. Pontoglio, M., Barra, J., Hadchouel, M., Doyen, A., Kress, C., Bach, J. P., Babinet, C. & Yaniv, M. (1996) *Cell* **84,** 575-85.

37. Lee, Y. H., Sauer, B. & Gonzalez, F. J. (1998) *Molecular & Cellular Biology* **18,** 3059-68.

38. Hiraiwa, H., Pan, C.-J., Lin, B., Akiyama, T. E., Gonzalez, F. J. & Chou, J. Y. (2001) *J. Biol. Chem.* **276,** 7963-7967.

39. Shih, D. Q., Bussen, M., Sehayek, E., Ananthanarayanan, M., Shneider, B. L., Suchy, F. J., Shefer, S., Bollileni, J. S., Gonzalez, F. J., Breslow, J. L. & Stoffel, M. (2001) *Nature Genetics* **27,** 375-82.

40. Dukes, I. D., Sreenan, S., Roe, M. W., Levisetti, M., Zhou, Y. P., Ostrega, D., Bell, G. I., Pontoglio, M., Yaniv, M., Philipson, L. & Polonsky, K. S. (1998) *Journal of Biological Chemistry* **273,** 24457-64.

41. Pontoglio, M., Sreenan, S., Roe, M., Pugh, W., Ostrega, D., Doyen, A., Pick, A. J., Baldwin, A., Velho, G., Froguel, P., Levisetti, M., Bonner-Weir, S., Bell, G. I., Yaniv, M. & Polonsky, K. S. (1998) *J Clin Invest* **101,** 2215-22.

42. Shih, D. Q., Screenan, S., Munoz, K. N., Philipson, L., Pontoglio, M., Yaniv, M., Polonsky, K. S. & Stoffel, M. (2001) *Diabetes* **50,** 2472-2480.

43. Chevre, J. C., Hani, E. H., Boutin, P., Vaxillaire, M., Blanche, H., Vionnet, N., Pardini, V. C., Timsit, J., Larger, E., Charpentier, G., Beckers, D., Maes, M., Bellanne-Chantelot, C., Velho, G. & Froguel, P. (1998) *Diabetologia* **41,** 1017-23.

44. Frayling, T. M., Bulamn, M. P., Ellard, S., Appleton, M., Dronsfield, M. J., Mackie, A. D., Baird, J. D., Kaisaki, P. J., Yamagata, K., Bell, G. I., Bain, S. C. & Hattersley, A. T. (1997) *Diabetes* **46,** 720-5.

45. Lehto, M., Tuomi, T., Mahtani, M. M., Widen, E., Forsblom, C., Sarelin, L., Gullstrom, M., Isomaa, B., Lehtovirta, M., Hyrkko, A., Kanninen, T., Orho, M., Manley, S., Turner, R. C., Brettin, T., Kirby, A., Thomas, J., Duyk, G., Lander, E., Taskinen, M. R. & Groop, L. (1997) *Journal of Clinical Investigation* **99,** 582-91.

46. Hansen, T., Eiberg, H., Rouard, M., Vaxillaire, M., Moller, A. M., Rasmussen, S. K., Fridberg, M., Urhammer, S. A., Holst, J. J., Almind, K., Echwald, S. M., Hansen, L., Bell, G. I. & Pedersen, O. (1997) *Diabetes* **46,** 726-30.

47. Menzel, R., Kaisaki, P. J., Rjasanowski, I., Heinke, P., Kerner, W. & Menzel, S. (1998) *Diabet Med* **15,** 816-20.

48. Pontoglio, M., Prie, D., Cheret, C., Doyen, A., Leroy, C., Froguel, P., Velho, G., Yaniv, M. & Friedlander, G. (2000) *EMBO Rep* **1,** 359-65.

49. Frayling, T. M., Evans, J. C., Bulman, M. P., Pearson, E., Allen, L., Owen, K., Bingham, C., Hannemann, M., Shepherd, M., Ellard, S. & Hattersley, A. T. (2001) *Diabetes* **50 Suppl 1,** S94-100.

50. Ohlsson, H., Karlsson, K. & Edlund, T. (1993) *EMBO Journal* **12,** 4251-9.

51. Leonard, J., Peers, B., Johnson, T., Ferreri, K., Lee, S. & Montminy, M. R. (1993) *Mol Endocrinol* **7,** 1275-83.

52. Miller, C. P., McGehee, R. E., Jr. & Habener, J. F. (1994) *Embo J* **13,** 1145-56.

53. Dutta, S., Gannon, M., Peers, B., Wright, C., Bonner-Weir, S. & Montminy, M. (2001) *Proceedings of the National Academy of Sciences of the United States of America* **98,** 1065-70.

54. Jonsson, J., Carlsson, L., Edlund, T. & Edlund, H. (1994) *Nature* **371,** 606-9.

55. Offield, M. F., Jetton, T. L., Labosky, P. A., Ray, M., Stein, R. W., Magnuson, M. A., Hogan, B. L. & Wright, C. V. (1996) *Development* **122,** 983-95.

56. Ahlgren, U., Jonsson, J., Jonsson, L., Simu, K. & Edlund, H. (1998) *Genes & Development* **12,** 1763-8.

57. Ben-Shushan, E., Marshak, S., Shoshkes, M., Cerasi, E. & Melloul, D. (2001) *J Biol Chem* **276,** 17533-40.

58. Wu, K. L., Gannon, M., Peshavaria, M., Offield, M. F., Henderson, E., Ray, M., Marks, A., Gamer, L. W., Wright, C. V. & Stein, R. (1997) *Mol Cell Biol* **17,** 6002-13.

59. Gerrish, K., Gannon, M., Shih, D., Henderson, E., Stoffel, M., Wright, C. V. & Stein, R. (2000) *Journal of Biological Chemistry* **275,** 3485-92.

60. Hart, A. W., Baeza, N., Apelqvist, A. & Edlund, H. (2000) *Nature* **408,** 864-8.

61. Clocquet, A. R., Egan, J. M., Stoffers, D. A., Muller, D. C., Wideman, L., Chin, G. A., Clarke, W. L., Hanks, J. B., Habener, J. F. & Elahi, D. (2000) *Diabetes* **49,** 1856-64.

62. Barbacci, E., Reber, M., Ott, M. O., Breillat, C., Huetz, F. & Cereghini, S. (1999) *Development* **126,** 4795-805.

63. Coffinier, C., Thepot, D., Babinet, C., Yaniv, M. & Barra, J. (1999) *Development* **126,** 4785-94.

64. Lindner, T. H., Njolstad, P R., Horikawa, Y., Bostad, L., Bell, G. I. & Sovik, O. (1999) *Human Molecular Genetics* **8,** 2001-8.

65. Bingham, C., Bulman, M. P., Ellard, S., Allen, L. I., Lipkin, G. W., Hoff, W. G., Woolf, A. S., Rizzoni, G., Novelli, G., Nicholls, A. J. & Hattersley, A. T. (2001) *American Journal of Human Genetics* **68,** 219-24.

66. Bingham, C., Ellard, S., Allen, L., Bulman, M., Shepherd, M., Frayling, T., Berry, P. J., Clark, P. M., Lindner, T., Bell, G. I., Ryffel, G. U., Nicholls, A. J. & Hattersley, A. T. (2000) *Kidney International* **57,** 898-907.

67. Nishigori, H., Yamada, S., Kohama, T., Tomura, H., Sho, K., Horikawa, Y., Bell, G. I., Takeuchi, T. & Takeda, J. (1998) *Diabetes* **47,** 1354-5.

68. Iwasaki, N., Okabe, I., Momoi, M. Y., Ohashi, H., Ogata, M. & Iwamoto, Y. (2001) *Diabetologia* **44,** 387-8.

69. Naya, F. J., Stellrecht, C. M. & Tsai, M. J. (1995) *Genes & Development* **9,** 1009-19.

70. Glick, E., Leshkowitz, D. & Walker, M. D. (2000) *J Biol Chem* **275,** 2199-204.

71. Naya, F. J., Huang, H. P., Qiu, Y., Mutoh, H., DeMayo, F. J., Leiter, A. B. & Tsai, M. J. (1997) *Genes & Development* **11,** 2323-34.

72. Qiu, Y., Sharma, A. & Stein, R. (1998) *Mol Cell Biol* **18,** 2957-64.

73. Sharma, A., Moore, M., Marcora, E., Lee, J. E., Qiu, Y., Samaras, S. & Stein, R. (1999) *Mol Cell Biol* **19,** 704-13.

74. Waeber, G., Delplanque, J., Bonny, C., Mooser, V., Steinmann, M., Widmann, C., Maillard, A., Miklossy, J., Dina, C., Hani, E. H., Vionnet, N., Nicod, P., Boutin, P. & Froguel, P. (2000) *Nature Genetics* **24,** 291-5.

75. Vinik, A. & Bell, G. (1988) *Hormone & Metabolic Research* **20,** 1-10.

76. Shimomura, H., Sanke, T., Hanabusa, T., Tsunoda, K., Furuta, H. & Nanjo, K. (2000) *Diabetes* **49,** 1597-600.

77. Duncan, S. A., Navas, M. A., Dufort, D., Rossant, J. & Stoffel, M. (1998) *Science* **281,** 692-5.

78. McPherson, C. E., Shim, E. Y., Friedman, D. S. & Zaret, K. S. (1993) *Cell* **75,** 387-98.

79. Shim, E. Y., Woodcock, C. & Zaret, K. S. (1998) *Genes Dev* **12,** 5-10.

80. Kuo, C. J., Conley, P. B., Chen, L., Sladek, F. M., Darnell, J. E. & Crabtree, G. R. (1992) *Nature* **355,** 457-61.

81. Parrizas, M., Maestro, M. A., Boj, S. F., Paniagua, A., Casamitjana, R., Gomis, R., Rivera, F. & Ferrer, J. (2001) *Molecular & Cellular Biology* **21,** 3234-43.

82. Boj, S. F., Parrizas, M., Maestro, M. A. & Ferrer, J. (2001) *Proc Natl Acad Sci U S A* **20,** 20.

83. Seol, W., Choi, H. S. & Moore, D. D. (1996) *Science* **272,** 1336-9.

84. Lee, Y. K., Dell, H., Dowhan, D. H., Hadzopoulou-Cladaras, M. & Moore, D. D. (2000) *Mol Cell Biol* **20,** 187-95.

85. Lai, E., Clark, K. L., Burley, S. K. & Darnell, J. E., Jr. (1993) *Proc Natl Acad Sci U S A* **90,** 10421-3.

86. Pani, L., Overdier, D. G., Porcella, A., Qian, X., Lai, E. & Costa, R. H. (1992) *Mol Cell Biol* **12,** 3723-32.

87. Costa, R. H., Grayson, D. R. & Darnell, J. E., Jr. (1989) *Mol Cell Biol* **9,** 1415-25.

88. Cereghini, S. (1996) *Faseb J* **10,** 267-82.

89. Lai, E., Prezioso, V. R., Smith, E., Litvin, O., Costa, R. H. & Darnell, J. E., Jr. (1990) *Genes Dev* **4,** 1427-36.

90. Lai, E., Prezioso, V. R., Tao, W. F., Chen, W. S. & Darnell, J. E., Jr. (1991) *Genes Dev* **5,** 416-27.

91. Ang, S. L., Wierda, A., Wong, D., Stevens, K. A., Cascio, S., Rossant, J. & Zaret, K. S. (1993) *Development* **119,** 1301-15.

92. Monaghan, A. P., Kaestner, K. H., Grau, E. & Schutz, G. (1993) *Development* **119,** 567-78.

93. Weinstein, D. C., Ruiz i Altaba, A., Chen, W. S., Hoodless, P., Prezioso, V. R., Jessell, T. M. & Darnell, J. E., Jr. (1994) *Cell* **78,** 575-88.

94. Sasaki, H. & Hogan, B. L. (1993) *Development* **118,** 47-59.

95. Ang, S. L. & Rossant, J. (1994) *Cell* **78,** 561-74.

96. Sund, N. J., Ang, S. L., Sackett, S. D., Shen, W., Daigle, N., Magnuson, M. A. & Kaestner, K. H. (2000) *Mol Cell Biol* **20,** 5175-83.

97. Sund, N. J., Vatamaniuk, M. Z., Casey, M., Ang, S. L., Magnuson, M. A., Stoffers, D. A., Matschinsky, F. M. & Kaestner, K. H. (2001) *Genes Dev* **15,** 1706-15.

98. Kaestner, K. H., Hiemisch, H. & Schutz, G. (1998) *Mol Cell Biol* **18,** 4245-51.

99. Felig, P., Pozefsky, T., Marliss, E. & Cahill, G. F., Jr. (1970) *Science* **167,** 1003-4.

100. Muller, W. A., Faloona, G. R. & Unger, R. H. (1971) *J Clin Invest* **50,** 2215-8.

101. Vidnes, J. & Oyasaeter, S. (1977) *Pediatr Res* **11,** 943-9.

102. Wise, J. K., Hendler, R. & Felig, P. (1973) *N Engl J Med* **288,** 487-90.

103. Guettet, C., Rostaqui, N., Mathe, D., Lecuyer, B., Navarro, N. & Jacotot, B. (1991) *Lipids* **26,** 451-8.

104. Philippe, J., Morel, C. & Prezioso, V R. (1994) *Mol Cell Biol* **14,** 3514-23.

105. Rudnicki, M. A., Braun, T., Hinuma, S. & Jaenisch, R. (1992) *Cell* **71,** 383-90.

106. Cornblath, M. & Schwartz, R. (1966) *Disorders of carbohydrate metabolism in infancy* (Saunders, Philadelphia,).

107. Friedman, J. M. & Halaas, J. L. (1998) *Nature* **395,** 763-70.

108. Krysiak, R., Obuchowicz, E. & Herman, Z. S. (1999) *Eur J Endocrinol* **140,** 130-6.

109. Unger, R. H. & Orci, L. (1976) *Physiol Rev* **56,** 778-826.

110. Holst, J. J. (1997) *Annu Rev Physiol* **59,** 257-71.

111. Mojsov, S., Weir, G. C. & Habener, J. F. (1987) *J Clin Invest* **79,** 616-9.

112. Cockell, M., Stolarczyk, D., Frutiger, S., Hughes, G. J., Hagenbuchle, O. & Wellauer, P. K. (1995) *Mol Cell Biol* **15,** 1933-41.

113. Vaisse, C., Kim, J., Espinosa, R., 3rd, Le Beau, M. M. & Stoffel, M. (1997) *Diabetes* **46,** 1364-7.

114. Grill, V., Adamson, U. & Cerasi, E. (1978) *J Clin Invest* **61,** 1034-43.

115. Tronche, F. & Yaniv, M. (1994) *Liver gene expression* (R.G. Landes, Austin).

116. Kollee, L. A., Monnens, L. A., Cecjka, V. & Wilms, R. M. (1978) *Arch Dis Child* **53,** 422-4.

117. Navas, M. A., Vaisse, C., Boger, S., Heimesaat, M., Kollee, L. A. & Stoffel, M. (2000) *Hum Hered* **50,** 370-81.

118. Mendel, D. B. & Crabtree, G. R. (1991) *J Biol Chem* **266,** 677-80.

119. Blumenfeld, M., Maury, M., Chouard, T., Yaniv, M. & Condamine, H. (1991) *Development* **113,** 589-99.

120. Byrne, M. M., Sturis, J., Menzel, S., Yamagata, K., Fajans, S. S., Dronsfield, M. J., Bain, S. C., Hattersley, A. T., Velho, G., Froguel, P., Bell, G. I. & Polonsky, K. S. (1996) *Diabetes* **45,** 1503-10.

121. Wang, H., Maechler, P., Hagenfeldt, K. A. & Wollheim, C. B. (1998) *Embo J* **17,** 6701-13.

122. Wang, H., Antinozzi, P. A., Hagenfeldt, K. A., Maechler, P. & Wollheim, C. B. (2000) *EMBO Journal* **19,** 4257-64.

123. Shih, D. Q., Navas, M. A., Kuwajima, S., Duncan, S. A. & Stoffel, M. (1999) *Proc Natl Acad Sci U S A* **96,** 10152-7.

124. Webb, G. C., Akbar, M. S., Zhao, C. & Steiner, D. F. (2000) *Proc Natl Acad Sci U S A* **97,** 5773-8.

125. MacDonald, M. J. & Kowluru, A. (1985) *Mol Cell Biochem* **68,** 107-14.

126. MacDonald, M. J., Kowluru, A. & Chang, C. M. (1985) *Metabolism* **34,** 600-3.

127. Lee, H. K., Lee, Y. K., Park, S. H., Kim, Y. S., Lee, J. W., Kwon, H. B., Soh, J., Moore, D. D. & Choi, H. S. (1998) *J Biol Chem* **273,** 14398-402.

128. Guillam, M. T., Hummler, E., Schaerer, E., Yeh, J. I., Birnbaum, M. J., Beermann, F., Schmidt, A., Deriaz, N., Thorens, B. & Wu, J. Y. (1997) *Nat Genet* **17,** 327-30.

129. Tsukuda, N. & Gabler, W. L. (1993) *J Periodontol* **64,** 1219-24.

130. Saez, E., No, D., West, A. & Evans, R. M. (1997) *Curr Opin Biotechnol* **8,** 608-16.

131. Chouard, T., Blumenfeld, M., Bach, I., Vandekerckhove, J., Cereghini, S. & Yaniv, M. (1990) *Nucleic Acids Res* **18,** 5853-63.

132. Asfari, M., Janjic, D., Meda, P., Li, G., Halban, P. A. & Wollheim, C. B. (1992) *Endocrinology* **130,** 167-78.

133. Waeber, G., Thompson, N., Nicod, P. & Bonny, C. (1996) *Mol Endocrinol* **10,** 1327-34.

134. Carty, M. D., Lillquist, J. S., Peshavaria, M., Stein, R. & Soeller, W. C. (1997) *J Biol Chem* **272,** 11986-93.

135. Melloul, D., Ben-Neriah, Y. & Cerasi, E. (1993) *Proc Natl Acad Sci U S A* **90,** 3865-9.

136. Dumonteil, E., Laser, B., Constant, I. & Philippe, J. (1998) *J Biol Chem* **273,** 19945-54.

137. Emens, L. A., Landers, D. W. & Moss, L. G. (1992) *Proc Natl Acad Sci U S A* **89,** 7300-4.

138. Nishigori, H., Tomura, H., Tonooka, N., Kanamori, M., Yamada, S., Sho, K., Inoue, I., Kikuchi, N., Onigata, K., Kojima, I., Kohama, T., Yamagata, K., Yang, Q., Matsuzawa, Y., Miki, T., Seino, S., Kim, M. Y., Choi, H. S., Lee, Y. K., Moore, D. D. & Takeda, J. (2001) *Proc Natl Acad Sci U S A* **98,** 575-80.

139. Lillioja, S., Mott, D. M., Spraul, M., Ferraro, R., Foley, J. E., Ravussin, E., Knowler, W. C., Bennett, P. H. & Bogardus, C. (1993) *N Engl J Med* **329,** 1988-92.

140. DeFronzo, R. A. (1997) *Neth J Med* **50,** 191-7.

141. Lauro, D., Kido, Y., Castle, A. L., Zarnowski, M. J., Hayashi, H., Ebina, Y. & Accili, D. (1998) *Nat Genet* **20,** 294-8.

142. Bruning, J. C., Michael, M. D., Winnay, J. N., Hayashi, T., Horsch, D., Accili, D., Goodyear, L. J. & Kahn, C. R. (1998) *Mol Cell* **2,** 559-69.

143. St-Onge, L., Wehr, R. & Gruss, P. (1999) *Curr Opin Genet Dev* **9,** 295-300.

144. Sander, M., Sussel, L., Conners, J., Scheel, D., Kalamaras, J., Dela Cruz, F., Schwitzgebel, V., Hayes-Jordan, A. & German, M. (2000) *Development* **127,** 5533-40.

145. Cirillo, L. A., McPherson, C. E., Bossard, P., Stevens, K., Cherian, S., Shim, E. Y., Clark, K. L., Burley, S. K. & Zaret, K. S. (1998) *Embo J* **17,** 244-54.

146. Marshak, S., Ben-Shushan, E., Shoshkes, M., Havin, L., Cerasi, E. & Melloul, D. (2001) *Diabetes* **50 Suppl 1,** S37-8.

147. Ohneda, K., Ee, H. & German, M. (2000) *Semin Cell Dev Biol* **11,** 227-33.

148. Perl, A. K., Wilgenbus, P., Dahl, U., Semb, H. & Christofori, G. (1998) *Nature* **392,** 190-3.

149. Bruning, J. C., Winnay, J., Bonner-Weir, S., Taylor, S. I., Accili, D. & Kahn, C. R. (1997) *Cell* **88,** 561-72.

150. Kido, Y., Burks, D. J., Withers, D., Bruning, J. C., Kahn, C. R., White, M. F. & Accili, D. (2000) *J Clin Invest* **105,** 199-205.

151. Withers, D. J., Burks, D. J., Towery, H. H., Altamuro, S. L., Flint, C. L. & White, M. F. (1999) *Nat Genet* **23,** 32-40.

152. Sussel, L., Kalamaras, J., Hartigan-O'Connor, D. J., Meneses, J. J., Pedersen, R. A., Rubenstein, J. L. & German, M. S. (1998) *Development* **125,** 2213-21.

153. Atwater, I., Rojas, E. & Soria, B. (1986) *Biophysics of the pancreatic gbs-cell* (Plenum Press, New York).

154. Dahl, U., Sjodin, A. & Semb, H. (1996) *Development* **122,** 2895-902.

155. Hauge-Evans, A. C., Squires, P. E., Persaud, S. J. & Jones, P. M. (1999) *Diabetes* **48,** 1402-8.

156. Mudaliar, S. & Henry, R. R. (2001) *Annual Review of Medicine* **52,** 239-57.

157. anonymous (1998) *Lancet* **352,** 837-53.

158. Zeng, Y., Ricordi, C., Lendoire, J., Carroll, P. B., Alejandro, R., Bereiter, D. R., Tzakis, A. & Starzl, T. E. (1993) *Surgery* **113,** 98-102.

159. Zandstra, P. W. & Nagy, A. (2001) **3,** 275-305.

160. Lee, S. H., Lumelsky, N., Studer, L., Auerbach, J. M. & McKay, R. D. (2000) *Nat Biotechnol* **18,** 675-9.

161. Johe, K. K., Hazel, T. G., Muller, T., Dugich-Djordjevic, M. M. & McKay, R. D. (1996) *Genes Dev* **10,** 3129-40.

162. Palacios, R., Golunski, E. & Samaridis, J. (1995) *Proc Natl Acad Sci U S A* **92,** 7530-4.

163. Brustle, O., Spiro, A. C., Karram, K., Choudhary, K., Okabe, S. & McKay, R. D. (1997) *Proc Natl Acad Sci U S A* **94,** 14809-14.

164. Deacon, T., Dinsmore, J., Costantini, L. C., Ratliff, J. & Isacson, O. (1998) *Exp Neurol* **149,** 28-41.

165. Assady, S., Maor, G., Amit, M., Itskovitz-Eldor, J., Skorecki, K. L. & Tzukerman, M. (2001) *Diabetes* **50,** 1691-7.

166. Lumelsky, N., Blondel, O., Laeng, P., Velasco, I., Ravin, R. & McKay, R. (2001) *Science* **292,** 1389-94.

167. Soria, B., Roche, E., Berna, G., Leon-Quinto, T., Reig, J. A. & Martin, F. (2000) *Diabetes* **49,** 157-62.

168. Pictet, R. L., Rall, L. B., Phelps, P. & Rutter, W. J. (1976) *Science* **191,** 191-2.

169. Kim, S. K. & Hebrok, M. (2001) *Genes Dev* **15,** 111-27.

170. Hebrok, M., Kim, S. K. & Melton, D. A. (1998) *Genes Dev* **12,** 1705-13.

171. Kim, S. K. & Melton, D. A. (1998) *Proc Natl Acad Sci U S A* **95,** 13036-41.

172. Hebrok, M., Kim, S. K., St Jacques, B., McMahon, A. P. & Melton, D. A. (2000) *Development* **127,** 4905-13.

173. Edlund, H. (2001) *Diabetes* **50 Suppl 1,** S5-9.

174. Ahlgren, U., Jonsson, J. & Edlund, H. (1996) *Development* **122,** 1409-16.

175. Teitelman, G., Alpert, S., Polak, J. M., Martinez, A. & Hanahan, D. (1993) *Development* **118,** 1031-9.

176. Pictet, R. L., Clark, W. R., Williams, R. H. & Rutter, W. J. (1972) *Dev Biol* **29,** 436-67.

177. Wessells, N. K. & Evans, J. (1968) *Dev Biol* **17,** 413-46.

178. Apelqvist, A., Li, H., Sommer, L., Beatus, P., Anderson, D. J., Honjo, T., Hrabe de Angelis, M., Lendahl, U. & Edlund, H. (1999) *Nature* **400,** 877-81.

179. Ma, Q., Chen, Z., del Barco Barrantes, I., de la Pompa, J. L. & Anderson, D. J. (1998) *Neuron* **20,** 469-82.

180. Jensen, J., Pedersen, E. E., Galante, P., Hald, J., Heller, R. S., Ishibashi, M., Kageyama, R., Guillemot, F., Serup, P. & Madsen, O. D. (2000) *Nat Genet* **24,** 36-44.

181. Gradwohl, G., Dierich, A., LeMeur, M. & Guillemot, F. (2000) *Proc Natl Acad Sci U S A* **97,** 1607-11.

182. Finegood, D. T., Scaglia, L. & Bonner-Weir, S. (1995) *Diabetes* **44,** 249-56.

183. Herrera, P. L., Huarte, J., Sanvito, F., Meda, P., Orci, L. & Vassalli, J. D. (1991) *Development* **113,** 1257-65.

184. Sander, M. & German, M. S. (1997) *J Mol Med* **75,** 327-40.

185. Li, H., Arber, S., Jessell, T. M. & Edlund, H. (1999) *Nat Genet* **23,** 67-70.

186. Harrison, K. A., Thaler, J., Pfaff, S. L., Gu, H. & Kehrl, J. H. (1999) *Nat Genet* **23,** 71-5.

187. Ahlgren, U., Pfaff, S. L., Jessell, T. M., Edlund, T. & Edlund, H. (1997) *Nature* **385,** 257-60.

188. Sosa-Pineda, B., Chowdhury, K., Torres, M., Oliver, G. & Gruss, P. (1997) *Nature* **386,** 399-402.

189. St-Onge, L., Sosa-Pineda, B., Chowdhury, K., Mansouri, A. & Gruss, P. (1997) *Nature* **387,** 406-9.

190. Kaestner, K. H., Katz, J., Liu, Y., Drucker, D. J. & Schutz, G. (1999) *Genes Dev* **13,** 495-504.

191. Lendahl, U., Zimmerman, L. B. & McKay, R. D. (1990) *Cell* **60,** 585-95.

192. Zulewski, H., Abraham, E. J., Gerlach, M. J., Daniel, P. B., Moritz, W., Muller, B., Vallejo, M., Thomas, M. K. & Habener, J. F. (2001) *Diabetes* **50,** 521-33.

193. Hunziker, E. & Stein, M. (2000) *Biochem Biophys Res Commun* **271,** 116-9.

194. Le Bras, S., Miralles, F., Basmaciogullari, A., Czernichow, P & Scharfmann, R. (1998) *Diabetes* **47,** 1236-42.

195. Miralles, F., Czernichow, P., Ozaki, K., Itoh, N. & Scharfmann, R. (1999) *Proc Natl Acad Sci U S A* **96,** 6267-72.

196. Miralles, F., Philippe, P., Czernichow, P. & Scharfmann, R. (1998) *J Endocrinol* **156,** 431-9.

197. Schuldiner, M., Yanuka, O., Itskovitz-Eldor, J., Melton, D. A. & Benvenisty, N. (2000) *Proc Natl Acad Sci U S A* **97,** 11307-12.

198. Bonner-Weir, S., Baxter, L. A., Schuppin, G. T. & Smith, F. E. (1993) *Diabetes* **42,** 1715-20.

199. Morshead, C. M., Reynolds, B. A., Craig, C. G., McBurney, M. W., Staines, W. A., Morassutti, D., Weiss, S. & van der Kooy, D. (1994) *Neuron* **13,** 1071-82.

200. Dahlstrand, J., Zimmerman, L. B., McKay, R. D. & Lendahl, U. (1992) *J Cell Sci* **103,** 589-97.

201. Bonner-Weir, S., Taneja, M., Weir, G. C., Tatarkiewicz, K., Song, K. H., Sharma, A. & O'Neil, J. J. (2000) *Proc Natl Acad Sci U S A* **97,** 7999-8004.

202. Otonkoski, T., Beattie, G. M., Mally, M. I., Ricordi, C. & Hayek, A. (1993) *J Clin Invest* **92,** 1459-66.

203. Sjoholm, A., Korsgren, O. & Andersson, A. (1994) *Endocrinology* **135,** 1559-65.

204. Trube, G., Rorsman, P. & Ohno-Shosaku, T. (1986) *Pflugers Arch* **407,** 493-9.

205. Yajima, H., Komatsu, M., Schermerhorn, T., Aizawa, T., Kaneko, T., Nagai, M., Sharp, G. W. & Hashizume, K. (1999) *Diabetes* **48,** 1006-12.

206. Susini, S., Roche, E., Prentki, M. & Schlegel, W. (1998) *Faseb J* **12,** 1173-82.

207. Roche, E., Farfari, S., Witters, L. A., Assimacopoulos-Jeannet, F., Thumelin, S., Brun, T., Corkey, B. E., Saha, A. K. & Prentki, M. (1998) *Diabetes* **47,** 1086-94.

208. Jonas, J. C., Sharma, A., Hasenkamp, W., Ilkova, H., Patane, G., Laybutt, R., Bonner-Weir, S. & Weir, G. C. (1999) *J Biol Chem* **274,** 14112-21.

209. Bonner-Weir, S. (2000) *J Mol Endocrinol* **24,** 297-302.

210. Weintraub, H., Davis, R., Tapscott, S., Thayer, M., Krause, M., Benezra, R., Blackwell, T. K., Turner, D., Rupp, R., Hollenberg, S. & et al. (1991) *Science* **251,** 761-6.

211. Rosenfeld, M. G. (1991) *Genes Dev* **5,** 897-907.

212. McGinnis, W. & Krumlauf, R. (1992) *Cell* **68,** 283-302.

213. Narimatsu, M., Maeda, H., Itoh, S., Atsumi, T., Ohtani, T., Nishida, K., Itoh, M., Kamimura, D., Park, S. J., Mizuno, K., Miyazaki, J., Hibi, M., Ishihara, K., Nakajima, K. & Hirano, T. (2001) *Mol Cell Biol* **21,** 6615-25.

214. Rudnick, A., Ling, T. Y., Odagiri, H., Rutter, W. J. & German, M. S. (1994) *Proc Natl Acad Sci U S A* **91,** 12203-7.

215. Gill, R. G. (1999) *Ann N Y Acad Sci* **875,** 255-60.

216. Martin, F. & Bedoya, F. J. (1990) *Transplantation* **50,** 551-3.

217. Wilmut, I., Schnieke, A. E., McWhir, J., Kind, A. J. & Campbell, K. H. (1997) *Nature* **385,** 810-3.

218. Wakayama, T., Tabar, V., Rodriguez, I., Perry, A. C., Studer, L. & Mombaerts, P. (2001) *Science* **292,** 740-3.

219. Weinberg, S. L., Burckhardt, G. & Wilson, F. A. (1986) *J Clin Invest* **78,** 44-50.

220. Higgins, C. F. (1995) *Cell* **82,** 693-6.

221. Chiang, J. Y. L. (1998) *Front Biosci* **3,** D176-93.

222. Stroup, D., Crestani, M. & Chiang, J. Y. (1997) *Am J Physiol* **273,** G508-17.

223. Janowski, B. A., Willy, P. J., Devi, T. R., Falck, J. R. & Mangelsdorf, D. J. (1996) *Nature* **383,** 728-31.

224. Peet, D. J., Turley, S. D., Ma, W., Janowski, B. A., Lobaccaro, J. M., Hammer, R. E. & Mangelsdorf, D. J. (1998) *Cell* **93,** 693-704.

225. Makishima, M., Okamoto, A. Y., Repa, J. J., Tu, H., Learned, R. M., Luk, A., Hull, M. V., Lustig, K. D., Mangelsdorf, D. J. & Shan, B. (1999) *Science* **284,** 1362-5.

226. Parks, D. J., Blanchard, S. G., Bledsoe, R. K., Chandra, G., Consler, T. G., Kliewer, S. A., Stimmel, J. B., Willson, T. M., Zavacki, A. M., Moore, D. D. & Lehmann, J. M. (1999) *Science* **284,** 1365-8.

227. Nitta, M., Ku, S., Brown, C., Okamoto, A. Y. & Shan, B. (1999) *Proc Natl Acad Sci U S A* **96,** 6660-5.

228. Goodwin, B., Jones, S. A., Price, R. R., Watson, M. A., McKee, D. D., Moore, L. B., Galardi, C., Wilson, J. G., Lewis, M. C., Roth, M. E., Maloney, P. R., Willson, T. M. & Kliewer, S. A. (2000) *Mol Cell* **6,** 517-26.

229. Lu, T. T., Makishima, M., Repa, J. J., Schoonjans, K., Kerr, T. A., Auwerx, J. & Mangelsdorf, D. J. (2000) *Mol Cell* **6,** 507-15.

230. Sinal, C. J., Tohkin, M., Miyata, M., Ward, J. M., Lambert, G. & Gonzalez, F. J. (2000) *Cell* **102,** 731-44.

231. Setchell, K. D., Schwarz, M., O'Connell, N. C., Lund, E. G., Davis, D. L., Lathe, R., Thompson, H. R., Weslie Tyson, R., Sokol, R. J. & Russell, D. W. (1998) *J Clin Invest* **102,** 1690-703.

232. Hagenbuch, B. & Meier, P. J. (1994) *J Clin Invest* **93,** 1326-31.

233. Hagenbuch, B., Stieger, B., Foguet, M., Lubbert, H. & Meier, P J. (1991) *Proc Natl Acad Sci U S A* **88,** 10629-33.

234. Tamai, I., Nezu, J., Uchino, H., Sai, Y., Oku, A., Shimane, M. & Tsuji, A. (2000) *Biochem Biophys Res Commun* **273,** 251-60.

235. Ogura, K., Choudhuri, S. & Klaassen, C. D. (2000) *Biochem Biophys Res Commun* **272,** 563-70.

236. Noe, B., Hagenbuch, B., Stieger, B. & Meier, P. J. (1997) *Proc Natl Acad Sci U S A* **94,** 10346-50.

237. Stieger, B. & Meier, P. J. (1998) *Curr Opin Cell Biol* **10,** 462-7.

238. de Vree, J. M., Jacquemin, E., Sturm, E., Cresteil, D., Bosma, P. J., Aten, J., Deleuze, J. F., Desrochers, M., Burdelski, M., Bernard, O., Oude Elferink, R. P & Hadchouel, M. (1998) *Proc Natl Acad Sci U S A* **95,** 282-7.

239. Powell, D. R. & Suwanichkul, A. (1993) *DNA Cell Biol* **12,** 283-9.

240. Christie, D. M., Dawson, P. A., Thevananther, S. & Shneider, B. L. (1996) *Am J Physiol* **271,** G377-85.

241. Wong, M. H., Oelkers, P., Craddock, A. L. & Dawson, P. A. (1994) *J Biol Chem* **269,** 1340-7.

242. Ishibashi, S., Goldstein, J. L., Brown, M. S., Herz, J. & Burns, D. K. (1994) *J Clin Invest* **93,** 1885-93.

243. Felker, T. E., Hamilton, R. L. & Havel, R. J. (1978) *Proc Natl Acad Sci U S A* **75,** 3459-63.

244. Manzato, E., Fellin, R., Baggio, G., Walch, S., Neubeck, W. & Seidel, D. (1976) *J Clin Invest* **57,** 1248-60.

245. Norum, K. R., Glomset, J. A., Nichols, A. V. & Forte, T. (1971) *J Clin Invest* **50,** 1131-40.

246. van Antwerpen, R., Chen, G. C., Pullinger, C. R., Kane, J. P., LaBelle, M., Krauss, R. M., Luna-Chavez, C., Forte, T. M. & Gilkey, J. C. (1997) *J Lipid Res* **38,** 659-69.

247. Laggner, P., Glatter, O., Muller, K., Kratky, O., Kostner, G. & Holasek, A. (1977) *Eur J Biochem* **77,** 165-71.

248. Austin, M. A. & Edwards, K. L. (1996) *Curr Opin Lipidol* **7,** 167-71.

249. Homanics, G. E., de Silva, H. V., Osada, J., Zhang, S. H., Wong, H., Borensztajn, J. & Maeda, N. (1995) *J Biol Chem* **270,** 2974-80.

250. Foger, B., Chase, M., Amar, M. J., Vaisman, B. L., Shamburek, R. D., Paigen, B., Fruchart-Najib, J., Paiz, J. A., Koch, C. A., Hoyt, R. F., Brewer, H. B., Jr. & Santamarina-Fojo, S. (1999) *J Biol Chem* **274,** 36912-20.

251. Mahley, R. W., Weisgraber, K. H., Innerarity, T., Brewer, H. B., Jr. & Assmann, G. (1975) *Biochemistry* **14,** 2817-23.

252. Konig, J., Cui, Y., Nies, A. T. & Keppler, D. (2000) *Am J Physiol Gastrointest Liver Physiol* **278,** G156-64.

253. Abe, T., Kakyo, M., Tokui, T., Nakagomi, R., Nishio, T., Nakai, D., Nomura, H., Unno, M., Suzuki, M., Naitoh, T., Matsuno, S. & Yawo, H. (1999) *J Biol Chem* **274,** 17159-63.

254. Kullak-Ublick, G. A., Hagenbuch, B., Stieger, B., Schteingart, C. D., Hofmann, A. F., Wolkoff, A. W. & Meier, P. J. (1995) *Gastroenterology* **109,** 1274-82.

255. Craddock, A. L., Love, M. W., Daniel, R. W., Kirby, L. C., Walters, H. C., Wong, M. H. & Dawson, P. A. (1998) *Am J Physiol* **274,** G157-69.

256. Oelkers, P., Kirby, L. C., Heubi, J. E. & Dawson, P. A. (1997) *J Clin Invest* **99,** 1880-7.

257. Wang, H., Chen, J., Hollister, K., Sowers, L. C. & Forman, B. M. (1999) *Mol Cell* **3,** 543-53.

258. Stolz, A., Hammond, L., Lou, H., Takikawa, H., Ronk, M. & Shively, J. E. (1993) *J Biol Chem* **268,** 10448-57.

259. Gordon, D. J., Probstfield, J. L., Garrison, R. J., Neaton, J. D., Castelli, W. P., Knoke, J. D., Jacobs, D. R., Jr., Bangdiwala, S. & Tyroler, H. A. (1989) *Circulation* **79,** 8-15.

260. Scriver, C. R. (1995) *The metabolic and molecular bases of inherited disease* (McGraw-Hill Health Professions Division, New York).

261. Fielding, C. J. & Fielding, P. E. (1995) *J Lipid Res* **36,** 211-28.

262. Sladek, F. M., Zhong, W. M., Lai, E. & Darnell, J. E. (1990) *Genes & Development* **4,** 2353-65.

263. Lehto, M., Bitzen, P. O., Isomaa, B., Wipemo, C., Wessman, Y., Forsblom, C., Tuomi, T., Taskinen, M. R. & Groop, L. (1999) *Diabetes* **48,** 423-5.

264. Hayhurst, G. P., Lee, Y. H., Lambert, G., Ward, J. M. & Gonzalez, F. J. (2001) *Mol Cell Biol* **21,** 1393-403.

265. Harrison, T. R. & Fauci, A. S. (1998) *Harrison's principles of internal medicine* (McGraw-Hill Health Professions Division, New York).

266. Xu, N. & Dahlback, B. (1999) *J Biol Chem* **274,** 31286-90.

267. Duncan, S. A., Nagy, A. & Chan, W. (1997) *Development* **124,** 279-87.

268. Lindner, T., Gragnoli, C., Furuta, H., Cockburn, B. N., Petzold, C., Rietzsch, H., Weiss, U., Schulze, J. & Bell, G. I. (1997) *Journal of Clinical Investigation* **100,** 1400-5.

269. Iwasaki, N., Ogata, M., Tomonaga, O., Kuroki, H., Kasahara, T., Yano, N. & Iwamoto, Y. (1998) *Diabetes Care* **21,** 2144-8.

270. Navas, M. A., Munoz-Elias, E. J., Kim, J., Shih, D. & Stoffel, M. (1999) *Diabetes* **48,** 1459-65.

271. Utermann, G., Kraft, H. G., Menzel, H. J., Hopferwieser, T. & Seitz, C. (1988) *Hum Genet* **78,** 41-6.

272. Boerwinkle, E., Menzel, H. J., Kraft, H. G. & Utermann, G. (1989) *Hum Genet* **82,** 73-8.

273. Bereket, A., Lang, C. H. & Wilson, T. A. (1999) *Horm Metab Res* **31,** 172-81.

274. Cardot, P., Chambaz, J., Cladaras, C. & Zannis, V. I. (1991) *J Biol Chem* **266,** 24460-70.

275. Krauss, R. M., Herbert, P. N., Levy, R. I. & Fredrickson, D. S. (1973) *Circ Res* **33,** 403-11.

276. Aalto-Setala, K., Weinstock, P. H., Bisgaier, C. L., Wu, L., Smith, J. D. & Breslow, J. L. (1996) *J Lipid Res* **37,** 1802-11.

277. Boisfer, E., Lambert, G., Atger, V., Tran, N. Q., Pastier, D., Benetollo, C., Trottier, J. F., Beaucamps, I., Antonucci, M., Laplaud, M., Griglio, S., Chambaz, J. & Kalopissis, A. D. (1999) *J Biol Chem* **274,** 11564-72.

278. Weng, W. & Breslow, J. L. (1996) *Proc Natl Acad Sci U S A* **93,** 14788-94.

279. Deeb, S. S., Takata, K., Peng, R. L., Kajiyama, G. & Albers, J. J. (1990) *Am J Hum Genet* **46,** 822-7.

280. Stoffel, M., Froguel, P., Takeda, J., Zouali, H., Vionnet, N., Nishi, S., Weber, I. T., Harrison, R. W., Pilkis, S. J., Lesage, S. & et al. (1992) *Proc Natl Acad Sci U S A* **89,** 7698-702.

281. Postic, C., Shiota, M., Niswender, K. D., Jetton, T. L., Chen, Y., Moates, J. M., Shelton, K. D., Lindner, J., Cherrington, A. D. & Magnuson, M. A. (1999) *J Biol Chem* **274,** 305-15.

282. Setchell, K. D., Lawson, A. M., Tanida, N. & Sjovall, J. (1983) *J Lipid Res* **24,** 1085-100.

283. Setchell, K. D., Yamashita, H., Rodrigues, C. M., O'Connell, N. C., Kren, B. T. & Steer, C. J. (1995) *Biochemistry* **34,** 4169-78.

284. Aalto-Setala, K., Bisgaier, C. L., Ho, A., Kieft, K. A., Traber, M. G., Kayden, H. J., Ramakrishnan, R., Walsh, A., Essenburg, A. D. & Breslow, J. L. (1994) *J Clin Invest* **93,** 1776-86.

285. Sehayek, E., Ono, J. G., Shefer, S., Nguyen, L. B., Wang, N., Batta, A. K., Salen, G., Smith, J. D., Tall, A. R. & Breslow, J. L. (1998) *Proc Natl Acad Sci U S A* **95,** 10194-9.

286. Levine, D. M. & Williams, K. J. (1997) *Clin Chem* **43,** 669-74.

287. Alam, J. & Cook, J. L. (1990) *Anal Biochem* **188,** 245-54.

288. Ananthanarayanan, M., Bucuvalas, J. C., Shneider, B. L., Sippel, C. J. & Suchy, F. J. (1991) *Am J Physiol* **261,** G810-7.

289. Bergwerk, A. J., Shi, X., Ford, A. C., Kanai, N., Jacquemin, E., Burk, R. D., Bai, S., Novikoff, P. M., Stieger, B., Meier, P. J., Schuster, V. L. & Wolkoff, A. W. (1996) *Am J Physiol* **271,** G231-8.

290. Sturis, J., Pugh, W. L., Tang, J. & Polonsky, K. S. (1995) *Am J Physiol* **269,** E786-92.

291. Lavery, D. J., Lopez-Molina, L., Fleury-Olela, F. & Schibler, U. (1997) *Proc Natl Acad Sci U S A* **94,** 6831-6.

292. Miller, R. D. & Riblet, R. (1995) *Nucleic Acids Res* **23,** 2339-40.